RESIDUAL RESPONSE OF REINFORCED CONCRETE BEAMS FOLLOWING FIRE EXPOSURE

By

Ankit Agrawal

A DISSERTATION

Submitted to
Michigan State University
in partial fulfillment of the requirements
for the degree of

Civil Engineering - Doctor of Philosophy

2020

ABSTRACT

RESIDUAL RESPONSE OF REINFORCED CONCRETE BEAMS FOLLOWING FIRE EXPOSURE

By

Ankit Agrawal

Reinforced concrete (RC) structures possess inherent fire resistance due to relatively low thermal conductivity, high thermal capacity, and slower strength degradation of concrete with temperature. Nonetheless, fire exposure results in varying reduction in strength and stiffness RC members because of irreversible temperature induced degradation in mechanical properties concrete and rebar. Thus, uncertainty regarding extent of reduction in load bearing capacity RC structures (members) necessitates post-fire assessment of residual capacity to facilitate repair and (or) return to service conditions. Specifically, RC beams or slabs are particularly susceptible to fire damage arising from convective effects (hot gases) and impingement by flames near the ceiling, which do not affect vertical members as significantly. This PhD dissertation develops a comprehensive understanding on the residual response of fire damaged RC beams after exposure to combined effects of fire and structural loading through detailed experimental and numerical studies. A novel three stage approach to evaluate residual response of RC beams following fire exposure is conceptualized to overcome deficiencies in current assessment approaches. The three stages comprise of; Stage 1: evaluating the member response at room temperature during service (load) conditions as present prior to fire exposure; Stage 2: evaluating member response during heating and cooling phases as present in a fire incident, and during extended cool down phase of the member to simulate conditions as occurring after fire is extinguished or burnout conditions are attained; and Stage 3: evaluating residual response of the fire damaged member following complete cool down to room temperature. The proposed approach can account for the influence of critical factors such as, distinct temperature dependent material properties of concrete and rebar during heating, cooling, and residual phases, fire induced residual deformations, load level, and restraint conditions present during fire exposure in evaluating residual response of RC beams. Experimental and numerical studies were conducted to develop needed data for establishing applicability and validity of the proposed approach for tracing residual response. Material level tests were undertaken to establish temperature dependent bond strength relations for interfacial bond between rebar and concrete. Full scale fire resistance tests followed by residual capacity evaluation tests were conducted on six RC beams having different configurations. As part of numerical studies, a three-dimensional finite element based numerical model was developed to implement the proposed three-stage approach for evaluating residual response of fire exposed concrete beams, using general purpose software ABAQUS. The novelty of the developed model lies in explicit consideration of distinct thermomechanical properties of concrete and rebar during heating and cooling phase of fire exposure and residual (after cool down) phase, as well as in incorporation of plastic deflections occurring during fire exposure into post-fire residual response analysis of RC beams. Predictions from the developed model were validated against response parameters measured during tests published in literature and conducted as part of this study. The validated model was applied to conduct parametric studies to quantify the effect of critical parameters, namely, fire severity, load level, axial restraint, cross-sectional dimensions, and cover to reinforcement, on residual response of RC beams following fire exposure. Finally, findings from experimental and numerical studies, together with that reported in literature, were utilized to develop a five-step rational approach combining physical testing with simplified and advanced calculation methods, for practical post-fire assessment of residual capacity in concrete structures.

brother Prate	n is dedicated to ek Agrawal, and ragement, I wou	my beloved wi	fe, Kanupriya.	Without their sup	port and

ACKNOWLEDGMENTS

I would like to express my deep gratitude to my advisor, Prof. Venkatesh Kodur for his continued support and guidance during the course of my studies. I am very grateful for his motivation and perseverance, and for providing an opportunity for a valuable learning experience.

I would also like to thank Prof. Neeraj Buch, Prof. Weiyi Lu, and Prof. Thomas J. Pence for joining my Ph.D. committee, and for their valuable advice throughout my education at Michigan State University.

I would like to thank my friends Anuj Shakya, Amir Arablouei, Mohannad Naser, Esam Aziz, Saleh Mohammad Alogla, Roya Solhmirzaei, Srishti Banerji, and Puneet Kumar for their support, particularly in the experimental part of this study.

I would also like to express my appreciation to Mr. Siavosh Ravanbakhsh (Sia) and Mr. Charles Meddaugh (Chuck), for their support and help during the experimental program in this research. Additionally, I would like to extend my thanks to Laura Taylor, Margaret Conner and Laura Post for all the administrative assistance they provided.

TABLE OF CONTENTS

LIST O	F TABLES	ix
LIST O	F FIGURES	X
СНАРТ	TER 1	1
1 INTE	RODUCTION	1
1.1	General	1
1.2	Residual capacity of fire exposed beams	
1.3	Factors governing residual response of fire exposed RC beams	6
1.4	Research objectives	
1.5	Layout of thesis	9
СНАРТ	TER 2	13
2 STA	ΓE-OF-THE-ART REVIEW	13
2.1	General	13
2.2	Experimental studies on fire exposed RC beams	14
2.3	Numerical studies	
2.4	Material properties during heating, cooling, and residual phases	23
2.4.1	Concrete properties	24
2.4.1.1		
2.4.1.2	r	
2.4.1.3	1 1	
2.4.1.4	6 T T	
2.4.1.5	1 1	
2.4.1.6	1 1	36
2.4.1.7	T T	
2.4.1.8	- r · · · · · · · · · · · · · · · · · ·	
2.5	Knowledge gaps	42
	TER 3	
3 EXPI	ERIMENTAL PROGRAM	
3.1	General	
3.2	Test to evaluate temperature induced bond degradation	59
3.2.1	Fabrication of specimens and test-setup	
3.2.2	Results from high temperature bond tests	
3.2.3	Temperature dependent residual bond strength relations	
3.3	Three-stage procedure for evaluating residual capacity	
3.4	Design and fabrication of concrete beams	
3.5	Test-setup and procedure	
3.5.1	Testing prior to fire exposure	
3.5.2	Testing during fire exposure conditions	67

3.5.3	Residual strength test	69
3.6	Results from tests	70
3.6.1	Response prior to fire exposure (Stage 1)	70
3.6.2	Response during fire exposure (Stage 2)	70
3.6.2.		
3.6.2.2	2 Structural response during fire exposure	75
3.6.2.3	3 Temperature induced spalling	79
3.6.3	Residual response of fire damaged beams (Stage 3)	
3.6.3.	1 Structural response	82
3.6.3.2	2 Crack patterns and failure modes	85
3.7	Summary	88
СНАРТ	TER 4	102
4 NUM	IERICAL MODEL AND VALIDATION	102
4.1	General	102
4.2	Development of finite element model	103
4.2.1	General approach	
4.2.2	Modeling assumptions	105
4.2.3	Analysis details	106
4.2.3.	Heat transfer analysis (Stage 2)	108
4.2.3.2	2 Structural analysis (Stages 1, 2, and 3)	112
4.2.4	Modeling interfacial bond between rebar and concrete	116
4.2.4.		
4.2.4.2	2 Bond-link element approach	117
4.2.5	Discretization of the beam	118
4.2.6	Temperature dependent material modeling	119
4.2.6.		
4.2.6.2	2 Modelling of reinforcing steel	124
4.2.6.3		
4.2.7	Failure criteria.	
4.2.8	Output results	128
4.3	Model Validation	129
4.3.1	Tests by Dwaikat and Kodur (Dwaikat and Kodur 2009c)	129
4.3.2	Tests by Kumar and Kumar (Kumar and Kumar 2003b)	
4.3.3	MSU test beams	
4.3.3.	Response during pre-fire conditions (Stage 1)	137
4.3.3.2	Response during fire conditions (Stage 2)	138
4.3.3.3		
4.3.3.4	<u> </u>	
4.4	Summary	
СНАРТ	TER 5	171
	AMETRIC STUDIES	
5.1	General	
5.2	Factors influencing fire response	
5.3	Parametric studies	

5.3.1	General	172
5.3.2	Range of parameters	173
5.3.3	Analysis details	174
5.4	Results of parametric studies	175
5.4.1	Effect of fire exposure	175
5.4.2	Effect of load level	177
5.4.3	Effect of axial restraint	178
5.4.4	Effect of varying size of beam	179
5.4.5	Effect of cover to reinforcement	181
5.5	Summary	182
СНАРТ	TER 6	197
6 APPI	ROACH FOR RESIDUAL CAPACITY ASSESSMENT	197
6.1	General	197
6.2	Approach for assessment	198
6.2.1	General procedure	198
6.2.2	Step 1: Establish fire characteristics	199
6.2.3	Step 2: Establish peak exposure (surface) temperatures experienced by struct	ural
	member	
6.2.4	Step 3: Classification of temperature induced damage during fire exposure	
6.2.5	Step 4: Estimating residual mechanical properties of concrete and rebar	204
6.2.6	Step 5: Evaluating residual capacity of fire-damaged reinforced concrete elements	
6.2.6.1	1 11	
6.2.6.2	2 Advanced analysis approach	209
6.3	Limitations of approach	
6.4	Summary	212
	TER 7	
7 CON	CLUSIONS AND RECOMMENDATIONS	
7.1	General	
7.2	Key findings	
7.3	Recommendations for future research	
7.4	Research impact	230
		232
	ix A: Worked Example for damage assessment of an office building floor after fire	233
		241
Append	ix C: Additional images taken during different stages of testing	249
PEEEDI	ENCES	250

LIST OF TABLES

Table 3-1. Concrete batch mix proportions used in fabrication of RC beams
Table 3-2. Test parameters varied in residual capacity tests
Table 3-3. Summary of measured response parameters for tested RC beams
Table 4-1. Relationships for high temperature thermal properties of concrete (Eurocode 2) 145
Table 4-2. Constitutive relationship for high temperature properties of concrete (Eurocode 2) 146
Table 4-3. Values for the main parameters of the stress-strain relationships of NSC and HSC at elevated temperatures (Eurocode 2)
Table 4-4. High temperature thermal properties of reinforcing steel (Eurocode 3)
Table 4-5. Constitutive relationships for high temperature properties of reinforcing steel (Eurocode 2)
Table 4-6. Values for the main parameters of the stress-strain relationships of reinforcing steel at elevated temperatures (Eurocode 2)
Table 4-7. Input parameters for defining concrete plasticity
Table 4-8. Summary of test parameters and results for beams used for validation
Table 5-1. Summary of test parameters and results used for parametric study
Table 5-2. Summary of varied parameters and results from parametric study
Table 6-1. Assessment of temperature reached by selected materials and components in fires 214
Table 6-2. A visual damage classification scheme for reinforced concrete elements
Table A-1. Key fire severity characteristics
Table A-2. Classification of temperature induced damage based on visual observation 237
Table A-3. Reduction factors for residual strength of concrete and reinforcing steel after exposure to high temperature
Table A-4. Calculated moment capacity before and after fire exposure

LIST OF FIGURES

Figure 1-1. Thermal and structural response of a typical RC beam subject to varying fire scenarios in a building compartment
Figure 1-2. Comparison of residual load-deflection response of the fire exposed RC beams and undamaged RC beam
Figure 1-3. Effect of load level on response of RC beam during and after fire exposure
Figure 2-1. Residual response of fire damaged beams reported in previous studies
Figure 2-2. Numerical predictions from previous studies on evaluating residual capacity of fire damaged concrete beams
Figure 2-3. Illustration depicting temperature induced deterioration in thermal properties of concrete as expected during heating, cooling, and residual phases of fire exposure
Figure 2-4. Variation of thermal conductivity of concrete with temperature based on Eurocode 2
Figure 2-5. Variation of specific heat of concrete with temperature based on Eurocode 2 47
Figure 2-6. Variation of density of concrete with temperature based on Eurocode 2
Figure 2-7. Illustration depicting temperature induced deterioration in mechanical properties of concrete as expected during heating, cooling, and residual phases of fire exposure
Figure 2-8. Variation of compressive strength of NSC with temperature (Kodur 2014)
Figure 2-9. Variation of compressive strength of HSC with temperature (Kodur 2014)
Figure 2-10. Variation of tensile strength of concrete with temperature
Figure 2-11. Variation of elastic modulus of concrete with temperature
Figure 2-12. Variation of residual compressive strength of concrete with temperature 51
Figure 2-13. Variation of elastic modulus of concrete with temperature
Figure 2-14. Variation of thermal strain of concrete with temperature during elevated (hot) and residual phases
Figure 2-15. Variation of creep strain of concrete with temperature (Gross 1975)

Figure 2-16. Total strain of concrete variation with temperature under different stress levels (Anderberg and Thelandersson 1976)
Figure 2-17. Typical relations for temperature dependent stress-strain relations of concrete during and after high temperature exposure
Figure 2-18. Variation of thermal conductivity of reinforcing steel with temperature based on Eurocode 2
Figure 2-19. Variation of specific heat of reinforcing steel with temperature based on Eurocode 2
Figure 2-20. Variation of yield strength of reinforcing steel as a function of temperature 55
Figure 2-21. Normalized residual strength of hot rolled reinforcing steel
Figure 2-22. Variation of thermal strain of reinforcing steel with temperature based on Eurocode
Figure 2-23. Residual stress–strain curves for reinforcing steel having yield strength of 420 MPa
Figure 2-24. Relative bond strength as a function of temperature (air-cooled specimens) 57
Figure 3-1. Test setup for residual bond strength tests after exposure to high temperature 92
Figure 3-2. Test data from DTP tests after exposure to high temperature for NSC and HSC specimens
Figure 3-3. Failure modes in NSC and HSC specimens at different temperatures
Figure 3-4. Flow chart illustrating proposed three stage approach for residual capacity assessment of RC structural members
Figure 3-5. Loading reinforcement, and instrumentation details of tested RC beams
Figure 3-6. Response of RC beams during Stage-1 loading at room temperature
Figure 3-7. Time–temperature curves for fire scenarios used in the fire tests
Figure 3-8. Measured rebar and concrete temperatures as a function of fire exposure time for tested RC beams
Figure 3-9. Mid-span deflection of beam tested beams as a function of time
Figure 3-10. Load–deflection response of fire damaged RC beams in residual strength tests 99

Figure 3-11. Crack and failure patterns in HSC and NSC beams after cool down from fire exposure and after residual capacity tests
Figure 4-1. Flow chart illustrating the three stages involved in residual capacity analysis 150
Figure 4-2. Discretization and element types adopted for thermal and structural analysis of RC beams
Figure 4-3. Transformation of uniaxial stress-strain relation to equivalent yield surface in the deviatoric plane comprising of stress invariants
Figure 4-4. Stress-strain relationship of concrete in compression at various temperature based on Eurocode 2
Figure 4-5. Stress-strain relationship of concrete in tension at various temperature based on Eurocode 2
Figure 4-6. Normalized compressive strength of concrete with maximum exposure temperature
Figure 4-7. Normalized residual strength of hot rolled reinforcing steel
Figure 4-8. Loading and reinforcement details of RC beams used for validation
Figure 4-9. Time-temperature curves for fire scenarios used in fire tests on beams B1 and B2 155
Figure 4-10. Comparison of predicted and measured cross sectional temperatures for beams B1 and B2 during fire exposure
Figure 4-11. Comparison of the predicted and measured mid-span deflections for beams B1 and B2 during fire exposure
Figure 4-12. Predicted and measured post-fire residual load-deflection response for beam B2 157
Figure 4-13. Expected residual thermal expansion (or shrinkage) strains versus residual plastic deformations across the section at mid-span for beam B2
Figure 4-14. Fire exposures for tested beams
Figure 4-15.Comparison of predicted and published temperature contours (EN 1992-1-2 2004) over the beam cross-section after heating of: (a) 0.5 h; (b) 1 h and (c) 1.5 h for validation 158
Figure 4-16.Comparison of predicted and measured post fire load-deflection response for tested beams

Figure 4-17. Expected residual thermal expansion (or shrinkage) strains versus residual plastic deformations across the section at mid-span for tested beams
Figure 4-18. Measured and predicted load-deflection response for room temperature analysis during Stage 1
Figure 4-19. Time–temperature curves depicting fire scenarios used in fire tests for HSCB1 HSCB2, and NSCB1 through NSCB4.
Figure 4-20. Comparison of measured and predicted temperatures for heating and cooling phase of testing during Stage 2
Figure 4-21. Comparison of measured and predicted mid span deflection progression with time during Stage 2
Figure 4-22. Predicted and measured post-fire residual load-deflection response of fire damaged beams during Stage 3
Figure 4-23. Effect of temperature induced bond degradation on fire behavior and residual response of RC beams following fire exposure
Figure 5-1. Illustration showing dimensions, loading and reinforcement details of typical bean (BX1) analyzed for parametric study
Figure 5-2. Parametric time-temperature curves for a total compartment area of 360 m ² , fire load density between 600 to 750 MJ/m ² and four opening factors (At). ($o = A_v \sqrt{h_{eq}}/A_t$) accounting fo different area of openings (A_v), equivalent height of openings (h_{eq}), and total area (A_t)
Figure 5-3. Effect of fire scenario on residual response of fire exposed RC beam BX1
Figure 5-4. Effect of load ratio for beam BX1 under fire exposure scenario DF2
Figure 5-5. Effect of axial restraint on fire performance and residual capacity of beams BX1, BX2 and BX3 under different fire exposure scenarios
Figure 5-6. Effect of cross section on fire response of RC beams under different fire exposures
Figure 5-7. Effect of fire scenario on residual load-deflection response in RC beams with varying cross section
Figure 5-8. Effect of varying cover to reinforcement on structural response during fire exposure DF5 and residual response following fire exposure
Figure 6-1. Response of a typical RC beam during and after fire exposure

Figure 6-2. Flowchart illustrating five step approach for rapid assessment of fire-damaged concrete structures
Figure 6-3. Melting of aluminum formwork supports indicating that the fire reached temperatures in excess of 650°C
Figure 6-4. Parametric time temperature curves for different compartment conditions calculated as per Eurocode 1
Figure 6-5. Color change of siliceous concrete, heated to temperatures ranging from 100°C to 1000°C
Figure 6-6. Temperature induced damage at surface level (outer layers) of fire exposed concrete slabs
Figure 6-7. Influence of temperature and post cooling storage period on compressive strength of concrete
Figure 6-8. Yield strength of different types of reinforcing steel after exposure to elevated temperature
Figure 6-9. Illustration of cross-sectional capacity using simplified analysis
Fig. A-1. Ground plan and structural layout of the office floor and reference numbers for structural elements
Fig. A-2. Cross-sectional dimensions and reinforcement details of beams and columns present in the fire exposed structure
Fig. A-3. Predicted time-temperature curve of the fire compartment
Fig. A-4. Geometry and reinforcement details of the fire damaged beams
Fig. C-1. Images of Normal Strength Concrete (NSC) beam prior to and during fire exposure 249
Fig. C-2. Typical strain localization (redder hues indicate greater tensile strains) at critical flexural span in NSC beam B3 at service load (about 50 kN); captured using Digital Image Correlation (DIC) setup

CHAPTER 1

1 INTRODUCTION

1.1 General

Fire represents a severe environmental condition structures may experience during their design life. Hence, structural members in buildings have to satisfy fire resistance requirements as fire safety is one of the key considerations in building design (ASTM E119-19 2019; EN 1992-1-2 2004). However, historical survey data clearly suggests that while fires do occur in structures, complete collapse of structural system due to fire is a rare event (Beitel and Iwankiw 2005). The probability of such failure in reinforced concrete (RC) structural members is even lower due to low thermal conductivity, high thermal capacity, and slower degradation of mechanical properties of concrete with temperature (Molkens et al. 2017; Tovey 1986). It is reasonable to assume, after most fire incidents, RC structures may be opened to re-occupancy with adequate repair and retrofitting, depending on severity of fire exposure (Kodur 2014; Park and Yim 2017; Van Coile 2015).

Nonetheless, extent of fire induced damage in RC structures is highly variable. In case of exposure to a severe fire, RC members might experience significant structural damage resulting from loss of concrete due to possible fire induced spalling, high rebar temperatures and relatively larger permanent deflections. Alternatively, exposure to moderate fire scenario may not result in noticeable deflections or loss of concrete section due to spalling, and thus loss of structural capacity may not be significant. Thus, there is uncertainty regarding load bearing capacity of RC members owing to temperature induced degradation in material properties and extent of redistribution of stresses within the RC member after fire. It is imperative to assess if sufficient residual capacity

exists in structural members prior to re-occupancy after the fire incident. Such an assessment forms also the basis for developing retrofitting (repair) measures in fire damaged RC structures.

When a RC structure is exposed to fire, RC beams (horizontal flexural members) located near the ceiling are often more susceptible to temperature induced damage, than vertical RC columns located at the corners of the structure. RC beams experience higher rise in temperature as compared to RC columns, due to rising convective currents (hot gases) that accumulate in upper layers close to ceiling. Also, smaller concrete cover requirements for RC beams than RC columns imply greater increase in rebar temperature in beams for similar fire exposures. In addition, tensile and bond strength of concrete, which are critical for transfer of tensile stresses from concrete to rebar in flexural members, deteriorate at a faster rate with temperature compared to compressive strength of concrete. Besides, temperature induced degradation, large thermal gradients develop across the depth of the RC beam as temperatures near the bottom (exposed) faces of the beam increase rapidly, and slabs present on top face provide thermal insulation. These increased stresses, coupled with deterioration in strength and stiffness properties of the RC beam, result in post-fire residual deflections (plastic strains), and hence greater reduction in residual capacity. Therefore, it is imperative to evaluate residual capacity of RC beams following a fire event.

At present, limited approaches are available for evaluating residual response of RC beams following fire exposure. Majority of existing approaches utilize modified room temperature strength equations, with temperature dependent strength reduction factors to account for temperature induced degradation in mechanical properties of concrete and reinforcing steel, to evaluate residual capacity. Current approaches do not account for realistic material properties of concrete and rebar during and after fire exposure (specifically during cooling phase), post-fire residual deflections, load level, and restraint conditions present during fire exposure in evaluating

residual capacity. In addition, a perfect bond is assumed between concrete and rebar during fire exposure and after cool down (residual state), which has been recently shown to yield unconservative predictions of residual capacity. Thus, there is a need for a rational approach that takes into account realistic fire exposure scenarios, structural conditions and residual mechanical properties, including temperature induced bond degradation, in evaluating residual capacity of fire exposed RC beams. To develop a better understanding of the problem, complexities involved in evaluating residual capacity assessment of fire exposed RC beams are discussed below.

1.2 Residual capacity of fire exposed beams

In most cases, significant residual capacity is retained in RC members following a fire incident. However, the residual capacity retained in the RC member is highly variable, and depends on both temperature history as well as structural conditions present during fire exposure. The different temperature histories (fire exposure scenarios) and structural conditions (load and restraint levels) influences elevated temperature response, and consequently residual capacity of a fire exposed RC beam, as illustrated through a typical example below.

Consider a high rise RC building with multiple floors under fire (see Figure 1-1a). Fire travels upwards through building floors, with limited floors being under fire at a given time. Furthermore, owing to some level of compartmentation provided in such buildings, fire spread occurs gradually from one compartment to another and does not affect the entire building at the same time. Thus, a system level analysis is generally not needed to evaluate damage due to fire in a RC building. Evaluating residual capacity of RC members within respective fire exposed compartments can provide reasonable approximation of extent of fire damage in structural members. There are multiple fire scenarios possible in a building compartment. Four such possible fire exposure

scenarios designated as DF1, DF2, DF3, and DF4, are shown in Figure 1-1b. These fire scenarios are calculated for different ventilation conditions, or opening factors (represented by 'O'), and are generally characterized by relatively rapid heating followed by a distinct cooling (decay) phase (see Figure 1-1b). Fire temperatures can rise rapidly in the first few minutes of heating phase, at a rate of 100°C-150°C per minute, as the fire attains post-flashover state, and heat up a RC beam in the building from below (see Figure 1-1c). This results in sectional temperatures to rise in both concrete and rebar present in the RC beam. However, the rate of temperature increase in rebar (and inner layers of concrete) as seen in Figure 1-1d, is almost 10 times lower than the rate of increase in fire temperatures due to thermal protection from concrete which has low thermal conductivity and high heat capacity. Thus, there are large temperature gradients between the exposed surface and inner layers of concrete. These thermal gradients lead to a rapid increase in the mid-span deflections of the beam. As fire exposure time progresses, temperature within the RC beam stabilizes and the effect of thermal gradients is less pronounced. Nonetheless, mid-span deflection in the RC beam continues to increase due to temperature induced degradation in strength and stiffness properties of concrete and rebar (see Figure 1-1d).

In fact, the RC beam fails due to excessive mid-span deflection as peak rebar temperature exceed 500°C under DF1 fire exposure, since the deflections exceed limiting deflection under fire conditions. In this case, there is no need for evaluating residual capacity as the beam has lost all its capacity and failed during fire exposure. In the remaining three fire scenarios (DF2, DF3 and DF4); mid-span deflections that occur during fire exposure begin to recover (revert back) just as the rebar temperature starts decreasing after attaining peak value. Note that the peak-rebar temperature, and consequently peak mid-span deflection in the beam occurs during cooling phase of fire exposure, owing to high thermal inertia of concrete. Upon complete cool down to room

temperature, there is an irrecoverable residual deflection in the beam resulting from plastic deformations that occurred in the loaded beam during fire exposure. This residual deflection varies greatly with fire exposure scenario, and greater peak rebar temperature results in greater residual deflection. Also, the post-fire residual deflections under load are significantly greater than pre-fire deflections indicating the reduction in stiffness of the beams due to fire damage.

The load-deflection response of the undamaged beam prior to fire exposure, as well residual response of the same beam after different fire exposure scenarios is shown in Figure 1-2. Residual deflections exist in fire damaged beams even when no load is acting on the beams. It can be seen that a greater reduction in capacity is seen in cases with higher post-fire residual deflection resulting from more severe fire exposure. Thus, there is significant variability in predicted residual capacity depending on fire exposure scenario.

Similarly, the effect of varying load levels on fire response and residual capacity can be seen in Figure 1-3a-b, depicting mid-span deflection during fire and post-fire load-deflection curves for varying load levels. Both the rate of rise and maximum deflection experienced during fire exposure are directly proportional to load level present during fire exposure. Also, greater load level results in greater degradation in residual capacity and higher residual deflections, even when the thermal (fire exposure) conditions are identical.

Thus, it can be inferred that both temperature (fire) history, as well as structural conditions present during fire exposure, influence the residual capacity of fire exposed RC beams. With these considerations, key factors that influence residual capacity of fire exposed RC beams are discussed in the following section.

1.3 Factors governing residual response of fire exposed RC beams

The extent of damage to a RC beam during a fire incident is influenced by a number of factors, including fire severity, residual mechanical properties of rebar and concrete, temperature induced bond degradation, load level, and restraint conditions present during fire exposure. Many of these factors are interdependent and can vary significantly in different scenarios.

The severity of fire exposure can influence residual capacity of RC beams significantly. Fire severity in a structure depends on fuel load density, ventilation characteristics, and geometrical parameters of the fire compartment (EN 1991-1-2 2002). Moreover, these factors may evolve with the growth of the fire, for instance, a sudden increase in ventilation can occur due to breakage of glass windows. Furthermore, presence of active fire protection systems such as sprinklers and fire fighter intervention can have significant effect on rate of fire temperature increase, peak fire temperature as well as time taken for fire temperature to cool down.

Properties of concrete and reinforcing steel vary during heating and cooling phases of fire exposure as well as upon cool down to ambient conditions (Kalaba et al. 2018). Thermophysical, mechanical and deformation properties of concrete change substantially during heating phase of fire exposure primarily due to breakdown of C-S-H gel and loss of moisture present in concrete (Chew 1993). The properties of concrete change further during cooling phase, due to micro-cracking and chemical changes occurring during heating. Also, load induced thermal strain (LITS, also referred to as transient thermal creep, drying creep or Pickett's effect (Bažant 1970; Khoury et al. 1985) occurs in concrete during the first heating cycle under load and does not recover upon cool down of a structural member (Gernay 2019; Kodur and Alogla 2017).

Post-fire residual properties of concrete upon cool down are also different from original properties or that during fire exposure. In particular, the residual compressive strength of concrete exposed

to temperatures in excess of 220°C continues to deteriorate and can be 10% lower than its value at elevated temperature, for 1 to 6 weeks after fire exposure (Nassif 2006).

Reinforcing steel exhibits reversibility in both thermal and mechanical properties as it cool downs to ambient conditions. Thermal properties of reinforcing steel can be considered completely reversible for engineering applications. However, post-fire residual yield strength of reinforcing steel depends on peak temperatures experienced during fire exposure, and undergoes partial recovery if exposure temperatures exceed 500°C (Neves et al. 1996a).

In addition to strength and stiffness degradation in concrete and rebar, bond between concreterebar deteriorates when temperatures at the interface exceed 400°C (Panedpojaman and Pothisiri 2014b) due to differential thermal expansion between rebar an concrete as well as temperature induced degradation in properties of concrete. Therefore, bond strength at residual state (after cool down) is lower than the original bond strength (Shamseldein et al. 2018).

Loading level and restraint conditions present during fire exposure can influence level of fire damage. Presence of higher loading (stress) or restraint influence stress history experienced in the RC beam during fire exposure. Consequently, these structural parameters affect residual capacity of fire exposed RC beams.

All critical factors discussed above need to be accounted for when evaluating residual capacity of fire exposed RC beams; which is currently lacking in majority of existing approaches. Therefore, residual strength evaluation of fire exposed RC beams becomes quite complex.

1.4 Research objectives

Based on above discussion, it is evident that evaluating residual capacity depends on temperature history as well as residual properties of materials, and structural conditions present during fire

exposure. Existing approaches do not account for all critical factors influencing residual response of RC beams following fire exposure. The overall aim of this thesis is to develop a general approach that accounts for critical factors in evaluating residual capacity of fire exposed RC beams. To this end, the following objectives are proposed as part of this research;

- Undertake a detailed state-of-the-art review on residual capacity of fire exposed RC beams, and identify knowledge gaps in literature.
- Develop a general approach to evaluate residual capacity of fire exposed RC beams. Implement the developed approach in a finite element based numerical model to trace residual response of fire exposed RC beams. This model is to account for geometric and material nonlinearities, distinct material properties of concrete and rebar during heating phase, cooling phase and residual (after cool down) phase of analysis, and temperature induced bond degradation. Moreover, effect of post-fire residual deflections on residual capacity of fire exposed RC beams is also to be incorporated in analysis.
- Conduct full scale tests on RC beams by exposing them to different fire exposure scenarios and load levels, followed by incrementally loading them to failure after cool down; to evaluate residual capacity of fire exposed RC beams.
- Validate the developed numerical model utilizing data generated from fire resistance tests, and also other data available in literature. For instance, measured cross sectional temperature, vertical deflections, post-fire residual deflection and residual load carrying capacity are to be validated with predictions from the developed finite element model.

- Conduct parametric studies using the validated model to quantify the influence of various critical parameters affecting the residual capacity of fire exposed RC beams.
 The varying parameters include fire severity, load level, restraint conditions and crosssectional dimensions of the beam.
- Develop rational guidance for assessing residual response of fire damaged concrete beams (based on the results obtained from fire tests and parametric studies) for realistic evaluation of residual capacity of fire exposed RC beams.

1.5 Layout of thesis

The research, undertaken to address the above objectives, is presented in seven chapters. Chapter 1 provides a general background to residual response of RC beams following fire exposure and lays out the objectives of the study. Chapter 2 summarizes a state-of-the-art review undertaken on the residual response of fire damaged RC beams. The review includes summary of reported experimental and analytical (numerical) studies, as well as reported approaches focused on evaluating residual response of RC beams following fire exposure, together with various properties of concrete and rebar in heating, cooling, and residual phases.

Chapter 3 presents fire resistance and residual capacity tests on two high strength (HSC) and four normal strength (NSC) concrete beams under varying fire exposure scenarios, and loading (stress) conditions. Data from these residual capacity tests is used to discuss comparative response of RC beams under these conditions. Chapter 4 describes a novel three stage approach to evaluate residual response of RC beams following fire exposure. The proposed approach is implemented in ABAQUS through a three-dimensional finite element based numerical model for predicting response of RC beams during pre-fire, during fire, and post-fire (residual) stages. Predictions from

the analysis are validated against relevant response parameters measured during fire tests and residual capacity tests.

Chapter 5 presents results from a parametric study on the influence of critical parameters on residual response of fire damaged RC beams. A detailed discussion on the trends along with the ranges of parameters governing the residual response of RC beams following fire exposure is also presented. In Chapter 6, rational guidelines for assessing fire damaged concrete structures, and simplified expressions for predicting residual capacity of fire damaged concrete beams are proposed. Results from the residual capacity tests conducted as a part of this research, and those available in published literature are utilized to verify the proposed simplified approach for evaluating residual response of fire damaged RC beams. Finally, Chapter 7 summarizes the main findings arising from the current study and lays out recommendations for future research.

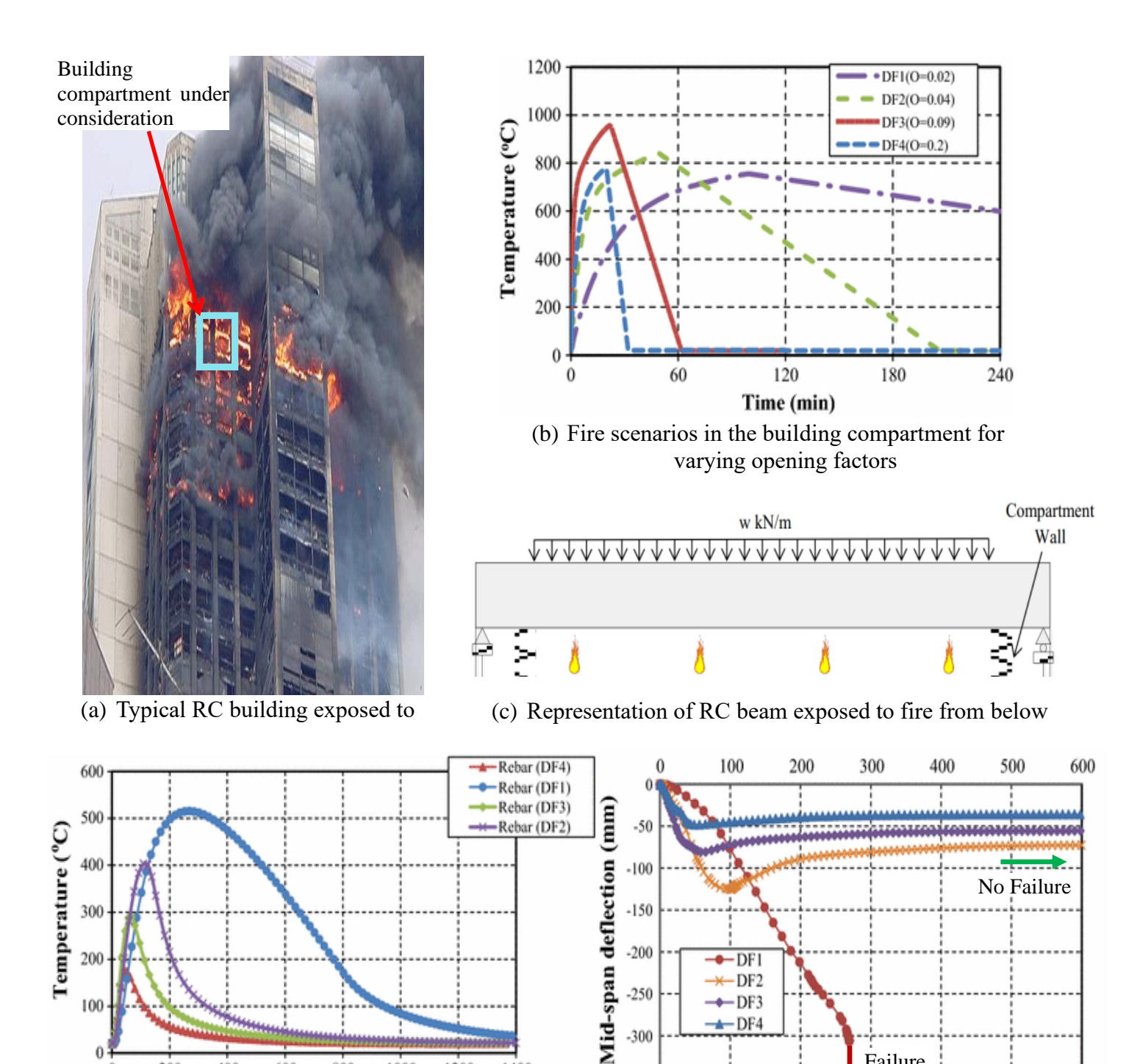


Figure 1-1. Thermal and structural response of a typical RC beam subject to varying fire scenarios in a building compartment

1000

1200

1400

-350

200

600

800

(d) Corner tension rebar temperature in beam

under different scenarios

Fire exposure time (min)

Failure

Fire exposure time (min)

(e) Mid-span deflections in RC beam

under different fire scenarios

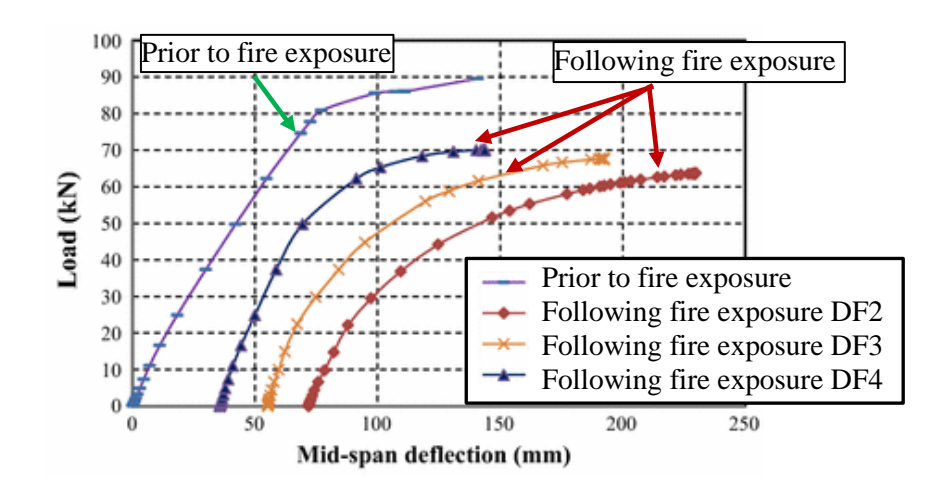


Figure 1-2. Comparison of residual load-deflection response of the fire exposed RC beams and undamaged RC beam

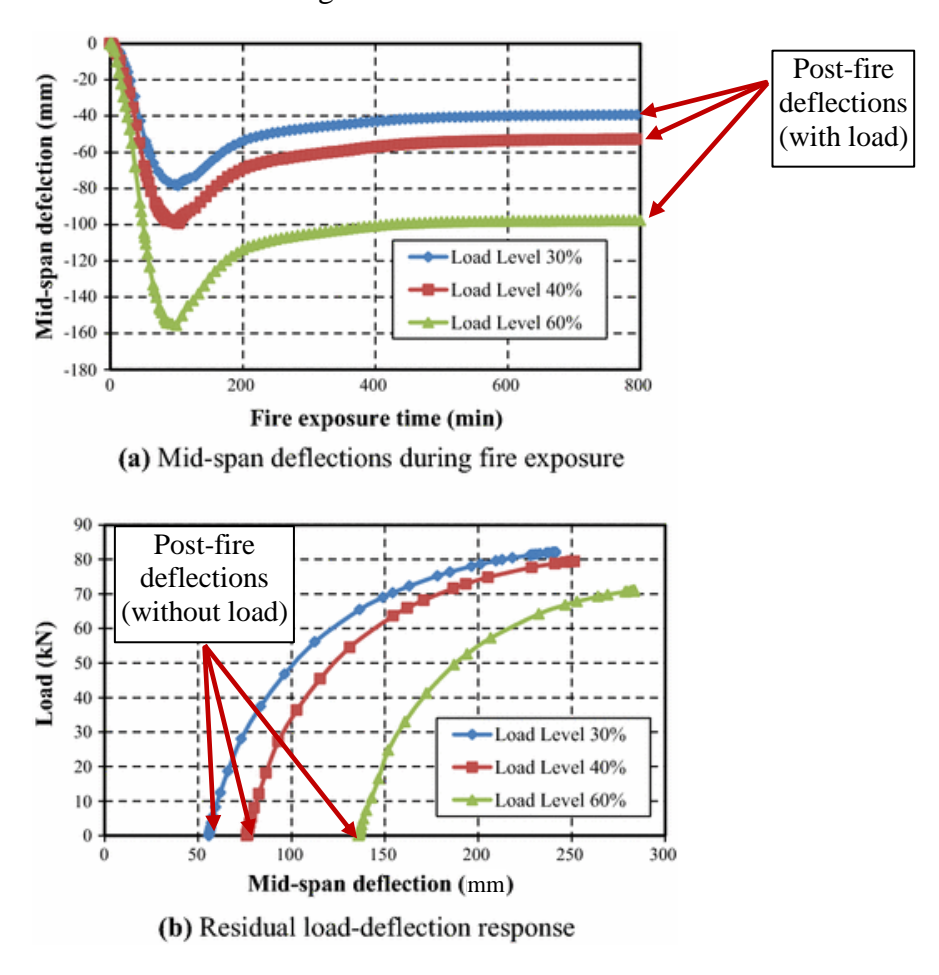


Figure 1-3. Effect of load level on response of RC beam during and after fire exposure

2 STATE-OF-THE-ART REVIEW

2.1 General

The extent of damage to concrete beams due to fire exposure is influenced by conditions existing just prior to the fire incident, as well as during complete fire exposure duration, including extended cooling phase when cross-sectional temperatures and deflections in the fire exposed member reverts back to ambient conditions. Furthermore, depending on severity of fire exposure, such RC flexural members (beams) may undergo varying levels of temperature induced damage, and there is uncertainty regarding extent of load bearing capacity retained in RC members after fire exposure (Kodur et al. 2014; Kodur and Agrawal 2016a, 2016b; Van Coile 2015). Therefore, it is imperative to assess if sufficient residual capacity exists in RC members prior to re-occupancy after the fire incident. Such an assessment also enables development of needed retrofitting (repair) measures. In the last four decades, significant number of experimental and numerical studies have been carried out to develop approaches for evaluating residual capacity of fire exposed RC beams. Majority of the tests employed standard heating regimes which do not represent realistic fire scenarios for simulating fire damage in the beams, prior to evaluating residual capacity. Current approaches relying on local material (concrete or steel) level testing (Alonso 2009; Awoyera and Akinwumi 2014; Gosain et al. 2008) of fire damaged members may not provide a reliable estimate of global structural damage. Previous structural level experimental approaches (Choi et al. 2013; El-Hawary et al. 1996; Kodur et al. 2010b; Kumar and Kumar 2003a; Thongchom et al. 2019; Xu et al. 2012) did not monitor conditions present during extended cooling phase of the member, including post-fire residual deflections, which significantly impact post-fire residual response (Kodur and Agrawal 2016a, 2016b). The effect of cooling phase of fire exposure, and load level

present in the member prior to fire exposure, on residual capacity were not considered explicitly in majority of the previous studies. This section presents the state-of-the-art review on evaluating residual capacity of fire exposed RC beams. Main experimental studies from literature are reviewed first, and then notable analytical (numerical) studies are discussed. In addition, current state of knowledge on high temperature material properties of concrete and rebar, and temperature induced bond degradation are reviewed as well.

2.2 Experimental studies on fire exposed RC beams

One approach to evaluate residual capacity of RC members is through full scale fire resistance tests, followed by residual capacity tests. There are relatively limited full scale tests to evaluate residual capacity of RC beams following fire exposure reported in literature (Choi et al. 2013; El-Hawary and Ragab 1996; Kodur et al. 2010a; Kumar and Kumar 2003a), as compared to studies investigated behavior of RC beams under fire (Abrams et al. 1976; Dwaikat and Kodur 2009b; Ellingwood and Lin 1991; Ellingwood and Shaver 1979; Kodur et al. 2007; Shi et al. 2004; Wu et al. 1993). These limited experimental studies available in literature have been reviewed in detail and discussed below briefly. Further, measured response parameters during fire tests and residual capacity tests in some of these studies are shown Figure 2-1.

Early research by Hawary et al. (El-Hawary and Ragab 1996) focused on evaluating residual capacity of RC beams after subjecting them to a constant elevated temperature for increasing durations. Three full scale beams having identical dimensions and reinforcement details were sustained at 650°C for 30, 60, and 120 minutes, respectively before being tested for residual capacity. As expected, a significant reduction in residual capacity proportional to the duration of heat exposure was measured with respect to the control (undamaged) beam. The residual capacity

in the tested beams varied between 61% to 88% of their room temperature capacity. Typical fire exposure and measured residual load-deflection response in these tests is shown in Figure 2-1a. No load was applied on the beams during heat exposure in these tests. Also, the fire scenario applied during tests was not realistic and did not have a distinct cooling phase. Further, residual deflections were not reported, and the residual capacity was evaluated using load-controlled testing procedure. Nonetheless, these experiments indicated an increase in ductility of the beams arising from thermal damage.

Kumar and Kumar (Kumar and Kumar 2003a) also tested five RC beams for residual capacity after fire exposure. These beams measuring at 3.96 m in span, were significantly longer than previously tested beams and were exposed to ISO 834 (ISO 834-1 1999) standard fire for 1 h, 1.5 h, 2 h and 2.5 h duration, respectively. Results indicated significant fire (temperature) induced damage and rise in mid-span deflections even when no load was applied during fire exposure, arising from thermal gradients experienced in the member during transient heating. In fact, one of the beams heated for 2.5 hours under ISO 834 standard fire was deemed to have failed during heating due to excessive deflection and could not be tested for residual capacity. Beams that did not fail during fire exposure retained 50% to 83% of their capacity relative to undamaged control beams. Similar to previous tests, these tests did not capture realistic fire damage as no load was applied on the tested beams during fire exposure. Also, the thermal and structural cooling behavior of the beams was not recorded. In addition, post-peak response of the fire damaged beams could not be captured accurately during these tests. Furthermore, the compressive strength of concrete utilized to fabricate these beams was extremely low (only 17 MPa), which is not representative of either NSC or HSC used in majority of modern concrete construction.

Kodur et al. (Kodur et al. 2010a) tested three RC beams for residual capacity after being exposed to design fire exposures with a decay phase. One of these beams was made of normal strength concrete (NSC), having average compressive strength 55 MPa, while the other two beams were made of high strength concrete (HSC) having average compressive strength 105 MPa. The beams were exposed to short design fire or long design fire under load to simulate realistic thermal and structural conditions. Based on the results of this study, the authors conclude that RC beams retain significant flexural capacity, after exposure to fire, especially when the temperature in reinforcing steel remains below 500°C. All beams retained significant residual capacity comparable to their room temperature design capacity due to reserve capacity in the beam prior to fire exposure from strain hardening and tension stiffening effects. Fire exposure scenarios adopted in these experiments, and subsequent residual load-deflection response is shown in Figure 2-1b. Unlike previous tests, these tests captured critical parameters governing residual capacity of fire damaged concrete beams. However, cooling phase conditions and their impact on residual capacity were not studied in these tests. Further, a load-controlled procedure was utilized to conduct residual capacity tests which may not capture post-peak response of the member with reliable accuracy. Choi et al. (Choi et al. 2013) tested eight beams to investigate the effect of effect of concrete strength, cover thickness, and heating period on the residual capacity of reinforced concrete beams. All beams were subject to fire exposure as per ISO 834 standard fire under sustained flexural loading to study effect of varying critical parameters on residual capacity. The authors concluded that beams fabricated using higher concrete compressive strength were susceptible to greater fire damage resulting from temperature induced damage (see Figure 2-1c). Also, concrete cover played a crucial role in restricting temperature ingress in tensile rebar, and hence impacted residual

capacity. Majority of the tested beams retained at least 80% of their room temperature capacity

even after undergoing significant fire damage. However, these tests had similar shortcomings as majority of the previous tests. Compressive strength of concrete used to fabricate tested beams was relatively low, measuring only 55 MPa, and the results are not applicable to HSC which has minimum compressive strength of 60 MPa. Furthermore, cooling phase response and post-fire residual deflections were not studied in these tests.

A more recent study by Thongchom et al. (Thongchom et al. 2019), investigated the effect of sustained service loading on residual flexural response of RC T-beams after exposed to elevated temperatures. Beams were heated to a constant elevated temperature, with and without sustained loads and then tested for flexural capacity. Test results clearly established reduction in residual capacity when the beams were subject to sustained loading prior to and during fire exposure. Nonetheless, these tests failed to capture effect of sustained loading during extended cooling phase of the member on post-fire residual deflections, and residual capacity. Moreover, the beams tested in this study were fabricated using concrete having maximum compressive strength of 43 MPa and results cannot be extrapolated to HSC members.

The above critical review highlights key knowledge gaps that exist in existing literature on tests to evaluate residual capacity of fire damaged RC beams. While these tests report that significant residual capacity is retained in RC beams after exposure to fire, the extent of recovery can vary widely depending on testing conditions. A major shortcoming of most of previous tests is that both the fire exposure scenarios and loading conditions did not represent realistic conditions possible in a typical building compartment. In addition, temperature and deflection history during fire exposure was not reported in majority of the studies, which is critical for establishing post-fire response of the beam. Most studies did not consider the impact of cooling phase of fire exposure, extended cooldown of the member and post-fire residual deflection on residual capacity.

Additionally, most of the previous studies did not study the influence of increasing load level and compressive strength (type of concrete i.e. NSC or HSC) on residual capacity of fire damaged concrete beams. Therefore, a detailed test program is needed tests to evaluate residual response of RC beams after exposure to realistic fire exposure and load (stress) level as experienced in a typical building compartment. Experimental data generated through such tests is critical for developing rational approaches to evaluate residual capacity after realistic compartment fires, and detailed validation of numerical models. Such a test program needs to explicitly consider cooling phase conditions of fire exposure and the member, post-fire residual deflections, compressive strength of concrete as well as load level present prior to and during fire exposure.

2.3 Numerical studies

Full-scale fire (and residual) tests are expensive and time consuming and thus, allow for limited number of parameters to be studied. Hence, numerical simulations can serve as a powerful alternative to fire tests at a fraction of the cost and time. Moreover, with numerical modelling, there are no limitations on the parameters that can be accounted for, in order to better understand the behavior of a structure.

Researchers have proposed numerical approaches for evaluating residual capacity of RC beams following fire exposure in the past (Bai and Wang 2011; Hsu and Lin 2008; Kodur et al. 2010a; Krešimir et al. 2016; Lakhani et al. 2014; Ožbolt et al. 2014; Thongchom et al. 2019). These approaches can be broadly categorized into two types, namely, simplified cross-sectional analysis and detailed finite element analysis. As part of simplified approach, room-temperature strength equations were applied for evaluating residual capacity, taking into consideration strength reduction factors based on high temperature exposure.

Hsu and Lin (Hsu and Lin 2008) proposed a simplified sectional approach to evaluate residual capacity of fire exposed RC beams. This approach involves dividing critical cross section into a number of strips and then calculating temperatures along each strip through a finite difference approach. Knowing temperatures across the cross section and strength-temperature relations of reinforcing steel and concrete, residual capacity of the fire exposed concrete beam was evaluated through a strain compatibility analysis. The authors concluded that this approach could capture temperature induced degradation in stiffness, shear capacity, and flexural capacity of fire exposed beams. Their results revealed that strength and stiffness properties of fire damaged beams deteriorate at different rates with increasing level of fire exposure. However, predictions by this approach were conservative when beams were exposed to relatively longer heating durations. Also, this approach assumed no cracking in the cross section and did not account for realistic structural and thermal (fire) conditions in evaluating residual capacity.

Kodur et al. (Kodur et al. 2010a) presented a simplified approach for evaluating residual capacity of flexural members based on peak rebar temperatures experienced during a fire. Peak rebar temperature was identified as the key parameter in ascertaining the level of damage sustained to the beam during fire exposure. As part of this method, an empirical equation was proposed for predicting maximum rebar temperatures under a specified parametric fire exposure. Once maximum temperatures attained in the rebar are calculated, residual capacity was computed using room-temperature strength design equations (Lakhani et al. 2014), but utilizing temperature dependent residual yield of reinforcing steel. Also, the width of the concrete cross section was reduced to account for temperature induced degradation in concrete properties. Predictions by this approach were found to be conservative as it accounted for cooling phase of fire exposure in calculating peak rebar temperature. Nonetheless, this approach did not capture sequential

deterioration in properties of concrete and reinforcing steel experienced during heating, cooling and residual phases. Moreover, effect of load level and post-fire residual deflections could not be accounted for in evaluating residual capacity through this approach.

Bai and Wang (Bai and Wang 2011), developed an hybrid approach employing finite element modeling using ANSYS software (ANSYS 2007), and subsequent cross sectional analysis. A two-dimensional thermal analysis was conducted using ANSYS (ANSYS 2007) software to determine peak cross-sectional temperatures in the fire exposed member. Subsequently, a fictitious reduced (effective) cross-sectional area is considered based on peak temperatures to calculate residual capacity. Based on a parametric study conducted using this approach, the authors inferred that increasing concrete or steel strength at room temperature has negligible influence on the rate of degradation in moment capacity due to fire exposure. Although this approach utilized advanced finite element software but lacked needed sophistication for incorporating effect of cooling phase and residual deflections in evaluating residual capacity. Also, the effect of varying load level or support conditions cannot be studied using this approach.

Lakhani et al. (Lakhani et al. 2014) proposed a simplified moment-curvature based approached to evaluate load-deflection response of fire damaged RC members. As per this approach, sectional temperatures were calculated for the entire duration of fire exposure using finite difference method. Subsequently, the residual capacity is calculated based on a moment-curvature analysis using temperature dependent residual mechanical properties of concrete and reinforcing steel. This approach could predict the yielding and ultimate residual load carrying capacity of fire damaged concrete beams. However, this approach did not consider distinct material properties during cooling phase of analysis. Further, it did not account for impact of residual deflections on residual capacity of fire damaged concrete members.

In the second type of approach, few researchers applied finite element models to trace the post-fire response of RC beams (Krešimir et al. 2016; Ožbolt et al. 2014; Thongchom et al. 2019). Ožbolt et al. (Ožbolt et al. 2014) proposed a transient three dimensional thermo-mechanical finite element model to simulate the behavior of RC beams exposed to elevated temperatures. The model was validated by comparing predictions against test data generated from post-fire residual strength tests (Kumar and Kumar 2003a). The load-carrying capacity and the initial stiffness of the beam reduced with the increase in duration of fire exposure. Moreover, results showed that on cooldown of the beam to room temperature; additional damage resulted in the beam due to thermally induced strains, as shown in Figure 2-2a. However, the analysis results deviated substantially from test data especially for beams that were heated for longer durations, as can be seen in results reported by the authors shown in Figure 2-2b. This is partly because the model does not account for distinct material properties during heating and cooling (decay) phases of fire. Moreover, the primary focus of the study was to study behavior of RC beams at elevated temperature rather than evaluation of post-fire residual capacity of RC beams.

Krešimir et al. (Krešimir et al. 2016) developed a numerical model for fire exposed concrete beams using a macroscopic space analysis developed for three-dimensional non-linear analysis of quasifragile materials, such as concrete. The developed model was applied to study different reinforcement configurations with varying levels of overlap in the tension region. Results indicated a significant degradation in load bearing capacities of the analyzed beams due to fire exposure. In addition, the configuration of reinforcement had significant impact on the ductility of the beams at failure, with greater overlapping resulting in significantly greater ductility. The authors highlighted the lack of comprehensive test data for detailed validation of the developed model.

Furthermore, distinct material properties during heating, cooling, and residual phases of analysis, as well as the impact of post-fire residual deflections were not incorporated in this model.

Thongchom et al. (Thongchom et al. 2019) developed a simplified three-dimensional numerical model using ANSYS finite element software (ANSYS 2007) to predict residual capacity of fire damaged T-beams. The model predicted distinct reduction in load carrying capacity for varying severity of fire (temperature) exposure. However, the developed model could not capture the effect of varying service load conditions due to simplifying assumptions made during analysis. The authors indicate that this model could only be applied to cases with low sustained service loads during fire exposure. Furthermore, reduction in compressive strength during cooling and subsequent post-fire residual conditions was not considered in analysis. Further, the impact of post-fire residual deflections and service loading during fire exposure on residual capacity of fire exposed beams could not be studied during the developed numerical model.

The above review illustrates that limited analytical studies were conducted to evaluate residual capacity of fire exposed RC beams. Most simplified cross-sectional approaches proposed in previous literature rely solely on heating phase of fire exposure to calculate temperature induced degradation in mechanical properties of concrete and reinforcing steel. However, such properties are not representative of those observed (residual mechanical properties) after cooldown following fire exposure. While concrete continues to display some level of strength loss even after cooling down, reinforcing steel regains partial yield strength depending on peak rebar temperatures. Further, the developed numerical models had several limitations and drawbacks, as they do not account for important factors namely distinct material properties during heating, cooling and residual phases, pre-fire loading and support conditions, temperature induced bond degradation,

and residual deflections. Thus, a reliable finite element based numerical model capable of incorporating key parameters needs to be developed.

2.4 Material properties during heating, cooling, and residual phases

Residual response of concrete members is governed by temperature induced degradation in material properties of constituent materials, namely, concrete and rebar, as well as the interfacial bond between them. Majority of the existing data on temperature dependent material properties of concrete and rebar is based on standard fire exposure wherein temperature increases continuously over time. Limited data exists on thermal properties, mechanical properties, deformation characteristics, and material specific properties such as temperature induced bond degradation during cooling (decay) phase of fire exposure, and post-fire residual conditions following complete cooldown. Although cooling and residual phase material properties of concrete and reinforcing steel are not well understood, reasonable assumptions based on heating phase material behavior can be made to capture residual response accurately. Specifically, many of the material properties are irreversible once high temperatures have been reached and therefore changes should not be considered to recover to their original room temperature values upon cooldown. Further, assumptions made based on elevated (hot) temperature behavior, along with limited experimental data on residual and cooling phase properties can be reasonably applied to develop distinct material property relations for different phases of fire exposure. These material properties include both thermal and mechanical properties of concrete and reinforcing steel.

Thermal properties of concrete and rebar during heating and cooling phases of fire exposure govern the temperatures experienced within the cross-section of the concrete member. These include thermal conductivity, and specific heat of constituent materials. These temperatures dictate the extent of deterioration in mechanical (strength and stiffness) properties experienced in the member during and after fire (residual conditions). Subsequently, deformation properties comprising of thermal expansion, creep, transient strain, and post-fire residual displacement (strain) which are a function of both temperature and stress conditions present prior to and during fire exposure influence response of concrete members exposed to fire. Notable residual deflections that exist in fire damaged concrete members primarily arise from irrecoverable deterioration in mechanical and deformation properties of concrete and hence impact their residual capacity.

Besides thermal, mechanical, and deformation properties, temperature induced degradation of the interfacial bond between them can influence residual response of RC members following fire exposure. In case of RC beams, wherein interfacial bond between concrete and rebar is critical in facilitating tensile stress transfer from concrete to rebar, significant reduction in post-fire residual stiffness or moment capacity may occur resulting from temperature induced bond degradation.

All the aforementioned properties vary as a function of temperature and stress as well as susceptible to changes in composition of concrete (e.g. moisture content, density, and type of aggregate). A clear understanding of these properties is critical for tracing residual response of fire damaged concrete structures. This section provides a review on temperature dependent properties of concrete and rebar during elevated (hot) conditions, cooling phase (after attaining peak temperatures) and post-fire residual conditions after complete cooldown. In addition to temperature dependent material properties of concrete and rebar, studies on temperature induced

2.4.1 Concrete properties

bond degradation are also reviewed here.

Concrete is a heterogeneous material comprising of cement paste, and aggregate with each component having different behavior at high temperatures. In addition, distinct chemo-physical changes in concrete give rise to distinct material properties during heating phase, cooling phase

and post-fire residual conditions. Thermal and mechanical properties of concrete during heating phase are relatively well established through comprehensive studies conducted by researchers in the past (Cheng Fu-Ping et al. 2004; Gawin et al. 2004; Khaliq and Kodur 2011; Kodur 2014; Li and Purkiss 2005; Shin et al. 2002; Youssef and Moftah 2007). In addition, constitutive relations for calculating material properties of concrete at elevated temperature are specified in codes namely, the Eurocode 2 (EN 1992-1-2 2004) and ASCE manual of practice (ASCE manual No. 78 1992). It should also be noted that while these material property relations are well established for normal strength concrete (NSC) with compressive strengths ranging from 40-50 MPa, there are relatively fewer material property models available for high strength concrete (HSC) having compressive strength greater than 70 MPa. In particular, the temperature dependent property models for concrete specified in the ASCE model (ASCE manual No. 78 1992) are primarily applicable to NSC, while Eurocode (EN 1992-1-2 2004) model is valid for both NSC and HSC. Accordingly, the Eurocode (EN 1992-1-2 2004) models that were adopted as part of this study are discussed in greater detail.

Concrete also exhibits distinct material properties during cooling phase, as the member cools down to ambient conditions, and post-fire residual conditions. Properties of concrete during cooling and residual phases were studied in the past but there is a large variation in reported results as they are sensitive to both composition of the concrete, and testing conditions. Thus, there is limited guidance on developing temperature dependent material property relations for concrete during cooling and residual phases. Nonetheless, depending on the magnitude of temperature experienced during heating phase and the type of property under consideration, concrete can experience partial recovery, no recovery or further deterioration during cooling and residual phases. Thus, given the temperature dependent relation for heating phase and extent of recovery (or further deterioration),

during and after cooldown, distinct material properties during cooling and residual phases can be estimated with reasonable accuracy. Key aspects of thermal, mechanical, and deformation properties of concrete as seen during heating, cooling and residual conditions that influence response of fire damaged concrete structures are reviewed in this section.

2.4.1.1 Thermal properties

Thermal properties during heating phase

Thermal conductivity, specific heat, and density of concrete govern temperature experienced within the concrete cross section. These properties display monotonic trends during heating phase of fire exposure, as illustrated in Figure 2-3, and were studied extensively in the past (Harmathy 1970; Khan 2002; Khoury et al. 2002; Kodur V. K. R. and Sultan M. A. 2003). Test data from these studies was used to develop empirical relations, such as those specified in Eurocode 2 (EN 1992-1-2 2004), and ASCE Manual of Practice (ASCE manual No. 78 1992), for calculating these properties as functions of elevated temperature.

The thermal conductivity, specific heat and density are expressed as a function of temperature for concrete in Eurocode 2 (EN 1992-1-2 2004), are plotted in, Figure 2-4, Figure 2-5, and Figure 2-6 respectively. It can be seen from Figure 2-4, Figure 2-5, and Figure 2-6 that temperature has significant effect on the thermal properties of concrete. Rather than specifying distinct relations for different types of concrete, Eurocode model conservatively defines lower and upper bounds for thermal conductivity of concrete as a function of temperature due to significant variation seen in test data. Similarly, temperature dependent specific heat of concrete as per Eurocode model conservatively assumes the same (lower bound) heat capacity models for both siliceous and carbonate aggregate concrete, and ignores significant increase in specific heat seen in carbonate aggregate concrete in the temperature range 600-800°C. Further, variation in specific heat with

varying moisture content is explicitly accounted for in specific heat calculations as per Eurocode 2 (EN 1992-1-2 2004), and is shown in Figure 2-5. Unlike thermal conductivity and specific heat, density of concrete is difficult to estimate as functions of temperature. Moreover, in limited test programs conducted in the past, test conditions, heating rate and other crucial parameters were not well reported and hence is not well established in literature. Nonetheless, Eurocode defines a linear decrease in density with increasing temperature as shown in Figure 2-4.

While current constitutive relations may not fully represent complex relationship between thermal properties and temperature, these empirical relations have been successfully utilized in a range of numerical and analytical studies to trace thermal response of concrete members exposed to monotonic heating (fire without cooling phase) with reasonable accuracy.

Thermal properties during cooling and residual phases

Thermal conductivity, specific heat and density of concrete undergo irreversible deterioration due to heating, and do not recover their original room temperature values during cooling and residual phases, as shown schematically in Figure 2-1. This can be primarily attributed to loss of capillary and chemically bonded water once temperatures in concrete exceed boiling point of water (~ 100°C), and this moisture is entrained to the external environment through compartment openings and flow of combustion products. This water is thus not available and does not re-enter in the material during cooling and, furthermore, part of the water that is released during heating was chemically bound and the physio-chemical reactions that liberate the molecules of water are not reversible resulting in irreversible changes in thermal properties of concrete during cooling phase. The thermal conductivity of concrete decreases with increasing temperature, and this reduction is also associated with the loss of moisture during heating (Khan 2002; Kodur 2014). Therefore, thermal conductivity of concrete is not reversible upon cooldown, and remains constant

corresponding to the peak temperature experienced during heating. Similarly, specific heat of concrete which sees a significant increase due to energy consumed during evaporation of water, does not experience recovery during cooling phase and residual conditions. Specific heat of concrete is constant depending on maximum temperature experienced in concrete during heating. Furthermore, during residual conditions, concrete hydrates partially once fire temperatures subside to room temperature conditions. Finally, the reduction in density of concrete is also irreversible and remains constant during cooling phase of fire exposure, and increases marginally during residual conditions due to re-hydration. It should be noted that thermal properties during residual conditions are not crucial for determining residual response of fire damaged concrete members, but may be relevant for subsequent retrofitting and repair measures. Thus, temperature dependent relations for thermal conductivity, specific heat, and density during heating phase can be adopted for cooling, and residual phases but with no recovery, as illustrated in Figure 2-1.

2.4.1.2 Mechanical properties

Mechanical properties during heating phase

Mechanical properties of concrete include compressive strength, tensile strength, and elastic modulus that influence strength and stiffness properties of concrete members during and after fire exposure. As compared to thermal properties, mechanical properties were studied more extensively as functions of temperature. Similar to thermal properties, mechanical properties of concrete deteriorate as temperatures increase monotonically during heating phase of fire exposure, as illustrated in Figure 2-7. Significant amount of test data is available for temperature dependent mechanical properties of both NSC and HSC fabricated using different types of aggregates.

Figure 2-8 and Figure 2-9 show the variation of concrete compressive strength with temperature for NSC and HSC, respectively. Figure 2-8 shows a large but uniform variation of the compiled

test data for NSC throughout the temperature range. However, Figure 2-9 shows a larger variation in the compressive strength with temperature for SC in the range 200°C to 500°C, and less variation above 500°C. This is mainly because fewer test data points were reported for temperatures higher than 500°C either due to the occurrence of spalling or due to limitations in the test apparatus. However, a wider variation is observed for NSC in this temperature range (above 500°C) when compared to HSC as seen from Figures 2-8 and Figure 2-9. This is mainly because of the higher number of test data points reported for NSC in the literature and also due to the lower tendency of NSC to spall under fire. The variations in the mechanical properties of concrete at high temperatures are quite high. These variations from different tests can be attributed to using different heating or loading rates, specimen curing, condition at testing (moisture content and age of specimen), and the use of admixtures.

Researchers have proposed different constitutive models for high temperature mechanical properties of concrete based on measured data from high temperature mechanical property tests. The most widely used constitutive models present in the Eurocode 2 (EN 1992-1-2 2004), ASCE Manual of Practice (ASCE manual No. 78 1992). These relations give the rate of degradation of concrete as a function of temperature only, and without any consideration to variations in other significant parameters such as rate of loading, heating, and material composition. While there is significant variation in reported test data, Eurocode 2 curve for both NSC and HSC provides a conservative lower bound estimate of temperature dependent reduction in compressive strength of concrete, as shown in Figure 2-8 and Figure 2-9. Consequently, Eurocode constitutive model is shown to produce reasonably accurate results for tracing structural response of fire exposed concrete members in a number of studies (Gao et al. 2013; Gernay 2019; Kodur and Agrawal 2016a, 2016b).

Tensile strength of concrete also undergoes deterioration as a consequence of increase in temperatures as experienced during heating phase of fire exposure. While there are relatively fewer studies on tensile behavior of concrete at elevated temperature, as compared to compressive strength, it is generally accepted that rate of degradation in tensile strength is significantly more rapid as compared to compressive strength, especially for temperatures less than 400°C. Also, the original room temperature strength of concrete does not appear to have a significant effect on the normalized tensile strength after heating to various temperatures. Degradation in tensile strength of concrete typically follows a linear trend for temperatures exceeding 400°C. Eurocode 2 recommends a linear decrease in tensile strength for temperatures exceeding 100°C. Deterioration in tensile strength of concrete as a function of temperature as reported in previous studies (Chang et al. 2006; EN 1992-1-2 2004; Harada et al. 1972; Park and Yim 2017) is plotted in Figure 2-10. The elastic modulus of concrete also undergo temperature induced degradation upon heating. The elastic modulus of heated concrete in compression is calculated by taking the secant modulus at 30% of the peak stress from compressive stress-strain relation of the concrete. As shown in Figure 2-11, the rate of reduction in elastic modulus with temperature is greater than that in the compressive strength. In addition, rate of temperature induced deterioration in elastic modulus is independent of compressive strength of concrete (Chang et al. 2006).

Mechanical properties during cooling phase

Studies on behavior of fire damaged concrete in the past (Chang et al. 2006; Li and Franssen 2011; Nassif 2006; Poon et al. 2001a) indicate that compressive strength, tensile strength, and elastic modulus do not recover to their initial room temperature values as temperature in concrete begins to diminish. Figure 2-7 illustrates this lack of recovery in mechanical properties of concrete typically experienced during cooling phase of fire exposure. The irreversible degradation in

mechanical properties of concrete can be mainly attributed to loss of chemically bonded water (moisture) present in the concrete matrix. Eurocode 4 (EN-1994-1-2 2008) guidelines recommend that cooling phase mechanical properties can be interpolated between elevated and residual properties (after cooldown).

Consideration of distinct material properties during cooling phase of fire exposure was highlighted relatively recently, especially for axially loaded members subjected to fires with a distinct cooling phase. Recent research based on numerical simulations have highlighted the possibility of collapse of reinforced concrete columns during or even after the cooling phase of a fire and one of the main mechanisms that lead to this type of failure is the additional loss of concrete strength during the cooling phase of the fire (Annerel and Taerwe 2011). The effect of cooling phase properties on response of flexural members is relatively less pronounced (Lu et al. 2015a). Thus, mechanical properties of concrete during cooling phase of fire exposure can be linearly interpolated between heating phase and residual properties.

Mechanical properties during residual conditions

Residual mechanical properties of concrete are primarily influenced by maximum temperatures experienced during the fire and time allowed for recovery after fire, as shown in Figure 2-12 and Figure 2-13. In fact, mechanical properties of concrete can undergo additional deterioration even after cooling down to room temperature as illustrated in Figure 2-7. The residual compressive strength of concrete experiencing temperatures of 220 °C or higher can decrease up to 20% of its elevated or hot-temperature strength in weeks following cooling down (Annerel and Taerwe 2011). More recent investigations suggest that the 'short term' or 'temporary phase' wherein the compressive strength of concrete does not recover can last until three years after fire exposure (Elsanadedy 2019). According to Eurocode 2 (EN 1992-1-2 2004), an additional loss of 10% in

compressive strength is considered during cooling from maximum to ambient temperature. After this short-term phase, concrete may eventually exhibit noticeable recovery in compressive strength. This is referred to as the 'long term' response of RC structures after fire exposure. With sufficient recovery time (more than 6 months) at room temperature, concrete may regain almost 90% of its original room-temperature compressive strength when subject to appropriate post-fire curing conditions (Poon et al. 2001b). Nonetheless, very limited data exists on the long-term recovery of concrete and is highly sensitive to post-fire storage temperature and moisture conditions which can vary greatly on a case to case basis. Thus, long-term recovery in post-fire mechanical properties of concrete, especially compressive strength can be ignored conservatively while evaluating residual capacity of fire damaged concrete members.

Also, the residual compressive strength of concrete can be utilized to estimate the corresponding reduction in tensile strength, and elastic modulus during post-cooling storage. Thus, mechanical properties of concrete during residual phase can be calculated by considering no recovery during cooling phase, and additional reduction on top of pre-existing deterioration during heating phase of fire exposure (Gernay 2019).

2.4.1.3 Deformation properties

Free thermal strain during heating phase

The coefficient of thermal expansion, which is defined as the change in a unit length of a material caused by a unit (degree) increase in temperature, is important as a measure of the structural movement and thermal stresses resulting from temperature changes (Harmathy 1970), particularly during monotonic heating.

Eurocode 2 (EN 1992-1-2 2004) provides two different models of thermal strain for carbonate and siliceous aggregate concrete; wherein siliceous aggregate concrete has higher rate of increase in

thermal strain. This variation of thermal strain of concrete with temperature fabricated using siliceous and carbonate aggregate as per Eurocode is plotted in Figure 2-14. At high temperatures (600°C to 800°C) most concretes no longer exhibit any expansion and contract in some cases, as shown in Figure 2-14.

Free thermal strain cooling phase and residual conditions

Free thermal strain of concrete exhibits partial recovery during cooling phase, as can be inferred from post-cooling (residual) thermal expansion (shrinkage) values plotted in Figure 2-14. Maximum temperature experienced during fire exposure governs the amount of recovery, and residual thermal strain experienced during cooling and residual phases of fire exposure respectively. Further, residual strains and hence thermal strains during cooling phase can be positive (residual elongation), or negative (residual shrinkage) after complete cooldown of the concrete as can be seen in Figure 2-14. The rather limited number of experimental results (Li and Franssen 2011; Schneider 1988b) on residual thermal deformation suggests that concrete thermal deformation can be considered as fully recoverable if the maximum temperature experienced is lower than 100°C. On the other hand, if the maximum temperature is in the range between 200°C and 400°C, minor residual shrinkage is to be expected. For greater peak temperature values, residual elongation is to be expected. As for the influence of the aggregate, concretes with siliceous aggregates exhibit larger residual thermal expansion than calcareous aggregate concretes. Results from the experiments performed by Li and Franssen (Li and Franssen 2011) suggest that the maximum temperature governs the amount of residual elongation, and that for maximum temperatures lower than 500°C, no significant residual elongation is to be expected. It is important to note that the magnitude of these thermal elongation (or shrinkage) strains during cooling phase and subsequent residual conditions is relatively smaller than those seen during heating phase.

Nonetheless, residual thermal strains (elongation or shrinkage) can influence extent of irrecoverable residual deflection experienced in concrete members.

Creep and transient strain during heating, cooling and residual phases

Creep is defined as the time-dependent plastic strain for a given stress level and temperature. Creep strain can be primarily attributed to movement of moisture in concrete and thus varies significantly with temperature induced moisture migration and degradation in as experienced during fire exposure. Elevated temperatures significantly accelerate the rate at which creep deformations occur in concrete (see Figure 2-15), resulting in significant deflections in concrete members. These strains also influence stress redistribution within the concrete cross-section, and hence play an important role in deflection progression during both heating, and cooling phases of fire exposure. In addition, these strains increase with increasing stress level (see Figure 2-16), and are irreversible in nature, and do not recover during cooling phase and subsequent residual conditions.

Besides creep strain due to moisture migration, concrete also experiences complex changes in moisture content and chemical composition of the cement paste. Further, there is a mismatch in thermal expansion between the cement paste and the aggregate. These changes in concrete during heating result in transient strain, which only occurs during the first time that concrete is heated under load, but not upon subsequent heating (Khoury et al. 1985), and is independent of time. Transient strain is essentially caused by the thermal incompatibilities between the aggregate and the cement paste (Khoury et al. 1985). During heating of concrete, there are Such mismatches lead to internal stresses and micro-cracking in the concrete constituents (aggregate and cement paste) and results in transient strain in the concrete (Khoury et al. 1985).

These transient strains occur during first-time heating of concrete under load, do not recover during cooling phase, and remain constant after cooldown (residual conditions) (Khoury et al. 1985).

Thus, adequate consideration to creep and transient strains is crucial for tracing response of concrete members during cooling phase, and residual conditions. It is important to note that Eurocode model for stress-strain response of concrete exposed to high temperature implicitly accounts for transient strains experienced during fire exposure. Thus, residual stress-strain relationship of concrete follows a similar trend as seen in elevated temperature stress-strain characteristics, as shown in Figure 2-17.

2.4.1.4 Reinforcing steel properties

The material properties of reinforcing steel that influence extent of fire damage in concrete members comprise of temperature dependent thermal properties, mechanical properties, and deformation properties. Unlike concrete, temperature dependent material properties of reinforcing steel are largely reversible, with some level of permanent deterioration in yield strength depending on peak temperatures experienced during fire. These aspects of temperature dependent material properties of reinforcing steel are reviewed further in this section.

2.4.1.5 Thermal properties

The thermal properties of reinforcing steel i.e. thermal conductivity and thermal capacity, depend on the type and temperature of the steel. Nonetheless, at higher temperatures as experienced during fire, the thermal properties of steel become more dependent on temperature and are less influenced by the steel composition (Kodur et al. 2010d). It can be seen in Figure 2-18 that thermal conductivity of steel decreases with temperature in an almost linear fashion. On the contrary, specific heat of steel varies considerably between 700°C and 800°C, as can be seen in Figure 2-19. In general, the specific heat of steel increases with an increase in temperature with a large spike occurring around 750°C. The spike in the specific heat at around 750°C is due to the phase change

that occurs in steel. There are minor variations in the models specified in design codes and standards for high-temperature thermal properties of steel.

It should be noted that the thermal conductivity of reinforcing steel is high in comparison with concrete and thus heat is distributed through steel rebars quite rapidly. In addition, steel reinforcement is embedded in concrete and is of very small area as compared to concrete. For these reasons, in fire resistance calculations steel reinforcement is generally assumed to be a perfect conductor, which implies that temperature is uniform within the steel area, and thus do not separately account for steel reinforcement in a thermal analysis. It has been shown that reinforcing steel has a small influence on the temperature distribution within the RC cross-section (Panedpojaman and Intarit 2016). Thus, thermal properties of reinforcing steel are not very important for predicting temperature distributions in RC members, during heating or cooling phase of fire exposure.

2.4.1.6 Mechanical properties

Mechanical properties of reinforcing steel include yield strength, ultimate strength and modulus of elasticity. These properties are generally represented by the stress-strain temperature relationships of steel. The literature review indicates that there is a large variation in the yield and ultimate strength of steel as illustrated through upper and lower bound values of test data in Figure 2-20. Some of this variation is due to the variation of steel composition and the lack of definition of the yield strength of steel (Neves et al. 1996a). The variation of yield strength of reinforcing steel as a function of temperature, specified in Eurocode 2 (EN 1992-1-2 2004) are also shown in Figure 2-20.

A review of the literature indicates that reinforcing steel recovers nearly all of its original yield strength upon cooling as long as heating temperatures do not exceed 500°C (Neves et al. 1996a;

Tao et al. 2013). However, for steel heated to temperatures above 500°C the residual strength starts to decrease gradually as shown in Figure 2-21. The behavior of reinforcing steel in the cooling phase (as a function of its residual properties) is crucial for modeling the response of RC structural members exposed to fire scenarios with a distinct cooling phase.

Deformation properties of reinforcing steel include thermal strain and creep strain. The thermal

2.4.1.7 Deformation properties

strain of reinforcing steel at elevated temperatures is directly related to the temperature rise and generally increases with temperature. Between 650-815°C thermal strain decreases, due to a phase transformation in the steel, before increasing again. The variation for the thermal strain as a function of temperature as per the Eurocode 2 (EN 1992-1-2 2004) is shown in Figure 2-22. Creep strain is the gradual increase in strain with time under a constant stress. Creep strain occurs due to the movement of dislocations in the slip plane (in the microstructure of steel). Normally, steel (metal) composition contains a variety of defects, for example solute atoms, that act as obstacles to dislocation movement. At room temperature, the amount and distribution of these defects remains almost uniform and thus creep strains occur at a very rate. However, at high temperatures, vacancies in the crystal structure can diffuse to the locations of a dislocation and cause the dislocations to move faster to an adjacent slip plane thereby allowing further deformation to occur. Thus, creep strain becomes significant at elevated temperatures, particularly above 450°C, and should be included in modeling the fire response of RC members. A review of the literature indicated that there is very little information on high temperature creep strain of reinforcing steel. The available creep models, such as the one proposed by Harmathy (Harmathy 1967), are based on Dorn's theory, which relates the creep strain to the temperature, stress, and time. Furthermore, Eurocode 2 (EN 1992-1-2 2004) model implicitly accounts for high

temperature creep in calculating temperature dependent stress-strain relations of reinforcing steel. These irreversible creep strains in reinforcing steel are a primary cause of post-fire residual deflections in concrete members, especially in case of tensile reinforcement in flexural members exposed to fire from below (Kodur and Agrawal 2016a, 2016b). Typical stress-strain relations of reinforcing steel after exposure to elevated temperature are shown in Figure 2-23.

2.4.1.8 Temperature induced bond degradation

Reinforced concrete is essentially a composite structural material that derives its utility from the combination of two materials i.e. concrete which is strong in compression, and steel that is strong in tension. Sustaining this composite action throughout the life of a structure necessitates effective stress transfer between steel and concrete. The mechanism facilitating this stress transfer is usually referred to as bond and is represented by a continuous stress field around the concrete-rebar interface. When an RC member is subjected to moderate loading (stress), the slip between reinforcing steel and concrete is minimal. However, under high loading (stress) conditions, local bond strength may be lower than the demand resulting in localized damage and significant movement between reinforcing steel and surrounding concrete. At elevated temperatures, the evolution of stresses at the rebar-concrete interface becomes progressively complex owing to degradation in strength and modulus properties of reinforcing steel and concrete at different rates, as well as differential thermal expansion between them. Thus, unlike bond between reinforcing steel and concrete at room temperature, investigating temperature dependent bond effects is inherently complex. Bond strength at elevated temperatures, similar to bond under ambient conditions, is influenced by a number of factors. Early tests by Bazant and Kaplan (Bazant and Kaplan 1996) broadly concluded that:

- Bond strength decreases with rise in temperature and the rate of reduction is higher than that of compressive strength of concrete.
- The temperature induced reduction in bond strength for ribbed bars is generally less than that for plain rounded (smooth) steel bars.
- Diameter of bars has little effect on bond strength reduction.
- Heating rate, saturation period and stress level during heating influences the results of bond tests at high temperatures.
- Concrete with carbonate aggregates shows slower rate of bond degradation than with quartz aggregates at elevated temperatures.
- The lower the concrete cover thickness, the higher is the reduction in bond strength.

Due to the complexity involved in experimentally evaluating bond degradation at elevated temperatures, there is a significant variation in reported data on bond strength. These differences arise primarily due to different rates of heating, different concrete (compressive) strengths, different embedment lengths and loading conditions that were present in specific bond tests. Therefore, consideration for all influencing parameters on bond strength degradation is essential for tracing the realistic fire response of RC structures.

Limited material level investigations on evaluating residual bond strength after high temperature exposure exist in literature. Temperature dependent bond strength as a function of temperature reported in previous studies is summarized in Figure 2-24. Some notable experimental studies on temperature induced bond degradation are reviewed here.

Early tests to study deterioration of bond with temperature were conducted by Diederichs and Schneider (Diederichs and Schneider 1981) through concentric pull out tests on NSC specimens in 20°C to 800°C temperature range under both steady state and transient thermal conditions. They

concluded that shape of the rebar (ribbed or smooth) has significant influence on bond strength besides temperature itself. Also, the rate of temperature induced bond strength degradation was found to be higher than the rate of degradation of respective strengths in concrete and reinforcement with temperature.

Morley and Royles (Morley 1983) studied bond behavior through concentric pull out tests on NSC specimens under four different test conditions. The concrete cover to the reinforcement was also varied during tests. Based on test results, the authors pointed out that bond strength at elevated (hot) temperature conditions was greater than residual (after cooldown) bond strength. Also, higher concrete cover led to relatively larger slip indicating a pull-through type of failure. Similar to previous study by Diederichs and Schneider (Diederichs 1981), the reduction in bond strength with temperature was found to be higher than the corresponding reduction in the compressive strength of concrete.

In a relatively recent study, Haddad et al. (Haddad et al. 2008) studied the effect of elevated temperature on the bond between steel reinforcement and fiber reinforced concrete members through double pull-out tension tests for temperatures ranging from 350 °C to 700 °C. The specimens were heated to a target temperature without any applied loading during heating, and then cooled down to room temperature before loading to failure. The authors concluded that significant reduction in bond strength between concrete-rebar occurs when temperatures at the interface exceed 400 °C.

Besides the aforementioned tests at the material level, limited numerical and analytical studies are reported on modeling temperature induced bond degradation between rebar and concrete. Pothisiri and Panedpojaman (Pothisiri and Panedpojaman 2012a) developed a mechanical model for predicting bond strength between rebar and concrete at elevated temperatures by incorporating

smear crack theory. Based on a parametric study conducted using the developed model, the authors concluded that bond strength predictions using empirical models developed using experimental data to be un-conservative when concrete cover thickness to rebar diameter ratio is less than two. At the structural level, very few studies are carried out to study the effect of temperature induced bond degradation on fire response of RC members. The variation of temperature induced bond between rebar and concrete was specifically considered only in four different studies by Huang (Huang 2010a), Gao et al. (Gao et al. 2013), Panedpojaman and Pothisiri (Panedpojaman and Pothisiri 2014c), and Kodur and Agrawal (Kodur and Agrawal 2017a). In these four studies, the authors incorporated the influence of bond degradation utilizing zero thickness bond-link (spring) elements in evaluating response of RC beams under fire. However, none of these studies investigated effect of temperature induced bond degradation on residual capacity of fire exposed RC beams.

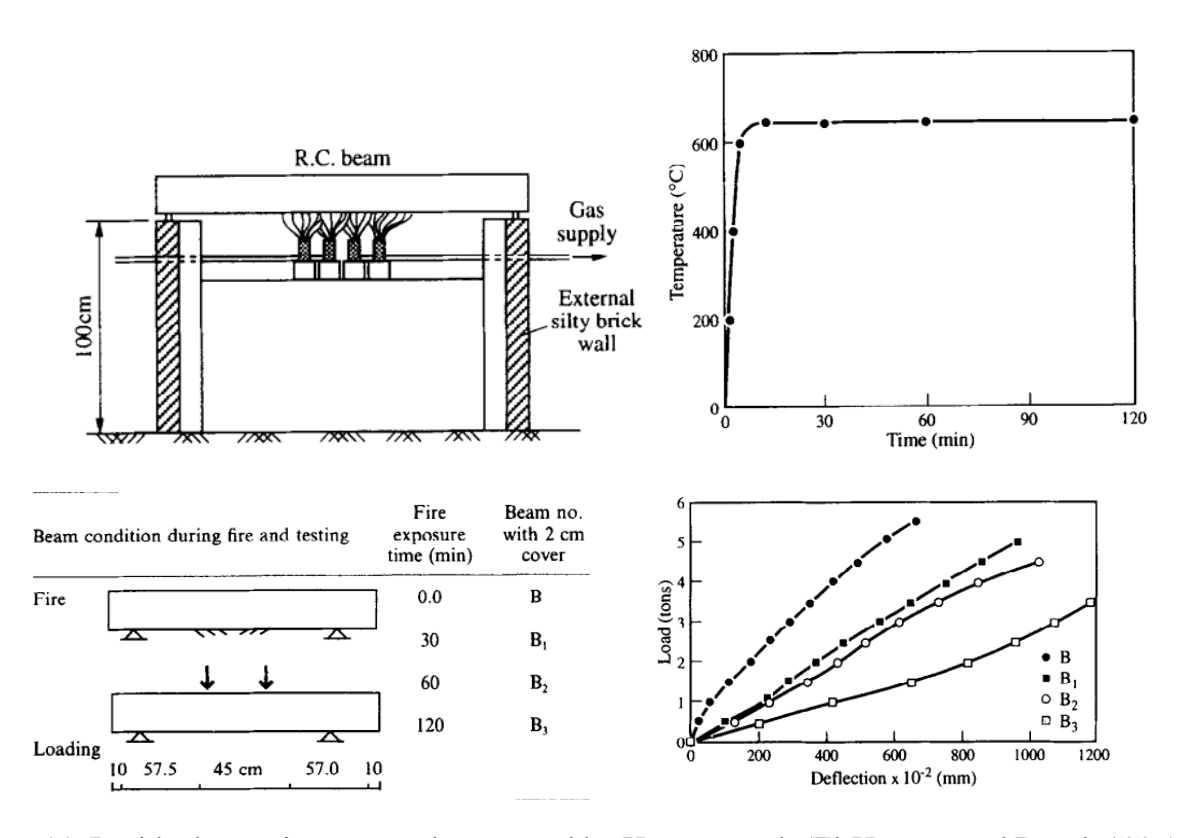
A main drawback in majority of reported experimental studies is that they relied on concentric pullout tests, which are now known to be unrepresentative of the stress state that occur in a flexural member (Tastani and Pantazopoulou 2010). Moreover, temperature at the concrete rebar interface was not monitored in any of the reported studies. Furthermore, only pull-out mode of failure was considered in previous studies with no consideration for splitting failure which is more probable during exposure to high temperatures. Finally, no numerical studies exist that quantify influence of temperature induced bond degradation on residual capacity of fire exposed RC beams. Thus, bod test data is needed at the material level to develop temperature dependent residual bond strength relations considering realistic stress state that occurs in flexural members as well as splitting failure mode. These relations can then be incorporated into numerical models, to investigate influence of temperature induced bond degradation on residual capacity of RC beams.

2.5 Knowledge gaps

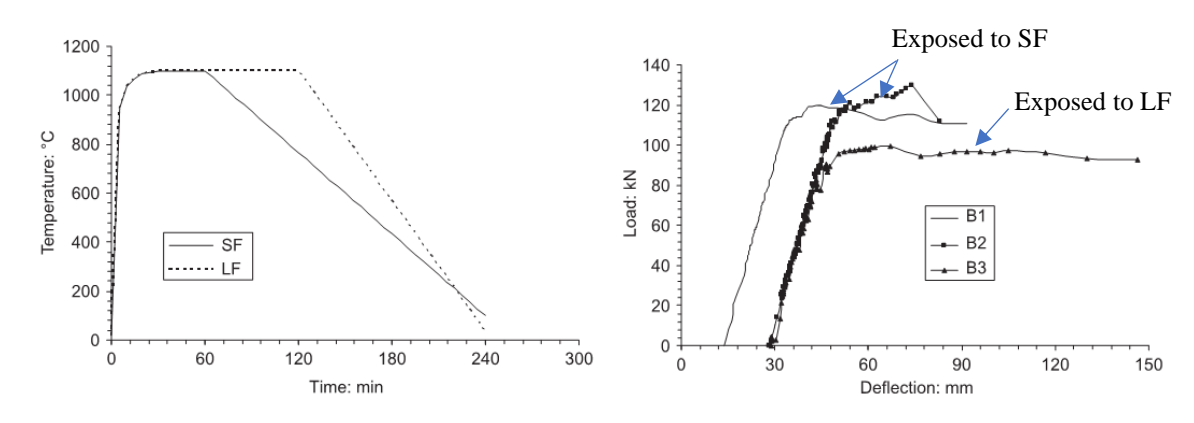
The state-of-the art review clearly indicates that there is a lack of studies and clearly established guidelines (approach) to evaluate residual capacity of fire exposed RC beams. This knowledge gap also includes effect of post-fire residual deflections, and temperature induced bond degradation on residual capacity of fire exposed RC beams. The following are some of the key areas where further research is needed:

- There is lack of test data on thermal and structural response of RC beams under full heating and cooling regime (till reaching ambient conditions). Such data from fire experiments is critical for developing rational approaches to evaluate residual capacity of fire exposed RC beams and validate developed analytical, numerical and finite element models.
- Limited experimental data exists on residual bond strength after exposure to high temperatures as encountered in a fire, which is representative of the stress state in a flexural member and accounts for splitting failure mode. Such data is critical for quantifying influence of temperature induced bond degradation on residual capacity of fire exposed RC beams, which is not considered in any of the previous studies.
- Prevalent analytical and numerical approaches for evaluating residual capacity rely on peak temperature experienced in the member alone. They do not account for distinct material properties exhibited by concrete during cooling and residual (after cooldown) phase of fire exposure. None of the previously developed models account for the effect of post-fire residual deflections on residual capacity of fire exposed RC beams.
- Effect of temperature induced bond degradation on residual response of fire exposed RC beams is not considered in any of the previous studies. Moreover, strain hardening in rebar as well as tension stiffening exhibited by concrete is ignored in most approaches.

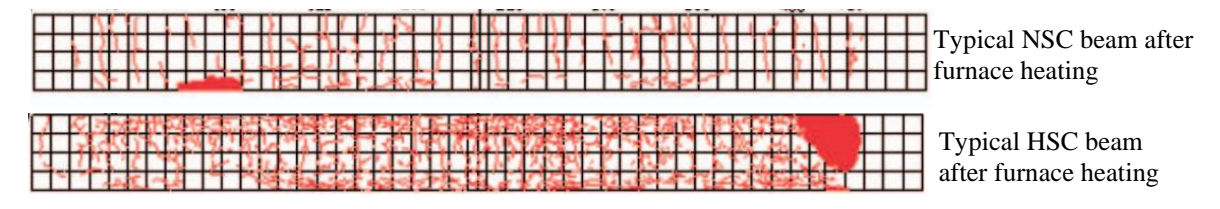
- No general approach or guidance is currently available for developing of reliable numerical models for tracing residual response of fire exposed RC beams.
- Effect of key factors such as fire exposure scenario, load level, restraint level and cross-sectional size of the beam is not studied or quantified in previous studies.



(a) Residual capacity test results reported by Hawary et al. (El-Hawary and Ragab 1996)

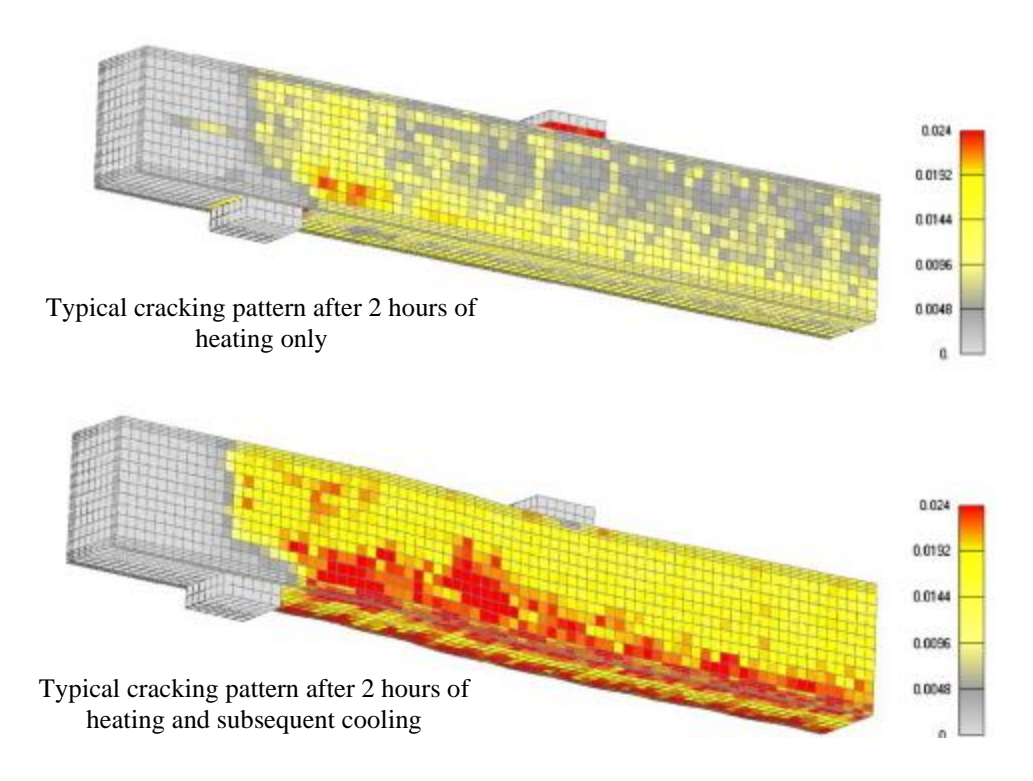


(b) Residual response of fire damaged beams reported by Kodur et al. (Kodur et al. 2010a)

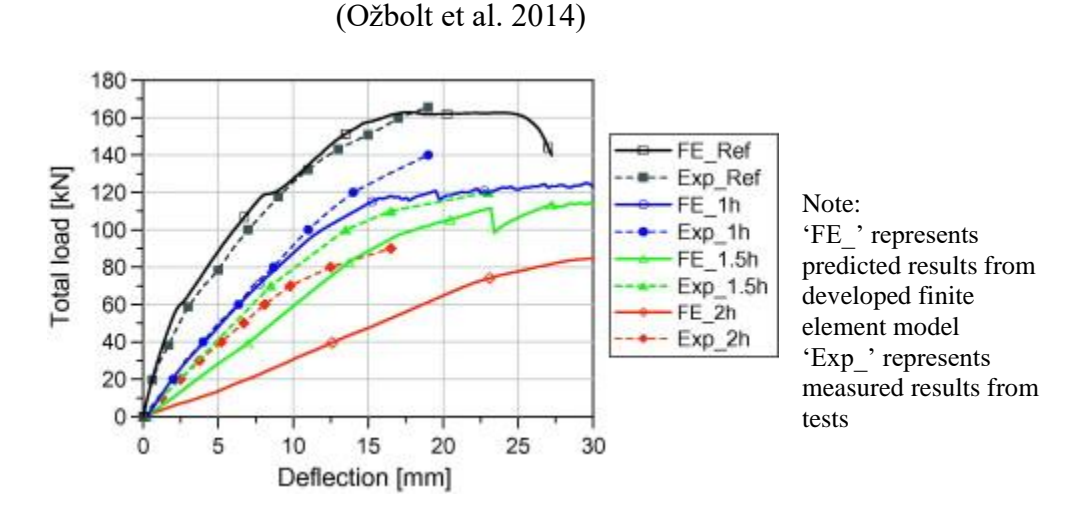


(c) Post-fire temperature induced cracking reported by Choi et al. (Choi et al. 2013)

Figure 2-1. Residual response of fire damaged beams reported in previous studies



(a) Influence of cooling on crack patterns in fire exposed beams analyzed by Ožbolt et al.



(b) Comparison of predicted and measured residual load-deflection response reported by Ožbolt et al. (Ožbolt et al. 2014)

Figure 2-2. Numerical predictions from previous studies on evaluating residual capacity of fire damaged concrete beams

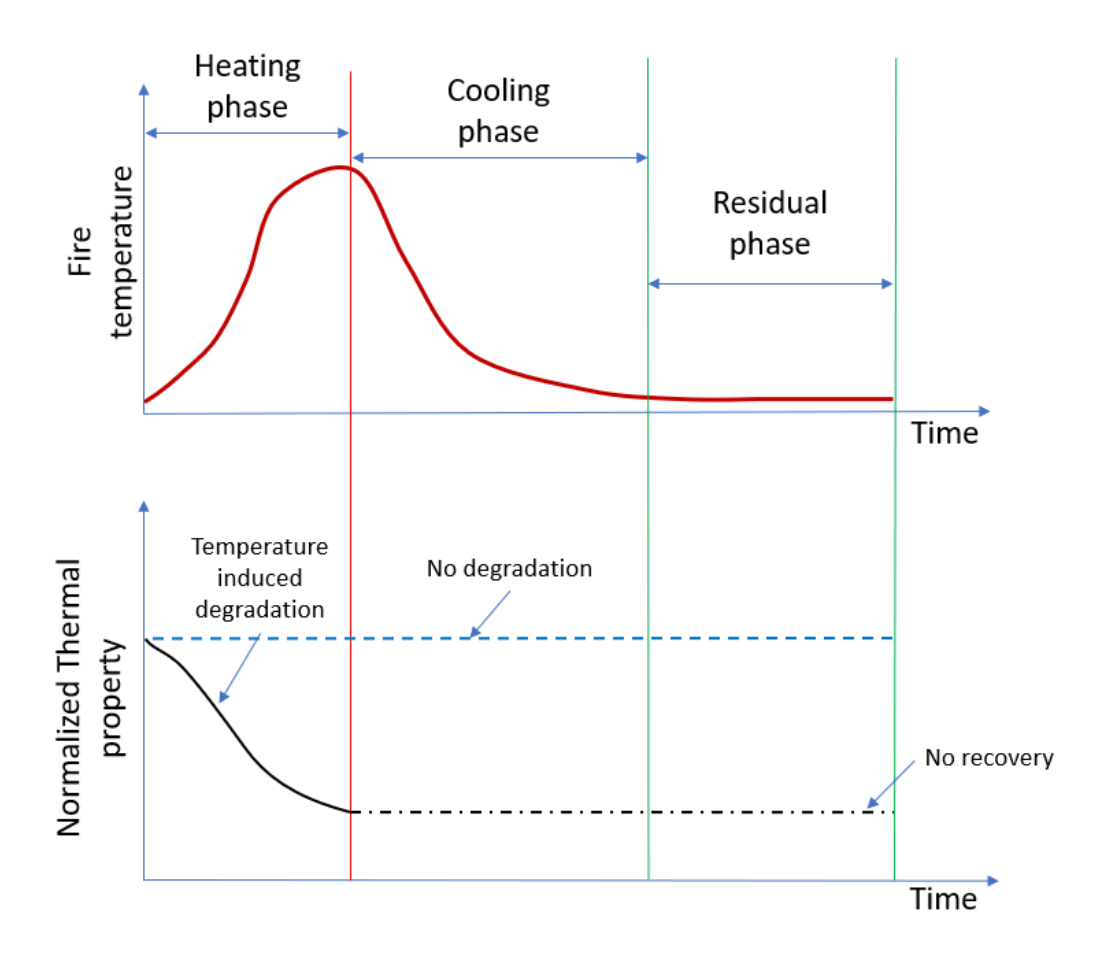


Figure 2-3. Illustration depicting temperature induced deterioration in thermal properties of concrete as expected during heating, cooling, and residual phases of fire exposure

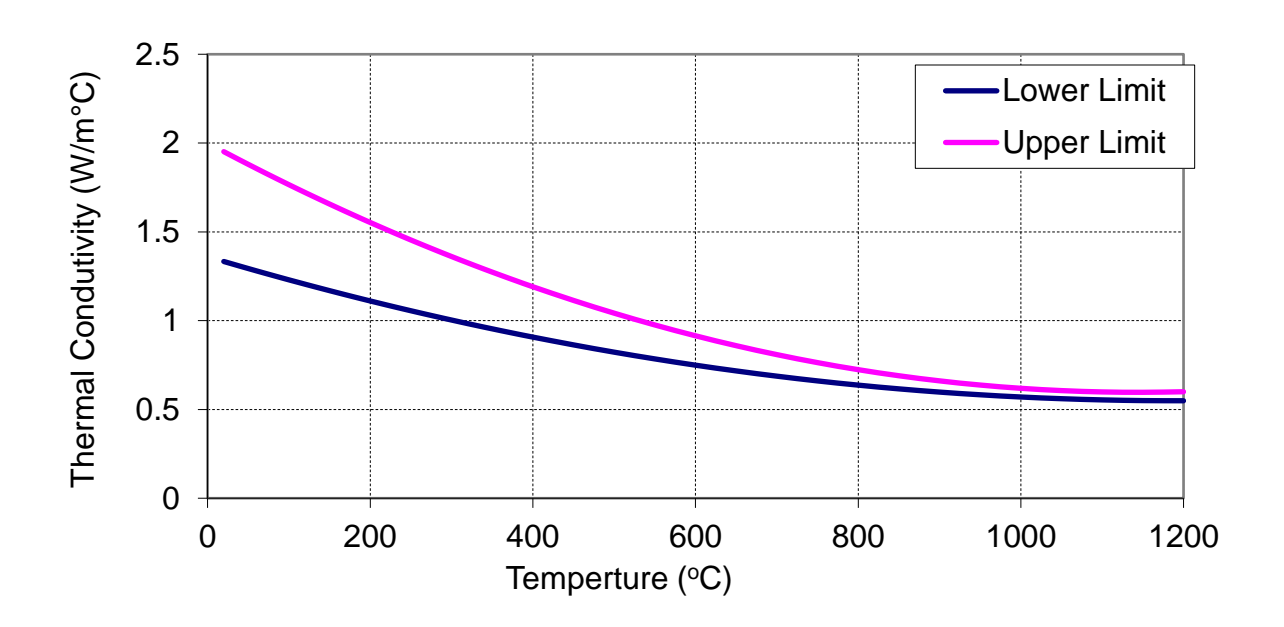


Figure 2-4. Variation of thermal conductivity of concrete with temperature based on Eurocode 2

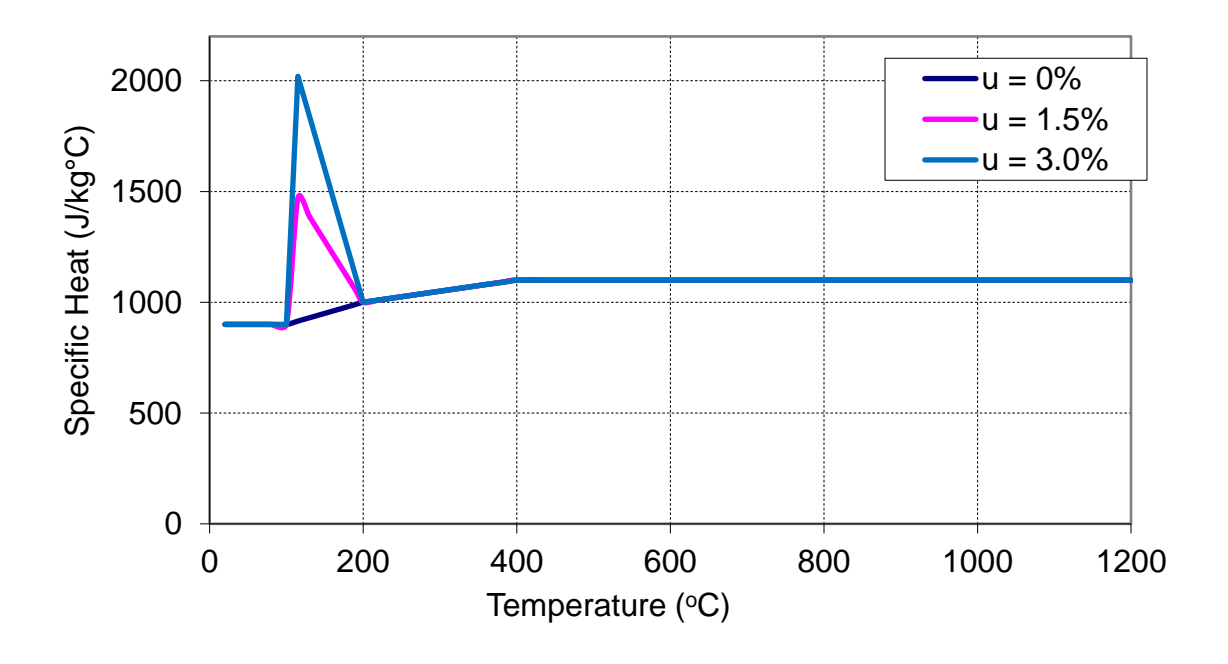


Figure 2-5. Variation of specific heat of concrete with temperature based on Eurocode 2

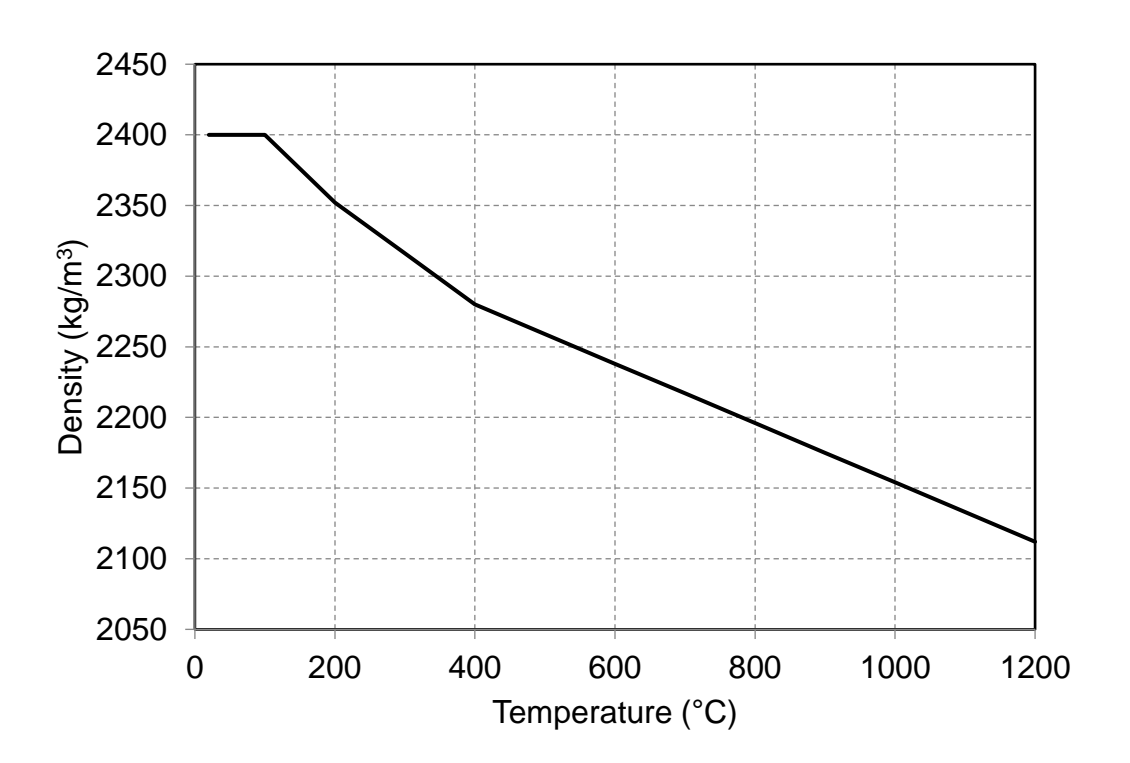


Figure 2-6. Variation of density of concrete with temperature based on Eurocode 2

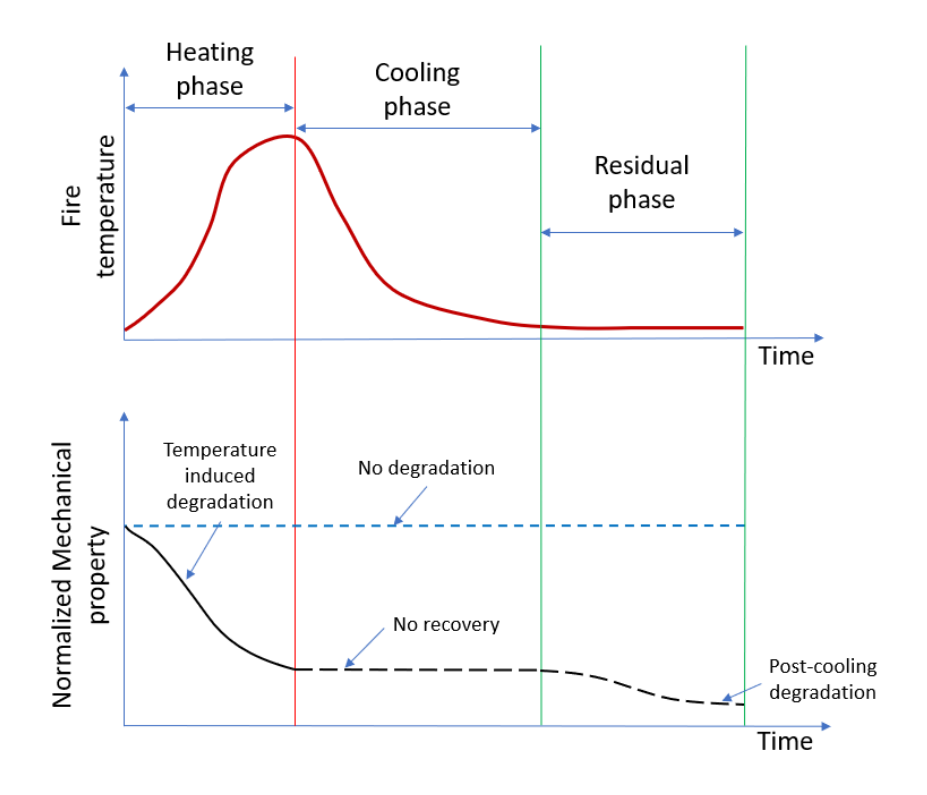


Figure 2-7. Illustration depicting temperature induced deterioration in mechanical properties of concrete as expected during heating, cooling, and residual phases of fire exposure

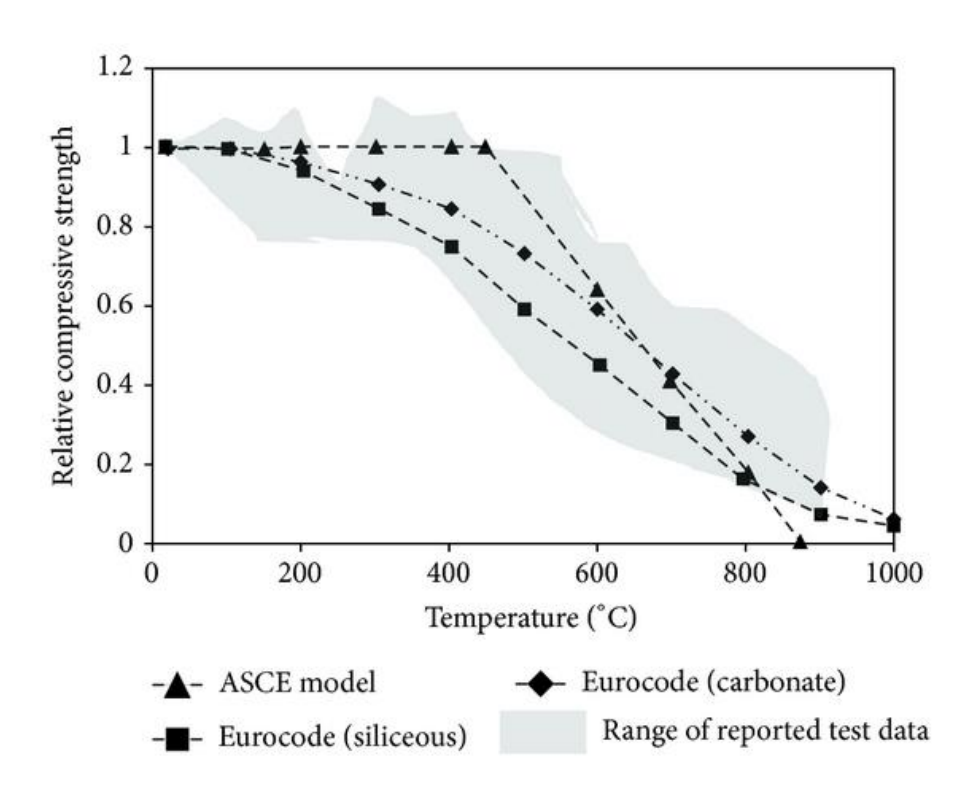


Figure 2-8. Variation of compressive strength of NSC with temperature (Kodur 2014)

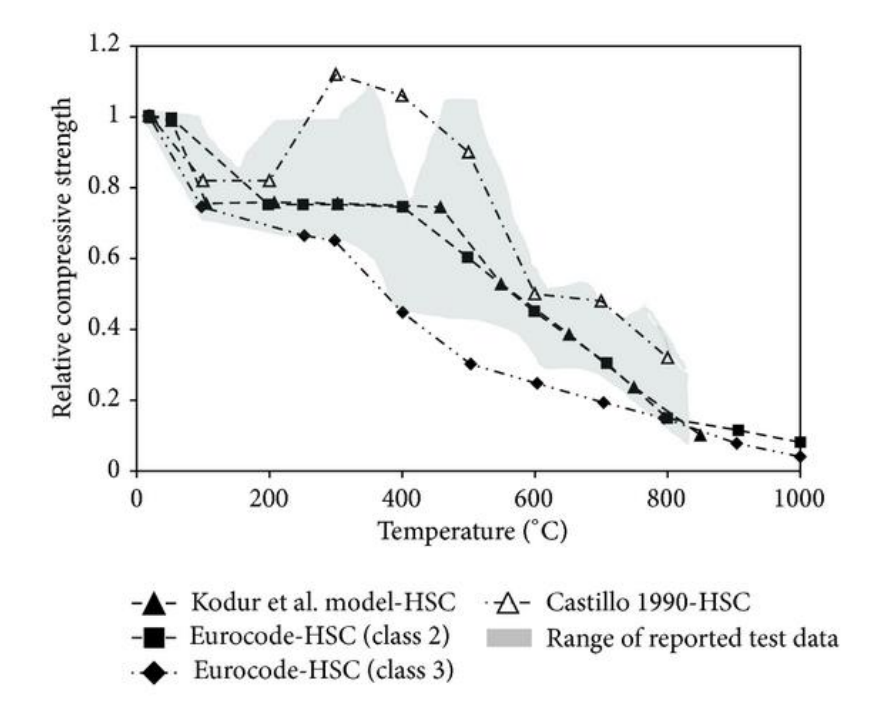


Figure 2-9. Variation of compressive strength of HSC with temperature (Kodur 2014)

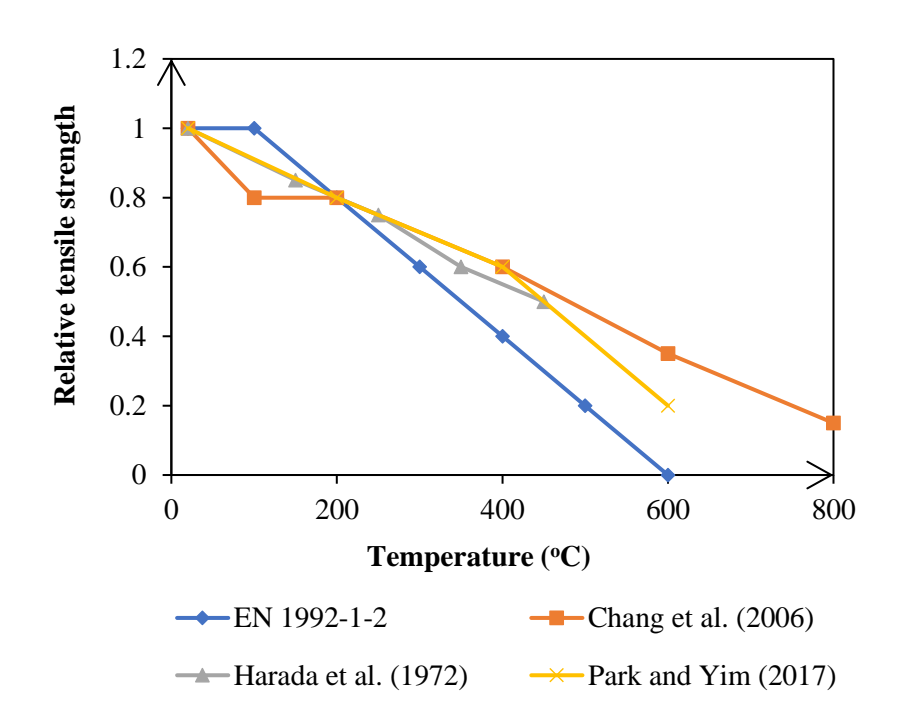


Figure 2-10. Variation of tensile strength of concrete with temperature

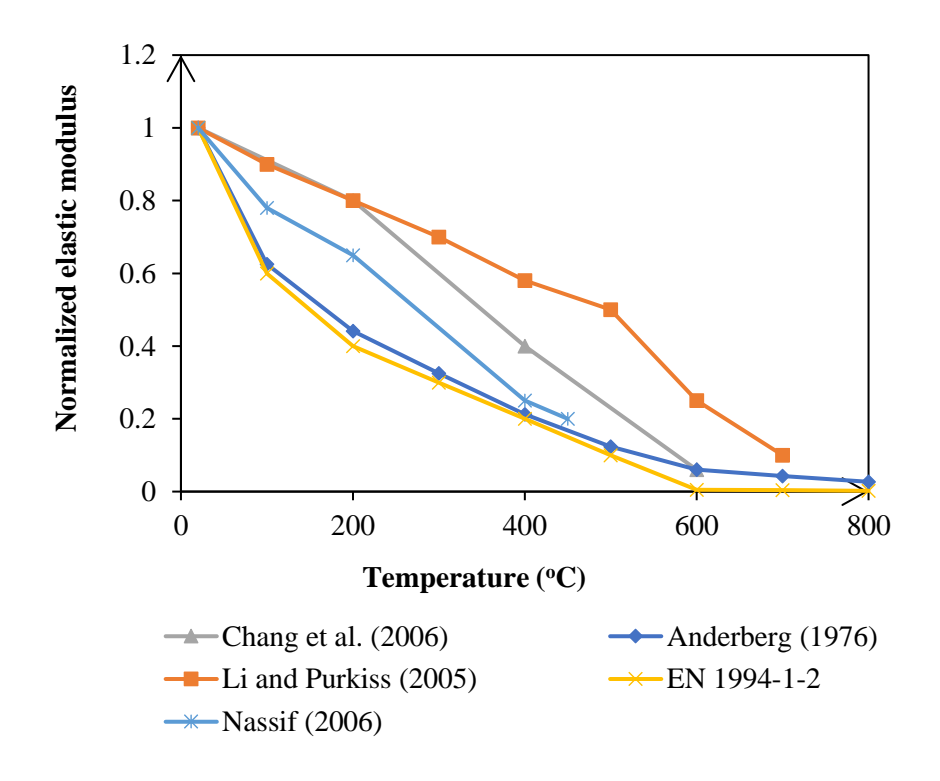


Figure 2-11. Variation of elastic modulus of concrete with temperature

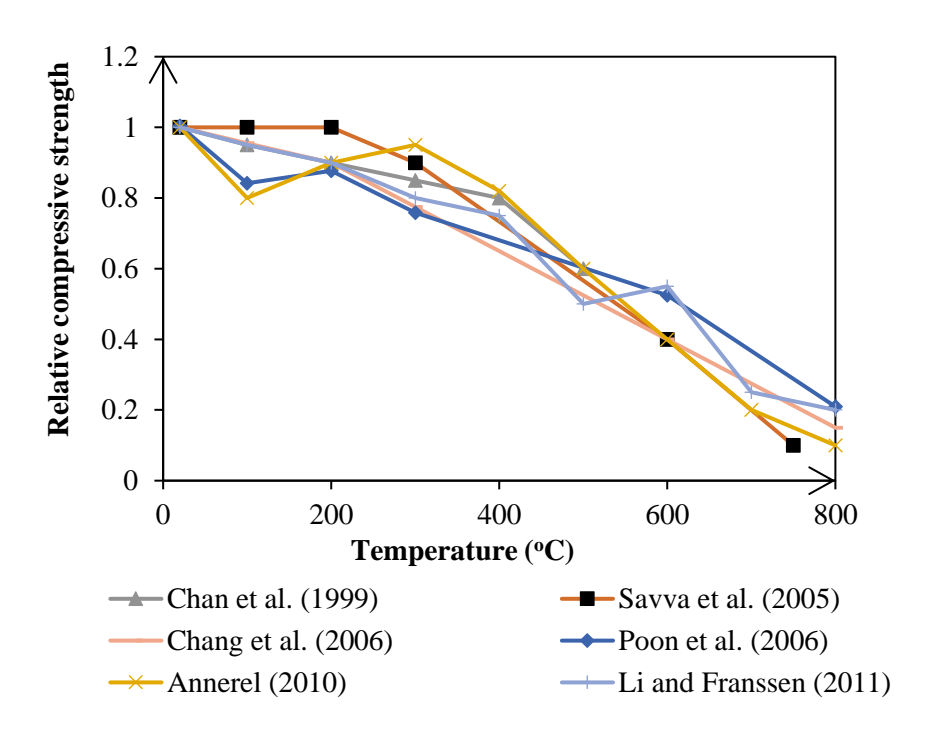


Figure 2-12. Variation of residual compressive strength of concrete with temperature

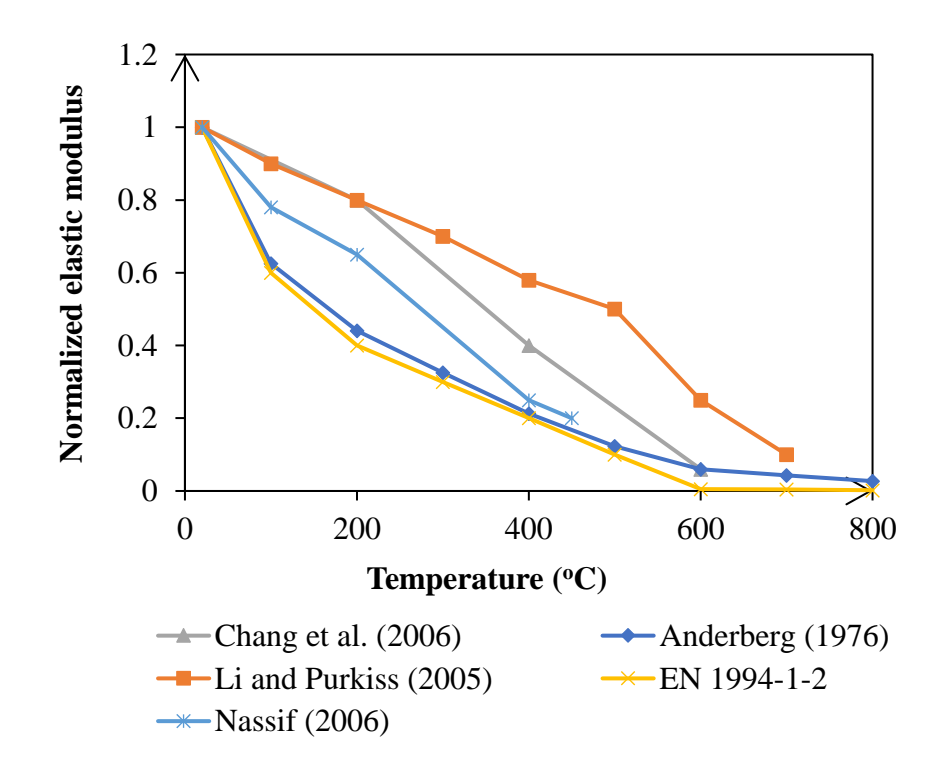


Figure 2-13. Variation of elastic modulus of concrete with temperature

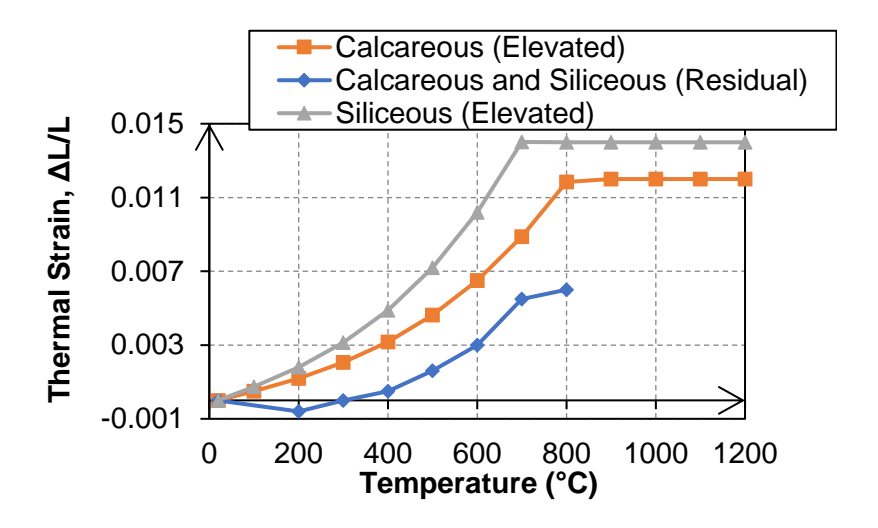


Figure 2-14. Variation of thermal strain of concrete with temperature during elevated (hot) and residual phases

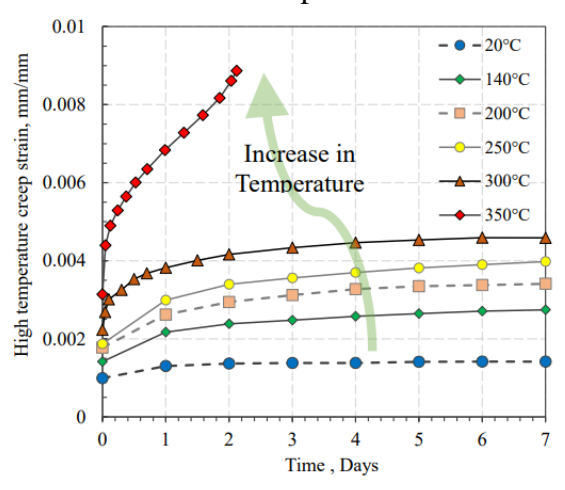


Figure 2-15. Variation of creep strain of concrete with temperature (Gross 1975)

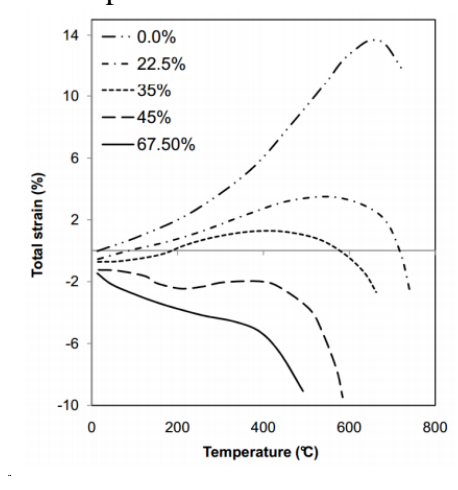
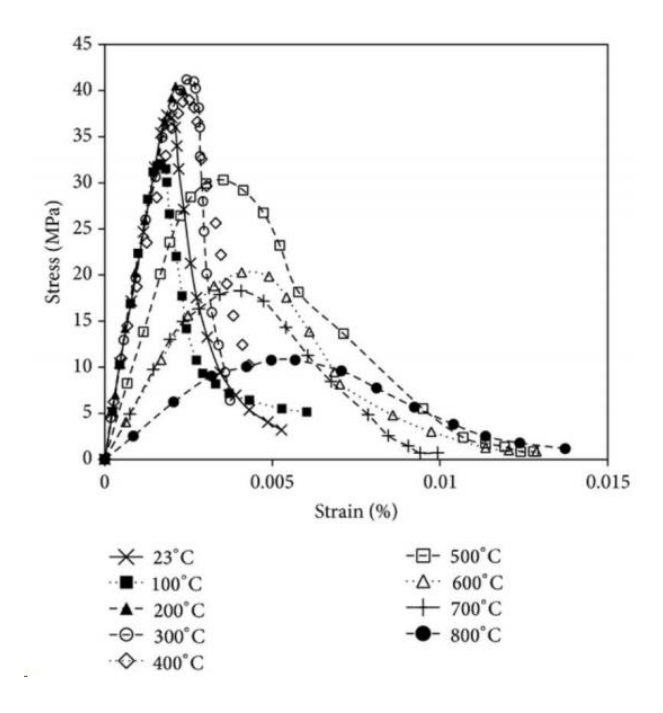
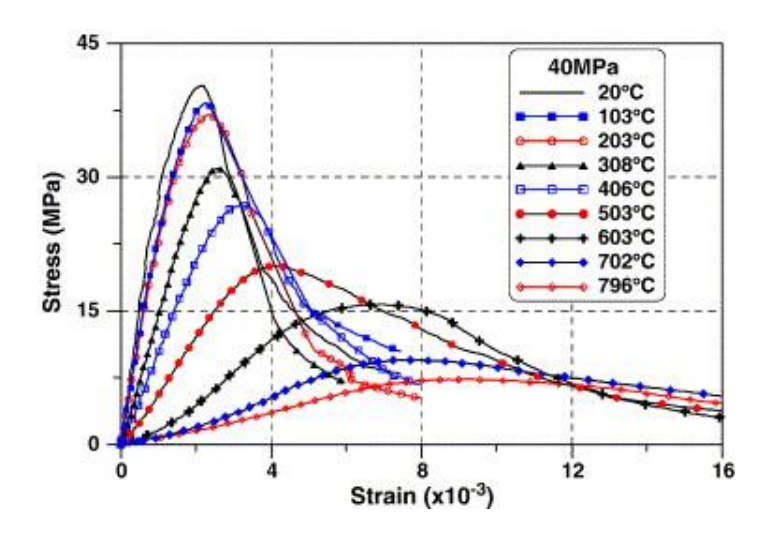


Figure 2-16. Total strain of concrete variation with temperature under different stress levels (Anderberg and Thelandersson 1976)



(a) Stress-strain cu2-15.rve of concrete at elevated temperature (Kodur 2014)



(b) Stress-strain curve of concrete during residual conditions (Chang et al. 2006)

Figure 2-17. Typical relations for temperature dependent stress-strain relations of concrete during and after high temperature exposure

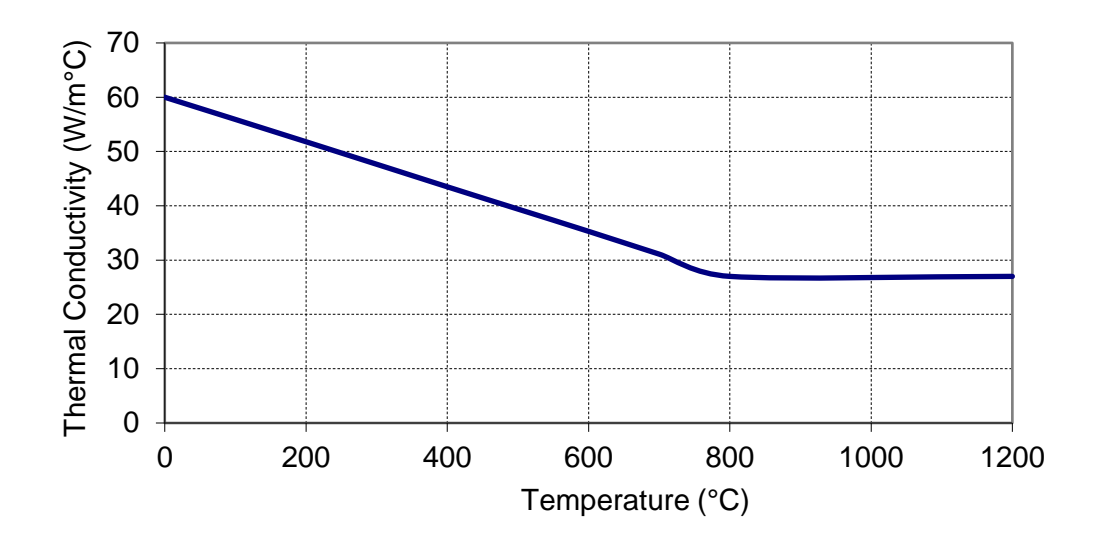


Figure 2-18. Variation of thermal conductivity of reinforcing steel with temperature based on Eurocode 2

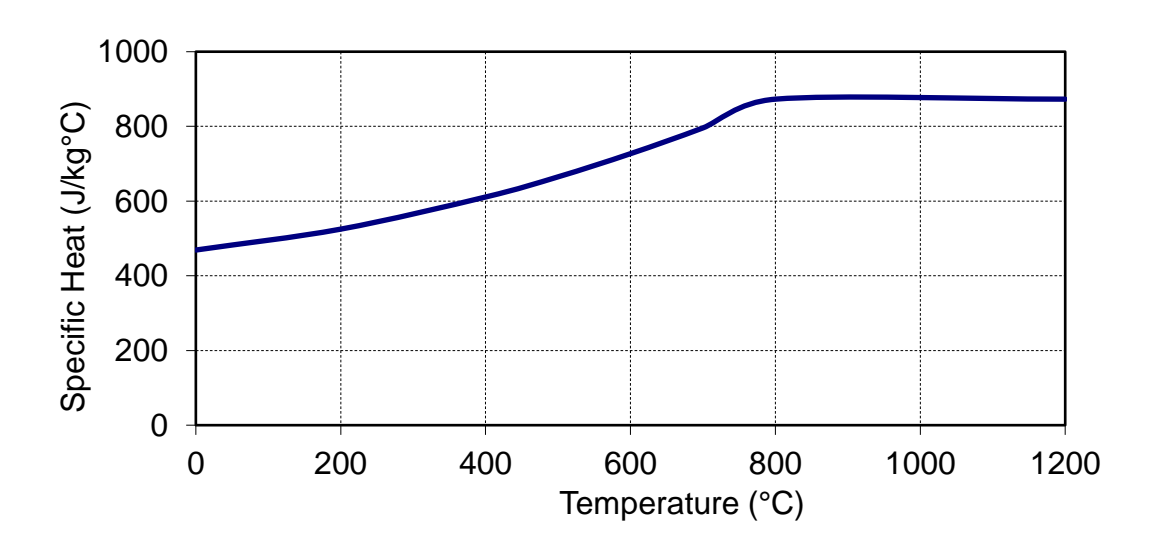


Figure 2-19. Variation of specific heat of reinforcing steel with temperature based on Eurocode 2

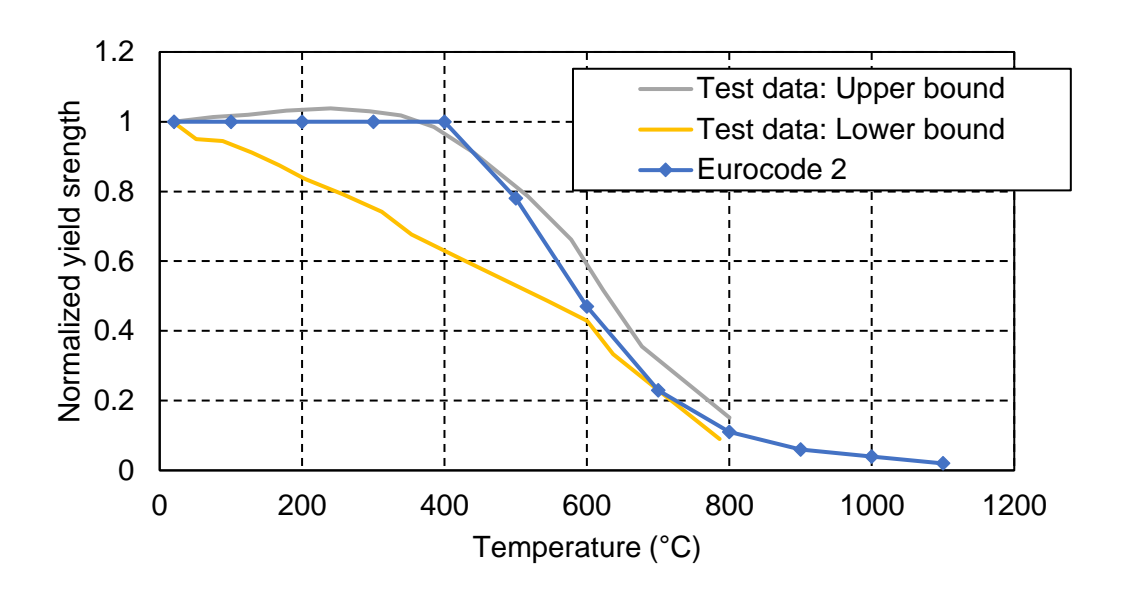


Figure 2-20. Variation of yield strength of reinforcing steel as a function of temperature

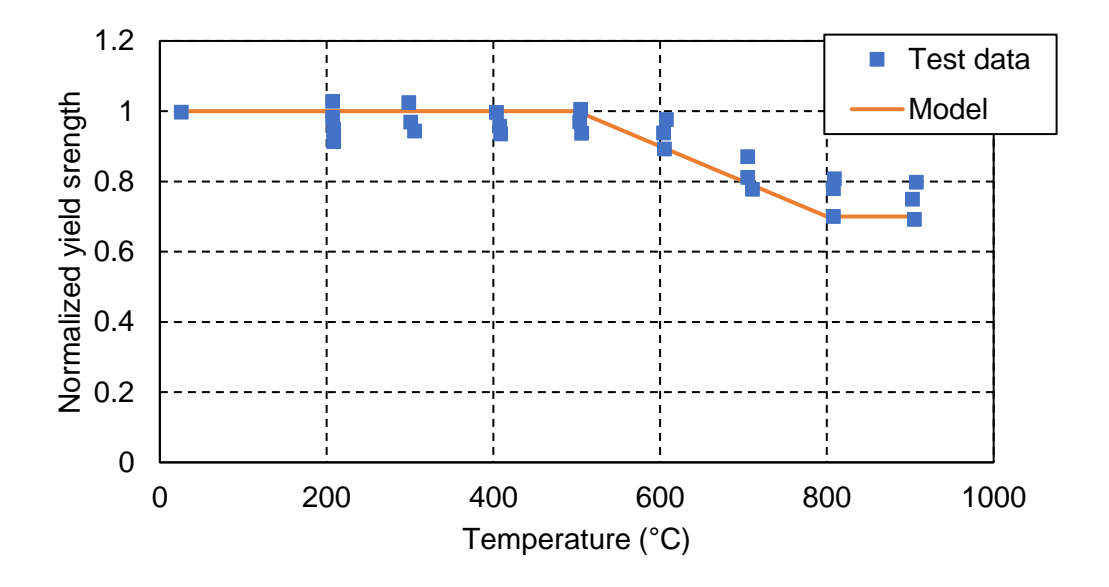


Figure 2-21. Normalized residual strength of hot rolled reinforcing steel

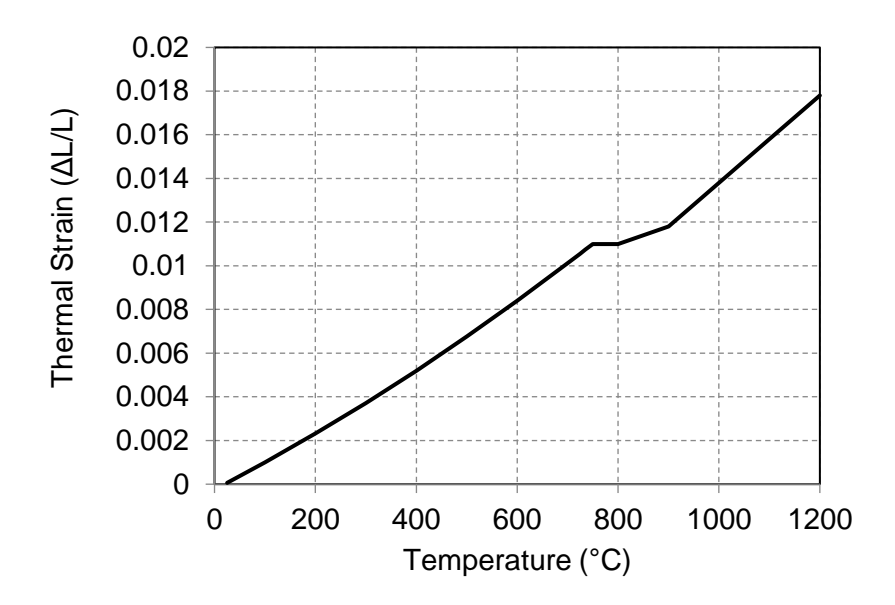


Figure 2-22. Variation of thermal strain of reinforcing steel with temperature based on Eurocode

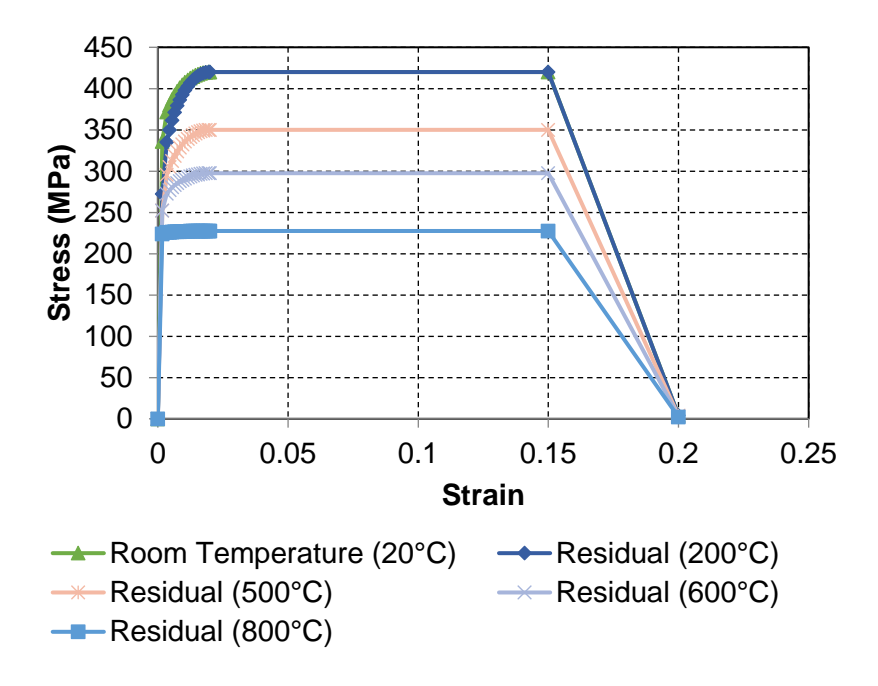


Figure 2-23. Residual stress-strain curves for reinforcing steel having yield strength of 420 MPa

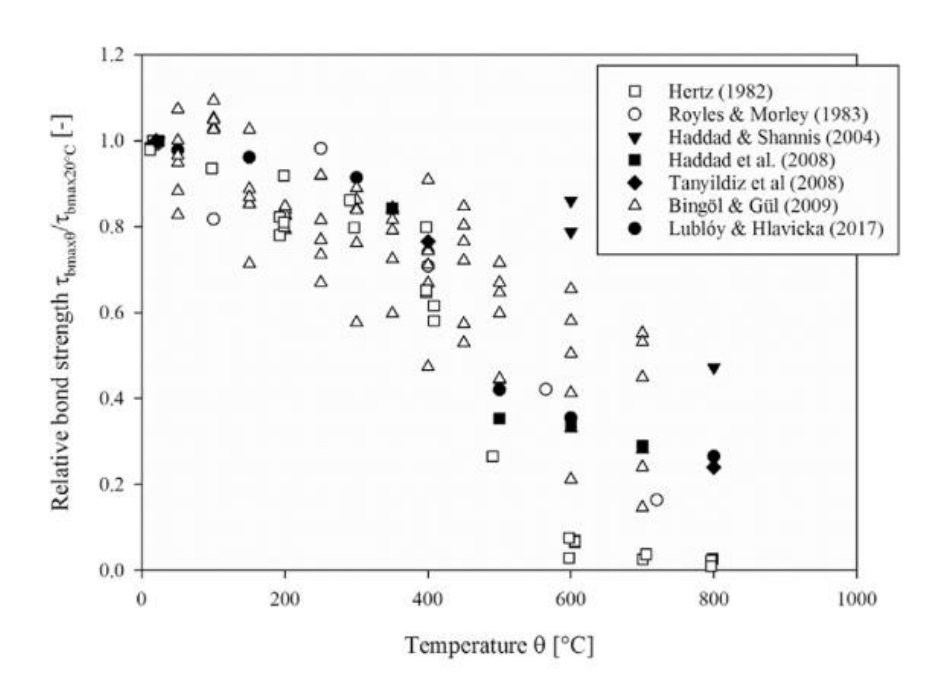


Figure 2-24. Relative bond strength as a function of temperature (air-cooled specimens)

3 EXPERIMENTAL PROGRAM

3.1 General

As summarized in the state-of-the-art review in Chapter 2, there are only limited experimental studies reported in literature on the residual response of fire exposed RC structural members. At the material level, limited test data exists on temperature induced bond degradation between rebar and concrete, especially in case of HSC. Moreover, majority of tests conducted in the past do not represent realistic stress state or failure mode as encountered in RC beams exposed to fire. At the structural level, no consistent procedure for experimental evaluation of residual capacity exists in published literature. Furthermore, majority of tests to evaluate residual capacity of RC beams rely solely on a standard heating regime and without any load acting on the beams during fire exposure, thus do not represent realistic (design) fire scenarios and stress conditions. In addition, temperature and deflection history during fire exposure, especially cooling phase, which is critical for establishing post-fire response of the beam, was not reported in majority of the studies. Further, local response and crack patterns were not reported in any of the residual capacity tests.

To overcome limitations at the material level, tests were conducted to evaluate residual bond strength between concrete and rebar. Unique test specimens that are representative of stress conditions in flexural members were fabricated using NSC and HSC (Agrawal and Kodur 2015, 2016). Data from tests was utilized to develop temperature dependent bond stress-slip relations that can be incorporated in numerical models. At the structural level, a general three-stage procedure for conducting residual capacity tests is developed (Agrawal and Kodur 2018, 2019, 2020) The developed test procedure is applied to evaluate residual capacity of two HSC and four NSC beams, after exposing them to fire scenarios representative of typical building compartments

with a distinct cooling phase as per the proposed test procedure. Thermo-structural behavior of each beam was traced through advanced instrumentation and visual observations during both heating phase of fire exposure, as well as extended cooling phase following fire decay. Following complete cooldown, the fire damaged beams were loaded incrementally to failure to evaluate residual flexural capacity. Data from these tests is utilized to compare relative performance of fire exposed HSC and NSC beams, and highlight critical parameters influencing residual capacity of fire damaged concrete members. Furthermore, these experiments provide needed data for validating finite element models developed to trace residual response of fire damaged beams in subsequent chapters of this dissertation. Details regarding, fabrication, fire test (elevated temperature exposure) procedure, residual testing procedure, measured response parameters, as well as RC beams are presented below.

3.2 Test to evaluate temperature induced bond degradation

Material level bond tests were conducted to develop simplified relations to calculate interfacial bond strength as a function of temperature for both HSC and NSC specimens. Details of the fabrication of specimens, high temperature double tension pull-out (DTP) tests, and temperature dependent residual bond strength relations are presented in this section.

3.2.1 Fabrication of specimens and test-setup

In order to develop temperature dependent bond strength relations for reinforced concrete, DTP specimens were fabricated using both NSC and HSC. Each DTP specimen comprised of a concrete prism (178 mm by 178 mm by 254 mm) with a concentric test rebar, anchored end to end, with four threaded anchor bars, at each corner on the other end (Figure 3-1a). This specimen configuration ensured presence of a longitudinal tensile stress, in the cover away from the ribs,

unlike the direct compression present parallel to the rebar axis, in a classical pullout test. In this manner, the stress conditions in this test were more representative of that encountered in the tensile region of flexural members. Once a specimen was placed in the tensile loading frame, it was first stressed to 30 percent of the measured room temperature strength. Furnace temperature was then increased at a constant rate of 5°C per minute until a predefined target temperature was reached, and then maintained for 30 minutes to allow the specimen to saturate at the target temperature. Finally, the specimen was allowed to cool down inside the furnace until it reached ambient temperature. It should be noted that a constant load could not be maintained on the specimen particularly during the later stages of heating due to free thermal expansion resulting in relaxation of tensile loads. Therefore, the effect of stress on the interfacial bond was only accounted for as a pre-load prior to heating of the specimen. The cooled down specimens were stored for 48 hours prior to heating, before being tested for residual bond strength. The test setup for both room temperature and high temperature tests is shown in Figure 3-1b.

3.2.2 Results from high temperature bond tests

Residual bond strength as a function of temperature, as well as measured bond stress-free-end-slip (BS-FES) relations from tests are plotted in Figure 3-2. It can be clearly seen that temperature induced bond strength degradation in HSC specimens occurs at a faster rate than that in NSC specimens. Also, a significant reduction in bond strength is seen (Figure 3-2a) in both HSC and NSC specimens when the exposure temperature is greater than 400°C. Furthermore, measured residual bond strength with temperature in the current study suggest that earlier tests utilizing classic pull-out tests (Diederichs 1981; Morley and Royles 1983; Reichel 1978) tend to be unconservative as they did could not capture splitting failure mode seen in the present study.

Besides temperature dependent bond strength, BS-FES relations were also measured during these tests. Results plotted in Figure 3-2b show that maximum slip increases for NSC specimens at

higher temperatures whereas it remains almost the same for HSC specimens. This indicates that failure of HSC specimens to occur in a brittle pattern than that of NSC specimens after exposure to high temperature. Thus, HSC specimens are more susceptible to longitudinal splitting cracks as a consequence of elevated temperature exposure. Furthermore, the failure mode changes in both NSC and HSC specimens with increasing temperatures (Figure 3-2a-b). A longitudinal crack develops in the specimen due to differential expansion between rebar and concrete. This crack causes loss of bond and causes a subsequent reduction in bond strength and eventual failure.

3.2.3 Temperature dependent residual bond strength relations

Test data was utilized to develop temperature dependent bond stress-slip relationships for both HSC and NSC specimens. These relationships account for degradation in bond strength and bond stiffness with increasing temperatures. A two-step procedure was adopted to develop these relations. As part of the first step, the degradation in bond strength with temperature for HSC and NSC respectively was developed using through polynomial regression on test data, and expressed as:

For NSC.

$$\frac{\tau_{max,T}}{\tau_{max,20}} = 1.0589 - 3 \times 10^{-3} T + 2 \times 10^{-6} T^2 \ (20^{\circ} C \le T \le 700^{\circ} C) \tag{3-1}$$

For HSC,

$$\frac{\tau_{max,T}}{\tau_{max,20}} = 0.984 + 9 \times 10^{-4} T - 7 \times 10^{-6} T^2 \ (20^{\circ} C \le T \le 400^{\circ} C)$$
 (3-2)

where, $\tau_{max,T}$ is the bond strength at temperature 'T' and $\tau_{max,20}$ is the bond strength at room temperature.

Secondly, a bilinear bond-stress-slip relationship is proposed based on a general relationship developed by Ulaga and Vogel (Ulaga et al. 2003), with suitable modifications for high temperature. The slip at maximum stress is assumed constant for all temperatures, which is

consistent with previous models. The generalized relationship bond stress-slip relationship is given as:

$$\tau_{b,T} = \begin{cases} \tau_{max,T} \left(\frac{s}{s_1} \right) & 0 \le s \le s_1 \\ \tau_{max,T} & s_1 < s \le s_2 \end{cases}$$
 (3-3)

where, $\tau_{b,T}$ represents bond stress, s represents slip in mm, s_1 represents slip at maximum bond stress (1 mm for NSC and 0.5 mm for HSC) and s_2 represents ultimate slip (3 mm for NSC and 2 mm for HSC) (Aslani and Samali 2013). The bond strength at room temperature is calculated using the generalized expression proposed by Aslani and Samali (Aslani and Samali 2013). These relations can be readily incorporated to explicitly account temperature induced bond degradation in evaluating residual capacity of fire damaged concrete beams. Further details on structural level tests to evaluate residual capacity of fire damaged beams are discussed in subsequent sections.

3.3 Three-stage procedure for evaluating residual capacity

In order to capture the realistic residual capacity of the member a three stage evaluation approach comprising of; Stage 1: evaluating the member response at room temperature during service (load) conditions as present prior to fire exposure; Stage 2: evaluating member response during heating and cooling phases as present in a fire incident, and during extended cool down phase of the member to simulate conditions as occurring after fire is extinguished or burnout conditions are attained; and Stage 3: evaluating residual response of the fire damaged member following complete cool down is proposed. A flowchart depicts these three distinct stages of residual capacity assessment through testing (or numerical modeling) in Figure 3-3.

Stage 1 of testing involves subjecting the member to load (stress) and boundary conditions, as present during pre-fire conditions. Loads need to be applied in small increments to simulate quasi-

static conditions, until service conditions are reached, and maintained constant using loadcontrolled technique, for a sustained period (typically 1 to 2 hours) until deflections in the member stabilize. During this stage of testing, the load-deflection response is to be monitored to establish initial (pre-fire exposure) stiffness of the structural member, as well as to ensure realistic level of cracking (damage) in the test specimen prior to fire exposure. Level of loading (stress) applied on the structural member during Stage 1 can have a significant influence on its performance during fire exposure in Stage 2 of testing. Also, response of the beams during Stage 1 of testing can be directly compared with structural response during Stage 3 of testing to gauge extent of fire damage. In Stage 2 of testing, extent of fire damage in the structural member, as occurring in a real fire incident, needs to be simulated. Thus, the loaded structural member is to be exposed to a realistic fire exposure scenario having a distinct cooling phase. It is also important to note that crosssectional temperatures within the structural member may remain significantly high for prolonged time following burnout conditions or after fire is extinguished, owing to high thermal inertia of concrete. In fact, cross-sectional temperatures within the structural member may not cool down to ambient conditions until 24 to 72 hours after fire has been extinguished, depending on size (thermal mass) of the member. Thus, loads on the member are to be maintained during complete duration of fire exposure, and until cross-sectional temperatures in the member revert back to ambient conditions. The load level maintained during this extended cooling phase of the member can also affect extent of recovery in the member. Thus, key parameters to be monitored during Stage 2 of testing include cross-sectional temperatures, deflections, temperature induced spalling, any restraint forces, and load level maintained during extended cool down of the member. Once the member cools down to ambient conditions, the member is unloaded to record recovery in post-fire deformations, and measure extent of irrecoverable (plastic) residual deformations.

Following complete cool down of the structural member to room temperature, and if there is no failure in Stage 2 of testing, residual response of the fire damaged member is traced in Stage 3 of testing. The post-fire residual response of the member is to be traced by incrementally loading the member to failure through a displacement-controlled loading technique. This ensures that the post-peak response, including softening state, of the tested member till actual failure to be captured accurately. During Stage 3 of testing, the load-deflection response, and modes of failure in the structural member are to be recorded. Details on fabrication of test specimens, test setup and procedure for each stage, and results from the tests are discussed in subsequent sections.

3.4 Design and fabrication of concrete beams

Six rectangular reinforced concrete beams (see Figure 3-4), designated as B1 to B6, were designed as per ACI 318 specifications (ACI 2008), and then fabricated for testing. Two of these beams, B1 and B2, were fabricated using HSC, while the other four beams, B3, B4, B5 and B6, were made of NSC. All six beams had three Ø19 mm bars as tensile reinforcement and two Ø13 mm bars as compressive reinforcement. The shear reinforcement in these beams comprised of Ø6 mm stirrups spaced at 150 mm along the length of the beam. The steel of the main reinforcing bars and stirrups had specified yield strength of 420 MPa and 280 MPa, respectively. Figure 3-4 shows the elevation and cross-sectional details of fabricated beams, together with the distribution of the stirrups.

Two batches of concrete were used for fabricating the RC beams. Beams B1 and B2 were fabricated from an HSC mix (batch 1), while beams B3, B4, and B5 were fabricated from an NSC mix (batch 2). The two batches of concrete were made with general-purpose Type I Portland cement, carbonate aggregate, and natural sand. The mix proportions of the two batches are shown in Table 3-1.

Silica fume (43 kg/m³) was added to the batch mix (batch 1) in order to obtain the targeted high strength in concrete. The HSC beams were moist cured in forms for 7 days, whereas the NSC beams were sealed in their forms for 7 days. All the specimens were then removed from the forms and stored in air maintained at about 25°C and 40% relative humidity. The HSC beams (B1 and B2) were stored for 8 years while the NSC beams (B3, B4, B5, and B6) were stored for 1 year prior to testing. The long curing periods ensured that these beams attained realistic moisture condition as observed in actual buildings. The average compressive (cylinder) strength of HSC, measured at 28 days and on test-day was 93 MPa and 106 MPa respectively, while for NSC 28 days and test-day compressive strength were measured to be 49 MPa and 62 MPa respectively. Also, after fire exposure and subsequent residual capacity tests on beams, cores were drilled from the unaffected (unexposed) support zones in each of the beams and tested for compressive strength of concrete and tensile strength of rebar. The average compressive strength of the drilled cores from HSC and NSC beams were measured to be about 104 MPa and 64 MPa respectively. The measured compressive strengths of drilled cores for each of the beams are also provided in Table 3-1.

The moisture condition (relative humidity) was measured on the day of the fire test as per ASTM E119 (ASTM 2007) recommendations. Also, the moisture content in the beams as a percentage of their weight was computed based on the measured relative humidity (Bazant and Thonguthai 1978) and porosity of the concrete estimated based on concrete mix proportions (Mindess et al. 2003). The calculated moisture content was relatively lower for HSC beams B1 and B2 (2.1% and 2.2%) as compared to NSC beams B3, B4, B5 and B5 (2.1%, 2.2%, 2.4%, and 2.5%), which were stored for a relatively shorter period as well (see Table 3-2). This can be attributed to higher water to cement ratio in the NSC mix as compared to the HSC mix. In addition, chemical bonding of 'free'

moisture present within pores, coupled with self-dessication due to limited permeability of HSC containing silica fume results in relatively lower moisture content over longer periods of time (Nilsson 2002).

The tested beams were instrumented with thermocouples and displacement transducers. Type-K chromel—alumel thermocouples (0.91 mm thick) were installed during fabrication at three different cross-sections in each beam for measuring concrete and rebar temperatures. Five thermocouples were also installed at the top side (unexposed side) of the beam. The location and numbering of the thermocouples (labelled TC1 to TC20) in three cross-sections along the span of the beam are shown in Figure 3-4. The deflection of each beam was measured by placing displacement transducers at mid-span, as well as at the location of one of the two point loads.

3.5 Test-setup and procedure

Each stage of testing was carried out in a specially designed test setup. The application of loads at room temperature (Stage 1), and subsequent fire exposure tests (Stage 2) on the six beams were carried out in the fire test furnace. Subsequently, upon complete cool down of the member residual capacity tests were conducted in a displacement controlled flexural loading test setup.

3.5.1 Testing prior to fire exposure

In Stage 1 of testing, each of the beams were setup in the loading frame-cum-heating furnace, and two point loads were applied incrementally through a load controlled procedure on the top face at 1.4 m from support ends. For all beams, except beam B4, each of the two point loads was 50 kN generating a bending moment of approximately 53% of the beam capacity according ACI 318 (ACI 2008), similar to load (stress) level typically present during pre-fire exposure conditions. To study the effect of load level on residual capacity, beam B4 was subjected to a relatively higher

load level of about 65% of design capacity, with each of the point loads being 60 kN. All six beams were tested under simply supported end conditions. The load was maintained on the beams through a load-controlled technique, till deflections stabilized, and then during Stage 2 of testing. During Stage 1, the load-deflection response and crack propagation in the beam were monitored.

3.5.2 Testing during fire exposure conditions

As part of Stage 2 of testing, HSC and NSC beams were exposed to fire in the MSU structural fire testing facility (Dwaikat 2009). This test facility was specially designed to subject structural members to representative thermal, load, and support conditions experienced during a fire. More details of the furnace are available elsewhere (Dwaikat 2009). The bottom and two side surfaces of each beam were exposed to fire, while a 50 mm layer of insulation (ceramic fiberfrax material) was utilized provided on the top surface of the beam. Such three-sided exposure is similar to conditions encountered in practice wherein a concrete slab is present on the top side of the beam prevents heat penetration from the top. Also, only middle 2.44 m length of the beam, of the total 3.96 m span was exposed to fire. Such exposure of the middle span of the beam are not exposed to fire directly. However, the ratio of the exposed to unexposed length is primarily due to limitations of fire test furnace, where the maximum fire exposed span cannot be more than 2.44 m.

The fire exposure on the beams comprised of a heating phase followed by a distinct cooling phase, as shown through time-temperature profile in Figure 3-5. HSC beams B1 and B2 were subject to rapid heating (more severe than ASTME119 standard fire (ASTM 2007), to simulate design fire exposures in a typical compartment. The heating phase lasted for 60 minutes in the case of beam B1 (indicated as SF1 in Figure 3-5, and 120 minutes in the case of beam B2 (refer LF1 in Figure 3-5). A rapid non-linear cooling phase of fire exposure was adopted for both beams B1 and B2 to

simulate fire-fighting or suppression intervention, and the beams were allowed to cool down naturally in air. For NSC beams heating was as per ASTM E119 (ASTM 2007) standard fire exposure; with 90 minutes heating for beams B3 and B4 (indicated as SF2 and SF3 in Figure 3-5) and 120 minutes of heating for beams B5 and B6 (indicated as LF2 and LF3 in Figure 3-5) respectively. Consequently, the duration of heating phase was equal to or greater than the prescriptive fire rating of the beams determined to be 90 minutes as per ACI 216 (ACI 216.1 2014). Similar to HSC beams, in order to study the effect of distinct cooling phase, a linear decay rate of approximately -6°C per minute during cooling phase of fire exposure was adopted for beams B1, B2, and B3, representing conditions when there is no fire-fighting intervention and the fire is allowed to decay on its own. Beam B4 however was allowed to cool at a rapid non-linear rate of approximately -80°C per minute, to simulate conditions when there is fire-fighting intervention and fire temperatures decay much more rapidly. These decay rates qualitatively highlight the influence of cooling phase on both compartment temperatures and residual response of RC beams. The chosen decay rates were governed by upper-bound and lower-bound limits achievable using the available test furnace, than a detailed study on compartment temperatures during actual fires with and without fire-fighter intervention. It is expected that cooling rates may differ in cases of water cooling, and other variations in cooling conditions. Further studies are needed for quantifying the effect of decay rates on residual response of fire damaged concrete members. It should be noted that the fire exposure scenarios adopted for beams B1 and B2 were identical as they were tested under different load level.

During fire tests, observations were made at every 5 minutes through the view ports in the furnace to record any noticeable fire induced spalling. It should be noted that these visual observations were qualitative in nature, and focused on recording time and location at which spalling occurred

(if any). The beam would be considered to have failed in case the hydraulic jack, with a stroke of 250 mm, could no longer maintain the load or the peak deflection in the beam exceeded L/20 as per ASTM E119 standard failure criterion (ASTM 2007).

Following end of fire exposure, representing extinguishing of fire in a building, the recovery of cross-sectional temperatures and deflections was monitored 24 hours after fire exposure to gauge extent of recovery in the strength and stiffness properties of the beams during extended cooling phase. After complete cool down, post-fire inspection was carried out to record fire induced spalling, rupture of reinforcement, and cracking of concrete in the tested beams. Also, a quantitative measurement of temperature induced spalling was carried out once beams were removed from the furnace after fire tests. Spalling measurements were carried out one week after fire exposure in order to record the upper bound magnitude of the overall volume of spalling.

3.5.3 Residual strength test

The fire damaged beams were stored for seven days following fire exposure after temperatures revert back to ambient conditions, to well as allow for any short term reduction in compressive strength of concrete during post-cooling storage (Torić et al. 2013). Subsequently, each beam was tested for residual capacity in a four-point loading set-up as part of Stage 3 of testing (see Figure 3-4). Two point loads at 1.4 m from the supports were applied on the top face of the beam through a displacement controlled actuator (MTS machine with a capacity of 1500 kN). A displacement controlled technique at 2 mm per min was adopted for loading the beam during residual strength test. The residual load-deflection response of each tested beam was recorded in incremental steps as the applied displacement (prescribed load) increased through LVDTs installed at mid-span and loading points of beams. Furthermore, observations relating to progression of cracking, as well as failure pattern, were made during residual capacity test on each beam.

3.6 Results from tests

Data generated from each stage of the above fire tests and residual capacity tests was utilized to evaluate comparative residual behavior of fire damaged NSC and HSC beams. Relevant response parameters measured during pre-fire conditions, fire exposure and extended cooldown, as well as residual conditions after complete cooldown is presented below.

3.6.1 Response prior to fire exposure (Stage 1)

The measured mid-span deflection in Stage 1 is plotted as a function of applied loading in Figure 3-6 for all six tested beams. As expected, deflection in all beams increases monotonically with increasing load. Furthermore, the response in all beams is almost linear until the onset of tensile cracking. This tensile cracking is primarily confined to the critical region between the two point loads, subject to a constant bending moment (flexural stresses). Pre-fire secant stiffness, calculated as the ratio of peak load over final deflection for each beam B1, B2, B3, B4, B5, and B6 was calculated to be 25kN/mm, 20.8 kN/mm, 8.8 kN/mm, 9.8 kN/mm, 9.1 kN/mm, and 7.2 kN/mm respectively. As expected, beams B1 and B4 fabricated using HSC exhibit significantly greater stiffness resulting from greater compressive strength of HSC. Also, noticeable reduction in secant stiffness of beam B2 can be attributed to greater applied load resulting in tensile cracking (softening) response. The calculated secant stiffness during Stage 1 of testing can be compared with post-fire stiffness to gauge extent of fire damage.

The applied load was maintained for at least 45 minutes after reaching peak load for each of the four tested beams to allow for the deflections to stabilize, and subjecting the beams to fire testing in Stage 2.

3.6.2 Response during fire exposure (Stage 2)

The thermal and structural response of beams was evaluated during heating and cooling phases of fire exposure, as well as during extended cool down of the beams; representing the period between fire being extinguished to the time at which cross-section of beams reverts back to room temperature. Subsequently, post fire-exposed state of the beams was evaluated by monitoring temperature induced residual deformation, spalling, crack patterns, and failure patterns. Beams B1, B2, B3, B4, and B6 did not fail during fire exposure and were tested for residual capacity, while beam B5 failed during fire exposure, and hence could not be tested for residual capacity. The varying test parameters together with summary of results of the tested beams are summarized in Table 3-2 and Table 3-3.

3.6.2.1 Thermal response during fire exposure

The thermal response of HSC and NSC beams (B1 through B6) during fire exposure are presented in Figurea-c by plotting rebar and concrete temperatures at different locations along the cross section, as a function of fire exposure time. Unlike fire temperatures that rose rapidly in the first few minutes, the sectional temperatures within the beam remained fairly low during initial phases of fire exposure. The temperatures within the cross section of all beams started to rise at about 10 to 15 minutes into fire exposure, when fire temperatures were already in excess of 700°C. Furthermore, a temperature plateau is seen at about 110°C in all six beams, at various measured locations within the beam cross-section. This temperature plateau is a consequence of the latent heat consumed by free capillary water present in the beam, as it changes state from liquid to vapor. As majority of this pore water evaporates, the temperatures in the rebar and concrete increase with fire temperature. Furthermore, measured data indicate that temperatures in concrete, as expected, get lower towards the inner zones of concrete core. This can be attributed to the low thermal conductivity and high thermal capacity of concrete which slows down heat penetration to inner concrete layers.

The effect of fire severity and concrete type on thermal response of beams B1 through B6 is evident in the plotted rebar and concrete temperatures, shown in Figurea-b. The fire temperatures rise rapidly in the first 15 minutes to almost 915°C in fire scenarios of SF1 and LF1, and about 730°C for fire scenarios of SF2, SF3, LF2, and LF3. Peak fire temperatures reach about 1100°C in SF1, 1250°C in LF1, 970°C for SF2, 990°C in SF3, 1030°C in LF2, and 1010°C LF3 respectively. Correspondingly, the measured cross-sectional temperatures in concrete and steel rebar increase monotonically during heating. It should also be noted that the rate of heating, especially for the first 50 minutes in fire scenarios SF1 and LF1, is relatively faster than adopted in fire scenarios SF2, SF3, LF2, and LF3. Consequently, temperature within outer layers of concrete (at 25 mm concrete depth in Figurea) in beams B1 and B2 increase at a faster rate than those measured in beams B3, B4, B5, and B6. The greater increase in temperatures in HSC beams can also be attributed to higher thermal conductivity resulting from higher compactness (lower porosity) of HSC. On the contrary, at larger depths i.e. mid-depth of the concrete cross section (see Figureb), the rate of temperature rise in NSC beams is relatively higher than temperature rise measured in HSC beams, despite the slower rate of heating adopted in the former case. This can be attributed to rapid heating adopted in fire exposure scenarios of HSC beams B1 and B2, resulting in high thermal gradients in the beam cross-section, especially in the outer layers of concrete. These thermal gradients in turn cause greater microcraking in HSC owing to its higher compactness and lower permeability as compared to that of NSC, resulting in increased porosity in HSC. The greater temperature induced damage and porosity (microcracking) reduces overall thermal conductivity of HSC and hence slows down temperature rise at deeper layers of concrete.

The rate of temperature rise in corner rebar is similar for all six beams, as shown in Figurec. This can be attributed to the increasing influence of microcracking in HSC beams within outer layers

(closer to fire exposed surface) of concrete cross-section, causing temperature rise in HSC beams to be slower, and hence similar to that measured in NSC beams. The peak rebar temperatures at the end of heating phase of 60 minutes for beam B1, and 90 minutes for beams B3 and B4, were measured to be 287°C, 390°C, and 385°C respectively. For beams B2, B5, and B6 however, the peak rebar temperatures at the end of heating phase lasting for 120 minutes were relatively higher, and measured to be 557°C, 480°C, and 465°C respectively. Thus rebar (and concrete) temperatures recorded in beams B2, B5 and B6 were higher by almost 200°C, when compared with the measured temperatures in beam B1, and almost 100°C greater than in beam B3 and B4, owing to longer burning duration (heating phase) of the applied fire exposure in the former case.

Cross-sectional temperatures in beams was monitored throughout cooling phase of fire exposure (representing extinguishing of the fire), as well as up to 24 hours after termination of fire exposure as the beams cooled down to room temperature. Since beam B5 failed at 230 minutes during fire exposure, temperatures were not recorded for this beam beyond point of failure (fire exposure). It can be seen that cross-sectional temperatures in all six beams continue to increase even as fire (gas) temperature begins to decay (see Figureb), owing to high thermal inertia of concrete. In fact, cross-sectional temperatures reach peak values during cooling (decay) phase of fire exposure in all six tested beams. Also, the effect of thermal inertia is more significant within inner layers of concrete (mid-depth of concrete cross-section) as compared to the outer layers. Consequently, temperatures measured in the outer layer (at 25 mm concrete depth) for all six beams begin to decrease soon after fire exposure temperature enters decay phase. Measured temperatures at concrete mid-depth however, start to decay at a significantly longer duration into fire exposure. In fact, in case of beam B5 which failed during fire exposure, the temperature at concrete mid depth show an increasing trend even as fire temperature reduce to almost half their peak value.

Peak temperatures at concrete mid-depth reach 200°C, 335°C, and 344°C at about 190 minutes, 297 minutes, and 300 minutes into the fire in beams B1, B3, and B4 respectively exposed to relatively shorter heating phases. For beams B2, B5 and B6, exposed to relatively longer fire exposure, temperatures at concrete mid-depth attain peak values of 315°C, 384°C, and 310°C at about 320 minutes, 230 minutes, and 260 minutes, well after peak fire temperatures have subsided. It is important to note that the cross-sectional temperature attained in NSC beams B3 and B4 are slightly higher than those measured in beam B1, even though peak fire temperatures are greater in the latter case by almost 200°C. This can be attributed to the longer burning (heating) duration, as well as slower cooling rate adopted in case of NSC beams B3 and B4. Also, the rate of decrease in temperatures at concrete mid-depth is slowest for HSC beam B2, even though it underwent faster cooling as compared to NSC beams B3 and B4. This again illustrates the influence of increased microcracking (porosity) in HSC beams resulting in lower thermal conductivity and hence greater thermal inertia of HSC.

Measured temperatures at corner rebar shown in Figurec indicate a similar trend as seen in concrete temperatures during decay phase of fire exposure for both HSC and NSC beams. The rebar temperatures continue to increase well into the decay phase of fire exposure. For beam B1 exposed to fire scenario SF1, having a heating phase of 60 minutes, tensile rebar temperatures continue to increase until about 90 minutes into fire exposure, attaining a peak value of 387°C. Similarly, for beam B3 and B4, exposed to fire scenario SF2 and SF3 having a heating phase of 90 minutes, tensile rebar temperatures attain a peak value of 521°C at 155 minutes and 510°C at 150 minutes into fire exposure respectively. In case of beams B2, B5, and B6, all of which were heated for 120 minutes under LF1, LF2 and LF3 fire scenarios, peak tensile rebar temperatures of 592°C, 583°C, and 500°C are experienced at 140 minutes, 190 minutes, and 146 minutes since beginning of fire

exposure in each case. Thus, the effect of thermal inertia is more pronounced in case of slower cooling rates as adopted in fire exposure scenarios SF2, SF3, and LF2.

In addition, the time taken in each beam to revert back to ambient temperature is significantly greater than duration of heating for all tested beams. As an illustration, time for temperatures at the mid depth of concrete to drop from peak temperature of 310°C to room temperature in beam B2 was more than 1400 minutes (or 24 hours), when the duration of the heating phase was 120 minutes (2 hours). This can be attributed to relatively high thermal inertia of concrete, as well as microcracking in concrete during fire exposure, which results in increased porosity and hence reduced thermal conductivity, and leads to prolonged retention of heat within the fire damaged beams.

3.6.2.2 Structural response during fire exposure

The structural response of HSC and NSC beams (B1 through B6) during fire exposure can be gauged by tracing measured mid-span deflection as a function of fire exposure time (see Figure 3-9). Similar trend in deflection progression in all beams can be seen during early stages (in the first 20 minutes) of fire exposure due to almost identical rise in cross-sectional temperatures. During this early stage of fire exposure, deflection rise is mainly governed by the level of applied loading and the thermal gradients that develop within the beam cross-section. As fire exposure progresses further, cross-sectional temperature within the beam rise and thermal gradients decrease along the depth. Mid-span deflection in beams continues to increase, but at relatively low rate, owing to gradual reduction in mechanical properties, especially elastic modulus of reinforcing steel. At this stage, HSC beams B1 and B2 (exposed to fire scenarios SF1 and LF1 respectively) experience more severe heating than NSC beams B3, B4, B5, and B6 (exposed to SF2, SF3, LF2, and LF3) and therefore undergo relatively larger deflections. As expected, beams B1 and B2

experience relatively faster temperature induced strength degradation as they are fabricated using HSC than beams B3, B4, B5, and B6 which are made of NSC.

Mid-span deflections in HSC beams B1 and B2 at the end of respective heating phases, lasting 60 minutes and 120 minutes respectively, were measured to be 15 mm and 35 mm, respectively owing to higher rebar temperatures in the latter case. In case of NSC beams B3 and B4, a higher mid span deflection of about 25 mm occurred in beam B4. as compared to 19 mm in case of beam B3, owing to higher load level in the former case after 90 minutes of heating. For beam B5 and B6 heated for 120 minutes as per ASTM E119 standard fire, almost identical mid span deflections of 25 mm and 27 mm were measured at the end of heating phase. Overall, NSC beams exhibit better response than HSC beams during heating phase of fire exposure.

NSC beam B5 failed at 230 minutes into fire exposure due to excessive deflections (see Figure 3-9), during cooling (decay) phase of fire, when furnace temperature dropped to 500°C (almost to half of its peak value). Consequently, the rebar temperatures also exhibited a decaying trend prior to failure and dropped by almost 60°C from their peak value. Nonetheless, rebar temperatures remained in excess of 500°C for almost 130 minutes prior to failure due to slower rate of cooling adopted in fire scenario LF2. Besides sustained temperature increase beyond 500°C, post-failure investigation indicated spalling in the cover region, combined with rupture of two of the three tensile rebar indicating excessive deflection (strain) in the mid-span region of the beam. Thus, although fire temperatures decayed substantially, reinforcing steel remained at temperatures in excess of 500°C wherein mechanical and creep strains in rebar increase at a significant rate resulting in large deflections and subsequent failure. Since beam B5 could not sustain applied loading throughout the duration of fire exposure (including cooling phase), it was deemed to have failed during Stage 2 of testing itself and was not tested for residual capacity in Stage 3 of testing.

HSC beams B1 and B2, as well as NSC beams B3, B4 and B6 did not fail during fire exposure. Progression of mid-span deflection in beams B1, B2, B3, B4, and B6 during cooling phase is also plotted in Figure 3-5. Correlating deflection progression in the beams with corresponding crosssectional temperatures plotted in Figure 3-3a-c, it can be inferred that level of mid-span deflection is influenced by the peak temperatures experienced in the tensile rebars, type of concrete (HSC or NSC), and load level on corresponding beam. For beam B1, mid-span deflection continues to increase until about 130 minutes into fire exposure, as the tensile rebar temperatures in the beam stay above 350°C. Similarly, mid-span deflection in beam B3, heated for 90 minutes, continues to increase until about 180 minutes into fire exposure, as long as rebar temperatures remain above, 350°C. Thus, there is a noticeable lag between recovery in mid-span deflections, and decay in tensile rebar temperatures which can be attributed to an almost 25% reduction in elastic modulus of reinforcing steel when experiencing temperatures in excess of 350°C (EN 1992-1-2 2004). Consequently, mid-span deflections begin to recover only after rebar temperatures drop below 350°C and reinforcing steel regains most of its original room temperature elastic modulus (stiffness). Also, it is important to note that peak mid-span deflection attained in both beams is almost identical (see Table 3-3) despite rebar temperatures in beam B3 being higher by almost 100°C than beam B1, due to slower rate of temperature induced mechanical property degradation in NSC as compared to that in HSC. In addition, the influence of load level on peak mid-span deflections can be seen in deflection response of NSC beams B3 and B4. An increased load level of about 20% present in beam B4 as compared to the load on beam B3 resulted in peak mid-span deflection to increase by almost 70% and this is mainly due to early yielding of steel reinforcement and increased mechanical and creep strains due to higher stress level present in beam B4. Furthermore, the rate of cooling adopted during fire exposure also affects level of recovery seen

in the fire exposed RC beams, as seen in beams B3 and B6. Although beam B3 experiences heating for 90 minutes, as compared to beam B6 heated for 120 minutes, recovery in mid-span deflections is relatively lower due to slower cooling adopted in the former case.

All five beams that did not fail during fire exposure attain a steady state mid-span deflection as rebar temperatures cool down to below 150°C. Significant residual deflection is left over in each of the fire exposed beams, and the beams do not completely revert back to their pre-fire configuration even after complete cool down. This is primarily due to irreversible temperature induced damage in concrete, which does not recover any of its strength and stiffness properties upon cool down to ambient conditions, as well as residual plastic strains in steel reinforcement and concrete. These residual deflections, with no load acting on the beams, were measured to be 6 mm, 12 mm, 14 mm, 27 mm, and 10 mm in beams B1, B2, B3, B4, and B6 respectively. Peak rebar temperature as well as rate of cooling and load level present, influence extent of residual deflections in beams following fire exposure. Residual deflection in HSC beam B2 which experienced greater peak rebar temperatures by about 200°C as compared to HSC beam B1, are greater by almost double than that measured in beam B1. The effect of cooling on extent of residual deflections can also be gauged by comparing response of NSC beams B3 and B6 which were cooled at different rates. Lower residual deflections result in NSC beam B6, as compared to NSC beam B3, due to the faster cooling adopted in the latter case. Besides rate of cooling, load level present during cooling phase also affects the magnitude of post-fire residual deflections. Residual deflections in HSC beam B2 are comparable to those measured in NSC beam B3, even though beam B3 experienced lower rebar temperatures by about 100°C. This can be attributed to the fact that load was maintained constant throughout the extended cooldown of the beam resulting in significant irreversible load induced thermal (creep) strains that did not recover during cooldown.

Furthermore, residual deflections in beam B4 subject to a higher load level by about 20% as compared to beam B3 subject to an almost identical fire exposure scenario were almost twice than those measured in the latter case. It is crucial to note that applied load was removed in beam B1 after 180 minutes during cooling phase, and after 300 minutes into fire exposure for beam B2, as rebar temperatures dropped below 300°C for both beams. However, the applied load was maintained constant for beams B3, B4 and B6 until they cooled down completely to ambient conditions. This difference in the unloading process of the beams B1 and B2 during Stage 2 of testing, combined with rapid cooling rate can be attributed to the significantly lower mid-span deflections as compared to residual deflections measured in beams B3, B4, and B6.

Therefore, beams B1, B2, B3, B4, and B6 did not fail during fire exposure as per applicable failure limit states according to ASTM E119 (ASTM 2007), and applied loads were removed to measure post-fire residual deflections. Residual capacity of these beams that did not fail during fire exposure was evaluated in Stage 3 of testing as described in the following section.

3.6.2.3 Temperature induced spalling

The extent of early stage (explosive) spalling in both HSC and NSC beams during fire exposure (heating phase) was monitored by taking visual observations through windows located on the sides of the furnace. Such type of early spalling, often occurs in HSC members, within the first 20 minutes of fire exposure (Dwaikat and Kodur 2009a; Hertz 2003; Kodur 2000; Kodur and Phan 2007) under rapid heating conditions with free water, coupled with moisture gradients in concrete, being the primary driving factors. Observations from fire tests indicated no explosive spalling in any of the tested beams. Beams B1 and B2 did not experience any noticeable spalling in spite of being made from HSC and this could be attributed to low free water (moisture content) present in the beams resulting from a prolonged storage period of about 8 years after fabrication. Since

moisture gradients that develop during heating are the main reason for explosive spalling, low moisture content within the beam prevented any explosive spalling. In case of NSC beams B3, B4, B5, and B6, no spalling occurred due to relatively higher permeability of NSC which prevented build-up of excessive pore pressure within the concrete layers.

No spalling was seen in the tested beams, even after fire temperatures begin to decay in the cooling period. Nonetheless, upon examination of fire exposed beams, 24 hours after fire exposure as they cooled down to ambient conditions, it was seen that the beams underwent some level of spalling during cooling phase. HSC beams, having lower water to cement ratio, underwent significant spalling confined to the bottom convex corners of the beam. This type of late stage spalling, also known as corner spalling or sloughing-off, can be attributed to thermal cracking, combined with thermo-mechanical stresses in the surface giving rise to a crack pattern, where cover concrete in corners fall-off due to stress induced from self-weight (Hertz 2003). In addition, there was significant surface pitting and peeling observed in beams B1 and B2 (see inset photo in Figure 3-10) with chunks of concrete (aggregate) falling-off from the surface as a result of decarbonation that occurs in calcareous aggregates at about 700°C (Razafinjato and Beaucour 2016). This damage occured in the beam as the Calcium Oxide (CaO) formed by decarbonation of calcite, rehydrated under ambient conditions and expanded, causing existing microcracks in concrete to widen (Razafinjato and Beaucour 2016; Xing et al. 2013). The extent of such damage was proportional to severity of fire exposure, with the volume of spalling in HSC beam B2 (experiencing higher cross-sectional temperatures) almost twice as that measured in beam HSC B1 (experiencing relatively lower cross-sectional temperatures). Also, chunks of aggregate continued to dislodge from the beam during the one-week storage period (prior to residual testing) after fire exposure.

Significant spalling in the cover region, with reinforcement exposed, was seen in beam B5 which failed during cooling phase of fire exposure. Nonetheless, this spalling occurred just prior to the failure of beam B5 (during fire exposure) and was caused due to the sudden rupture of tensile rebar. Besides this cover spalling prior to failure of the beam, no surface pitting and very limited corner spalling was seen in the NSC beams upon cool down to ambient conditions; i.e. 24 hours after fire exposure. This can be attributed to higher moisture content present in the NSC, as well as presence of much higher free water in capillary pores as compared to that in HSC. Majority of corner spalling in NSC beams was seen to occur in the fire exposed (bottom) convex corners of the beam, while it was stored under ambient conditions for a period of one week before prior to undertaking residual capacity tests. Minimal temperature-induced spalling (less than 0.1% of total beam volume) occurred in beams B3, B4 and B6, relative to spalling in beams B1 and B2, but the mechanism of spalling in all beams during cool down was similar, and could be attributed to a large volume expansion of decarbonated calcite resulting in debonding of carbonate aggregates from the cementitious concrete matrix, combined with radial cracking (Razafinjato and Beaucour 2016; Xing et al. 2013).

Surface pitting and corner spalling did not reach the tension rebar level in any of the beams B1, B2, B3, B4 or B6. Nonetheless, such type of temperature induced spalling (corner sloughing) can reduce the volume of cover concrete surrounding tensile rebar, and hence lower the extent of tension stiffening effect in concrete resulting in lower post-fire residual capacity. In addition, this type of temperature induced damage limited to the surface of the structural member can influence choice of retrofitting strategies for reinstating such fire damaged RC beams (Alonso 2009).

3.6.3 Residual response of fire damaged beams (Stage 3)

Beam B5, made of NSC, failed during fire exposure due to excessive deflections and hence there was no need to test this beam for residual capacity. Other beams B1, B2, B3, B4, and B6, which

did not fail during fire exposure, were tested for residual capacity evaluation by incrementally loading them to failure. The load-deflection response, progression of cracking, and failure mode were traced during these residual capacity tests.

3.6.3.1 Structural response

The mid-span deflection in each tested beam was measured through LVDTs installed on the beams. The measured load-deflection response for beams, B1, B2, B3, B4, and B6 is plotted in Figure 3-10. Beams B1 and B2 made of HSC, depict four phases in deflection progression i.e., linear response (marked as A-B in Figure 3-10), onset of yielding in steel reinforcement (marked as B in Figure 3-10), plastic deformation with strain hardening of steel reinforcement (marked as B-C in Figure 3-10), and finally, crushing of concrete located at extreme compression fiber immediately followed by plastic deformation until failure (marked as D-E in Figure 3-10). Beams B3, B4 and B6 made of NSC however, exhibit only three key phases in deflection progression i.e., linear response (marked as A'-B' in Figure 3-10), onset of yielding in steel reinforcement (marked as B' in Figure 3-10), and plastic deformation with strain softening until failure (marked as B'-C' in Figure 3-10).

In the first phase for both HSC beams (see A-B in Figure 3-10) and NSC (see A'-B' in Figure 3-10), load-deflection response of fire damaged beams follow a linear progression as seen in a cracked section, until the onset of yielding in steel reinforcement. This can be attributed to extensive tensile cracking and temperature induced material degradation that occur in the beams during fire exposure. In case of the HSC beams, the stiffness of beam B1 is about 20% greater than beam B2 (see Figure 3-10) owing to higher temperature (fire) induced damage in the latter case. Also, stiffness of HSC beam B2 is greater than any of the NSC beams B3, B4 and B6, despite experiencing lower peak rebar temperatures by almost 80°C. This can be attributed to lower room

temperature strength and stiffness properties of NSC as compared to HSC, as well as greater level of damage arising from slower cooling and sustained loading adopted in case of beams B3, B4, and B6. Furthermore, the stiffness of NSC beam B3 is almost 10% higher than beam B4 which was subjected to a higher load level. This is despite the fact that compressive strength of cores drilled from unaffected support zones of beam B4 was almost 8% higher compared to those from beam B3. This indicates that higher load level present during fire exposure has detrimental effect on residual stiffness of fire damaged RC beams. Thus, stiffness of the fire exposed RC beams is governed by peak temperatures experienced in the cross-section, and type of concrete (concrete strength), and level of loading present on beams during fire exposure.

The second phase of load-deflection response is characterized by onset of yielding in tensile steel reinforcement. In case of HSC beams, onset of yielding occurs at a load of 99 kN in beam B1, and approximately 90 kN in beam B2. This reduction in load at which yield occurs can be attributed irrecoverable reduction in yield strength of reinforcing steel, as well as compressive strength of concrete due to higher cross-sectional temperatures experienced in beam B2 as compared to beam B1. In fact, peak rebar temperatures in beam B2 exceeded 500°C unlike those experienced in beam B1 which remained below 400°C, and reinforcing steel recovered only part of its yield strength (Neves et al. 1996b). In case of NSC beams B3, B4, and B6, which experienced peak rebar temperatures of 521°C, 510°C and 500°C respectively, yielding occurred at a load of 91 kN, 99 kN, and 93 kN respectively. Counterintuitively, beam B4 which was subject to greater load level during fire exposure yielded at a higher load, by about 10%, as compared to beam B3 exposed to identical fire exposure. This can partly be attributed to higher compressive strength of concrete in beam B4, as well as relatively lower peak rebar temperatures experienced in the beam. It should also be noted that HSC beam B2 which experienced greatest magnitude of peak rebar temperatures

yielded at similar loads, as compared to NSC beams B3, B4 and B6 which experienced significantly lower rebar temperatures. This can be attributed to higher (room temperature) concrete strength of HSC beam B2, as compared to that of NSC beams B3 B4, and B6. Thus, peak rebar temperature attained during fire exposure and concrete strength determine yielding load of HSC and NSC beams. However, the effect of load level on yield load of fire damaged RC beams was found to be very limited.

Once yielding occurred, HSC beams B1 and B2 exhibited a strain hardening response with a sustained increase in load level as mid-span deflection increase (see B-C in Figure 3-10) in the third phase. On the contrary, NSC beams (B3, B4 and B6) exhibited a strain softening response after yielding (see B'-C' in Figure 3-10). The different response in two groups of beams is primarily due to higher compressive strength concrete in HSC beams. In fact, compression rebars in NSC beams experienced buckling soon after yielding of tensile steel reinforcement, as concrete under compression in top layer fail and experience crushing. HSC beams did not fail during the third phase of load-deflection progression, with load carrying capacity of beams B1 and B2 increasing by almost 12%. On the other hand, both NSC beams B3, B4, and B6 failed, due to crushing of concrete under compression and buckling of compressive reinforcement. Therefore, strain hardening of steel reinforcement has significant influence on post-yielding response of HSC beams than NSC beams.

HSC beams B1 and B2, exhibited a fourth phase of load-deflection response (marked as D-E in Figure 3-10) characterized by a sudden drop in load carrying capacity, of about 18% in beam B1, and 19% in beam B2 and accompanied with visible crushing of concrete at the extreme (top) compression layers. This crushing of concrete under compression led to redistribution of internal forces within the section, and thus the beam continued to deflect in a plastic fashion until failure,

i.e. when the beam could not resist any further increment in applied loading. In case of beams B3, B4 and B6 however, a progressive decrease in load level is seen as soon as extreme compression fiber underwent crushing. Thus, sufficient compressive cross-section was not available in case of NSC beams for redistribution of internal forces as seen in HSC beams following crushing failure of concrete in the compression face.

The peak load in beams B1, B2, B3, B4, and B6, prior to failure, was measured to be 112 kN, 102 kN, 91 kN, 99 kN, and 93 kN respectively. These peak residual load capacity values represent a recovery of 70%, 64%, 65%, 70%, and 66% respectively with respect to actual (not design) room temperature capacity of tested beams, calculated to be 160 kN for HSC beams, and 140 for NSC beams, when accounting for tension stiffening in concrete and strain hardening in steel reinforcement (Kodur and Agrawal 2016a). However, the measured residual capacity of all five beams is comparable to the computed room temperature design capacity of 92.7 kN for NSC beams and 94.5 kN for HSC beams, computed as per ACI 318 (ACI 2008). Thus, following a fire incident, fire damaged beams may satisfy design limit state from strength consideration, but need to be retrofitted to arrive at comparable level of safety (capacity) as existed prior to the fire incident.

3.6.3.2 Crack patterns and failure modes

In order to illustrate the influence of concrete type (strength), fire exposure scenario and load level on extent of fire damage and failure modes during residual capacity tests, observed crack patterns during residual capacity tests for beams B1, B2, B3, and B4 are shown in **Error! Reference source n ot found.**a-h. Flexural failure is said to have occurred if crushing (compressive cracking) at the upper surface of the specimen or yielding of tensile reinforcement occurred. Beam B5 is not discussed in this section as it failed during fire exposure and was not tested for residual capacity.

Also, crack patterns for beam B6 were very similar to beams B3 and B4 and hence have been omitted to avoid repetition.

Upon cool down to ambient conditions, 24 hours after fire exposure, vertical cracks were seen in all four beams (B1, B2, B3, and B4) especially between the points of load application and fire exposed span. These flexural cracks resulted from structural loading applied during fire exposure and temperature induced degradation in tensile strength of concrete during fire exposure. Due to surface condition of HSC beams (B1 and B2), it was not possible to record the crack width and spacing of these flexural cracks after cool down of these beams. However, observations from NSC beams B3 and B4 indicated that these cracks were less than 0.05 mm wide with an average spacing of 150 mm, coinciding with the placement of stirrups. Also, increasing load level in case of NSC beam B4 resulted in marginally wider cracks that extended deeper towards the top face of the beam. Minor shear cracks with crack width less than 0.05 mm were also observed in all four tested beams indicating some loss in shear capacity due to fire exposure.

In addition to flexural cracks, tensile splitting cracks along the length of the reinforcing bars were seen primarily in HSC beams B1 and B2 after they cooled down to room temperature. For beam B1, these tensile splitting cracks (see Error! Reference source not found.a) were about 0.8 mm. F or beam B2 subject to a more severe fire exposure, these tensile splitting cracks (see Error! Reference source not found.b) were significantly wider and measured to be almost 1.5 mm in width. This indicates that these tensile cracks were formed due to differential thermal expansion between rebar and HSC, particularly when rebar temperature exceeded 500°C, coupled with temperature induced degradation in tensile and bond strength of concrete (Huang 2010b; Kodur and Agrawal 2017b; Panedpojaman and Pothisiri 2014a; Pothisiri and Panedpojaman 2012b). These tensile splitting cracks were not visible during heating phase of fire exposure in beams B1

and B2 and developed during the cooling (decay) phase of fire exposure. Such tensile splitting cracks were not seen in NSC beams B3 and B4 (and B6) indicating differential thermal expansion between NSC and rebar may not be as significant as in the case of HSC. However, significant surface crazing was observed on the beam surface typically observed in concrete structural members exposed to fire.

All five beams failed in flexural mode, resulting from crushing of concrete in extreme compressive fibers (top layers) of the beam cross section, as seen in Error! Reference source not found.e-h. I n case of HSC beams B1 and B2, flexural crack patterns were governed by temperature induced degradation experienced during fire exposure. For HSC beam B1, average spacing of flexural cracks was approximately 110 mm having a maximum width of 1 mm. Flexural cracks were spaced relatively farther in HSC beam B2 at approximately 160 mm and having a greater crack width of about 2.5 mm at failure. The differences in flexural cracking patterns for beams B1 and B2 were a consequence of different levels of temperature induced bond degradation at the rebar-concrete interface. Beam B1 experienced lower sectional temperatures closer to fire exposed layers of concrete, and hence higher level of bond strength is retained at rebar-concrete interface. Therefore, tensile stresses developed in rebars could be transferred more effectively to surrounding concrete, resulting in cracks that are smaller in width and closely spaced. On the other hand, due to higher levels of temperature induced bond degradation leading to lower bond strength, wider flexural cracks with further spacing occurred in beam B2.

For NSC beams B3 and B4 (and B6) however, while there was no loss of bond between rebar and concrete, presence of pre-existing cracks due to differential expansion between rebar and concrete, as well as significant loss in tensile strength of concrete surrounding rebar governed cracking pattern at failure. Pre-existing tensile cracks in the NSC beams widened prior to failure.

Furthermore, these cracks were located close to stirrups in the beams and did not vary greatly with different fire exposure and load levels. For NSC beams B3 and B4 (and B6) flexural cracks had a similar average crack spacing of 80 mm with maximum width of about 0.8 mm at failure.

3.7 Summary

Both material level and structural level tests were conducted to evaluate residual capacity of fire damaged HSC and NSC beams. The following observations can be drawn based on presented results:

- Concrete type (compressive strength) and peak interfacial temperature influence
 extent of deterioration in bond strength between rebar and concrete. This deterioration
 occurs at a more rapid rate for high strength concrete than normal strength concrete
 specimens.
- A three-stage procedure is needed to capture key parameters in evaluating residual capacity of fire damaged beams. The approach comprises of evaluating response in three sequential stages, namely, during pre-fire exposure condition; during fire exposure comprising of heating and cooling phases of fire, followed by complete cool down of the member to ambient temperature; and then finally during residual conditions after cooldown.
- Duration of heating, rate of cooling during fire exposure, and compressive strength of
 concrete, have significant influence on residual capacity of fire damaged concrete
 beams. Longer heating duration (followed by slower rate of cooling) results in higher
 temperature induced degradation in rebar and concrete, resulting in lower residual
 capacity.

- Cooling phase adopted in fire exposure scenario is a critical parameter that can influence residual capacity of fire damaged beams significantly. Abrupt failure of RC beams can occur during cooling phase of fire exposure when the cooling (phase) is at a slower rate (about -6°C per minute) following rapid heating phase in a severe fire. Alternatively, a rapid cooling rate (about -80°C per minute) can result in significant recovery under similar loading and heating conditions.
- Irrecoverable plastic deformations develop in concrete beams during cool down following fire exposure. The level of deformation is directly proportional to peak rebar temperatures experienced within the concrete beam if load level is maintained constant. Further, these deformations are significantly larger for higher load level during fire exposure, and if applied load is maintained during cooling phase of fire exposure.
- Fire exposed concrete beams recover significant flexural capacity with respect to their
 design capacity, provided rebar temperatures do not exceed 500°C. Due to higher
 compressive strength of concrete, HSC beams retain higher residual capacity
 following fire exposure, as compared to NSC beams, provided no early stage spalling
 of concrete occurs during fire exposure.

Table 3-1. Concrete batch mix proportions used in fabrication of RC beams

Mix design	NSC	HSC
Beams fabricated	B1 and	B3, B4, B5
Total cement (kg/m ³)	B2 512.5	and B6 389.9
Silica fume (kg/m³)	42.7	NA
Water (kg/m ³)	129.8	156.4
Coarse aggregate (maximum size 25 mm)	1078.4	1036.9
Fine aggregate (kg/m ³)	684.3	830.1
Water reducing agent (kg/m ³)	15.0	1.9
Slump (mm)	100	100
Water/cement ratio	0.25	0.4
Air content %	2.7	1.7
Unit weight (kg/m ³)	2463	2415
Design compressive strength: MPa	103	42
28-day compressive strength: MPa	93 ± 0.3	58.6 ± 0.2
Test day compressive strength: MPa	106	62

Table 3-2. Test parameters varied in residual capacity tests

Beam designation		Concrete type	Support conditions	Fire resistance (ACI 2016): min		humidity	content	Measured fire resistance (min)	Volume	
B1	SF1				50(53%)	72	2.1	No Failure	3.2	
B2	LF1	HSC	SS	90	50(53%)	774	2.2	No Failure	1.5	
В3	SF2	NSC				50(53%)	91.8	2.6	No Failure	0.1
B4	SF3				60 (65%)	87.5	2.5	No Failure	0.1	
B5	LF2				50(53%)	86.6	2.5	230	0.5	
B6	LF3				50(53%)	89.8	2.6	No failure	0.1	

Table 3-3. Summary of measured response parameters for tested RC beams

Beam designation	Design (actual) capacity: kN	Peak rebar temperature: °C	Peak mid-span deflection: mm	Residual deformation: mm	Residual capacity: kN (% ratio)
B1 (SF1)	94 (160)	387	33	6	112 (70%)
B2 (LF1)		592	53	11	102 (64%)
B3 (SF2)	94 (140)	521	31	14	91 (65%)
B4 (SF3)		510	54	27	99 (70%)
B5 (LF2)		580	122	-	-
B6 (LF3)		500	54	27	93 (66%)

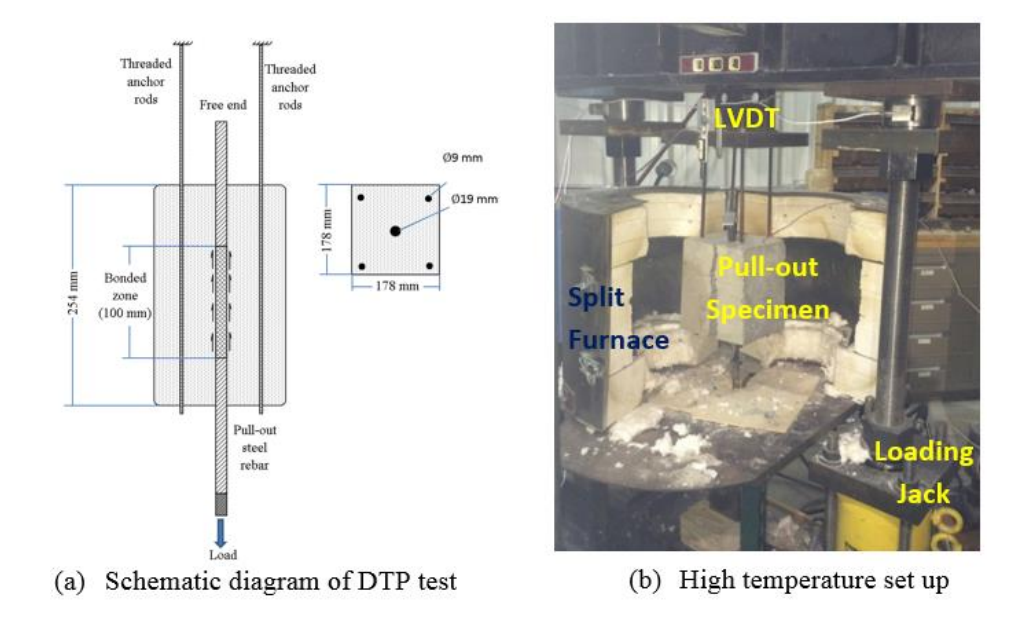


Figure 3-1. Test setup for residual bond strength tests after exposure to high temperature

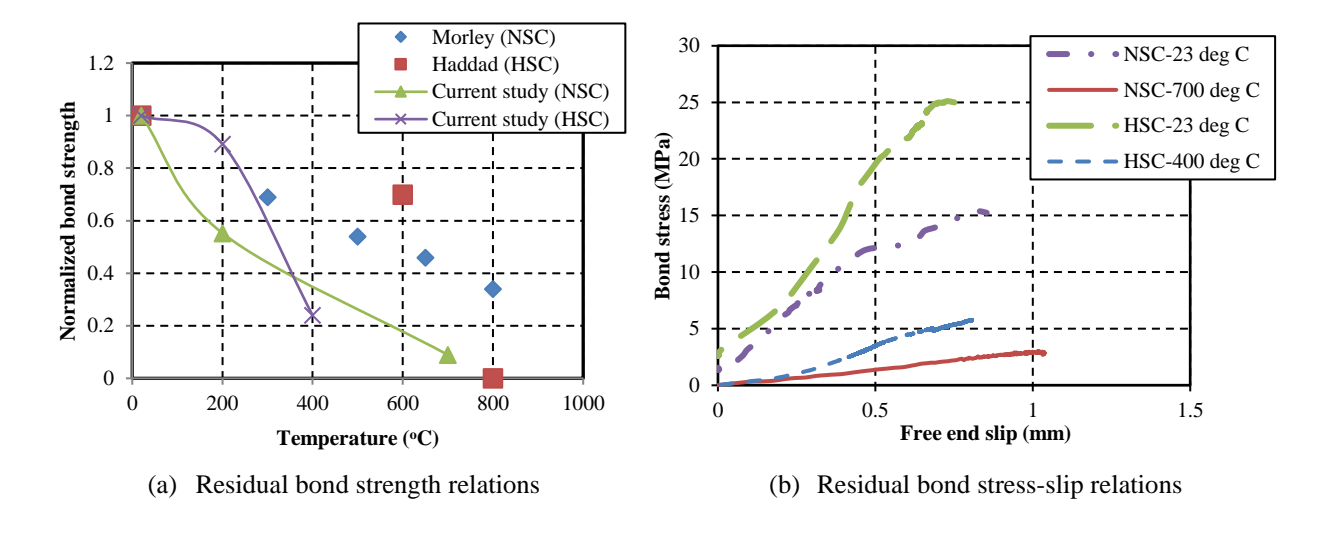


Figure 3-2. Test data from DTP tests after exposure to high temperature for NSC and HSC specimens



(a) Normal strength concrete (NSC) specimens

400°C



(b) High strength concrete (HSC) specimens

Figure 3-3. Failure modes in NSC and HSC specimens at different temperatures

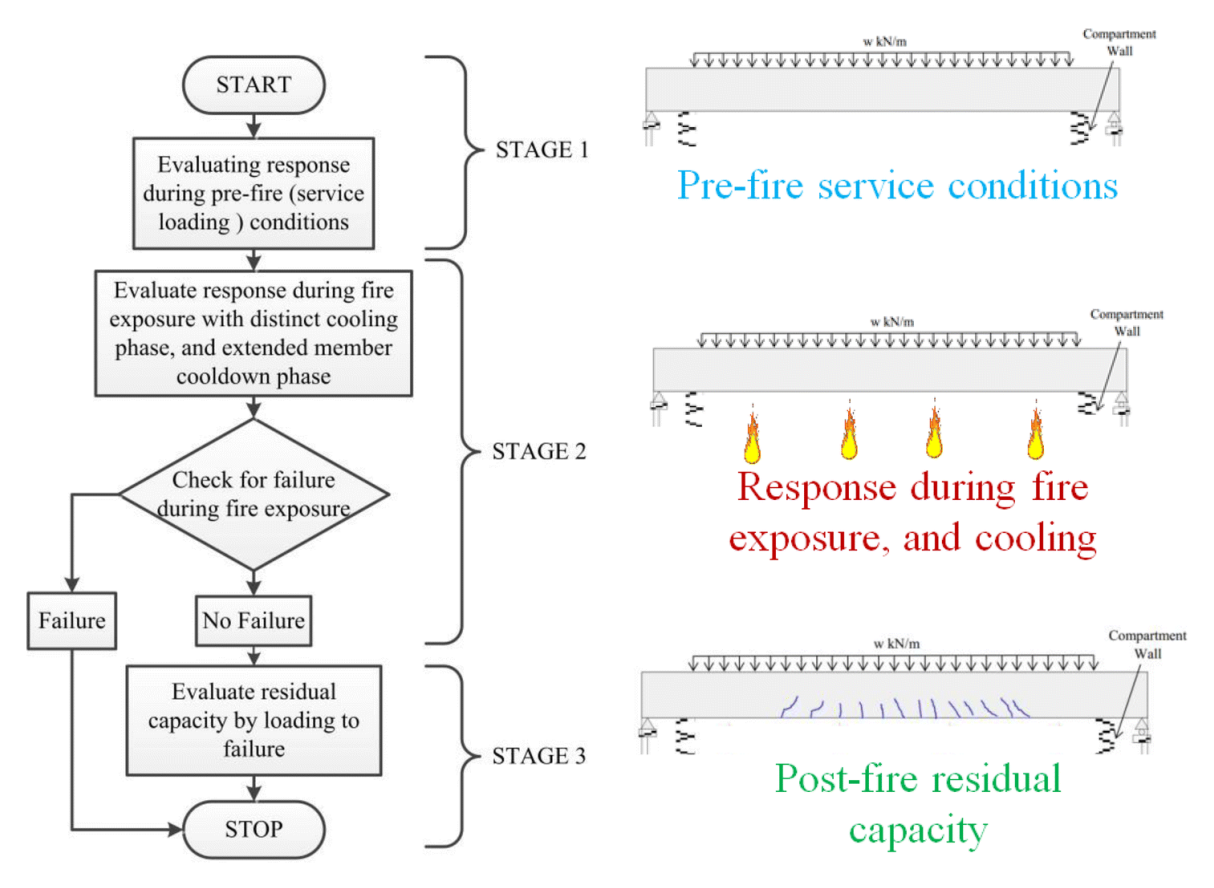
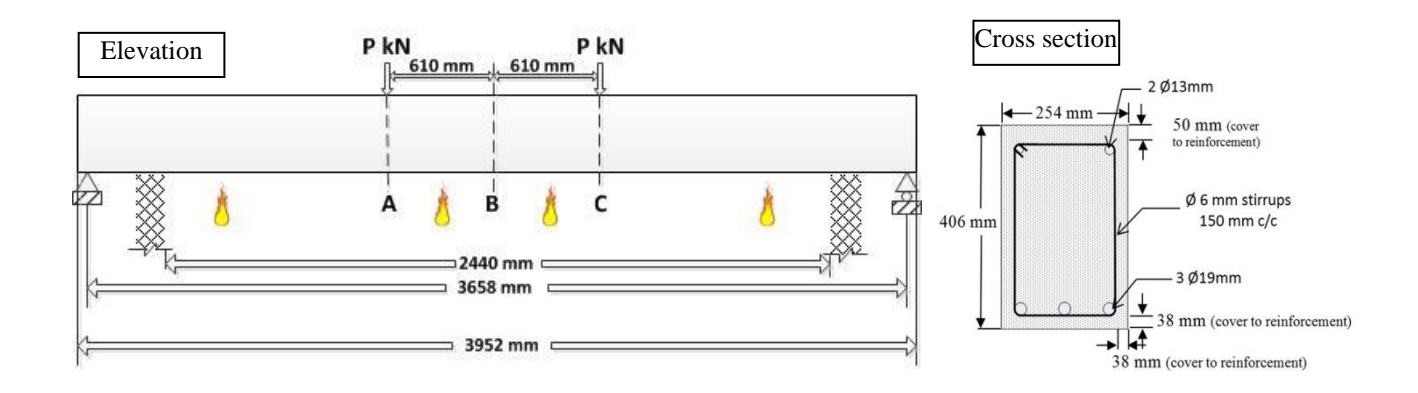


Figure 3-4. Flow chart illustrating proposed three stage approach for residual capacity assessment of RC structural members



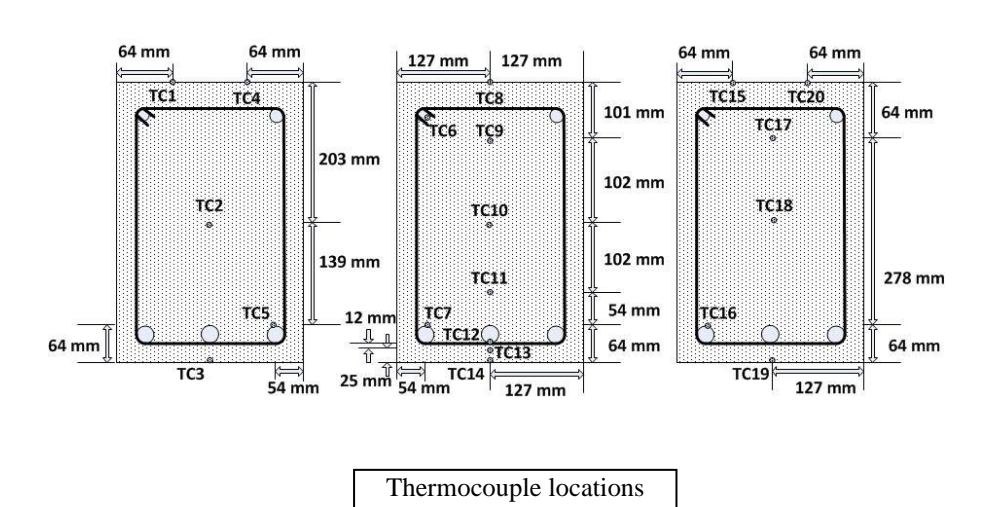


Figure 3-5. Loading reinforcement, and instrumentation details of tested RC beams

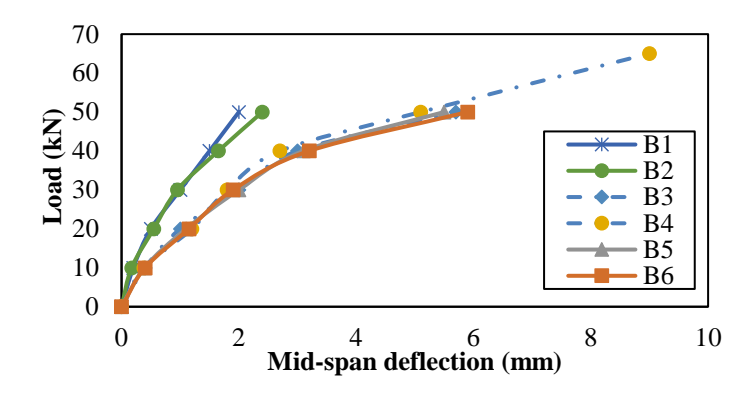


Figure 3-6. Response of RC beams during Stage-1 loading at room temperature.

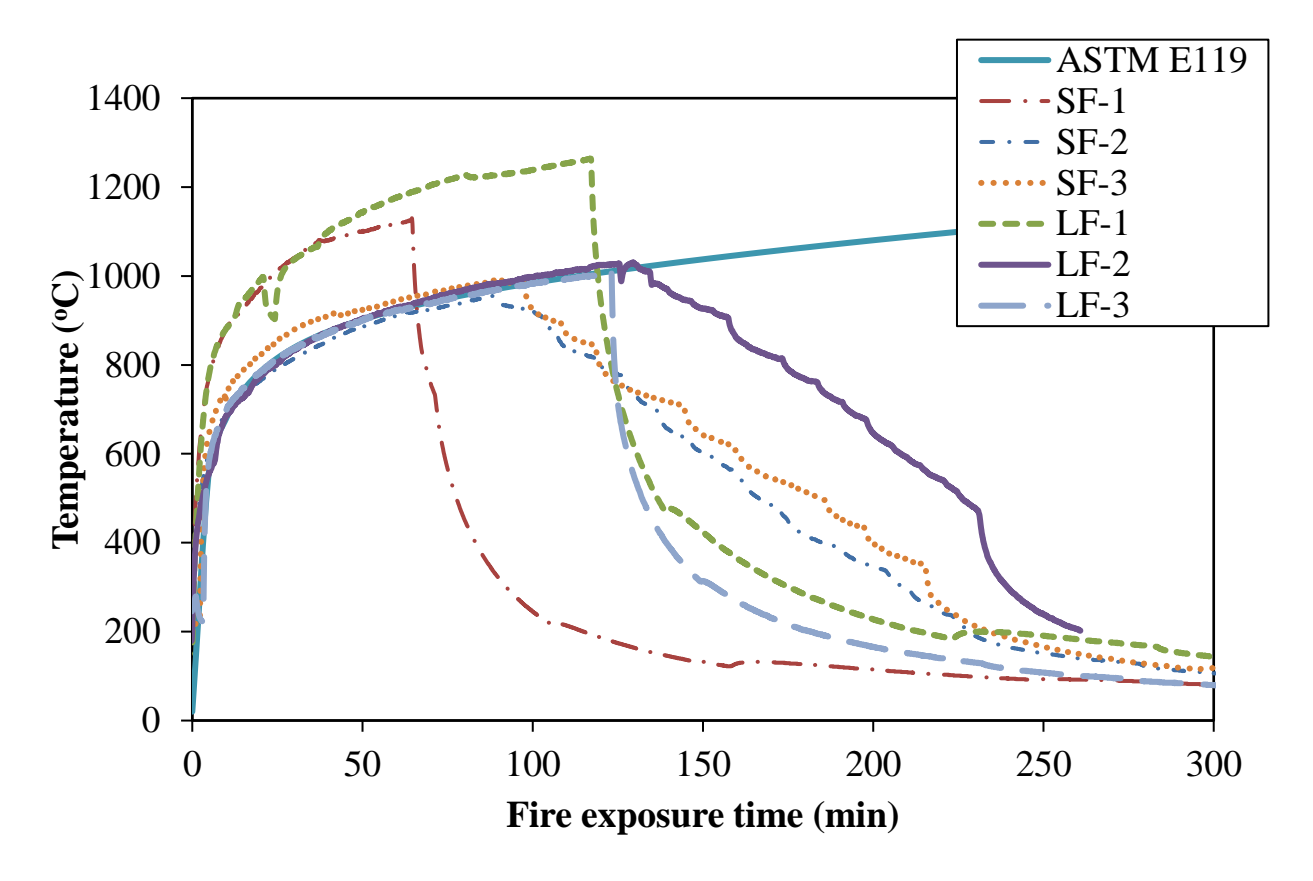
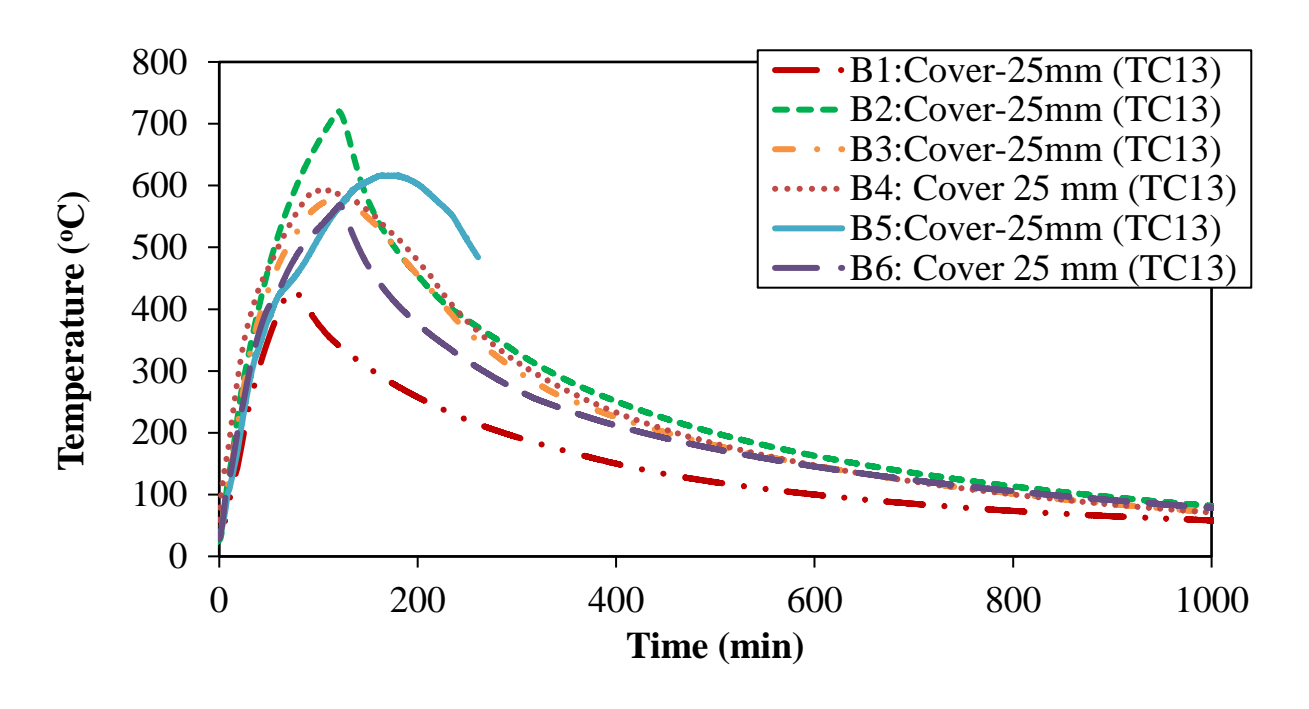
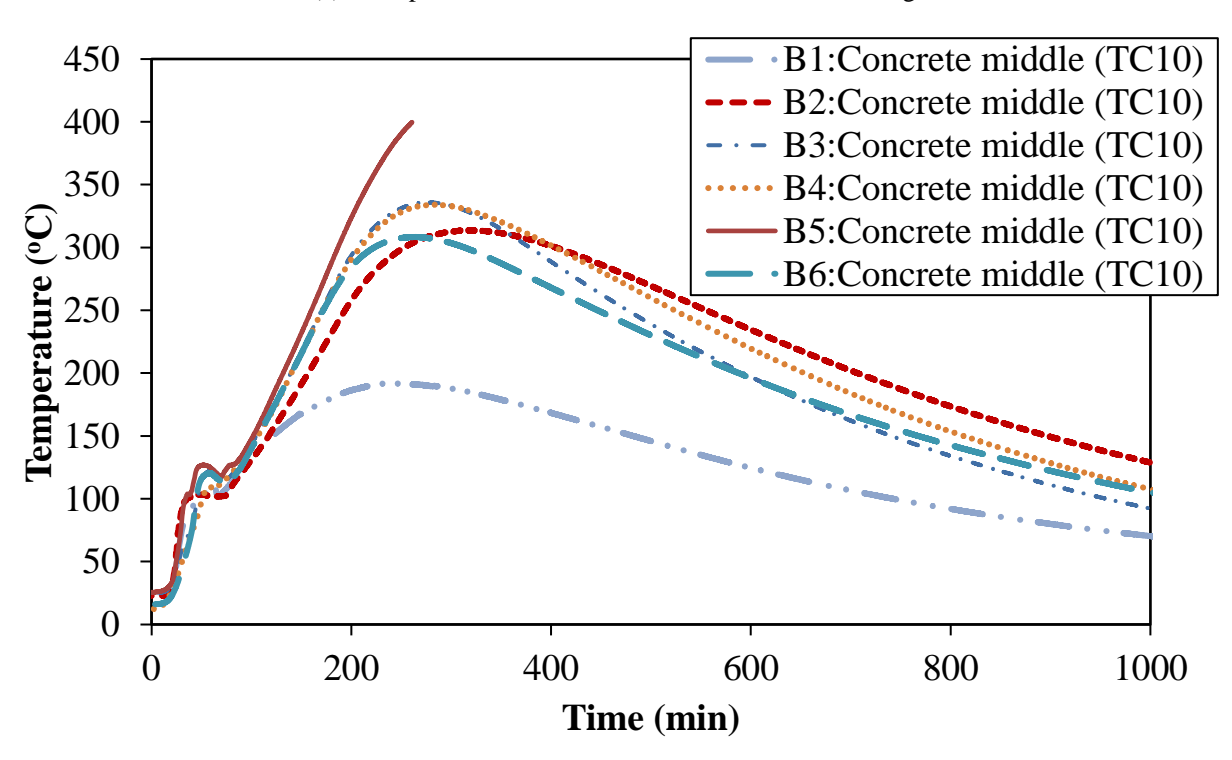


Figure 3-7. Time—temperature curves for fire scenarios used in the fire tests



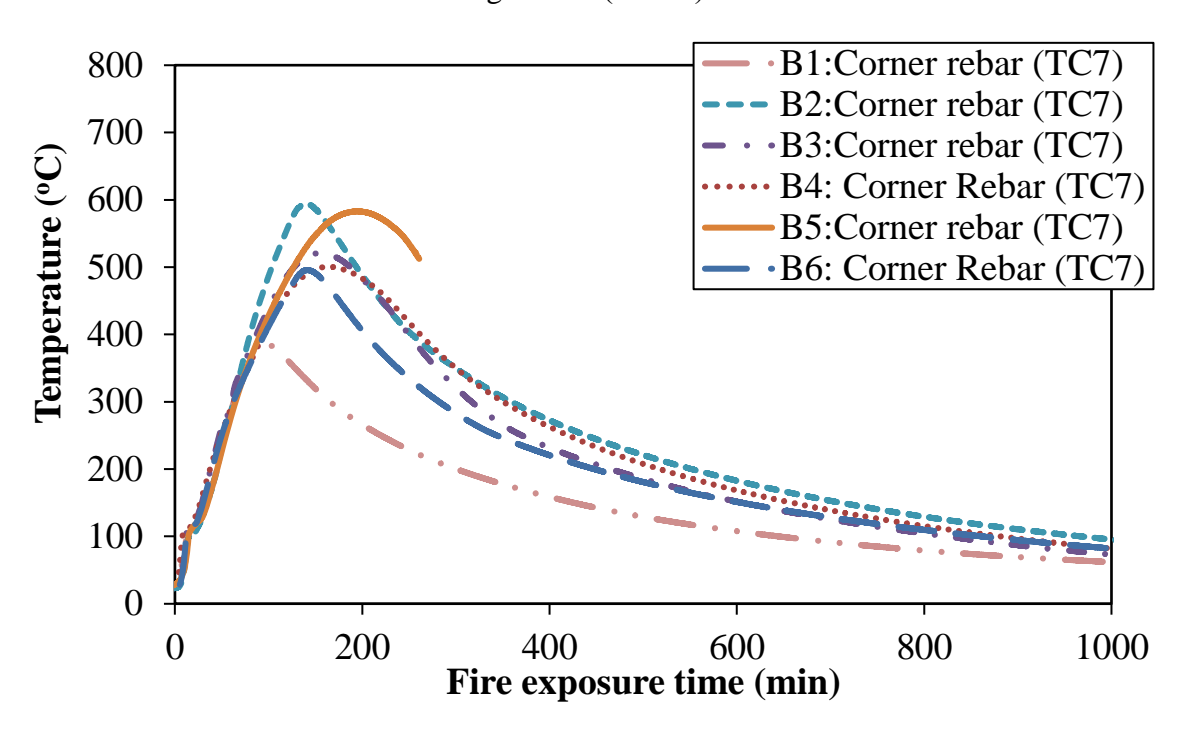
(a) Temperatures in concrete cover for beams B1through B6



(b) Temperatures in concrete mid-depth for beams B1 through B6

Figure 3-8. Measured rebar and concrete temperatures as a function of fire exposure time for tested RC beams

Figure 3-8 (cont'd).



(c) Temperatures in rebar for beams B1 through B6

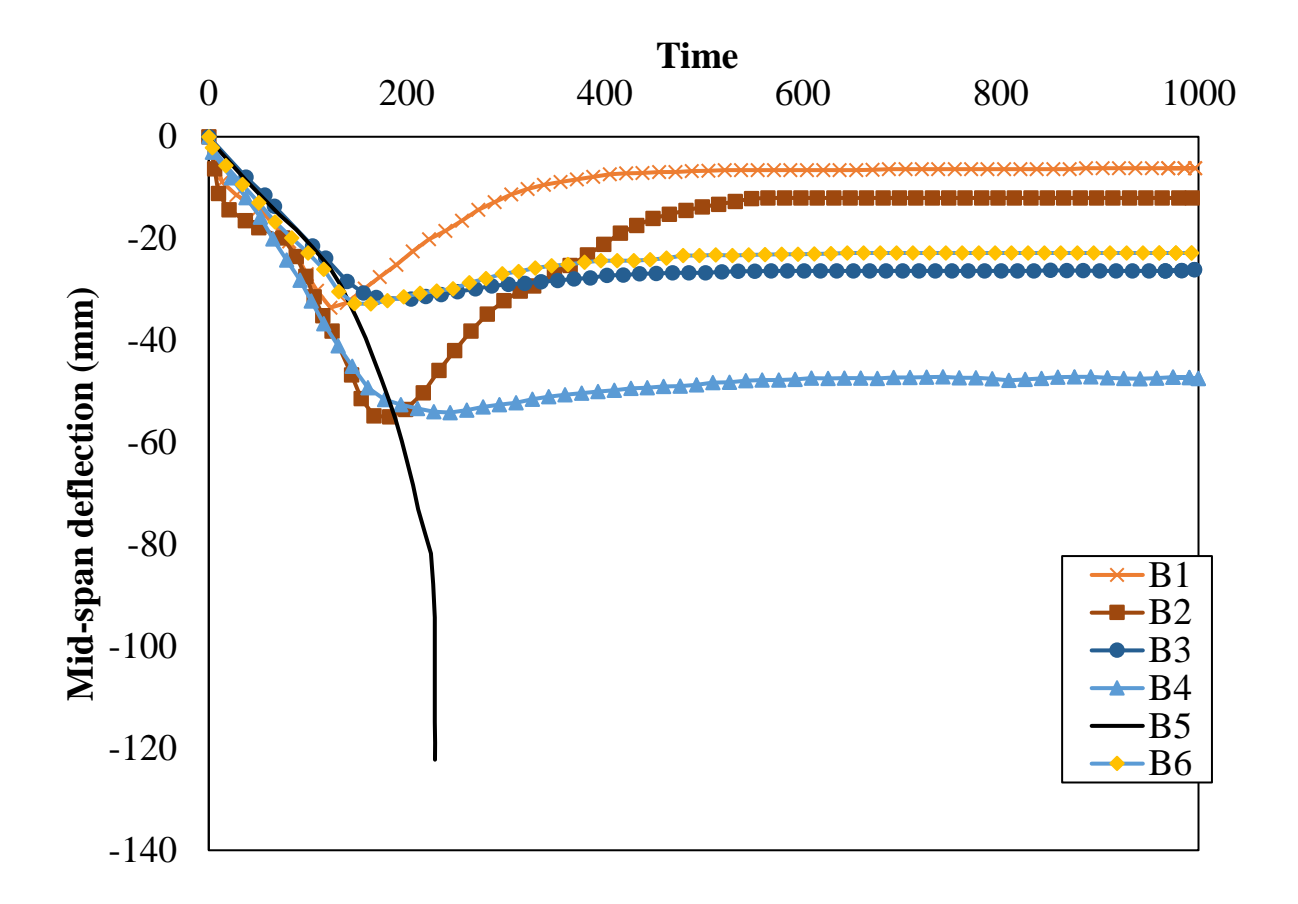


Figure 3-9. Mid-span deflection of beam tested beams as a function of time

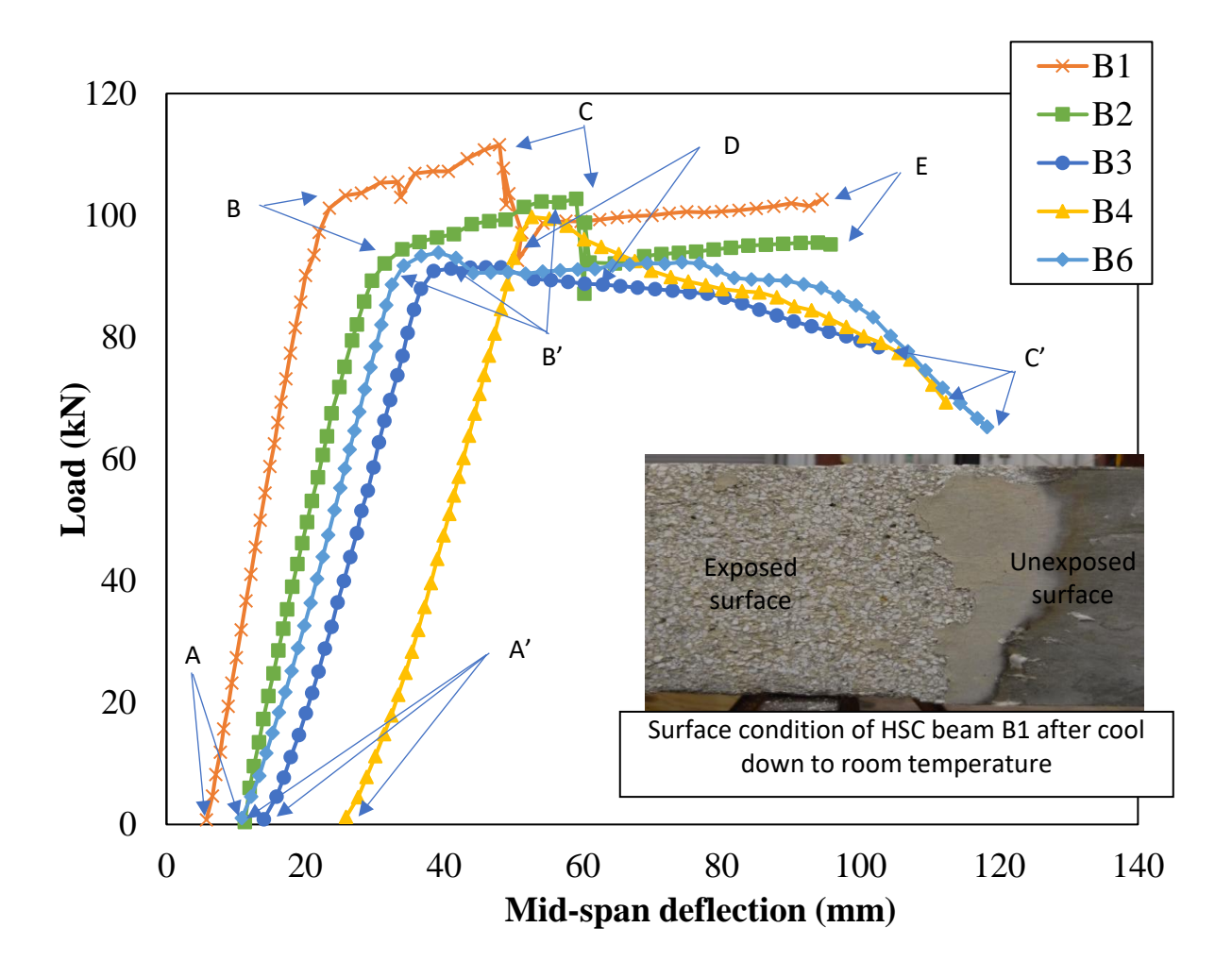


Figure 3-10. Load-deflection response of fire damaged RC beams in residual strength tests



(a) Beam B1 at the beginning of residual tests



(b) Beam B2 at the beginning of residual tests



(c) Beam B3 at the beginning of residual tests



(d) Beam B4 at the beginning of residual tests



(e) Beam B1 at failure



(f) Beam B2 at failure

Figure 3-11. Crack and failure patterns in HSC and NSC beams after cool down from fire exposure and after residual capacity tests

Figure 3-11 (cont'd).



(g) Beam B3 at failure



(h) Beam B4 at failure

4 NUMERICAL MODEL AND VALIDATION

4.1 General

Residual capacity of fire damaged concrete members can be calculated through two types of approaches, namely, simplified sectional analysis or advanced numerical models. Simplified sectional approaches are based on modified room-temperature strength equations with appropriate strength reduction factors to account for temperature induced degradation. Such approaches are straightforward to apply but do not account for realistic temperature dependent material properties of concrete and reinforcing steel as seen during cooling, and do not account for full extent of physical damage experienced by the structure resulting from fire exposure.

Alternatively, three-dimensional thermo-mechanical finite element models can be utilized to simulate the behavior of RC beams exposed to elevated temperatures. Such models can account for high temperature material properties and different strain components and generate detailed output parameters to trace the response of fire damaged concrete members. Nonetheless, there is limited information available for developing such numerical models to trace residual response of fire damaged concrete structures. Moreover, none of the previous prediction models accounted for distinct material properties specific to cooling (decay) phase of fire exposure. In addition, effect of service conditions (load level, extent of cracking etc.) present prior to and during fire exposure, as well as influence of residual deflections occurred during fire exposure on residual capacity of fire exposed concrete members is not addressed in any of the previous studies.

To overcome some of the above drawbacks, an approach for predicting residual capacity and residual deflections of fire exposed RC beams is proposed (Kodur and Agrawal 2016b, 2020). The novelty of the current approach lies in the consideration of distinct material properties of

reinforcing steel and concrete during heating and cooling phases of fire exposure and residual (after cool down) phase, as well as in incorporation of plastic deflections occurring during fire exposure of RC beams into post-fire response analysis. A finite element based numerical model to trace the complete response of concrete members from pre-fire exposure stage to post-fire exposure stage after complete cooldown of RC beams is developed in this dissertation.

4.2 Development of finite element model

The extent of structural damage in a fire exposed RC beam is influenced by a number of factors including load level, support conditions, properties of concrete and reinforcement as well as level of fire severity. A general approach and finite element model to evaluate residual capacity of fire damaged concrete beams are discussed in subsequent sections.

4.2.1 General approach

For evaluating post-fire residual response of RC members, three stages of analysis are required to account for all these parameters. The three stages of analysis for evaluating residual capacity of fire exposed RC members comprise of, evaluating actual capacity of the member at room temperature, i.e. prior to fire exposure (Stage 1), fire resistance analysis during exposure to fire; including cooling phase of fire exposure (Stage 2) and finally, post-fire residual analysis after complete cool down of the member (Stage 3). A flow chart in Figure 4-1 illustrates various steps required for evaluating residual strength of fire exposed RC beams. This analysis procedure can be implemented using any finite element based package, such as ABAQUS (Hibbitt, Karlsson & Sorensen 2012a).

In Stage 1, room temperature capacity of the RC beam is evaluated through a detailed finite element analysis by gradually incrementing the load on the structural member till failure occurs. Alternatively, a conservative estimate of ultimate capacity can also be established using specified

strength equations in design standards (ACI 2008). The room temperature capacity determined in Stage 1 can give an idea on the extent of reserve capacity present in the member and is utilized to assess relative load level on the beam prior to fire exposure during Stage 2. Also, the capacity calculated during Stage 1 can be useful to gauge the extent of degradation in capacity in the member following fire exposure. It should be noted that for this stage of analysis, room temperature mechanical properties of concrete and reinforcing steel are to be utilized.

In Stage 2 of the analysis, the response of RC beam is evaluated under a given fire exposure scenario, load level, and boundary conditions. Realistic loads that are present during a typical fire event are to be applied on the beam prior to undertaking thermo-mechanical analysis during fire exposure. The time-temperature curve for the entire duration of fire exposure can be approximated using fire growth models or empirically through parametric curves (EN 1991-1-2 2002). The Stage 2 of the analysis is to be carried out at various time increments till the failure of the beam or till burnout conditions occur. At the end of each time increment, response parameters from thermal and structural analysis are to be utilized to check the state of the RC beam under different failure limit states. In this stage, temperature dependent thermal and mechanical properties of concrete and reinforcing steel, that are distinct during heating and cooling phases of fire exposure, are to be input into ABAQUS (Hibbitt, Karlsson & Sorensen 2012a).

Following the cooling down of the beam, and if there is no failure of the beam in Stage 2, Stage 3 of the analysis is to be carried out. The temperature induced residual stress and strains that exist in the beam after fire exposure are reflected in the form of residual deflections. These residual deflections result from accumulation of damage in the beam due to fire exposure and loading. This state of the beam is the initial state for Stage 3 of analysis. In this stage of the analysis, the cooled down RC beam is loaded incrementally till failure and the structural response of the beam is traced.

The residual capacity corresponds to maximum load that the beam can carry prior to attaining failure. For this analysis, residual properties of concrete and steel reinforcement are required.

The novelty of the three approach developed as part of this dissertation lies in the consideration of distinct material properties of reinforcing steel and concrete during heating and cooling phases of fire exposure and residual (after cool down) phase, as well as in incorporation of plastic deflections occurring during fire exposure of RC beams in to post-fire residual response analysis. The proposed approach is implemented through a detailed numerical model developed in a finite element based computer program ABAQUS (Hibbitt, Karlsson & Sorensen 2012a). The model is validated in different stages by comparing predictions against experimental data generated from published literature (Dwaikat and Kodur 2009c; Kumar and Kumar 2003b), and tests conducted as part of this dissertation.

4.2.2 Modeling assumptions

The following assumptions are made in the development of the numerical model:

Interfacial bond between tensile rebar and concrete is assumed to be perfect i.e., no bond-slip, or modeled explicitly using zero length bond link elements. In cases when perfect bond is assumed, the total strain in the steel reinforcement is assumed to be equal to that in the concrete. The assumption is quite accurate for the compression zone of concrete where no crack occurs. On the contrary, cracks may occur in the tensile zone causing weakness in the bond between concrete and reinforcement, and resulting in some level of slip of tensile reinforcement. However, over a length that includes several cracks (beam segment), the average strain in both the reinforcement and the concrete is approximately equal (Kodur and Dwaikat 2008). In cases when finite bond-slip is assumed, zero length bond-link elements are applied to appropriately model temperature dependent bond-slip expected due to tensile cracking of concrete.

- No loss of concrete cross-section resulting from fire induced spalling is assumed in the concrete member. This assumption typically holds true for normal strength concrete (NSC) with concrete compressive strengths of 70 MPa or lower and for cases when there is minimal spalling during high temperature exposure (Kodur and Dwaikat 2008).
- Concrete is assumed to not exhibit any recovery in strength and stiffness properties typically observed several months following fire exposure. The current model only considers the immediate and short-term (few weeks) reduction in post-fire residual mechanical properties of concrete in evaluating residual capacity.
- It is assumed that transient creep strain in concrete is recoverable during cooling phase of analysis. in concrete during heating and cooling phases of analysis. It is preferable to not consider this strain as recoverable during cooling using a more sophisticated explicit model. However, this reversibility assumption for transient creep does not lead to a large error in deflection predictions for RC beams, since a relatively small area of concrete is under compression (Lu et al. 2015b).
- Temperature dependent thermal properties of concrete and reinforcing steel; i.e. thermal conductivity, heat capacity and thermal expansion are completely reversible from heating to cooling phase. The effect of decrease in heat capacity due to loss of moisture as well as residual thermal expansion (or shrinkage), in concrete during cool down is neglected for simplicity.

4.2.3 Analysis details

Two sub-models, namely, thermal and structural models, are needed to carry out three stages of analysis for establishing residual response of a fire damaged member. A structural model is needed to carry out strength analysis in Stages 1, 2, and 3, while Stage 2 of the analysis requires a thermal model to undertake heat transfer calculations to compute sectional (or member) temperatures in

the RC beam. Also, the modeling of fire exposed RC beams is undertaken using sequentially coupled thermo-mechanical analysis procedure. This procedure assumes that the mechanical (structural) analysis is driven by temperatures obtained from an independent thermal analysis, but no reverse dependency exists.

In Stage 1 of analysis requiring only the structural sub-model, room temperature capacity of the RC beam is to be determined using detailed finite element analysis. Alternatively, undamaged load carrying capacity can be calculated using strength equations present in design standards (ACI 2008). In Stage 2, the beam is subjected to a specified load level taken to be a percentage of the ultimate capacity of the beam (based on the estimated loading present during fire exposure) and a realistic time-temperature curve resulting during fire exposure (EN 1991-1-2 2002). The response of the RC beam during fire exposure in Stage 2 is traced through two sets of discretization models, one for undertaking thermal analysis and the other for undertaking mechanical (strength) analysis. Temperatures calculated from thermal analysis at each time step are imported at corresponding nodes in the structural model of the RC beam. Subsequently, temperature dependent thermal and mechanical properties of concrete and reinforcing steel are utilized to carry out structural analysis for the entire time history of fire exposure, including cooling phase.

During the structural analysis in Stage 2, failure is evaluated by applying relevant deflection or deflection rate failure limit states (discussed in further detail in Section 4.2.6). Following cooling of the fire exposed RC beam, residual load-bearing capacity of the beam is evaluated by undertaking Stage 3 analysis, through loading the beam, in increments, until failure is attained. It should be noted that the time history of a given structural (or thermal) model can be divided into sequential steps in ABAQUS (Hibbitt, Karlsson & Sorensen 2012a) with the response state (i.e. stresses, strains and temperatures) of the beam being in each step of the analysis. Accordingly,

residual stresses and strains from Stage 2 of analysis are explicitly included as an initial state before carrying out Stage 3 of analysis.

The finite element formulation of the thermal and structural models, spatial and temporal discretization of the beams, temperature dependent constitutive model, input parameters, and output results of the numerical model are discussed in detail in this section

4.2.3.1 Heat transfer analysis (Stage 2)

A transient heat transfer model is needed for computing temperature distribution within the cross-section of a structural member. Such an analysis assumes that the temperature at the boundary surface of the member is known, and calculates temperature within internal layers of the cross-section by applying fundamental laws of heat transfer. In the case of a fire exposed member, heat transfer within the member (solid) occurs by the virtue of conduction and can be described by the Fourier equation, relating the temperature, T, at each point of the continuum to the time, t, as:

$$\rho c \frac{\partial T}{\partial t} = \nabla [k \nabla T] + Q \tag{4-1}$$

where, k is the thermal conductivity components expressed in W/m. $^{\circ}$ C, ρ is the density of solid in kg/m 3 , c is the specific heat of solid in J/kg. $^{\circ}$ C and Q is the time rate of heat generated per unit volume by hydration of cement in concrete within the body (W/m 3) and may be predicted by empirical equations.

Solution to heat conduction requires a set of boundary and initial conditions (for the time dependent problems) which may be linear or non-linear. These may be classified as:

 Boundary conditions of the first kind or the Dirichlet boundary condition where the temperature is prescribed along the boundary surface as:

$$T = T_0 (4-2)$$

 Boundary condition of the second kind or Neumann boundary condition where the derivative of the temperature i.e., the fluxes are prescribed over the boundary as:

$$k\frac{\partial T}{\partial n} + q = 0 \tag{4-3}$$

where, n, is the unit normal vector to the surface and, q, is the time rate of heat transferred between the environment and concrete surface per unit area, expressed in W/m^2 .

The outward heat flux, q, comprises of the components, q_c (heat flux lost due to convection), and, q_r (heat flux lost from long wave radiation). Convection component is expressed in terms of compartment temperature, T_0 , and convection heat transfer coefficient, h_c , as:

$$q_c = h_c(T - T_o) \tag{4-4}$$

The heat transfer between the surface of concrete and surroundings due to long wave radiation, i.e., thermal irradiation, q_r , can be expressed by Stefan-Boltzman's radiation law that is in a simplified form as:

$$q_r = h_r(T - T_0) \tag{4-5}$$

where,

$$h_{r} = C_{s} \varepsilon [(T + T^{*})^{4} - \alpha (T + T^{*})^{4}]$$
(4-6)

In the above expression, h_r , is the radiative heat transfer coefficient, C_s is the Stefan-Boltzman's constant equal to 5.667 x 10^{-8} W/m² °K⁴, ϵ is the emissivity coefficient relating the radiation of the concrete surface (gray) to that of an ideal black body ($0 \le \epsilon \le 1$); and T^* is a constant equal to 273 which is used to convert the temperature from degree Celsius (°C) to degree Kelvin (°K), α , the emissivity of the surroundings, is given by:

$$\alpha = 1 - 0.261 \exp[-7.776 \times 10^{-4} (T_0)^2]$$
(4-7)

Applying differential equation (4-1) in conjunction with the appropriate boundary conditions leads to strong form of the solution. However, the finite element based solutions rely upon weak formulation of the problem within the definite domain. To this end, Galerkin weighted residual principle has been employed which assumes an approximate function for the unknown temperature variable at elemental level and yields the following form:

$$\int_{V^{(e)}} [N]^T \rho c \frac{\partial \widetilde{T}}{\partial t} dV - \left(\int_{V^{(e)}} [N]^T \nabla [k \nabla \widetilde{T}] + [N]^T Q \right) dV = 0$$
(4-8)

where, [N] represents the element shape function matrix, ρ represents the density of the material.

A discretized approximation is usually taken as C° (linear integration) continuous in the scalar field variable represented by, \widetilde{T} , and at elemental level is given in terms of elemental nodal degree of freedom represented by, T^{e} , as:

$$\tilde{T} = [N]\{T^e\} = [N_1 N_2 N_3 \dots N_n]\{T^e\}$$
(4-9)

Equation (4-4) upon using Green's theorem, can be decoupled into a domain and a boundary term as:

$$\rho c \int_{V^{(e)}} [N]^T \frac{\partial \widetilde{T}}{\partial t} dV + \int_{V^{(e)}} [\nabla N]^T k [\nabla \widetilde{T}] dV - \int_{V^{(e)}} [N]^T Q dV + \int_{S^{(e)}} [N]^T q dS = 0 \tag{4-10}$$

Using equation (4-5), the above expression in the notational form maybe rewritten as:

$$[C^e] \{\dot{T}^e\} + [K^e] \{T^e\} = \{F^e\}$$
 (4-11)

where, $[C^e]$: the heat capacity matrix, $[K^e]$: the element conductivity matrix and $\{F^e\}$: the thermal load vector are given by:

$$[\mathsf{C}^{\mathsf{e}}] = \rho \mathsf{c} \int_{\mathsf{V}(\mathsf{e})} [\mathsf{N}]^{\mathsf{T}} [\mathsf{N}] \mathsf{d} \mathsf{V} \tag{4-12}$$

$$[K^{e}] = \int_{V^{(e)}} [\nabla N]^{T} k [\nabla N] dV + (h_{v} + h_{r}) \int_{S^{(e)}} [N]^{T} [N] dS$$
(4-13)

$$\{F^{e}\} = \int_{V^{(e)}} [N]^{T} Q dV + (h_{c} + h_{r}) \int_{S^{\{e\}}} [N]^{T} T_{o} dS$$
(4-14)

Once the local element characteristic matrices are established, they can be assembled into global temperature matrix at the structural level represented by {T} as following:

$$[C]\{\dot{T}\} + [K]\{T\} = \{F\}$$
 (4-15)

where, [C] and [K] are the global heat capacity and conduction matrices, {F} represents the assembled thermal load vector resulting from the convective and radiative heat fluxes.

This spatial discretization coupled with an implicit backward difference algorithm for time marching yields nodal temperatures within the discretized member for the complete time history of fire exposure. These calculated temperatures are utilized to evaluate appropriate temperature dependent mechanical properties and thermal strain during fire resistance analysis in Stage 2 of analysis, as well as residual properties based on peak temperatures in Stage 3 of analysis.

4.2.3.2 Structural analysis (Stages 1, 2, and 3)

A structural model is needed in conjunction with the heat transfer model to trace structural response during room temperature capacity evaluation (Stage 1), fire exposure (Stage 2), and residual conditions (Stage 3). This structural (stress) analysis model is developed using the principal of virtual work, and displacement-based finite element technique to trace structural response of the member. Given an equilibrium configuration of a continuum, a virtual displacement represents an imaginary change in configuration resulting in no change in loads or stresses, and admissible displacements that does not violate compatibility or displacement boundary conditions. Thus, internal work resulting from quasi-static virtual displacements can be

equated to external work by applying nodal loads and body forces. This principal of virtual work can be stated as:

$$\int_{V^{(e)}} \{\delta \epsilon\}^{T} \{\sigma\} dV = \int_{V^{(e)}} \{\delta u\}^{T} \{F\} dV + \int_{V^{(e)}} \{\delta u\}^{T} \{\emptyset\} dV$$
 (4-16)

The displacement $\{u\}$ can be interpolated over an element using the appropriate shape function matrix, and nodal displacement degrees of freedom of an element, that is:

$$\{u\} = [N]\{d\} \tag{4-17}$$

Now, the strain tensor $\{\varepsilon\}$ can be decomposed into a mechanical (stress-dependent) strain $\{\varepsilon_m\}$, and thermal strain $\{\varepsilon_T\}$, as:

$$\{\varepsilon\} = \{\varepsilon_m\} + \{\varepsilon_T\} \tag{4-18}$$

It should be noted that no explicit stress and temperature dependent transient creep strain components are considered in this formulation. It is assumed that the transient creep strain is specified implicitly as part of the temperature dependent mechanical strain.

Also, displacements $\{d\}$, and mechanical strains can be related using the strain-displacement matrix [B], as:

$$\{\varepsilon_m\} = [B]\{d\} \tag{4-19}$$

and,

$$[B] = [\partial][N] \tag{4-20}$$

Therefore using equations (4-17) and (4-19), we obtain:

$$\{\delta u\}^T = \{\delta d\}^T [N]^T \tag{4-21}$$

and,

$$\{\delta\varepsilon\}^T = \{\delta d\}^T [B]^T \tag{4-22}$$

Finally, we can substitute equations (4-18), (4-21) and (4-22) in equation (4-16), with due consideration for initial strain and stress to obtain:

$$\{\delta d\}^{T} \begin{pmatrix} \int_{V^{(e)}} \{B\}^{T}[D][B] dV - \int_{V^{(e)}} \{B\}^{T}[D] \{\epsilon_{T}\} dV - \int_{V^{(e)}} \{B\}^{T}[D] \{\epsilon_{0}\} dV - \int_{V^{(e)}} \{B\}^{T}[D]^{T} \{\emptyset\} dV - \int_{V^{(e)}} [N]^{T} \{\emptyset\} dV \end{pmatrix} = 0$$

$$(4-23)$$

Vectors $\{\delta d\}$ and $\{d\}$ are independent of coordinates, and hence are constant with respect to integration over the volume. Finally, equation (4-23) can be re-written as:

$$[k]{d} = {r_e}$$
 (4-24)

and,

$$[k] = \int_{V(e)} \{B\}^{T}[D][B]dV$$
 (4-25)

$$\begin{aligned} \{r_e\} &= \int_{V^{(e)}} \{B\}^T [D] \{\epsilon_T\} dV + \int_{V^{(e)}} \{B\}^T [D] \{\epsilon_0\} dV + \int_{V^{(e)}} \{B\}^T \{\sigma_0\} dV \\ &+ \int_{V^{(e)}} [N]^T \{F\} dV + \int_{V^{(e)}} [N]^T \{\emptyset\} dV \end{aligned} \tag{4-26}$$

where, [k] represents the element stiffness matrix, and $\{r_e\}$ represents the consistent element nodal loads arising from all sources (equivalent forces from thermal strain, equivalent forces from initial strain, equivalent forces from initial stress, concentrated forces applied at nodes, and body forces applied throughout the volume), except element deformation.

The element level matrices obtained in this manner are then assembled into global structural level matrices by rearranging, and adding overlapping terms when necessary. This leads to the well known classical stiffness-displacement equation that can be stated as:

$$[K]{D} = {R}$$
 (4-27)

And thus,

$$\{D\} = [K]^{-1}\{R\} \tag{4-28}$$

where, [K] represents the global stiffness matrix, {D}, represents the global displacement vector, and {R} represents the global load vector.

The global displacements can be calculated using equation (4-28). An implicit Newton-Raphson's method, with automatic incrementation is utilized to update the stiffness matrix and calculate

displacements in the structure for each time step. Both material, and geometric non-linearities are explicitly included in the model. Also, residual stresses and strains from the previous step of the analysis can be carried over to the next stage of the analysis using this formulation.

4.2.4 Modeling interfacial bond between rebar and concrete

The rebar-concrete interfacial bond can be either assumed to be perfect, or be modeled to account for finite bond-slip. Both approaches for modeling interfacial bond between rebar and concrete as utilized in the present study are discussed in sections below.

4.2.4.1 Bond-link element approach

Interfacial bond between rebar and concrete can be modeled through detailed discretization of the structure in region surrounding reinforcement, wherein both ribs of the reinforcement and the concrete lugs are modeled explicitly. Alternatively, a phenomenological modeling can be utilized in which local bond-slip is idealized as bond-link elements. In the present work, only phenomenological models of bond are utilized due to complexity in terms of effort and long computational time, involved in finite element analysis of RC structures.

Two common types of models are utilized in previous studies for modelling the bond characteristics between concrete and reinforcing steel at ambient temperature. The first type of model utilizes a 'bond-link element' having no physical dimensions (having coincident nodes) to connect the concrete and reinforcing steel elements at the nodes (Jendele and Cervenka 2006). In the second type of model, the contact surface between concrete and reinforcing steel is simulated using 'bond-zone connect' elements characterized by a distinct material law considering the properties of the bond zone (Keuser and Mehlhorn 1987; Kwak and Kim 2001; Schäfer 1975). Since these models assume a continuous connection between the concrete and reinforcing steel, a relatively fine mesh within the bond zone is needed for achieving reasonable accuracy. When modelling global response of RC structures, the bond-link element approach provides a reasonable

compromise between accuracy and computational efficiency and is utilized to model interfacial bond in the present study.

4.2.4.2 Bond-link element approach

As per the bond-link element approach, the concrete and the reinforcing steel are represented by two different sets of elements, and node pairs at the interface (i.e. at the same location) are connected using interfacial spring elements (shown in Figure 4-3). Three spring elements are used at each node pair: one to represent the shear bond behavior according to a bond-slip relationship and the other two to represent the normal bond behavior in the vertical direction; the latter are assumed to be rigid for simplicity by assigning large spring stiffness to the normal springs. It is assumed that the slip between reinforcing steel and concrete is related only to the longitudinal axis direction. Hence, at ambient temperature the bond force between the concrete and reinforcing steel bar for the bond element is obtained as:

$$F_x = A\tau_b \tag{4-29}$$

where, F_x : the bond force between the reinforcing steel bar and concrete for the bond element; A: the contact-area between the reinforcing steel bar and concrete for the bond element, that is A = UL, where U is the perimeter of the steel bar and L is the length of the steel bar which contributes to the node connected by the bond element; τ_b the average bond stress between the concrete and reinforcing steel bar related to the bond element.

The average bond stress (τ_b) can be calculated using temperature dependent empirical bond stress—slip relationship discussed in Section 3.2.3.

4.2.5 Discretization of the beam

For applying the above analytical procedure, the RC beam is to be discretized into finite elements that can accurately capture response of concrete, and rebar respectively. The finite element-based software package ABAQUS (Hibbitt, Karlsson & Sorensen 2012a), used to develop numerical models for tracing residual response contains an extensive library of elements suited for different types of analysis problems. For the thermal sub-model in 3D space (needed in Stage 2 of the analysis), concrete and reinforcement are discretized using DC3D8 element (8 noded linear brick element) and DC1D2 element (2 noded link element) respectively, available in ABAQUS (Hibbitt, Karlsson & Sorensen 2012b) library, having nodal temperature (NT11) as the only active degree of freedom. A tie constraint is used to apply temperatures from concrete to reinforcing steel bars at that location. The surface areas of DC3D8 elements assumed to be exposed to fire are subject to appropriate convection and radiation thermal boundary conditions that occur from fire (ambient air) to the beam. According to EN 1991-1-2 (EN 1991-1-2 2002), the convective heat transfer coefficient is taken to be 25 W/m² °C on fire exposed surface, consistent with the recommended value for cellulosic fires in building compartments. For the un-exposed surfaces, a convective coefficient of 9 W/m² °C is used to account for the effects of heat transfer through radiation. Further, the emissivity for radiative heat transfer at the exposed surfaces of the concrete member is taken as 0.8 as per Eurocode recommendations.

For the structural analysis (needed in Stages 1, 2 and 3 of analysis), the RC beam is discretized using eight-noded continuum elements (C3D8) and two-noded link elements (T3D2) for concrete and reinforcing steel respectively. This approach has been used effectively to model reinforcement explicitly wherein nodes of reinforcement are coincident with corresponding nodes of concrete (Gao et al. 2013; Pothisiri and Panedpojaman 2012a). A discretized view of a typical discretized beam is shown in Figure 4-2.

Since RC beams undergo large deflections during high temperature exposure, the effect of geometric and material non-linearity is to be taken into consideration and this is done through Lagrangian method (Hibbitt, Karlsson & Sorensen 2012b). The material nonlinearity is automatically accounted for through temperature dependent stress-strain relations specified in the models. The Newton–Raphson method is employed as the solution technique with a tolerance limit of 0.02 on the displacement norm as the convergence criterion (Rafi et al. 2008; Wu and Lu 2009). Also, line search function is activated to achieve rapid convergence (Crisfield 1982; Schweizerhof 1993). Similar analysis parameters have yielded results with sufficient accuracy and efficiency in earlier studies (Gao et al. 2013).

4.2.6 Temperature dependent material modeling

Distinct constitutive models for concrete and reinforcing steel are defined using specific temperature-dependent material property relations. These include mechanical property relations at room temperature (Stage 1), thermal and during fire exposure including cooling (Stage 2), and during residual (Stage 3) phases of analysis. To generate such data for thermal and mechanical material property variation with temperature, available relations in codes of practice and literature can be utilized with appropriate modifications. Key aspects of modeling the behavior of concrete and reinforcing steel in the present study are discussed in this section.

4.2.6.1 Modelling of concrete

Material properties of concrete at elevated temperature as experienced during fire exposure have been studied extensively in the past few decades, and this information is widely available in literature, and some design standards. Correspondingly, material properties of concrete were defined using published relations. It should be noted that majority of these property relations have been validated for standard fire exposure conditions which assume a monotonic increase in temperature with time. Thus, appropriate modifications were made to accurately capture effects of

that specific material properties of concrete that are irreversible once high temperatures are attained are not reversed during cooling, or residual phase of analysis.

Thermal properties

The thermal conductivity and heat capacity of concrete are defined according to EN 1992-1-2 (EN 1992-1-2 2004); and the density of concrete is taken to have a constant value of 2300 kg/m³. Since HSC is typically denser than NSC, lower bound conductivity was utilized for NSC while upper bound thermal conductivity was used for HSC. This assumption was based on extensive numerical studies in previous work (Lakhani et al. 2013) on thermal analysis of RC beams similar to those analyzed in the present study. The effect of moisture in concrete is implicitly considered by introducing a latent heat of evaporation component to the heat capacity of concrete; the value of this latent heat is denoted by C_{c,peak}, when the temperature is between 100°C and 115°C, and decreases linearly when the temperature is between 115°C and 200°C. C_{c,peak} is equal to 1470 J/(kg.°C) and 2020 J/(kg.°C) respectively, for the moisture contents of 1.5% or 3.0% by weight. For other moisture contents, a linear interpolation is adopted. Constitutive relations to define temperature dependent thermal properties of concrete are summarized in Table 4-1.

Constitutive model parameters

A damaged plasticity constitutive model (Lubliner et al. 1989) is adopted to model the material behavior of both normal strength and high strength concrete, involving strong nonlinearity and different failure mechanisms under compression and tension (crushing or cracking). This model assumes that user specified uniaxial stress-strain relations can be converted into stress-equivalent plastic strain curves and this is automatically done from the user-provided inelastic strain data (see Figure 4-3). The effective compressive and tensile cohesion stresses determine evolution of the

yield surface for analyzing multiaxial load cases. The yield surface used in this constitutive model for the different evolution of strength under tension and compression is based on Lee and Fenves's (Lee and Fenves 1998) modification of Lubliner et al.'s (Lubliner et al. 1989) yield function. In addition, the Drucker-Prager yield criterion is utilized for determining failure through both normal and shear stress. Correspondingly, a non-associative flow rule with the Drucker-Prager hyperbolic function is utilized to define the flow potential function for calculating plastic strain increments. The yield surface and flow potential can be defined using specific input parameters as summarized in Table 1. The dilation angle denoted by ψ , controls the amount of plastic volumetric strain developed during plastic shearing and is assumed constant during plastic yielding. Typically, for concrete a dilation angle of $\psi=31^0$ is used, and this is therefore also chosen herein. The value of flow potential eccentricity $\epsilon = 0.1$ ensures that the material has almost the same dilatation angle over a wide range of configuring pressure stress values. The ratio of the equibiaxial compressive yield stress and uniaxial compressive strength denoted by σ_{b0}/σ_{c0} is assumed to be 1.16 based on experimental data. The ratio of the second stress invariant on the tensile median to that on the compressive median at initial yield denoted by K_c is chosen to be 1.0 so that the yield surface has a perfect cone shape in the three-dimensional space, consistent with Drucker-Prager criterion described previously. Besides these constitutive parameters, the viscosity parameter denoted by μ is used for the visco-plastic regularization of the concrete constitutive equations. The default value is 0.0 to ensure that the analysis is rate independent.

The constitutive parameters utilized to define the shape of the yield surface and flow potential as described above, are assumed constant with temperature since their evolution with increasing temperatures are not available. Therefore, appropriate temperature dependent uniaxial material

properties are specified to define compressive and tensile behavior of concrete during room temperature, heating, cooling, and residual behavior of concrete.

Compressive behavior

Typical response of concrete under compression is assumed to be linear elastic until the initial yield surface is reached. The subsequent yield surfaces (i.e. loading surfaces) are controlled by a hardening variable, which is a function of the equivalent plastic strain. Therefore, based on the concept of effective stress and equivalent plastic strain, it is possible to find loading surfaces under multiaxial compression from the uniaxial compressive stress-strain relationship. In the present study, the Eurocode model (EN 1992-1-2 2004) is adopted to define the uniaxial compressive stress-strain relation of concrete at elevated temperatures (refer Table 4-2). While the general relations for NSC and HSC remain identical, different temperature dependent degradation factors specified in the Eurocode model (EN 1992-1-2 2004) were utilized to model the behavior of NSC and HSC. The compressive response of concrete (NSC or HSC) is assumed to be linear elastic until the axial stress reaches the initial uniaxial yield stress which is taken to be 0.33 f_{c.T} (f_{c.T} denotes the uniaxial compressive strength of concrete at temperature T). This is followed by a strain-hardening curve up to the peak compressive stress and then a descending branch representing the post-peak softening behavior of concrete. Stress-strain relations of concrete as a function of temperature are plotted in Figure 4-4.

Tensile behavior

The stress-strain relation for concrete in tension is represented by a triilinear relationship. Before cracking, the tensile behavior of concrete is assumed to be linear elastic. Subsequently, the behavior of cracked concrete is simulated using a smeared crack model in the sense that it does not track individual macro cracks. Constitutive calculations are performed independently at each

integration point of the FE-model and the presence of cracks enters the calculations by affecting the stress and material stiffness associated with the integration point. In this smeared crack model, crack initiates when the specified yield surface (i.e. which is the same as the failure surface for tension-dominated behavior) is reached. Consequently, the tensile stress at the integration point gradually decreases while the strain increases (referred to as tension softening). The tensile strength of concrete at elevated temperatures is assumed to vary as per Eurocode 2 (EN 1992-1-2 2004) but with some modifications to avoid the conditions where the tensile strength becomes zero at relatively low temperatures (600° C). A value of ε_{ct} (ultimate strain in tension) that lies between 0.002 and 0.004, independent of temperature, have been assumed in literature (Terro 1998). Identical bi-linear tensile relations were adopted for NSC and HSC, with the only distinction that the tensile cracking stress for HSC was greater than NSC owing to greater compressive strength of the latter. The tensile stress-strain relations of concrete utilized in this study are plotted in Figure 4-5.

Strain decomposition

The evolution of strain of concrete (NSC or HSC) at elevated temperatures can be grouped under four parts: the free thermal strain, the instantaneous stress-induced strain, the classical creep strain, and the transient creep strain (Khoury et al. 2002) as shown in the following expression:

$$\varepsilon_{\text{tot}} = \varepsilon_{\text{th}}(T) + \varepsilon_{\sigma}(\sigma, T) + \varepsilon_{\text{cr}}(\sigma, T, t) + \varepsilon_{\text{tr}}(\sigma, T)$$
(4-30)

where ε_{tot} is the total strain; t is the fire-exposure time; ε_{σ} is the stress-induced strain obtained from the above-mentioned constitutive law; ε_{th} is the free thermal strain and is determined according to Eurocode 2; ε_{cr} is the classical creep strain and can be ignored due to its small value compared to the other three components; and ε_{tr} is the transient creep strain which is defined as a function of stress and temperature. Transient creep appears only during the first heating cycle but not during

the subsequent cooling and heating cycles (Khoury et al. 1985). It is noted that the uniaxial compressive stress–strain relation provided by the Eurocode 2 has implicitly incorporated the effect of transient creep as pointed out in previous studies (Gao et al. 2013; Kodur and Dwaikat 2008). In addition, transient creep exists for concrete in compression rather than in tension. Therefore, the transient creep strain is not considered as an explicit strain component in the present FE model. Also, the phenomenon of temperature induced spalling is not considered in the present model for simplicity. Besides, no structurally significant spalling was observed in any of the normal strength or high strength concrete beams tested in the present study. Temperature dependent stress-strain relations for concrete are specified in Table 4-2 and Figure 4-4.

4.2.6.2 Modelling of reinforcing steel

Thermal properties

The temperature-dependent variations of thermal conductivity and specific heat capacity of steel as specified in Eurocode 2 are incorporated in the present FE model. The density of steel is assumed to be constant at 7800 kg/m³.

Constitutive model parameters

An isotropic hardening model based on von mises plasticity theory is used to describe the deformation hardening behavior for reinforcing steel. This model assumes that the initial yield surface expands uniformly without translation and distortion as plasticity occurs. The size increase in the yield surface depends on the stress, hardening property, and temperature. Temperature dependent elastic modulus and yield stress as a function of plastic strain are needed to calibrate this constitutive model for modeling behavior of reinforcing steel under fire conditions. An identical constitutive law is adopted for reinforcing steel for defining tensile and compressive behavior.

Elasto-plastic behavior

The uniaxial elasto-plastic response of reinforcing steel is governed by its elastic modulus and yield stress as a function of plastic strain. The elastic modulus of reinforcing steel decreases with increasing temperature. Also, the temperature dependent stress-strain relations including elastic and plastic response of reinforcing steel of steel at elevated temperatures includes two parts: the free thermal strain ε_{th} and the stress-induced strain ε_{σ} (i.e. tensile stress-strain curve). Similar to concrete, transient creep strain is accounted for implicitly in the stress-strain relation according to EN 1992-1-2.

4.2.6.3 Incorporating distinct cooling phase and residual properties

Temperature of constituent materials increases monotonically during heating phase. However, this study focuses on modeling the residual response concrete beams under realistic fire exposure necessitating calculation of appropriate material properties during cooling and residual phases, respectively. These properties are calculated by appropriately modifying temperature material properties described in the previous section. The material properties that need to be modified include compressive strength of concrete, and yield strength of reinforcing steel.

Compressive strength of concrete during cooling and residual phases can impact residual response significantly. Experimental data on concrete compressive strength after exposure to elevated temperature indicates that concrete does not recover its initial compressive strength, while cooling to ambient (room) temperature. In fact, it experiences an additional loss of strength compared to the value reached at maximum reached temperature, i.e. additional degradation occurs during cooling (Molkens et al. 2017). This additional loss of strength is assumed to be 10% less than the peak strength attained at the maximum temperature. During the cooling phase, a linear interpolation between the elevated and residual compressive strength after cool down is adopted

(EN 1991-1-2 2002). This assumption is based on Eurocode 4 (EN-1994-1-2 2008) recommendations and has been shown to yield accurate results in predicting residual capacity of RC columns immediately after cool down (Gernay 2019). The normalized compressive strength of concrete for both elevated and residual conditions in shown in Figure 4-6.

The residual yield strength in rebars depends mainly on the maximum temperature reached in the steel reinforcement. Provided the temperature of hot-rolled reinforcing steel does not exceed 500 °C, reinforcing steel will recover almost 100% of its initial room-temperature yield strength upon cooling (Neves et al. 1996b). However, when heating to above 500°C, reinforcing steel regains only part of its initial strength (see Figure 4-7). The ratio between ultimate strength and yield strength which is about 1.5 at room temperature, also decreases with increasing temperatures and becomes 1 at around 800°C. This suggests that strain-hardening becomes less prominent at very high temperatures (Neves et al. 1996a).

In addition to distinct material properties during cooling and residual phases of analysis, modeling material response during cooling phase poses a unique challenge owing to thermal inertia of concrete. The onset of cooling phase in fire temperatures does not coincide with the cooling phase within the cross-section of the heated beam itself. In fact, cross sectional temperatures within the beam continue to increase for a significant duration even after fire temperatures begin to decay owing to thermal inertia of concrete. Thus, each element within the concrete cross-section enters cooling phase at different times of the analysis. A state dependent solution procedure that assigns cooling phase properties automatically given the temperatures are increasing (heating phase) or decreasing (cooling phase) is needed to accurately model response during cooling phase, has been done by implementing a FORTRAN user subroutine

Accordingly, a user subroutine – UFIELD was implemented in FORTRAN to assign appropriate material properties by checking the rate of increment of temperature at each time step during fire exposure. Mechanical properties were completely irrecoverable for concrete and partially recoverable for reinforcing steel depending on peak temperatures. Moreover, unloading can take place along the branch defined by the unloading stiffness, that is somewhat higher that the initial stiffness. In this way, the irrecoverable strain components (i.e. transient creep strain) are implicitly accounted for. Also, additional damage in concrete was considered based on maximum temperature information stored in the subroutine during high temperature analysis. Appropriate high temperature material properties could thus be applied in calculations during cooling and residual phases of analysis, respectively (see Figure 4-6 and Figure 4-7).

4.2.7 Failure criteria

In undertaking residual strength analysis of a RC beam, different failure criteria are to be applied at each stage of the analysis depending on the applicable failure limit states. In Stage 1 of analysis (at ambient conditions), for evaluating capacity of the beam prior to the fire exposure, strength limit state generally governs the failure, characterized by runaway deflections where the beam cannot sustain any increase in load. In Stage 2 of the analysis (under fire exposure), a RC beam experiences high temperatures and high mid-span deflections due to degradation in strength (moment or shear capacity) and stiffness properties of concrete and reinforcing steel. In addition to strength criterion, deflection limit state is a reliable performance index to evaluate failure during fire exposure. Accordingly, the failure of the beam is said to occur (BS476-20 1987) when:

- The maximum deflection in the beam exceeds L/20 (mm) at any fire exposure time, or
- The rate of deflection exceeds L²/9000d (mm/min)

Where, L=span length of the beam (mm) and d = effective depth of the beam (mm).

It is important to note here that the aforementioned deflection limit states are developed for isolated RC beams tested under standard fire conditions in the laboratory and therefore may not apply to beams under realistic loading and fire scenarios. However, failure times obtained from the above deflection based limits would be conservative under most practical saturations.

To evaluate residual capacity after exposure, in Stage 3 (after cooling down of the beam), strength and extent of residual deflections generally govern failure.

4.2.8 Output results

Displacements, stresses and temperature fields are the primary output variables that are generated during different stages of analysis. In Stage 1 of analysis, failure of the beam is ascertained based on strength limit state or when any further increment in applied load leads to instability (runaway deflection). In Stage 2 of analysis, at each time step, the output from the thermal analysis, namely nodal temperatures, is applied as a thermal body load on the structural elements (nodes) to evaluate the structural response of RC beam under fire exposure. An identifier to ascertain if the material is under heating or cooling phase to apply the appropriate material properties is updated in the structural analysis using subroutine UFIELD provided in ABAQUS (Hibbitt, Karlsson & Sorensen 2012b). Also, the maximum temperature experienced at each node during thermal analysis is used to calculate residual mechanical properties to be used for the residual capacity evaluation in Stage 3 of analysis, when necessary. In Stage 3 of analysis, the load deflection response is utilized to evaluate residual load carrying capacity of a fire exposed reinforced concrete beam. Furthermore, the sectional capacity at failure is calculated by integrating stresses experienced within the concrete and reinforcing steel, as generated in ABAQUS (Hibbitt, Karlsson & Sorensen 2012b), to ascertain failure based on moment capacity or shear capacity criteria.

4.3 Model Validation

The validity of the developed finite element based numerical model is first established through comparison with published test data from residual capacity tests on four RC beams by Dwaikat and Kodur (Dwaikat and Kodur 2009) and Kumar and Kumar (Kumar and Kumar 2003b), respectively. In addition, measured response during residual capacity tests on six fire damaged beams conducted as part of this study, and reported in Chapter 3, was also utilized to validate the developed model. Novel data generated in these tests provides additional validation of the model especially during pre-fire exposure and extended cooling phase stages of analysis in evaluating residual capacity.

4.3.1 Tests by Dwaikat and Kodur (Dwaikat and Kodur 2009c)

Two concrete beams tested under fire exposure by Dwaikat and Kodur (Dwaikat and Kodur 2009c) were analyzed by applying the above numerical procedure to validate the proposed approach. The characteristics of the beam, together with the summary of the results are tabulated in Table 2. These beams are made of normal strength concrete (designated B1 and B2 as per Table 2) and there was no observed spalling in these beams during fire exposure. The dimensions and reinforcement details of both these beams are identical and are shown in Figure 4-8a. Both beams were tested under two point loading of 50 kN (as depicted in Figure 4-8a) which produced a bending moment equal to 55% of the beam capacity, as per ACI 318 (ACI 2008) capacity equation. In the tests, one of the beams was subjected to ASTM E119 (ASTM E119-19 2019) standard fire and the other beam was subjected to a short design fire (SF) as illustrated in Figure 4-9. In the fire tests, the authors applied loading 30 min before the start of the fire and this loading was maintained till no further increase in deflections occurred. This was selected as the initial condition for the deflection of the beam. The load was then maintained constant throughout the duration of fire exposure. In test for beam B1, failure occurred in the beam after 180 minutes of fire exposure.

In case of beam B2, failure did not occur during fire exposure and this beam was tested for residual capacity after cooldown to ambient conditions. In the residual test, the beam was subjected to incremental loading at the rate of 3 kN/min till failure occurred.

These two beams were analyzed in ABAQUS (Hibbitt, Karlsson & Sorensen 2012a) by applying the above discussed procedure. The validation process included comparison of thermal and structural response predictions from the analysis with that reported in the two fire tests on beams B1 and B2. Temperatures predicted by the analysis and those measured in the tests are compared in Figure 4-10. It can be seen that temperatures in concrete and reinforcing steel in beam B1 exposed to ASTM E119 (ASTM E119-19 2019) standard fire time-temperature curve rose steadily until failure. In beam B2, exposed to a Short Design Fire (SF), the rate of temperature increase is slightly higher than in the case of beam B1 during the heating phase of the fire. This can be attributed to the steep rise in the fire temperature during early stages of fire exposure. After attaining a maximum value, cross-sectional temperatures start to drop in the beam due to presence of a decay phase in this design fire exposure. It is interesting to note that peak temperatures in beam B2 occur during the decay phase of the fire exposure. This can be attributed to thermal inertia of concrete, which leads to a lag between fire temperatures and the temperatures within beam cross section. Overall, measured and predicted temperatures at various locations in beams B1 and B2 in Figure 4-10 indicate that there is close agreement between predicted and measured values during the fire test.

The measured and predicted mid-span deflection response in two beams, B1 and B2, during the fire test is shown in Figure 4-11. It can be seen that mid-span deflections increase during early stages of fire exposure due to degradation of strength and stiffness properties of concrete and reinforcing steel with temperature. Since temperatures in beam B1 continue to increase steadily

during the entire duration of fire exposure, failure occurs due to significant degradation in properties of concrete and reinforcing steel after about 180 minutes of fire exposure. For beam B2 however, due to presence of cooling phase, the temperatures experienced in concrete and reinforcing steel of the beam are relatively lower and a recovery in mid-span deflection is seen during the decay phase of fire. It can be seen in Figure 4-11 that the predicted mid-span deflections from the developed model agree well with measured response during the fire test.

Finally, the measured and predicted load-deflection response in beam B2, which did not fail during fire exposure, is presented in Figure 4-12. There is an unrecoverable deflection during fire exposure which was assumed to be the initial state for the residual strength analysis. The predicted load deflection response by the finite element model is very similar to the measured response during the test. These residual deflections represent the state of structural damage in the beam resulting from fire exposure and the extent of damage depending on load level, boundary conditions, and temperature induced degradation in material properties. While deflection prediction during fire exposure is lower than test data, the final residual deflection predicted by the model is relatively higher than the measured value during tests. This difference can be attributed to the fact that cooling phase properties adopted in the study are based on Eurocode 2 (EN 1991-1-2 2002) provisions which are conservative and lead to higher prediction of post fire residual deflections. Also, there is uncertainty regarding the adopted process in unloading of the beam in experiments after fire exposure before carrying out the residual test. Moreover, since test data is available only for first 300 min, no comparison could be made with predicted deflection beyond 300 minutes while the beam continued to cool down to room temperature. It should also be noted that the predicted residual capacity from ABAQUS (Hibbitt, Karlsson & Sorensen 2012b) is higher than room temperature capacity computed as per ACI 318 (ACI 2008). This is mainly

due to the beneficial effect of strain hardening of steel reinforcement which is not taken into account in ACI 318 (ACI 2008) strength design equations (Kodur et al. 2010c). The beam failed in flexural mode during numerical simulations and this agrees with experimentally observed failure mode.

Overall, predictions from the proposed model are in good agreement with the reported test data. The slight differences in deflection predictions can be attributed to minor variations in idealization adopted in the analysis, such as stress-strain relationship of steel and concrete. However, it is important to note that the predicted load-deflection curve in Stage 3 follows a very similar trend to the experimentally measured values.

Furthermore, to illustrate the influence of residual deflections on post-fire response of the beam, residual response of fire exposed beam B2 is evaluated from a single stage simplified analysis (without residual deflections), and three stage analysis (with residual deflections). Maintaining all other relevant analysis parameters identical, the load-deflection response of the beam is calculated using post-fire residual properties of concrete and reinforcing steel based on its temperature history. This implies there is no residual deflection in the beam at the start of the analysis in evaluating residual response. Figure 4-12 shows the difference between the post-fire response of the beam without considering residual plastic deflections as opposed to the three stage detailed analysis procedure proposed in this study. The residual load-carrying capacity of the RC beam without incorporating residual deflections in the beam is calculated to be (153 kN) which is significantly higher (approximately 26% more) than that obtained using a three stage (120.8 kN) procedure, when residual deflections are included. Moreover, it is not possible to predict residual deflections occurring in the beam after fire exposure using a single stage procedure. This

comparison clearly infers that accounting residual deflections is critical in evaluating realistic residual capacity in fire exposed RC beams.

Finally, in order to re-examine the assumption made to neglect residual shrinkage (or expansion) in analysis, the magnitude of residual plastic strains occurring at the critical section (mid-span) are compared with expected strains from residual thermal expansion or shrinkage (Figure 4-13). The strains from thermal expansion are calculated based on the maximum temperature attained at each node of the cross section during the entire fire regime (Schneider 1988a). While the strains from residual thermal expansion (shrinkage) is significant, they are still generally lower, varying from 0.012% to 0.6%, as compared to temperature induced residual plastic strains ranging from 0.03% to 1.5%.

4.3.2 Tests by Kumar and Kumar (Kumar and Kumar 2003b)

The model is further validated by comparing analysis predictions against data from another four beams tested by Kumar and Kumar (Kumar and Kumar 2003b). These beams were made of normal strength concrete and the dimensions and reinforcement details of these beams were identical and are shown in Figure 4-8b. The test parameters and results of the chosen beams and is summarized in Table 2.

One of the beams was tested by loading to failure, without any exposure to fire, and this served as the control or reference specimen. In the fire tests, four beams were subjected to ISO 834 standard fire exposure from three sides. The exposure duration varied from 1, 1.5, 2 and 2.5 hours respectively. During fire exposure tests in this study, no superimposed (external) load was applied on the beams. The heated beams were then allowed to cool naturally to ambient temperature and subsequently tested under four point bending (Figure 4-8b) in load control mode. The load-deflection response for the control beams and beams with 1, 1.5 and 2 hours fire exposure was reported by the authors (Kumar and Kumar 2003b). However, the beam that was heated for 2.5

hours showed excessive deflections and failed during fire exposure. Hence, no residual capacity test is performed on this beam.

The response of the control beam (without fire exposure) and three beams subjected to 1, 1.5 and 2 hours of fire exposure, is simulated by applying the above proposed approach in ABAQUS (Hibbitt, Karlsson & Sorensen 2012a). For the thermal analysis the heating scenario is assumed to be according to ISO 834 (ISO 834-1 1999) standard fire, as in the fire tests. The cooling of the beam is simulated through a linear decrease of air temperature, following fire exposure, for a period of two hours. The respective fire curves are illustrated in Figure 4-14. The temperature across the beam cross section during fire exposure was not recorded during the fire tests. In order to establish confidence regarding the thermal analysis procedure, a beam with a cross-section of 160×300 mm is analyzed. Temperature contours predicted by the model after 0.5, 1 and 1.5 hours of fire exposure are plotted in Figure 4-15. These temperature contours are in good agreement with corresponding contours provided by Eurocode 2 (EN 1992-1-2 2004) for similar exposure and thus establishes the validity of the thermal analysis procedure.

A comparison of measured and predicted load–deflection response for the reference beam (with no heating) is shown in Figure 4-16a. The total load is plotted as a function of deflection measured during static four point bending. Test data shows that post-peak response of the beam could not be captured since the test was load controlled. In the response predicted by the numerical model, the post-peak response shows sudden drop of load which indicates imminent failure. Figure 4-16a shows that for the reference beam, there is good agreement between measured and numerically predicted load-deflection response.

The load-deflection response for the beams tested for residual capacity after fire exposure is also presented in Figure 4-16b-d. Although no loads were applied during fire exposure, residual

deflection of 18 mm, 22 mm and 28 mm was measured in tests for beams Beam 1, Beam 2 and Beam 3 respectively. The predicted values of residual deflections are in close agreement with test data (refer Table 2). However, in this case, the residual deflections predicted by the model are lower than that observed experimentally. This can be attributed to the fact that significant fire induced spalling was reported in the beams as the beam cooled down to room temperature and before residual tests could be carried out. This is especially important in the case of Beam 3, wherein excessive spalling had been reported due to prolonged fire exposure. In the case of Beam 1 (with 1 h exposure), the residual capacity was found to be approximately 83% of the reference beam. Also, the predicted response by the model, for the case when the beam is exposed to 1 hour of fire exposure, is in good agreement with its experimental counterpart. It can be seen that for the cases of 1.5 and 2 hours of fire exposure i.e. Beam 2 and Beam 3, the ultimate load carrying capacity reduces significantly (approximately 50% of the reference beam). This reduction occurs due to rapid degradation in mechanical properties of reinforcing steel and concrete. The residual capacity predicted by the model is higher than that measured experimentally for Beam 2 and Beam 3. This is attributed to the fact that during fire experiment, reduction in cross-section due to spalling was reported after 1.5 to 2 h of fire exposure. Spalling of concrete due to high temperature exposure is not explicitly accounted in the currently developed numerical model. Hence, the residual capacity predicted by the current model for Beam 2 and Beam 3 tends to be slightly higher than that measured during tests. It should also be noted that all beams failed in flexural mode. Moreover, the overall response of beams became more ductile with greater duration of fire exposure as can be observed from the overall deflection trend plotted in Figure 4-16b-d.

Overall, good agreement between the predictions and the test data demonstrate the validity of the proposed approach in evaluating residual capacity of RC beams. However, it should be noted that

the model overestimates the residual flexural capacity of RC beams in all cases, especially when spalling occurred in the beams. This can be attributed to the fact that loss of bond between reinforcing steel and concrete, as well as fire induced spalling is not explicitly considered in the current model.

Again, the residual thermal expansion (or shrinkage) strains are compared with permanent deflections occurring due to temperature induced degradation at the critical section (mid-span) for all three beams (refer Figure 4-17). The comparison of these strains shows that the expected residual thermal expansion (or shrinkage) strains are relatively small as compared to the magnitude of residual plastic strains occurring at the same location. The residual expansion (or shrinkage) for all the three beams varies between 0.06% (shrinkage) to 0.6% (expansion) which is relatively lower than the magnitude of plastic strains that are between 1.1% to 2.3% for the three beams validated in this section. A single stage analysis without incorporating residual deflections yields significantly higher values of residual capacity as compared to a three stage analysis proposed in this study (Figure 16b-d). The post-fire residual capacity, not accounting for residual deflections is calculated to be 152 kN, 132 kN and 113 kN for tests carried out after 1 h, 1.5 h and 2 h of fire exposure respectively. These predictions are higher by 9%, 15% and 10% respectively when compared with the corresponding predictions made by the proposed three stage analysis that incorporates residual deflections.

4.3.3 MSU test beams

Two HSC and four NSC beams, tested for residual capacity as part of this study, were analyzed further to validate predictions by the model during each stage of analysis. More details on the characteristics of the beams, fire scenarios, load level, support conditions, and residual test parameters are discussed in Chapter 3. Details on the input parameters used in analysis are summarized in Table 2 and Figure 4-8c. Since comprehensive data was collected in the tests,

detailed validation was undertaken in each stage of analysis. Predictions from the numerical model are compared with response parameters during Stage 1, Stage 2, and Stage 3 of analysis to highlight the validity of the model.

4.3.3.1 Response during pre-fire conditions (Stage 1)

As part of Stage 1 analysis, the room temperature load carrying capacity of both HSCB1 (identical to HSCB2) and NSCB1 (identical to NSC2 through NSCB4) are evaluated, and results from Stage 1 analysis are presented in the form of load—mid-span deflection response of the beam in Figure 4-18. It can be seen that the mid-span deflections for both HSCB1 and NSCB1 increase linearly with load till yielding of reinforcing steel followed by nonlinearity resulting from onset of material and geometric nonlinearity incorporated in the analysis. In the nonlinear range of response, the mid-span deflection increases at a faster pace with small increments in loading and this is mainly due to spread of plasticity in the steel reinforcement. Finally, both HSCB1 and NSCB1 attain failure when they can no longer sustain any further increase in load. As expected, the elastic stiffness of HSCB1 prior to onset of tensile cracking is about 22% greater than that of NSCB1 owing to significantly greater tensile strength of HSC than NSC. However, the ultimate load carrying capacity of HSCB1 is greater by about 12% than that of NSCB1 as both beams are underreinforced and their ultimate load carrying capacity is governed by yield strength of reinforcement rather than compressive strength of concrete. It is important to note that the predicted capacity for both HSCB1 and NSCB1 at room temperature is higher than calculated using ACI 318 (ACI 2008), and this can be attributed to beneficial contribution of strain hardening of the steel reinforcement, which is conservatively not accounted for in ACI 318 (ACI 2008) design equations (see Table 2). Furthermore, the predicted displacements for both beams are in agreement with measured test data during pre-loading prior to fire tests during Stage 2 of testing. In fact, the average pre-fire secant

stiffness calculated as the ratio of peak load over final deflection for each beam measured prior to fire tests is within 10% of the corresponding predictions by the numerical model for HSCB1 and NSCB1, respectively. This comparison further demonstrates the ability of the model to predict room temperature response for both HSC and NSC beams prior to fire exposure.

4.3.3.2 Response during fire conditions (Stage 2)

In Stage 2 analysis, both thermal and structural response of the RC beam under fire exposure is evaluated. The fire exposure scenarios comprising of distinct heating and cooling phases (see Figure 4-19), as well as pre-fire loading conditions applied as inputs for thermal and structural analysis in the model are in accordance with those applied during tests (summarized in Chapter 3). The validity of the predictions by the model is established by comparison with measured temperatures and deflections plotted in Figure 4-20 and Figure 4-21. Figure 4-20a-b show the predicted and measured corner tensile rebar temperatures as a function of fire exposure time for tested beams HSCB1, HSCB2, and NSCB1 through NSCB4. It can be seen that there is good agreement between the measured and predicted average rebar temperatures throughout the heating phase of fire exposure for the two HSC and four NSC beams. The predicted peak rebar temperature at the end of heating phase of fire exposure are within 4% of the measured temperatures for all six beams (see Figure 4-20). Similarly, measured and predicted temperatures at two different locations i.e. concrete cover (25 mm from exposed bottom face), and mid-depth of concrete section (203 mm from exposed bottom) are shown in Figure 4-20. It can be seen that predicted temperatures match well with the measured temperatures within concrete cross-section establishing validity of temperature ingress for both HSC and NSC beams during heating phase of fire exposure.

The decay or cooling phase in each of the tested beam is marked by a decrease in fire temperatures. However, temperatures at the corner tensile rebar and two concrete cross-section locations displays a significant lag as compared to fire temperatures. Figure 4-20 clearly shows that predicted temperatures effectively capture this progressive lag in decay phase within the inner layers of the concrete cross section similar to temperatures measured during tests. Minor variations in the magnitude of cooling phase temperatures can be attributed to the assumption that thermal properties of both NSC and HSC during are the same as heating due to the lack of data on the thermal properties in the cooling phase.

Overall, the numerical model predicts cross-sectional temperatures at corner rebar and concrete mid-depth locations governing overall thermal response with sufficient accuracy for six tested beams. This comparison includes both heating and cooling phases of fire exposure. Further, both experimental and numerical results highlight the influence of cooling phase on thermal response of the fire exposed concrete beams. It should be also noted that accurate temperature predictions in HSC beams confirm the assumption and experimental observation that no noticeable temperature induced spalling occurred in the beams during fire exposure.

The mid-span deflections for the tested beams HSCB1, HSCB2, and NSCB1 through NSCB4 are compared in Figure 4-21. The figures show that measured and predicted deflection response of the tested beams is in good agreement depicting monotonic increase during heating phase of fire exposure. The predicted deflections for HSC beams is generally higher than those for NSC beams owing to faster degradation of strength and stiffness of HSC at elevated temperatures. Consistent with cross-sectional temperatures, mid-span deflections do not recover as soon as fire temperatures begin to decay. In fact, beam NSCB1 fails during cooling phase of fire exposure indicated by a rapid increase in rate of deflection and does not depict any recovery. The numerical model predicts failure of the beam at 240 minutes into fire exposure compared to a failure time of 230 minutes measured during the test. Thus, the developed model can accurately predict response of the

concrete beams during cooling phase of fire exposure. The five remaining beams (HSCB1, HSCB2, NSCB3, and NSCB4) sustain the entire duration of fire exposure and subsequent cooling (burn-out conditions). These beams depict varying level of recovery during cooling phase of fire exposure governed by rate of decay in fire temperature and load level present during cooling phase of fire exposure. The predicted recovery in mid-span deflections from the numerical model agrees well with measured response during fire tests. Also, the post-fire residual deflections representing the extent of stress and temperature induced degradation in the beams corresponds well with experimental conditions. The predicted residual deflection for HSCB2 is almost double than that of residual deflection for HSCB1 reflecting the same trend as seen in measured response. Similarly, the post-fire residual deflection predicted for NSCB2 subject to a higher load level than remaining NSC beams demonstrates the capability of the numerical model to accurately capture effect of load during cooling phase on deterioration in mechanical properties of the beam. It should be noted that although the trends in residual deflection predictions agree well with measured response during tests, significant difference exists between the predicted and measured magnitude of residual deflection. This can be attributed to lack of reliable data on unloading modulus of fire damaged concrete after cool down. Residual capacity of beams that did not fail during fire exposure is evaluated in Stage 3 of analysis.

4.3.3.3 Residual response after cool down (Stage 3)

Residual response of the five beams that did not fail during fire exposure is traced through incremental loading in Stage 3 of analysis. The load–deflection response from residual capacity analysis for all five beams is plotted in Figure 4-22 and the results from the analysis are summarized in Table 2.

The predicted residual response of the fire damaged NSC and HSC beams depicts three key phases of deflection progression, i.e. linear response, onset of yielding in steel reinforcement, and plastic deflection with until failure (see Figure 4-22) consistent with experimentally observed. Moreover, the numerical model captures distinct post-peak hardening response typical of HSC beams and softening response depicted by NSC beams in evaluating residual capacity. It can be inferred from the results that developed model can accurately capture deterioration in strength and stiffness properties of fire damaged RC beams with due consideration to fire severity and loading conditions present during cooling phase of fire exposure. Also, the numerical model explicitly accounts for post-fire residual deflection in evaluating residual capacity. It should also be noted that he predicted residual capacity in is higher than room temperature capacity computed as per ACI 318 (ACI 2008). This is mainly due to the effect of strain hardening of steel reinforcement which is not taken into account in ACI 318 (ACI 2008)strength design equations.

Overall, good agreement between the predictions and the test data authenticate the validity of the proposed approach in evaluating residual capacity of RC beams.

4.3.3.4 Effect of temperature induced bond degradation

In order to investigate the influence of temperature induced bond degradation on post-fire residual capacity, beams HSCB1 and NSCB1 were analyzed for two different assumptions for bond between reinforcing steel and concrete. In the analysis, all factors except the extent of temperature induced bond slip are kept identical for comparison. The two levels of fire induced bond degradation considered in the fire resistance analysis are, namely: (a) perfect bond; (b) generalized residual bond-slip model proposed in section 3.2.3.

The structural response of beams HSCB1 and NSCB1 under fire exposure and after fire exposure for two analysis cases of temperature dependent bond degradation is plotted in Fig. 9a-b. It can be

seen that different assumptions for interfacial bond between rebar and concrete has an influence on both the fire and post-fire residual response of RC beams. The peak deflection during fire exposure increases marginally by about 2% for NSCB1, and 6% for HSCB1, when temperature induced bond degradation is incorporated in analysis. However, the level of recovery during cool down of the beam is more significantly impacted by temperature induced bond degradation with residual deflection for beams NSCB1 and HSCB1 increasing by almost 4% and 8%, respectively, when temperature induced bond degradation is included in analysis (see Figure 8a). This greater effect on recovery can be attributed to the irrecoverable nature of bond degradation which further reduces the overall stiffness of the respective beams.

The effect of temperature induced bond degradation is fairly limited on post-fire residual capacity of the fire damaged concrete beams. Residual capacity of the fire damaged beams reduces by about 4% for NSCB1 and 7% for HSCB1 in the case when temperature induced bond degradation is explicitly incorporated in analysis as compared to when perfect bond is assumed (see Figure 8b). This variation in residual capacity can be attributed to the fact that in the case of temperature induced bond degradation, the magnitude of stress transfer from surrounding concrete to steel reinforcement is lower and is governed by temperature dependent bond strength while under a perfect bond scenario, all the tensile stress in concrete gets transferred to the steel reinforcement. This results in a faster degradation in predicted moment capacity when temperature induced bond degradation is incorporated in the model since all the tensile stress in concrete cannot be transferred to the reinforcing steel due to loss in bond strength. Consequently, residual response of HSCB1 having relatively higher tensile strength of concrete is more sensitive to different assumptions of temperature induced bond degradation as compared to NSCB1. Overall, temperature induced bond degradation does not significantly impact residual response of fire damaged concrete beams due

to significant reduction in tensile strength and hence tension stiffening capacity available in the RC beam.

4.4 Summary

A three-dimensional finite element based numerical model is developed to trace the residual response of fire damaged RC beams. Based on the information provided, the following observations can be made:

- The proposed numerical model is capable of tracing the response of RC beams in three stages of analysis, namely, pre-fire stage (Stage 1), fire exposure stage including cooling phase (Stage 2), and post-fire residual phase (Stage 3).
- This numerical model developed in ABAQUS software (Hibbitt, Karlsson & Sorensen 2012b), accounts for distinct temperature dependent material properties of concrete and reinforcing steel during heating, cooling and residual phases, strain hardening in steel reinforcement, tensile cracking in concrete, geometrical nonlinearities, realistic fire exposure with distinct cooling, and level of residual deflections in calculating residual response of the fire exposed member.
- Output parameters from the numerical model include sectional temperatures, mid-span
 deflection, and residual capacity of fire damaged concrete beams. In addition, fire induced
 residual stresses and strains (deflections) arising from deterioration in strength and stiffness
 of the beams due to fire exposure are incorporated in evaluating residual capacity.
- Predictions from the model compare well with measured test data on normal strength concrete beams, and high strength concrete beams.
- Temperature induced bond degradation has limited influence on heating phase and moderate influence on cooling phase behavior of RC beams under fire exposure. Further,

the impact of considering temperature induced bond degradation on residual capacity of fire damaged concrete beams is limited owing to irrecoverable tensile damage to concrete in the fire exposed regions. Thus, perfect bond may be assumed for evaluating residual capacity with reasonable accuracy.

Table 4-1. Relationships for high temperature thermal properties of concrete (Eurocode 2)

		Normal strength and high strength concrete
Thermal Conductivity (W/m K)	All types	$Upper\ limit: \\ k_c = 2 - 0.2451\ (T/100) + 0.0107\ (T/100)2 \\ for\ 20^{\circ}C \leq T \leq 1200^{\circ}C \\ Lower\ limit: \\ k_c = 1.36 - 0.136\ (T/100) + 0.0057\ (T/100)2 \\ for\ 20^{\circ}C \leq T \leq 1200^{\circ}C$

	Specific heat (J/kg°C)
	$c = 900,$ for $20^{\circ}C \le T \le 100^{\circ}C$
	$c = 900 + (T - 100), \qquad for 100^{\circ}C < T \le 200^{\circ}C$
	$c = 1000 + (T - 200)/2$, for $200^{\circ}C < T \le 400^{\circ}C$
$C_{i,o}^{\circ}C$	$c = 1100,$ for $400^{\circ}C < T \le 1200^{\circ}C$
Specific heat (J/kg°C)	Density change (kg/m ³)
t ()	$\rho = \rho(20^{\circ}C) = Reference\ density$
iea	for $20^{\circ}C \le T \le 115^{\circ}C$
ic h	$\rho = \rho(20^{\circ}C) (1 - 0.02(T - 115)/85)$
cifi	for $115^{\circ}C < T \le 200^{\circ}C$
Spe	$\rho = \rho(20^{\circ}C) (0.98 - 0.03(T - 200)/200)$
ر	for $200^{\circ}C < T \le 400^{\circ}C$
	$\rho = \rho(20^{\circ}C) (0.95 - 0.07(T - 400)/800)$
	for $400^{\circ}C < T \le 1200^{\circ}C$
	Thermal Capacity = $\rho \times c$

Strain	Siliceous aggregate	$ \varepsilon_{th} = -1.8 \times 10^{-4} + 9 \times 10^{-6} T + 2.3 \times 10^{-11} T^{3} $ $ for 20^{\circ}C \leq T \leq 700^{\circ}C $ $ \varepsilon_{th} = 14 \times 10^{-3} $ $ for 700^{\circ}C < T \leq 1200^{\circ}C $
Thermal Strain	Carbonate aggregate	$arepsilon_{th} = -1.2 \times 10^{-4} + 6 \times 10^{-6} T + 1.4 \times 10^{-11} T^3$ $for \ 20^{\circ}C \le T \le 805^{\circ}C$ $arepsilon_{th} = 12 \times 10^{-3}$ $for \ 805^{\circ}C < T \le 1200^{\circ}C$

Table 4-2. Constitutive relationship for high temperature properties of concrete (Eurocode 2)

	Normal strength and high strength concrete
Stress-strain relationships	$\sigma_{c} = rac{3 \varepsilon \ f_{c,T}^{'}}{arepsilon_{c1,T} \left(2 + \left(rac{arepsilon}{arepsilon_{c1,T}} ight)^{3} ight)} \ \ , arepsilon \leq arepsilon_{cu1,T}$
S-S.	For $\varepsilon_{c1(T)} < \varepsilon \le \varepsilon_{cu1(T)}$, the Eurocode permits the use of linear as well as nonlinear
res	descending branch in the numerical analysis.
St	For the parameters in this equation refer to Table 4-3

Table 4-3. Values for the main parameters of the stress-strain relationships of NSC and HSC at elevated temperatures (Eurocode 2)

Tomp	Тото	NSC						HSC		
Temp. °F	Temp. °C	Siliceous Agg.			Calcareous Agg.			$f_{c,T}^{'}/f_c^{'}(20^{\circ}C)$		
1		$\frac{f_{c,T}^{'}}{f_c^{'}(20^{\circ}C)}$	<i>Ec1,T</i>	Ecu1,T	$\frac{f_{c,T}^{'}}{f_c^{'}(20^{\circ}C)}$	<i>Ec1,T</i>	Ecu1,T	Class1	Class2	Class3
68	20	1	0.0025	0.02	1	0.0025	0.02	1	1	1
212	100	1	0.004	0.0225	1	0.004	0.023	0.9	0.75	0.75
392	200	0.95	0.0055	0.025	0.97	0.0055	0.025	0.9	0.75	0.70
572	300	0.85	0.007	0.0275	0.91	0.007	0.028	0.85	0.75	0.65
752	400	0.75	0.01	0.03	0.85	0.01	0.03	0.75	0.75	0.45
932	500	0.6	0.015	0.0325	0.74	0.015	0.033	0.60	0.60	0.30
1112	600	0.45	0.025	0.035	0.6	0.025	0.035	0.45	0.45	0.25
1292	700	0.3	0.025	0.0375	0.43	0.025	0.038	0.30	0.30	0.20
1472	800	0.15	0.025	0.04	0.27	0.025	0.04	0.15	0.15	0.15
1652	900	0.08	0.025	0.0425	0.15	0.025	0.043	0.08	0.113	0.08
1832	1000	0.04	0.025	0.045	0.06	0.025	0.045	0.04	0.075	0.04
2012	1100	0.01	0.025	0.0475	0.02	0.025	0.048	0.01	0.038	0.01
2192	1200	0	_	-	0	_	-	0	0	0

Table 4-4. High temperature thermal properties of reinforcing steel (Eurocode 3)

Thermal conductivity (W/m K)	$k_s = \begin{cases} 54 - 3.33 \times 10^{-2} T & 20^{\circ} C \le T < 800^{\circ} C \\ 27.3 & 800^{\circ} C \le T \le 1200^{\circ} C \end{cases}$
Specific heat (J/kg K)	c_{S} $= \begin{cases} 425 + 7.73 \times 10^{-1}T - 1.69 \times 10^{-3}T^{2} + 2.22 \times 10^{-6}T^{3} & 20^{\circ}C \leq T < 600^{\circ}C \\ 666 + \frac{13002}{738 - T} & 600^{\circ}C \leq T < 735^{\circ}C \\ 545 + \frac{17820}{T - 731} & 735^{\circ}C \leq T < 900^{\circ}C \\ 650 & 900^{\circ}C \leq T \leq 1200^{\circ}C \end{cases}$
Thermal strain	$\varepsilon_{ths} = \begin{cases} 1.2 \times 10^{-5}T + 0.4 \times 10^{-8}T^2 - 2.416 \times 10^{-4} & 20^{\circ}C \leq T \leq 750^{\circ}C \\ 1.1 \times 10^{-2} & 750^{\circ}C < T \leq 860^{\circ}C \\ 2 \times 10^{-5}T - 6.2 \times 10^{-3} & 860^{\circ}C < T \leq 1200^{\circ}C \end{cases}$

Table 4-5. Constitutive relationships for high temperature properties of reinforcing steel (Eurocode 2)

$$\sigma_{S} = \begin{cases} \varepsilon_{s}E_{s,T} & \varepsilon_{s} \leq \varepsilon_{sp,T} \\ f_{sp,T} - c + (b/a) \left(a^{2} - \left(\varepsilon_{py,T} - \varepsilon_{p}\right)^{2}\right)^{0.5} & \varepsilon_{sp,T} < \varepsilon_{s} \leq \varepsilon_{sy,T} \\ f_{sy,T} & \varepsilon_{sy,T} < \varepsilon_{s} \leq \varepsilon_{st,T} \\ f_{sy,T} \left(1 - \frac{\varepsilon_{p} - \varepsilon_{pt,T}}{\varepsilon_{pu,T} - \varepsilon_{pt,T}}\right) & \varepsilon_{st,T} < \varepsilon_{s} \leq \varepsilon_{su,T} \\ 0.0 & \varepsilon_{s} > \varepsilon_{su,T} \end{cases}$$
Parameters
$$\varepsilon_{sp,T} = \frac{f_{sp,T}}{E_{s,T}} & \varepsilon_{py,T} = 0.02 \quad \varepsilon_{st,T} = 0.15 \quad \varepsilon_{su,T} = 0.2$$
Functions
$$a^{2} = \left(\varepsilon_{sy,T} - \varepsilon_{sp,T}\right) \left(\varepsilon_{py,T} - \varepsilon_{sp,T} + \frac{c}{E_{p,T}}\right)$$

$$b^{2} = c\left(\varepsilon_{sy,T} - \varepsilon_{sp,T}\right) E_{s,T} + c^{2}$$

$$c = \frac{\left(f_{sy,T} - f_{sp,T}\right)^{2}}{\left(\varepsilon_{sy,T} - \varepsilon_{sp,T}\right) E_{s,T} - \left(f_{sy,T} - f_{sp,T}\right)}$$
Values of $f_{sp,T}, f_{sy,T}, E_{s,T}, \varepsilon_{st,T}$ and $\varepsilon_{su,T}$ can be obtained from Table 4-6

Table 4-6. Values for the main parameters of the stress-strain relationships of reinforcing steel at elevated temperatures (Eurocode 2)

		sy,T fyk	$\frac{f}{f}$	sp,T f yk	$\frac{E_{s,T}}{E_s}$	
Steel temp. T°C	Hot rolled	Cold worked	Hot rolled	Cold worked	Hot rolled	Cold worked
1	2	3	4	5	6	7
20	1	1	1	1	1	1
100	1	1	0.68	0.77	1	1
200	1	1	0.51	0.62	0.90	0.87
300	1	1	0.32	0.58	0.80	0.72
400	1	1	0.13	0.52	0.70	0.56
500	0.78	0.26	0.07	0.14	0.60	0.4
600	0.47	0.21	0.05	0.11	0.31	0.24
700	0.23	0.15	0.03	0.09	0.13	0.08
800	0.11	0.09	0.02	0.06	0.09	0.06
900	0.06	0.04	0.01	0.03	0.07	0.05

Table 4-6 (cont'd).

1000	0.04	0.03	0.01	0.02	0.04	0.03
1100	0.02	0.03	0.01	0.02	0.02	0.02
1200	0	0	0	0	0	0

Table 4-7. Input parameters for defining concrete plasticity.

Plasticity Parameter	Assumed Value
Dilatation angle	31°
Flow potential eccentricity	0.1
Ratio of biaxial to uniaxial stress	1.16
Yield surface shape parameter	1
Viscosity parameter	0

Table 4-8. Summary of test parameters and results for beams used for validation

Study	Beam designati on	Fire exposu	Maximum rebar temperature: °C		Residual deformation: mm		Residual load bearing capacity: kN	
		re	Measu red	Mod el	Measur ed	Model	Measur ed	Model
Dwaika t and	B1	ASTM E119	577	579	-	-	-	-
Kodur (2009)	B2	SF	493	496	13.7	20.9	119.5	120.8
	Referenc e beam	None	-	-	-	-	166	168
Kumar	Beam 1	ISO 834 (1 h)	Not Measur ed	576	18	16	139	140
and Kumar (2003)	Beam 2	ISO 834 (1.5 h)	Not Measur ed	648	22	20	119	120
	Beam 3	ISO 834 (2 h)	Not Measur ed	706	28	23	90	101
	HSCB1	SF1	387	398	6	9	112	115
MCII	HSCB2	LF1	592	616	11	12	102	107
MSU Test	NSCB1	SF2	521	541	14	17	91	92
beams	NSCB2	SF3	510	519	27	28	99	86
beams	NSCB3	LF2	580	612	-	-	-	-
	NSCB4	LF3	500	518	11	13.5	93	89

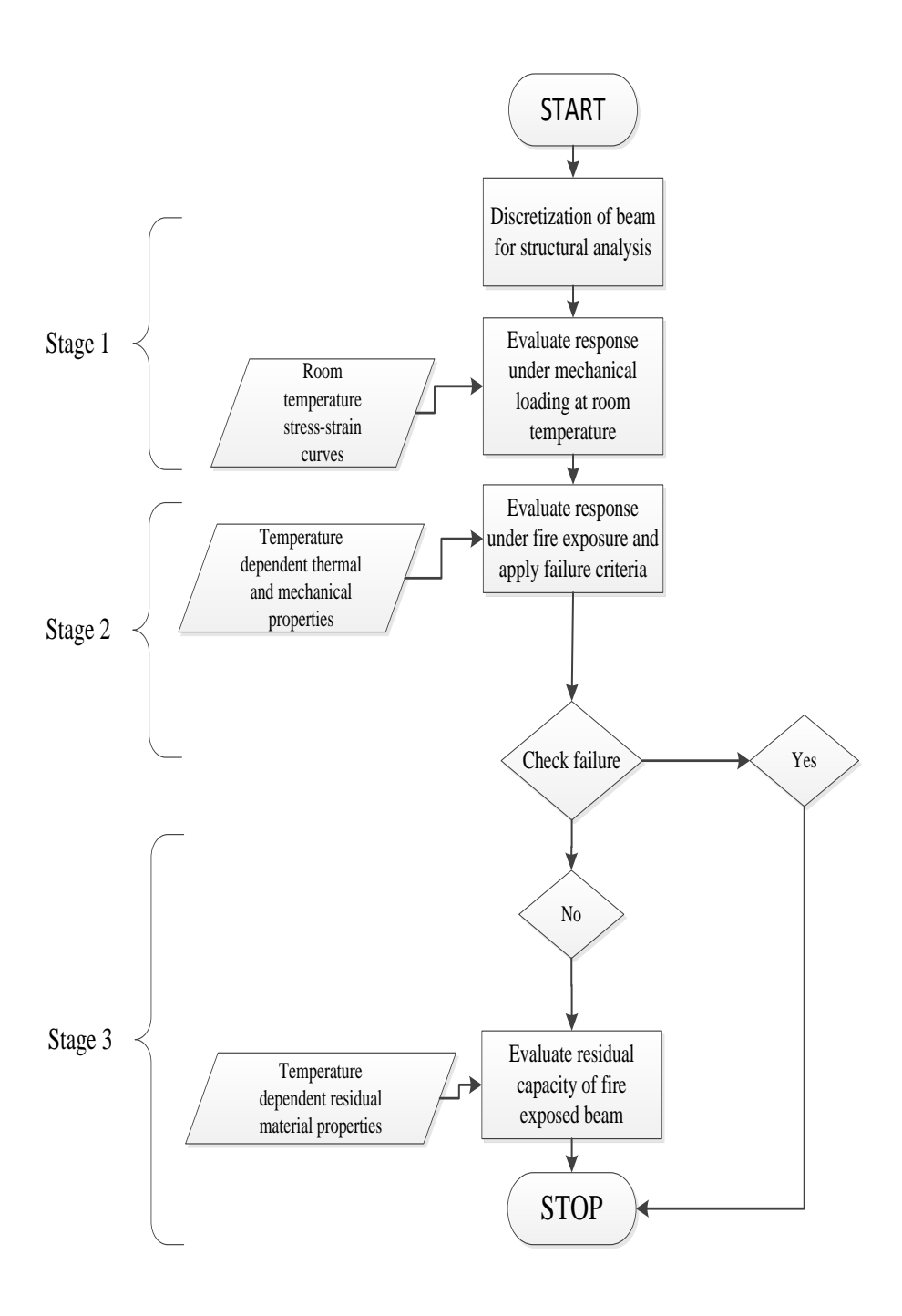


Figure 4-1. Flow chart illustrating the three stages involved in residual capacity analysis.

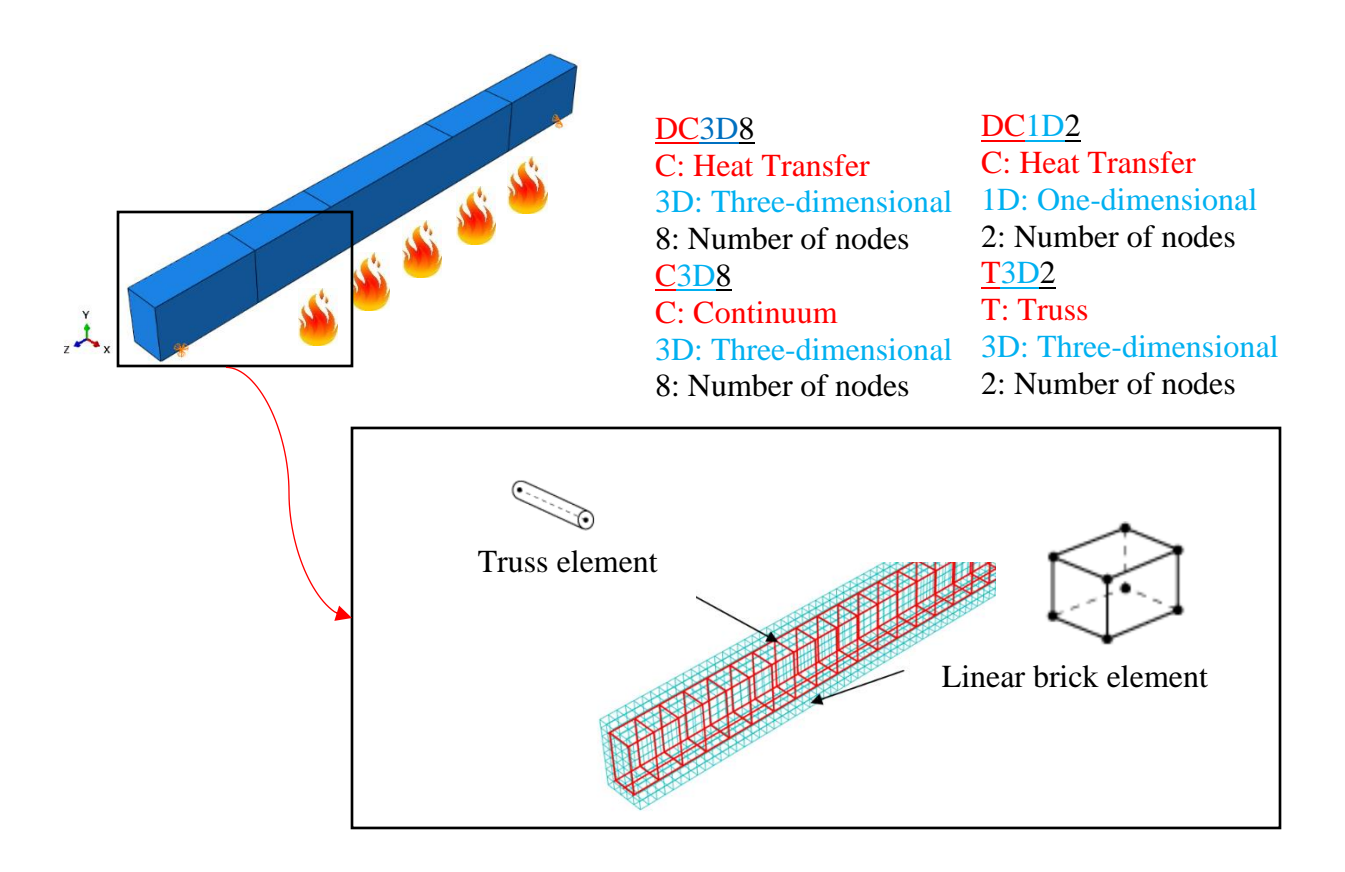


Figure 4-2. Discretization and element types adopted for thermal and structural analysis of RC beams.

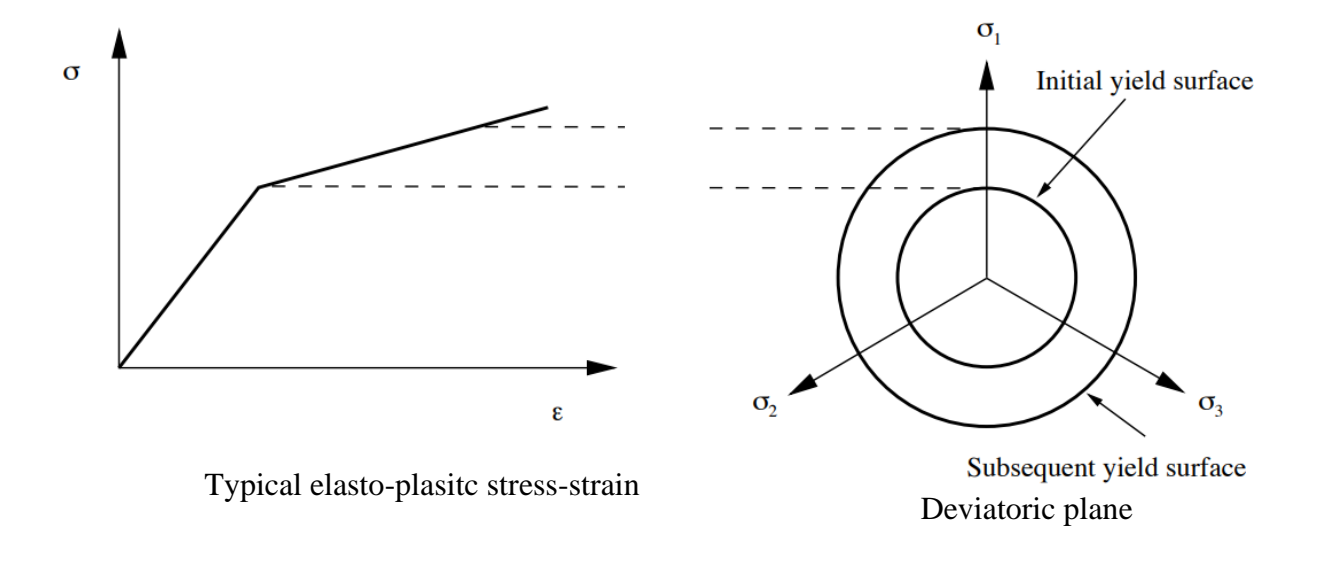


Figure 4-3. Transformation of uniaxial stress-strain relation to equivalent yield surface in the deviatoric plane comprising of stress invariants.

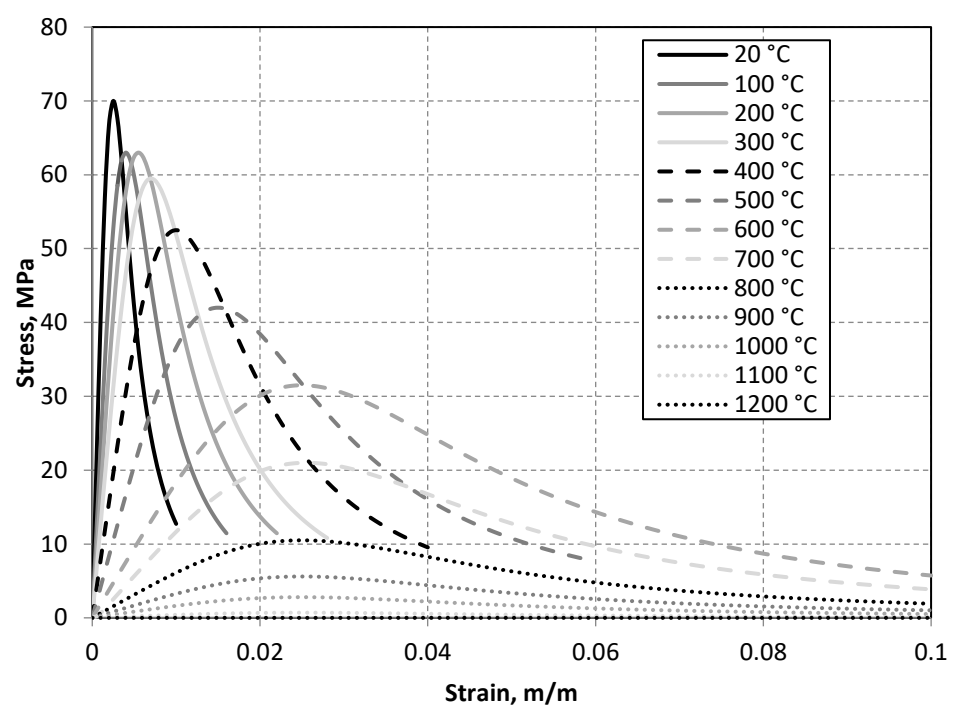


Figure 4-4. Stress-strain relationship of concrete in compression at various temperature based on Eurocode 2

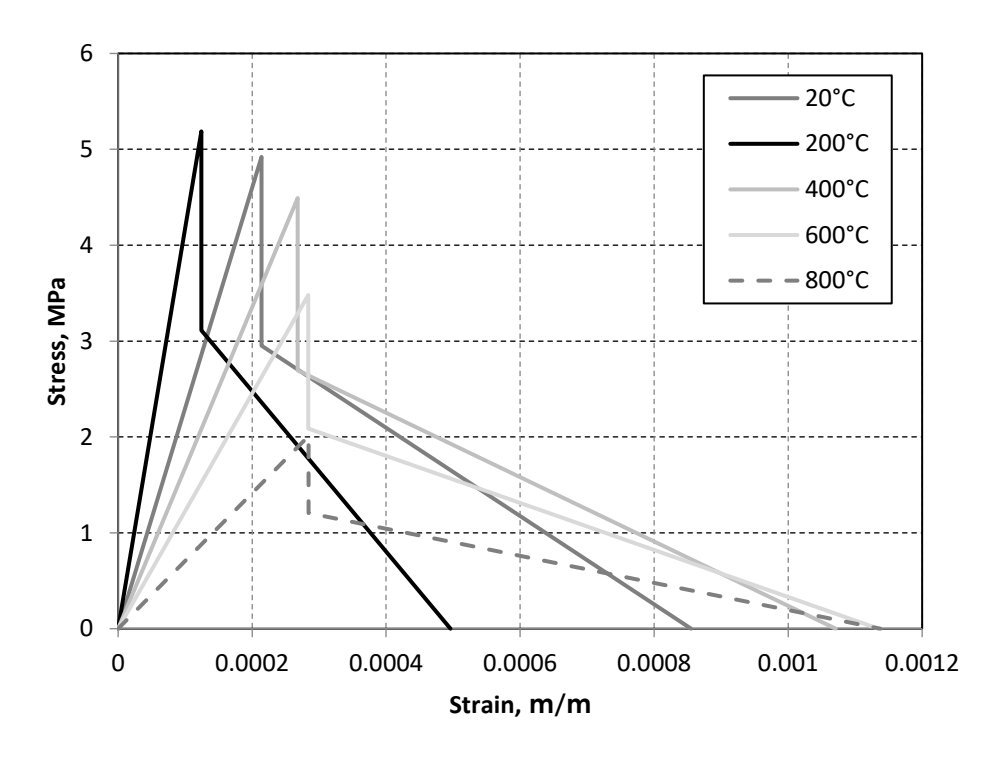


Figure 4-5. Stress-strain relationship of concrete in tension at various temperature based on Eurocode 2

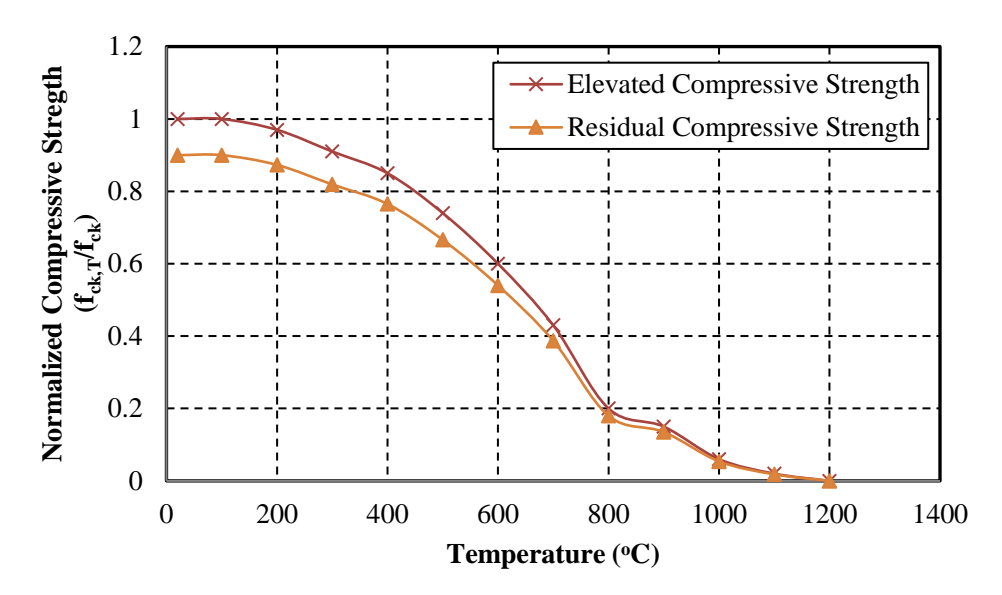


Figure 4-6. Normalized compressive strength of concrete with maximum exposure temperature

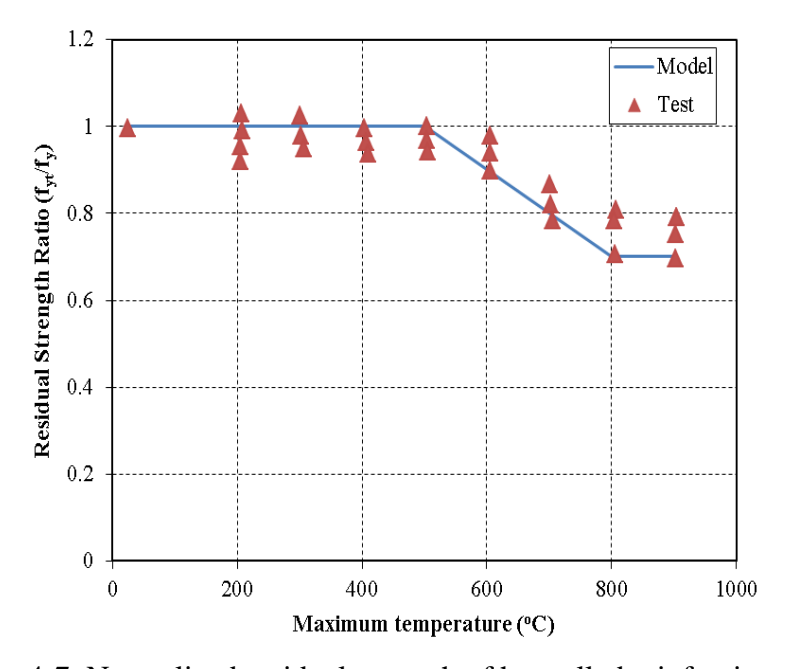
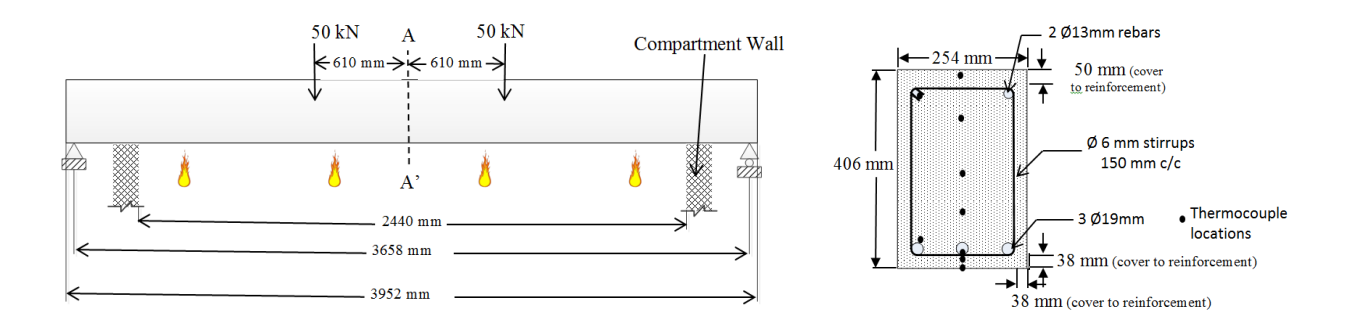
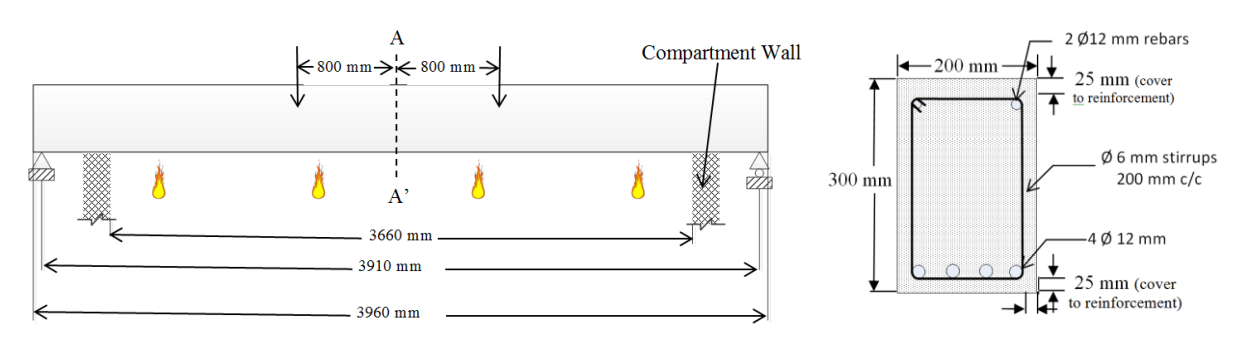


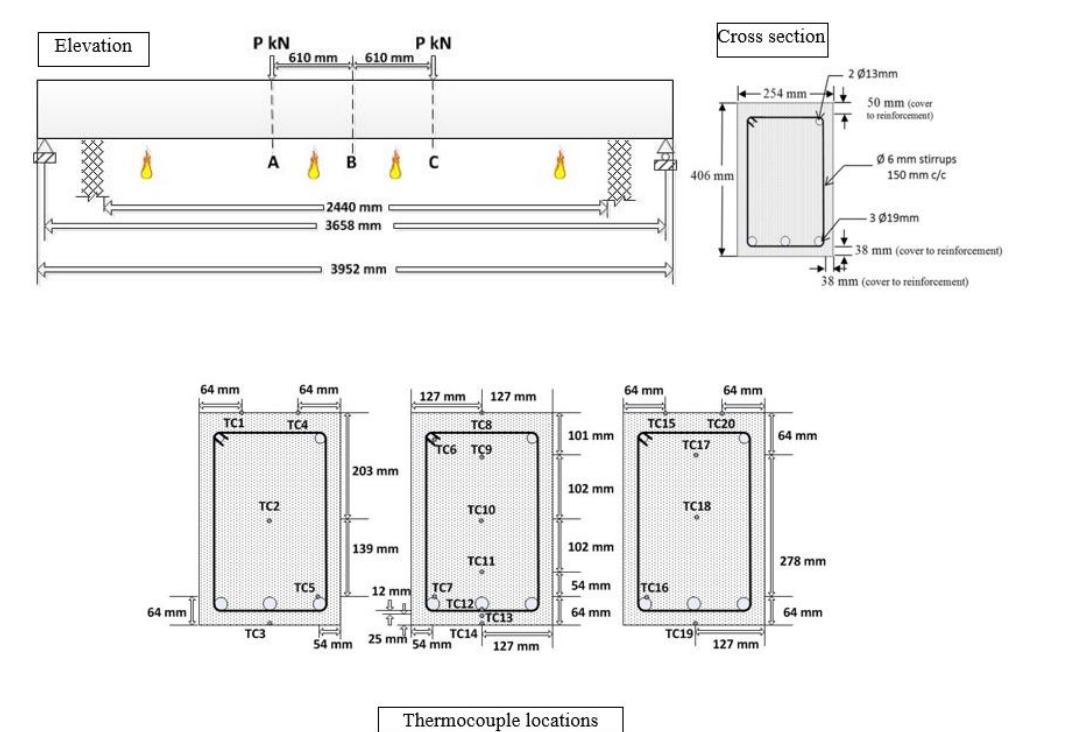
Figure 4-7. Normalized residual strength of hot rolled reinforcing steel



(a) Elevation and cross-section of beams 'B1' and 'B2'



(b) Elevation and cross-section of beams 'Reference beam', 'Beam 1', 'Beam 2', 'Beam 3' and 'Beam 4'



(c) Elevation and cross-section of beams HSCB1, HSCB2, and NSCB1 through NSCB4

Figure 4-8. Loading and reinforcement details of RC beams used for validation

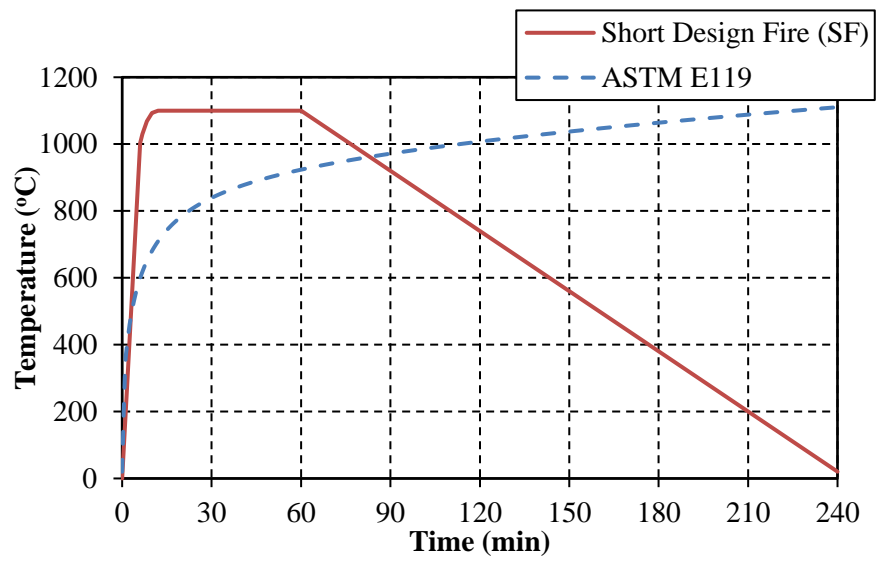
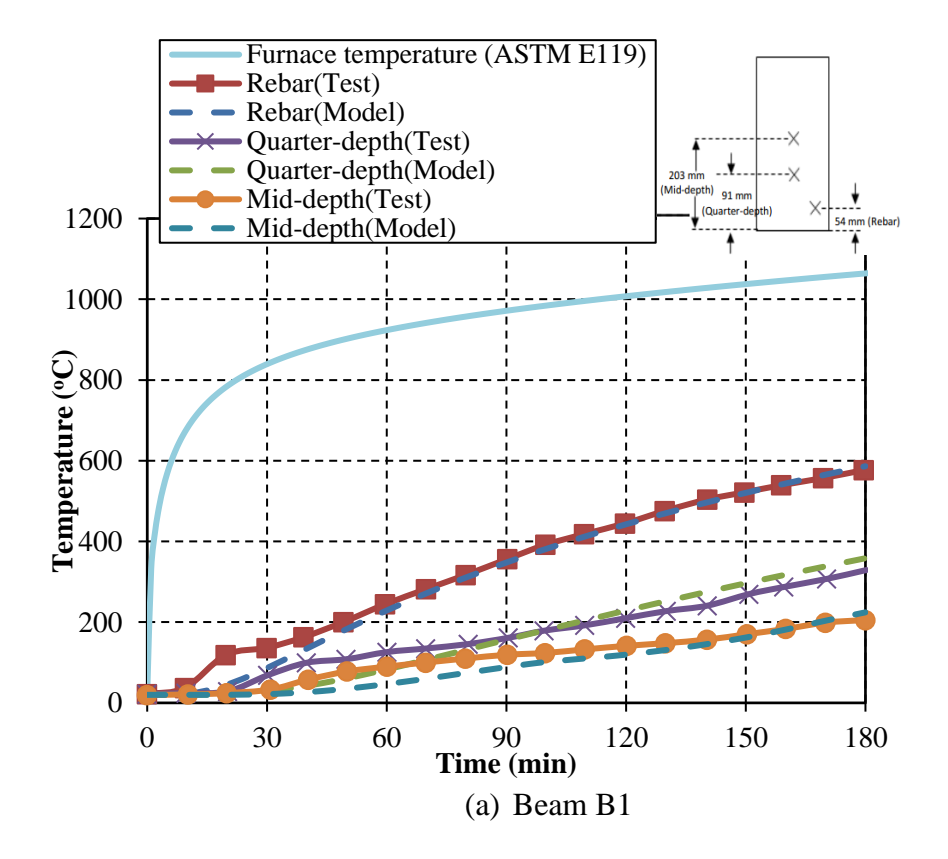


Figure 4-9. Time-temperature curves for fire scenarios used in fire tests on beams B1 and B2



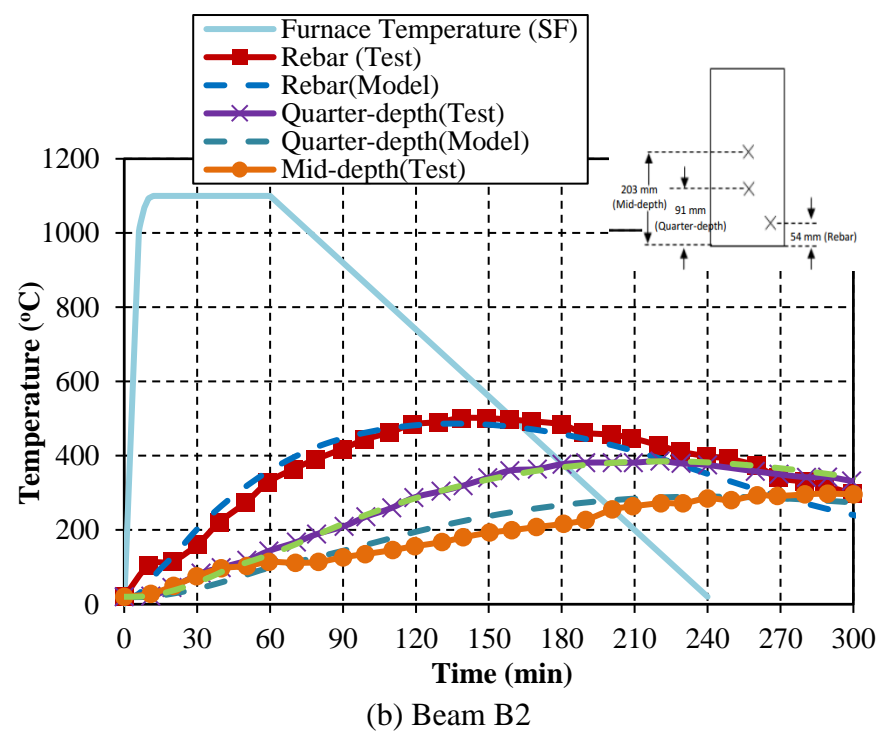


Figure 4-10. Comparison of predicted and measured cross sectional temperatures for beams B1 and B2 during fire exposure

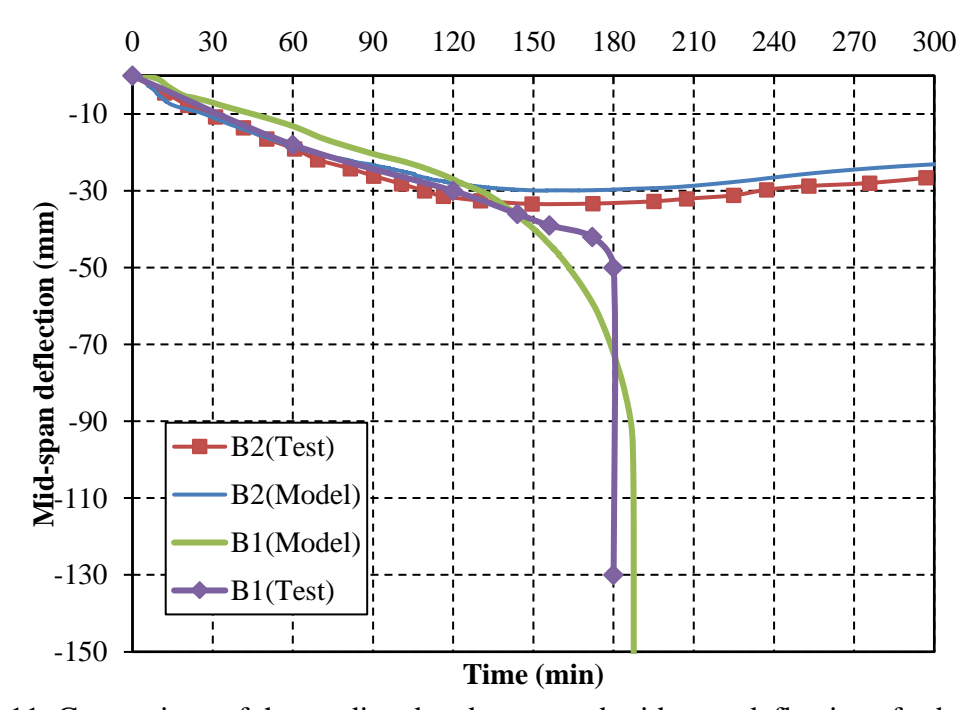


Figure 4-11. Comparison of the predicted and measured mid-span deflections for beams B1 and B2 during fire exposure

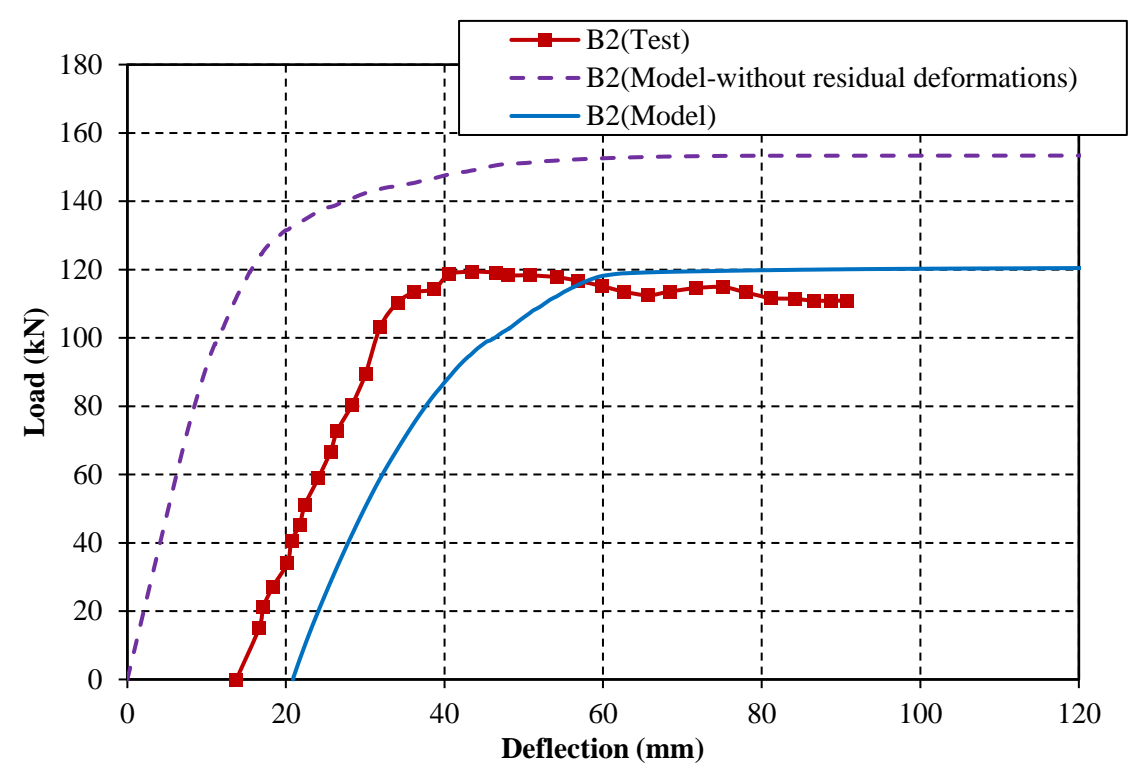


Figure 4-12. Predicted and measured post-fire residual load-deflection response for beam B2

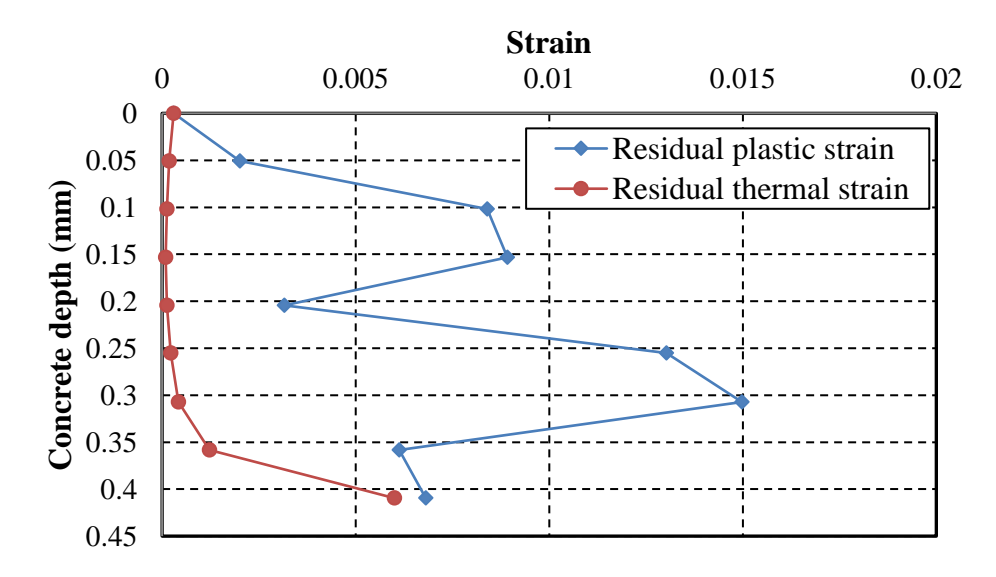


Figure 4-13. Expected residual thermal expansion (or shrinkage) strains versus residual plastic deformations across the section at mid-span for beam B2

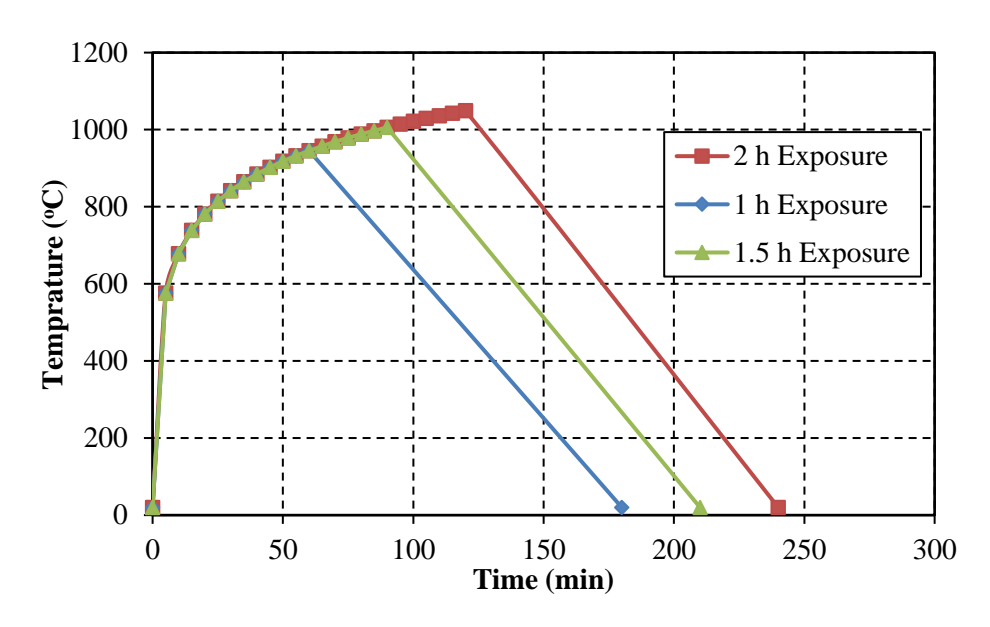


Figure 4-14. Fire exposures for tested beams

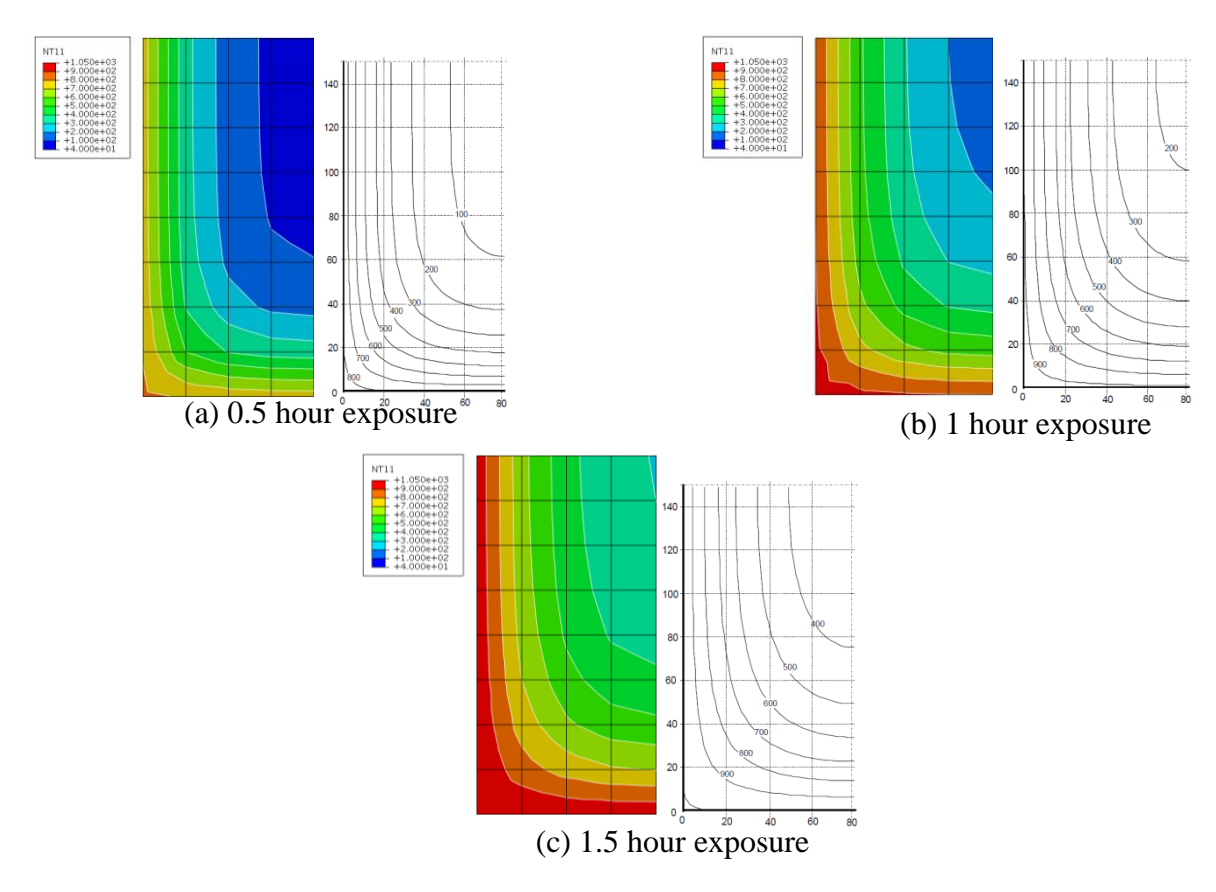
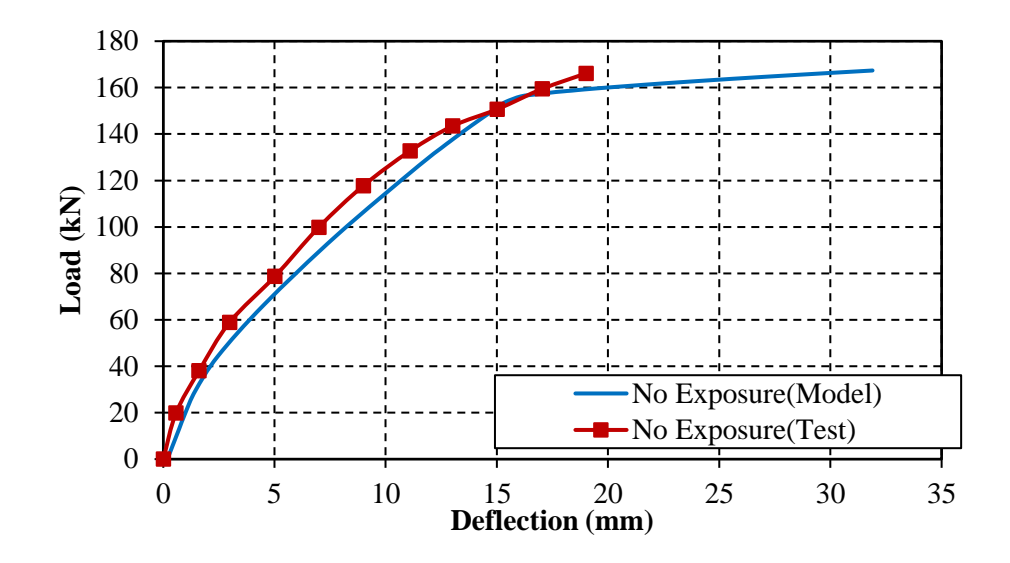


Figure 4-15.Comparison of predicted and published temperature contours (EN 1992-1-2 2004) over the beam cross-section after heating of: (a) 0.5 h; (b) 1 h and (c) 1.5 h for validation



(a) No exposure (room temperature testing)

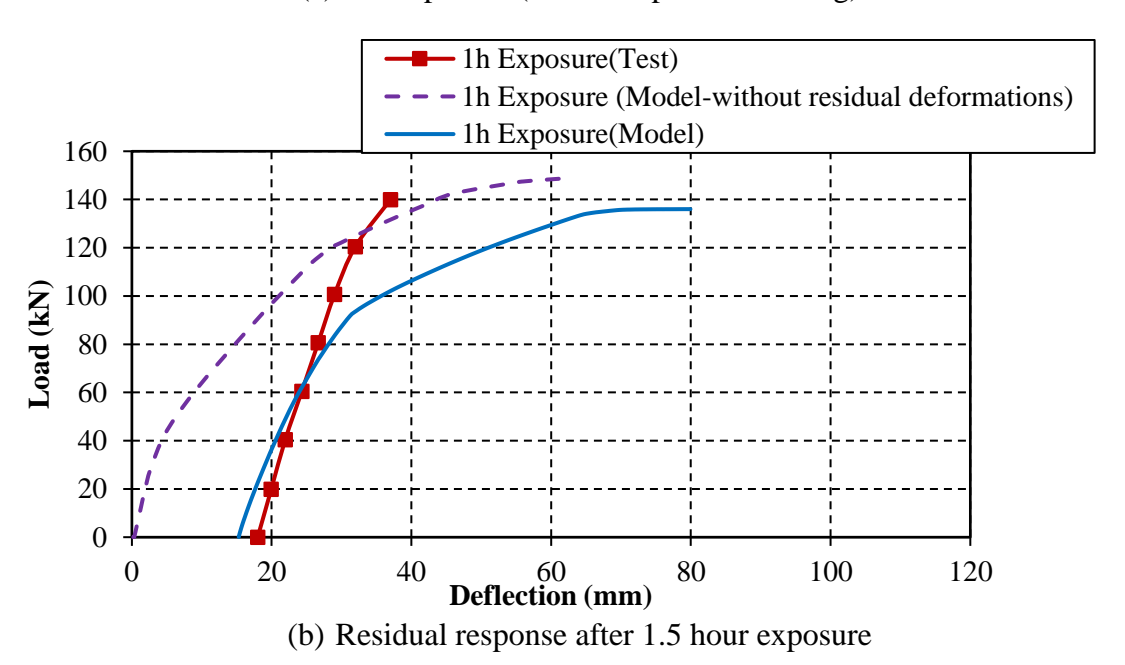
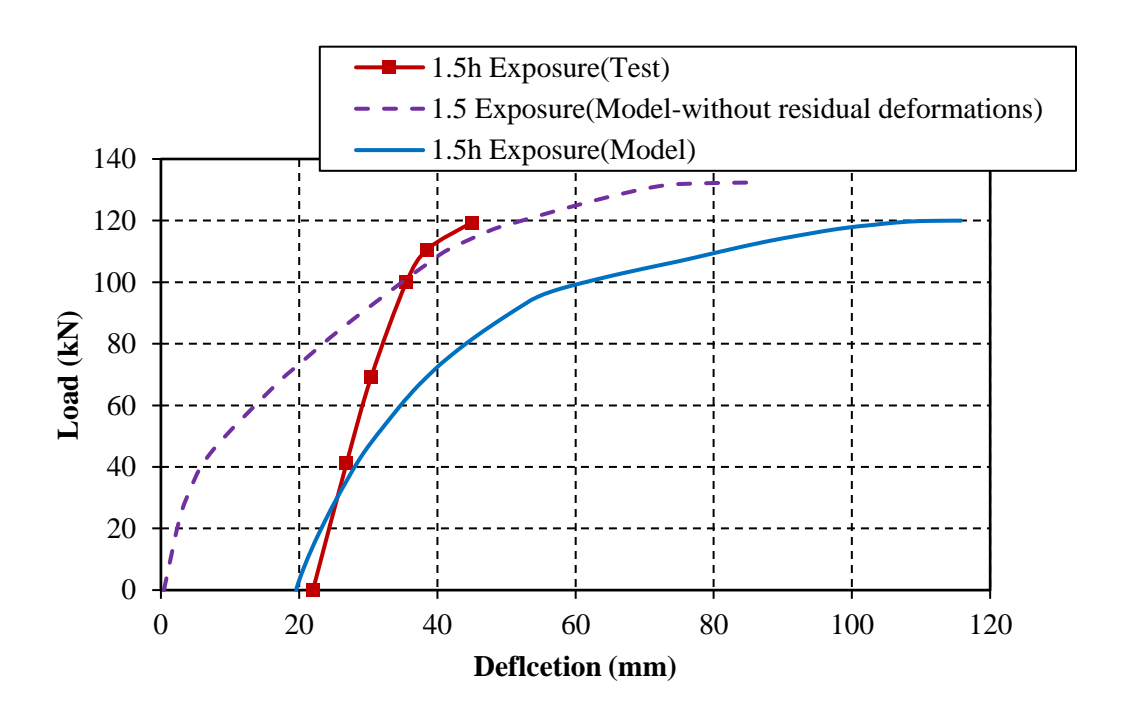
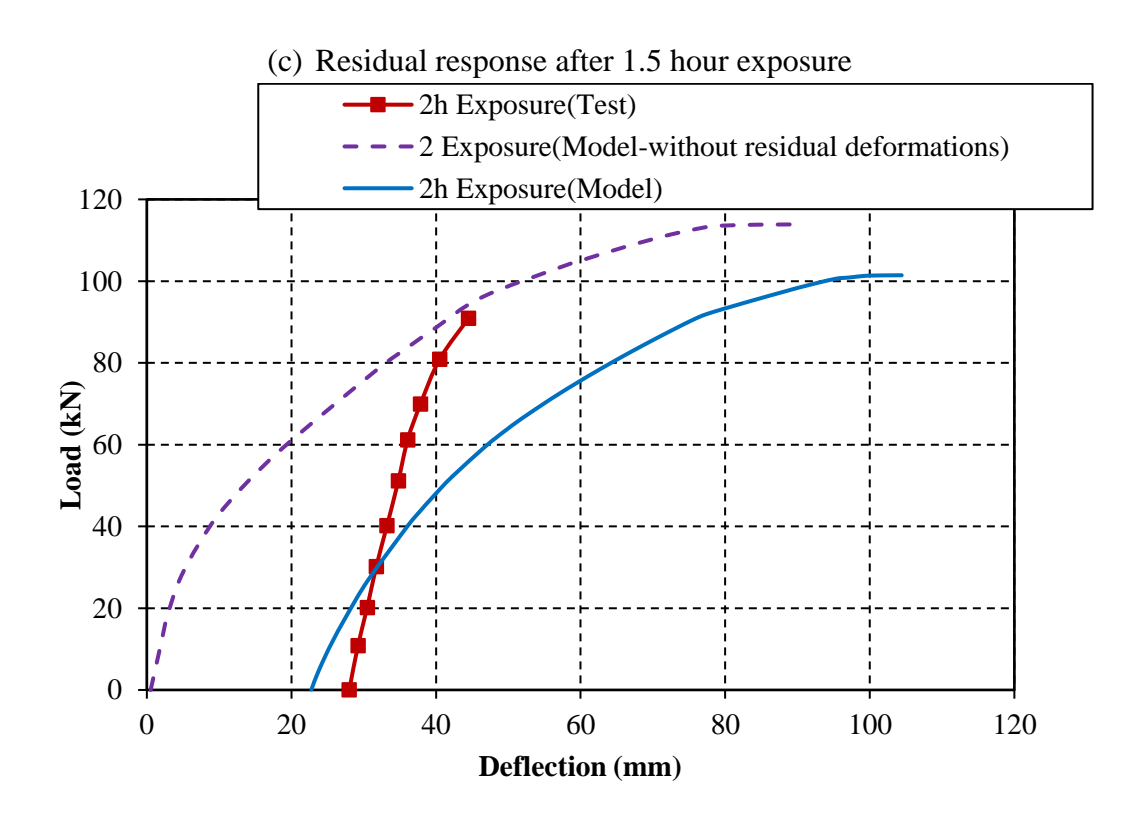


Figure 4-16.Comparison of predicted and measured post fire load-deflection response for tested beams

Figure 4-16 (cont'd).





(d) Residual response after 2 hour exposure

Figure 4-17. Comparison of predicted and measured post fire load-deflection response for tested beams

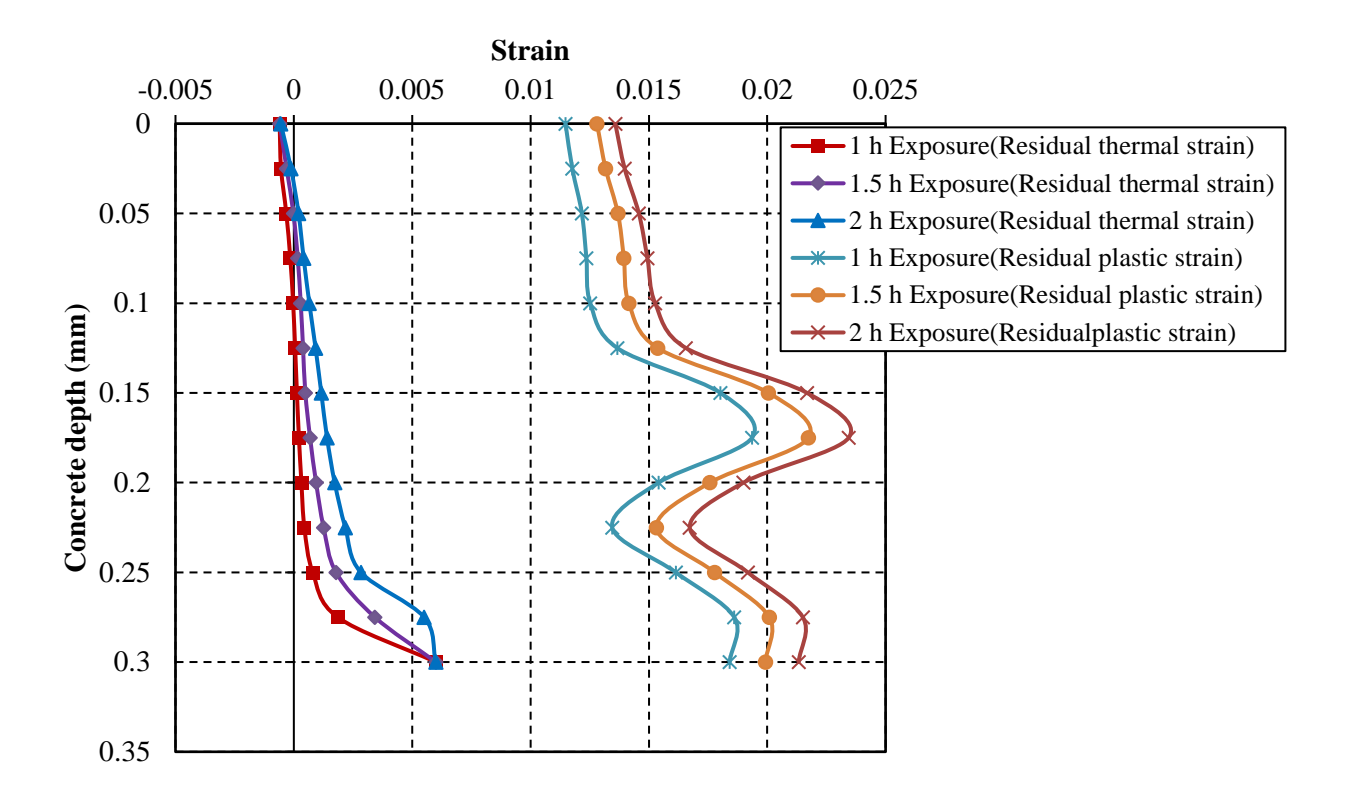


Figure 4-18. Expected residual thermal expansion (or shrinkage) strains versus residual plastic deformations across the section at mid-span for tested beams

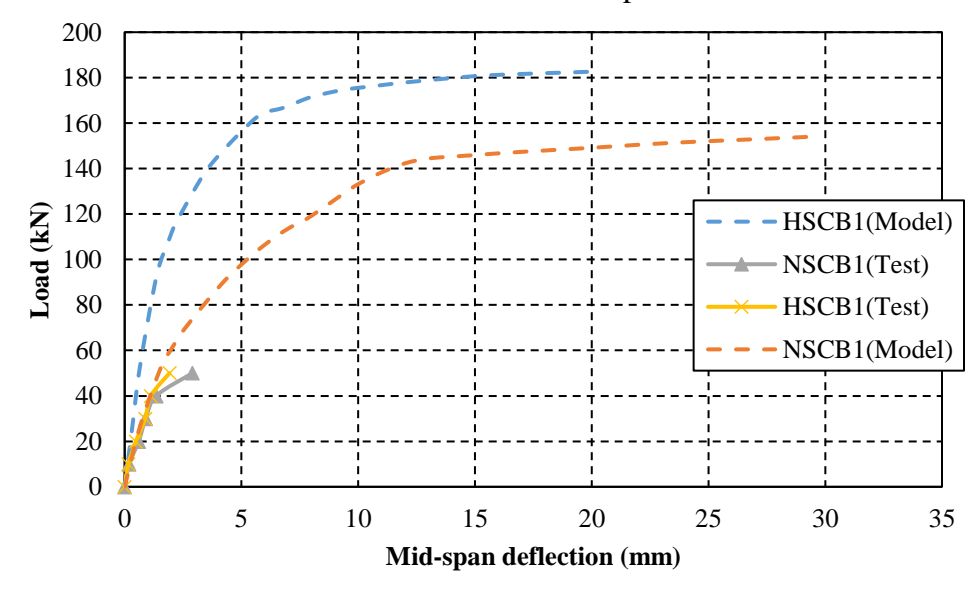


Figure 4-19. Measured and predicted load-deflection response for room temperature analysis during Stage 1.

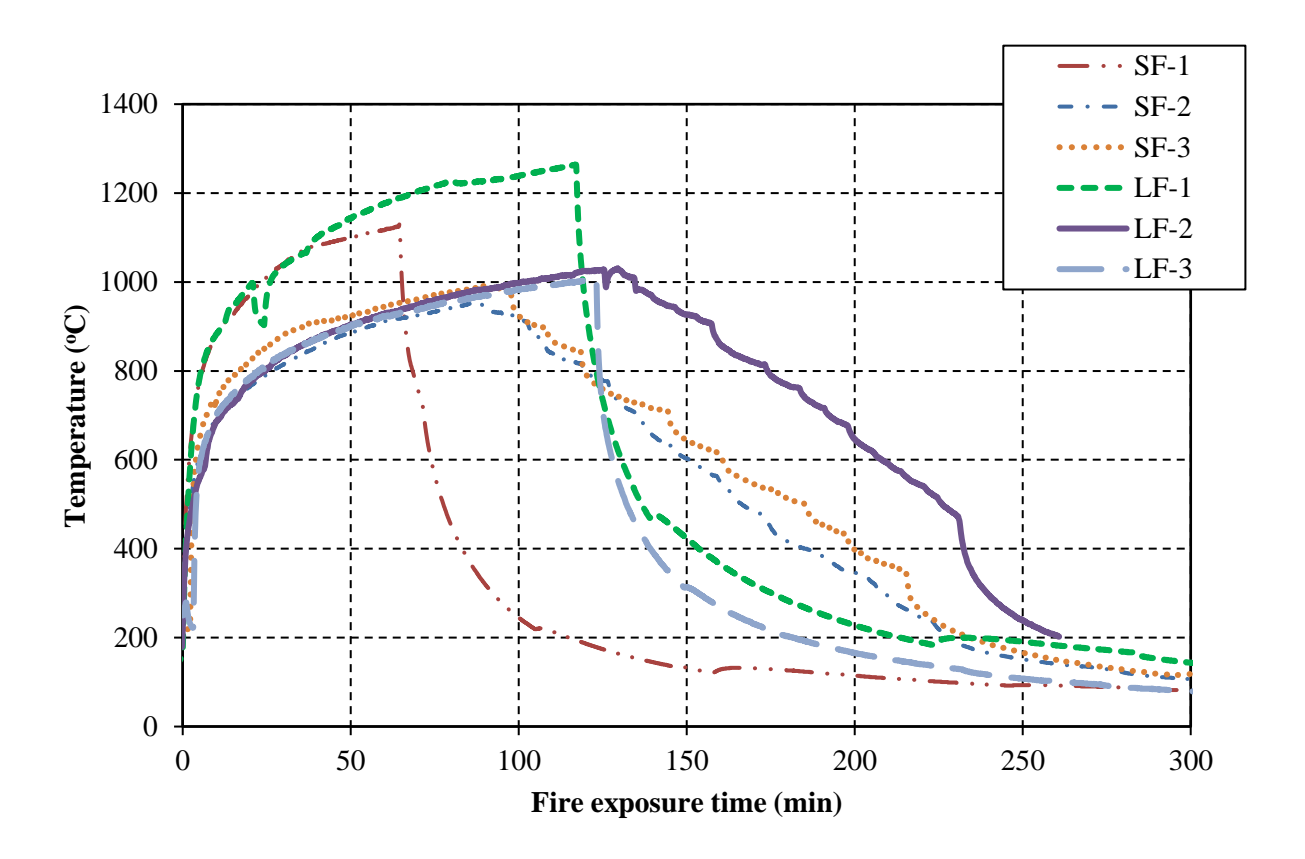
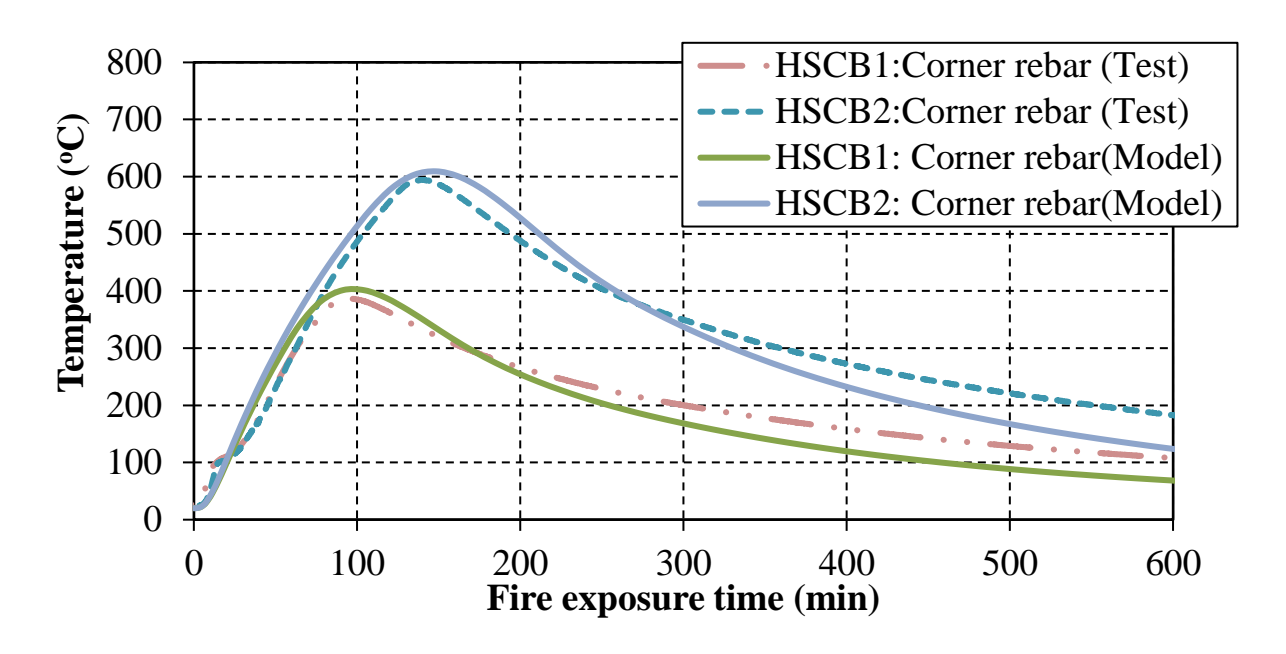
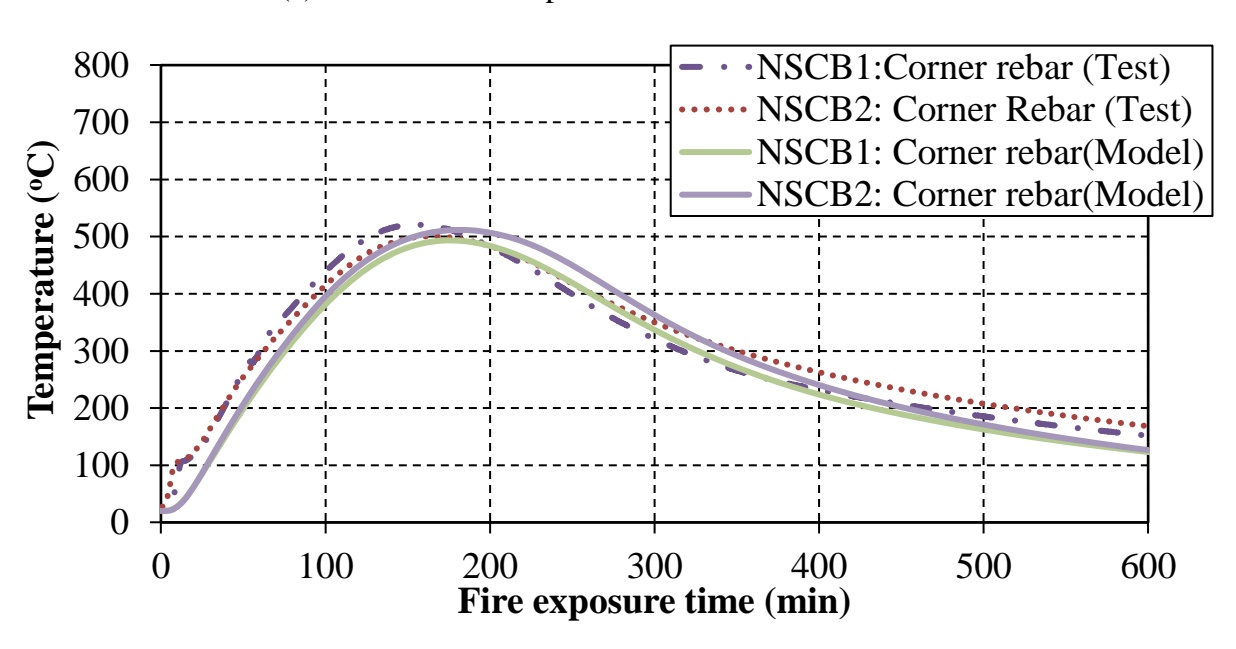


Figure 4-20. Time—temperature curves depicting fire scenarios used in fire tests for HSCB1, HSCB2, and NSCB1 through NSCB4.



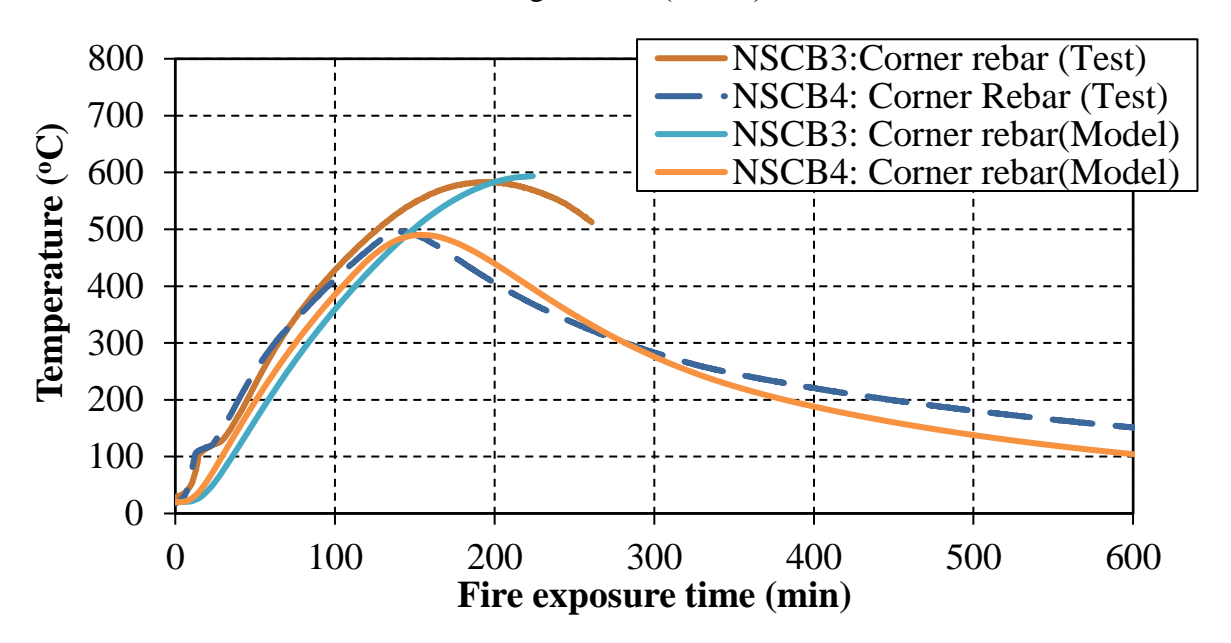
(a) Corner rebar temperatures for HSCB1 and HSCB2



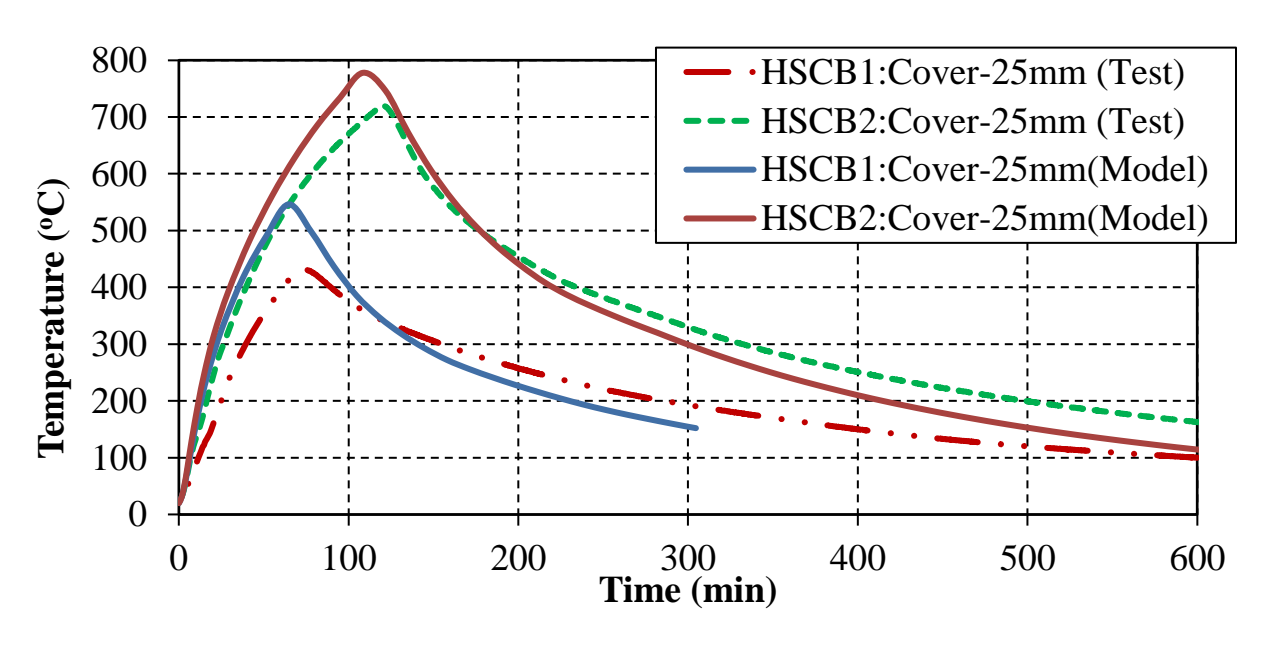
(b) Corner rebar temperatures for NSCB1 and NSCB2

Figure 4-21. Comparison of measured and predicted temperatures for heating and cooling phases of testing during Stage 2.

Figure 4-20 (cont'd).

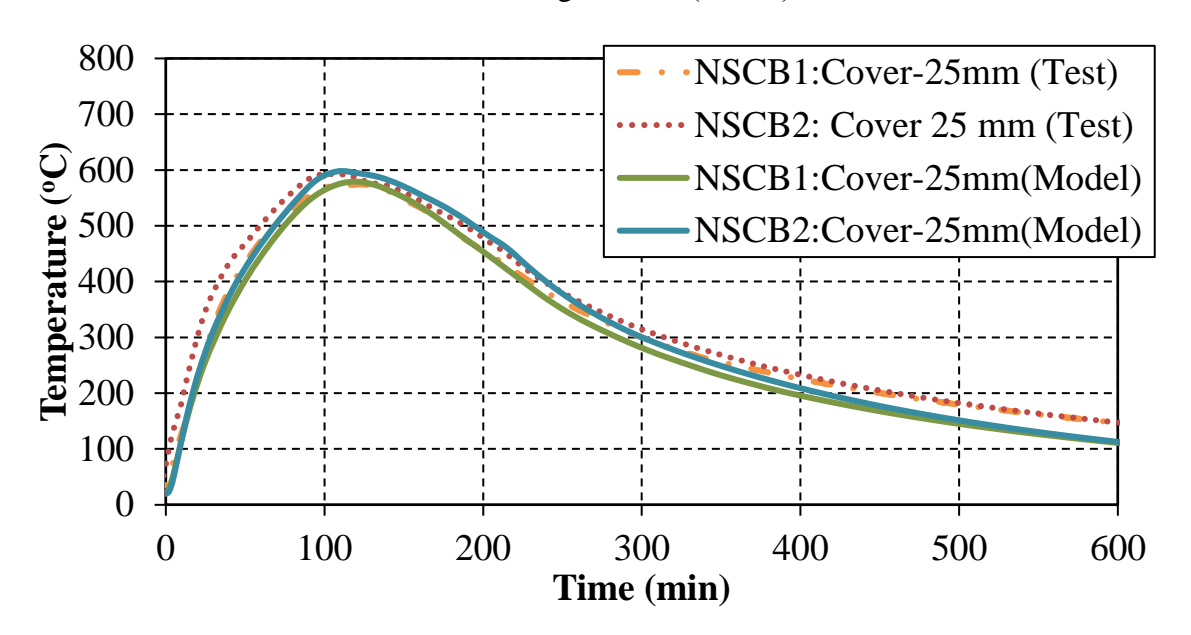


(c) Corner rebar temperatures for NSCB3 and NSCB4

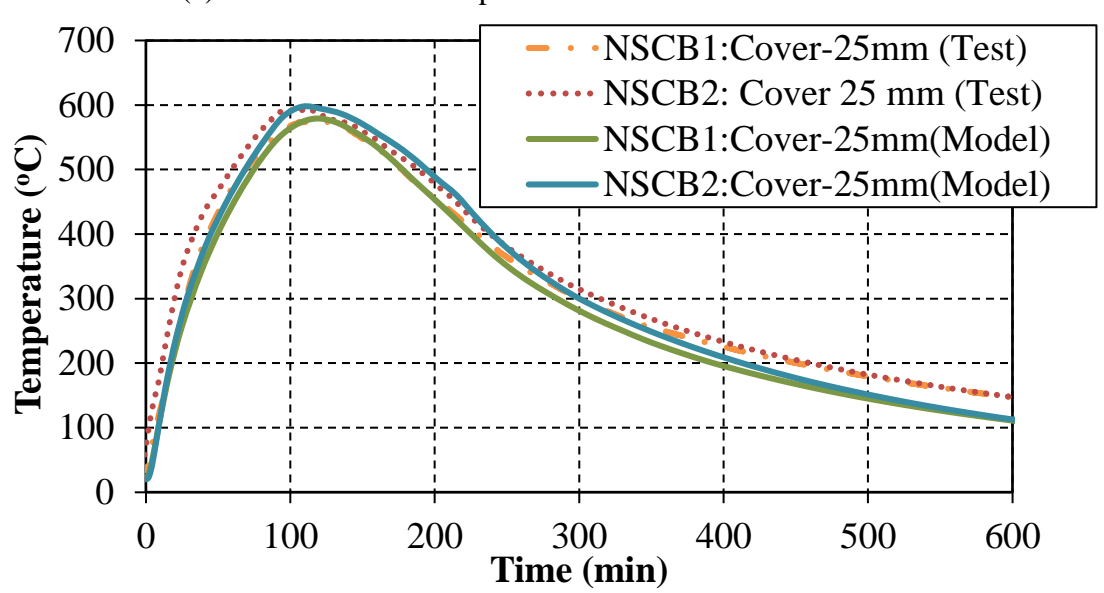


(d) Concrete cover temperatures for HSCB1 and HSCB2

Figure 4-20 (cont'd).

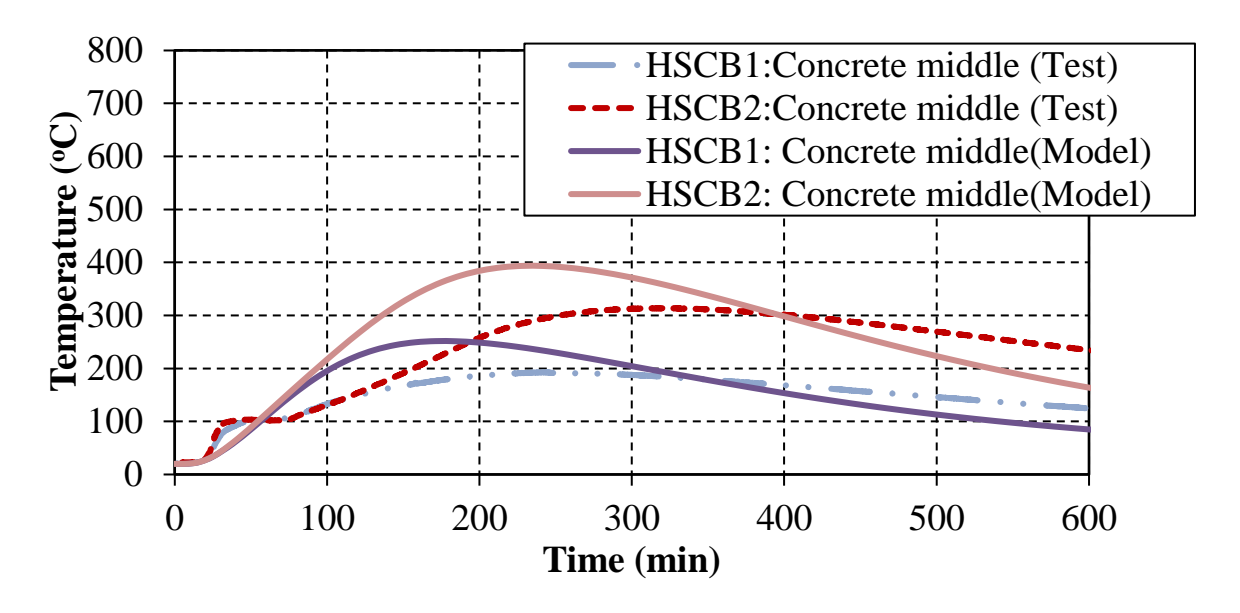


(e) Concrete cover temperatures for NSCB1 an NSCB2

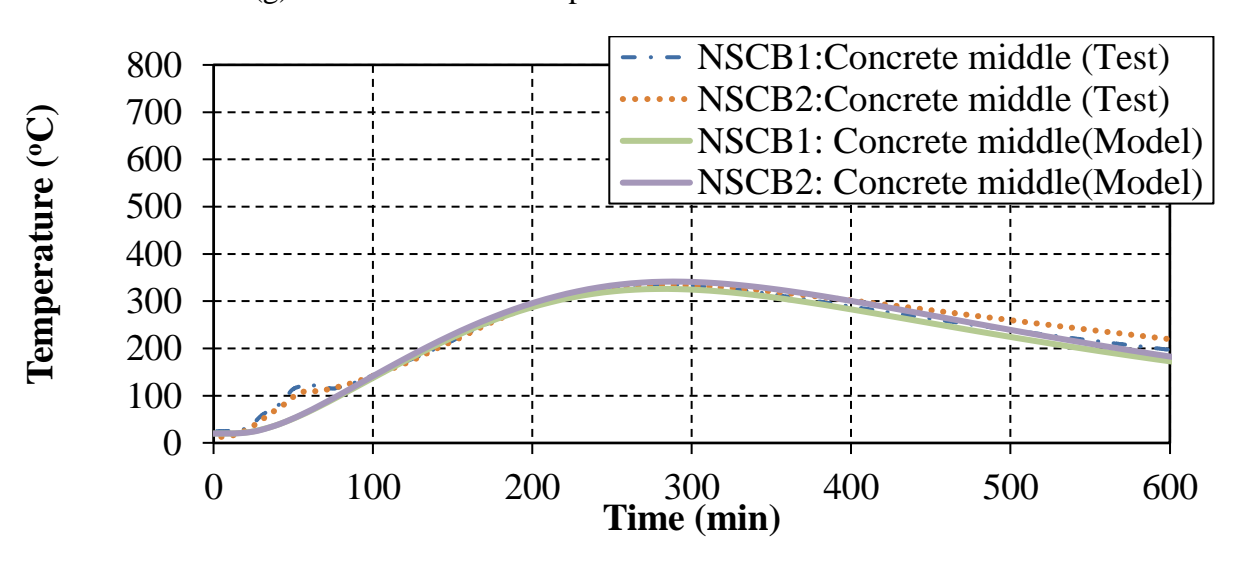


(f) Concrete cover temperatures for NSCB1 an NSCB2

Figure 4-20 (cont'd).

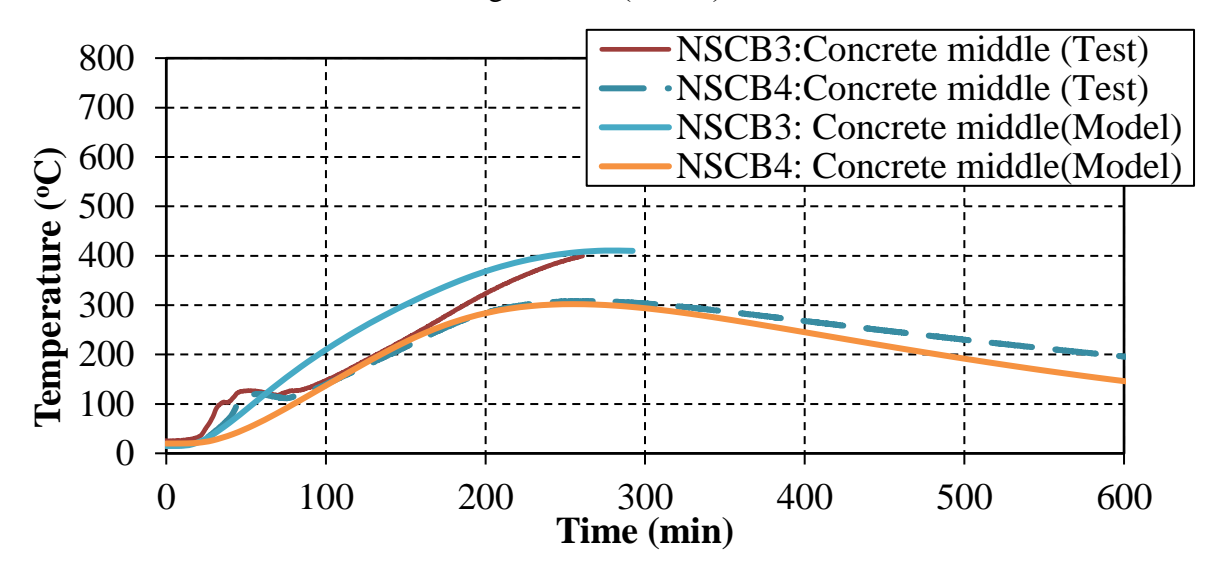


(g) Concrete middle temperatures for HSCB1 and HSCB2

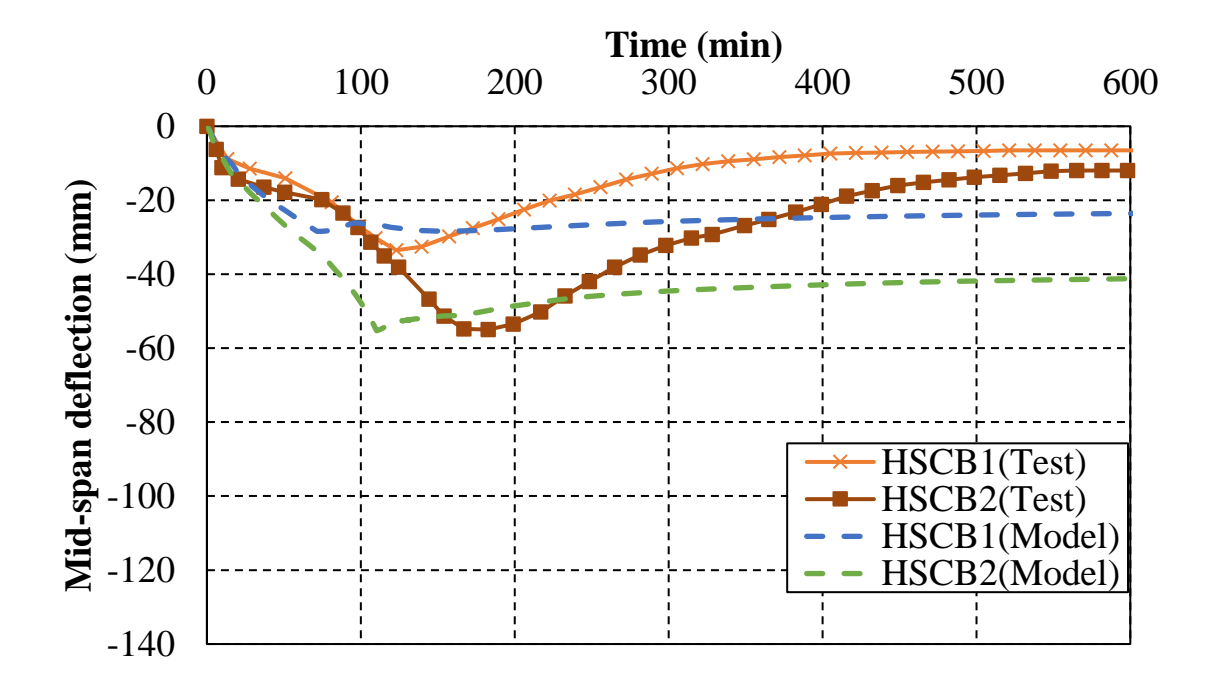


(h) Concrete middle temperatures for NSCB1 and NSCB2

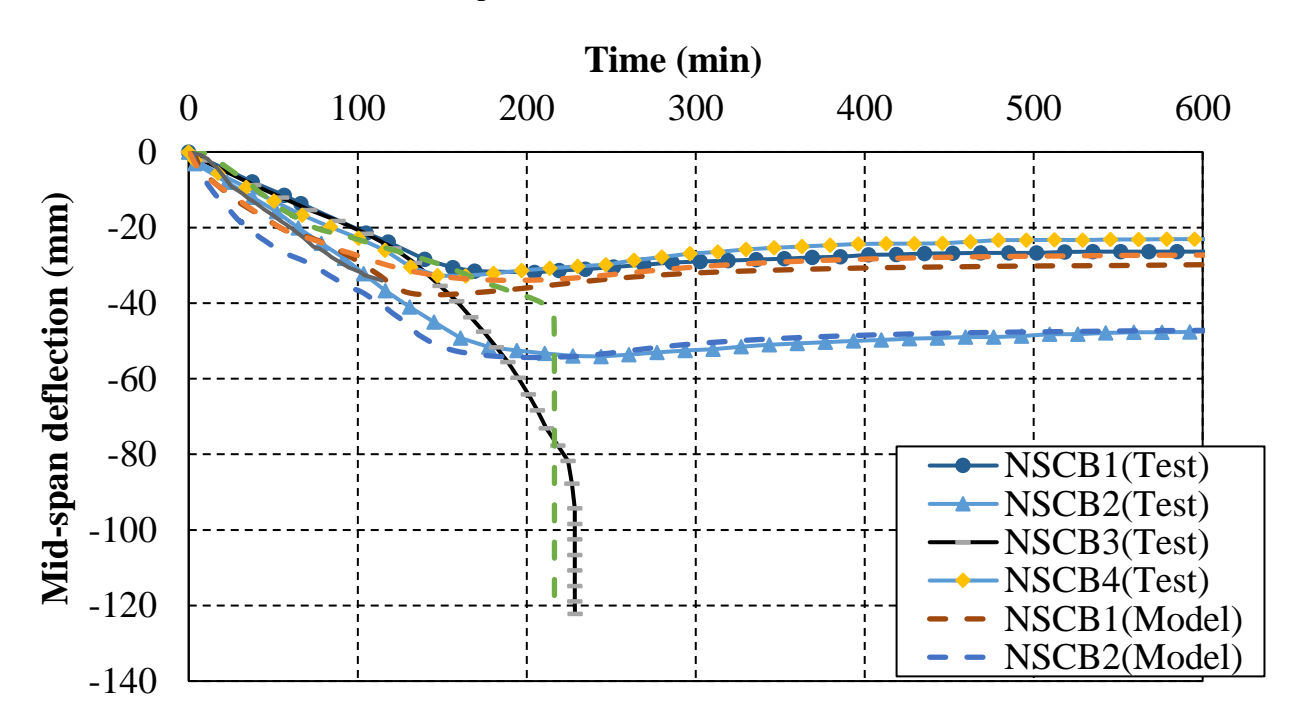
Figure 4-20 (cont'd).



(i) Concrete middle temperatures for NSCB1 through NSCB4

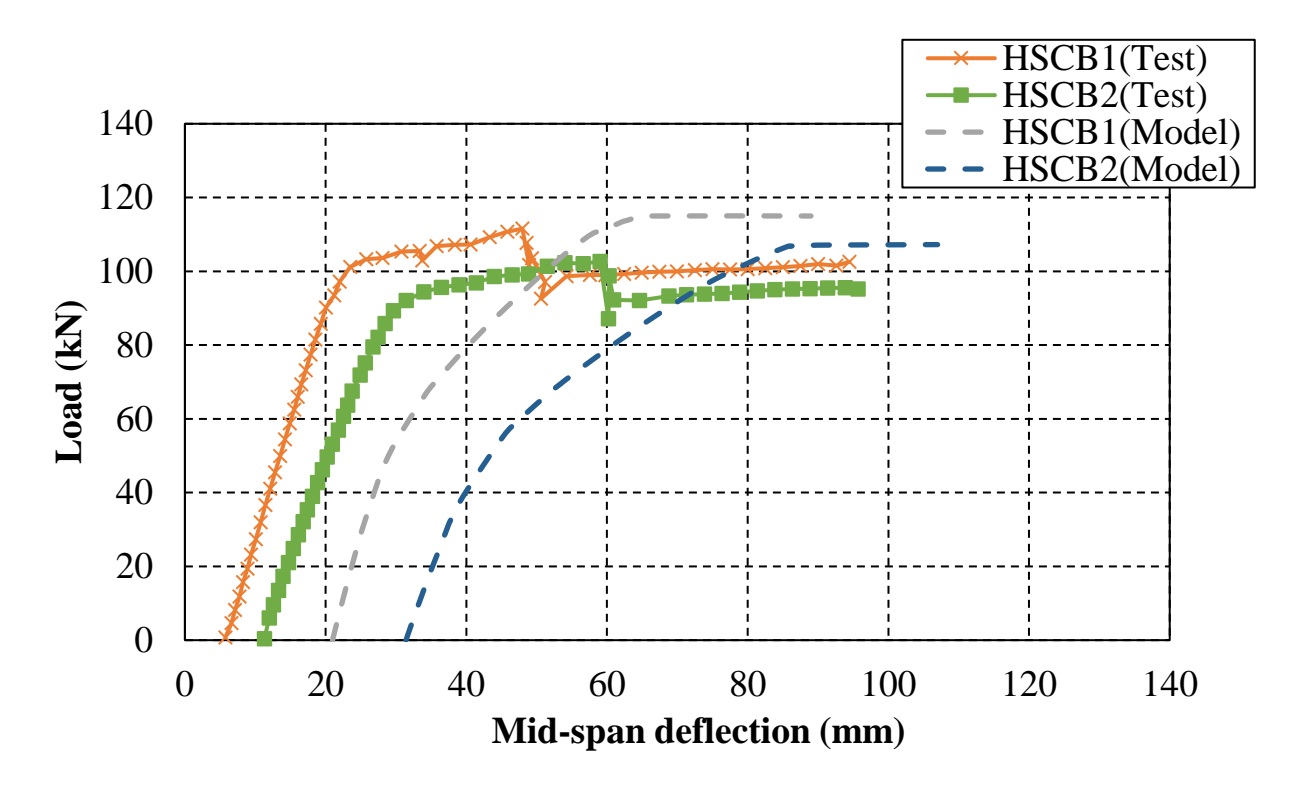


(a) Mid-span deflections for HSC B1 and HSCB2

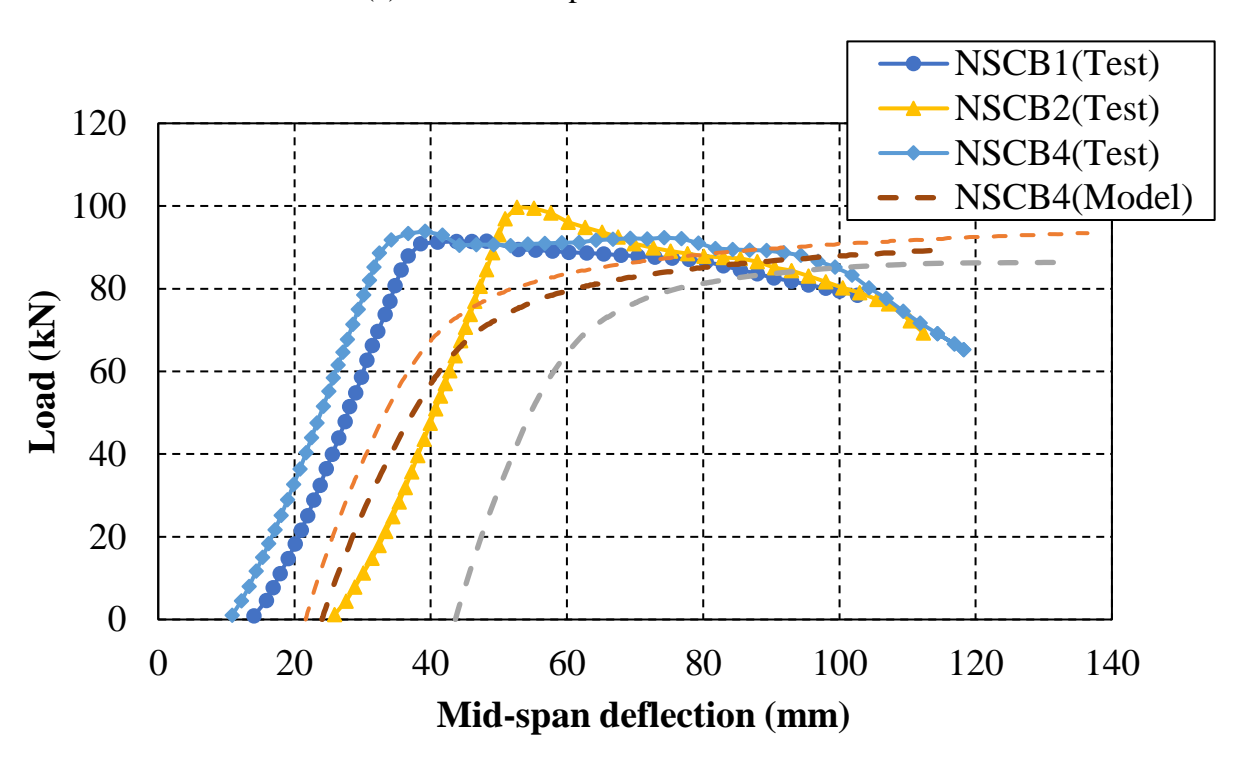


(b) Mid-span deflections for NSCB1 through NSCB4

Figure 4-22. Comparison of measured and predicted mid span deflection progression with time during Stage 2.

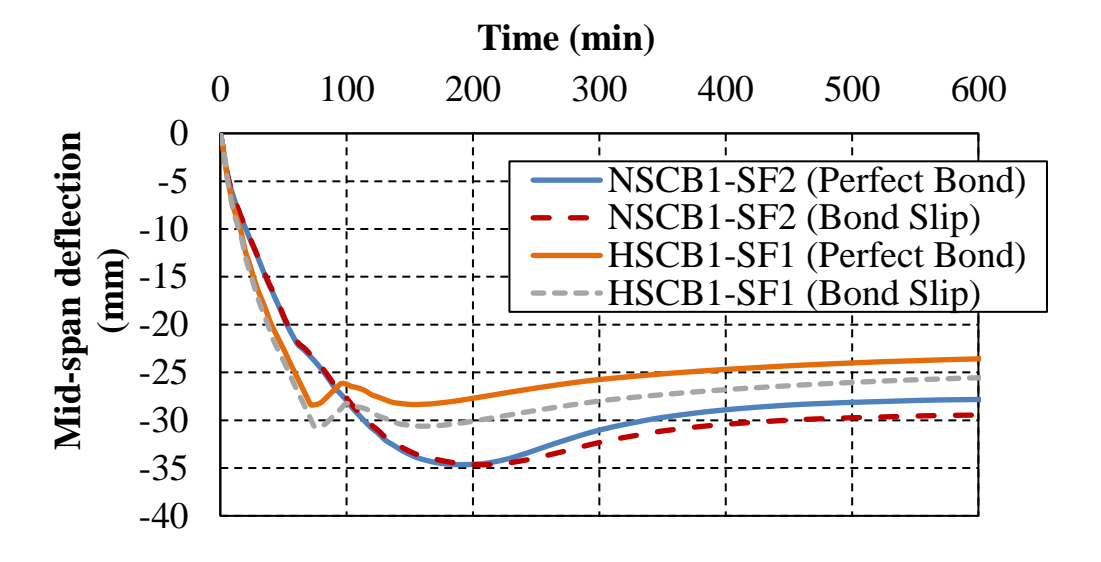


(a) Residual response for HSCB1 and HSCB2

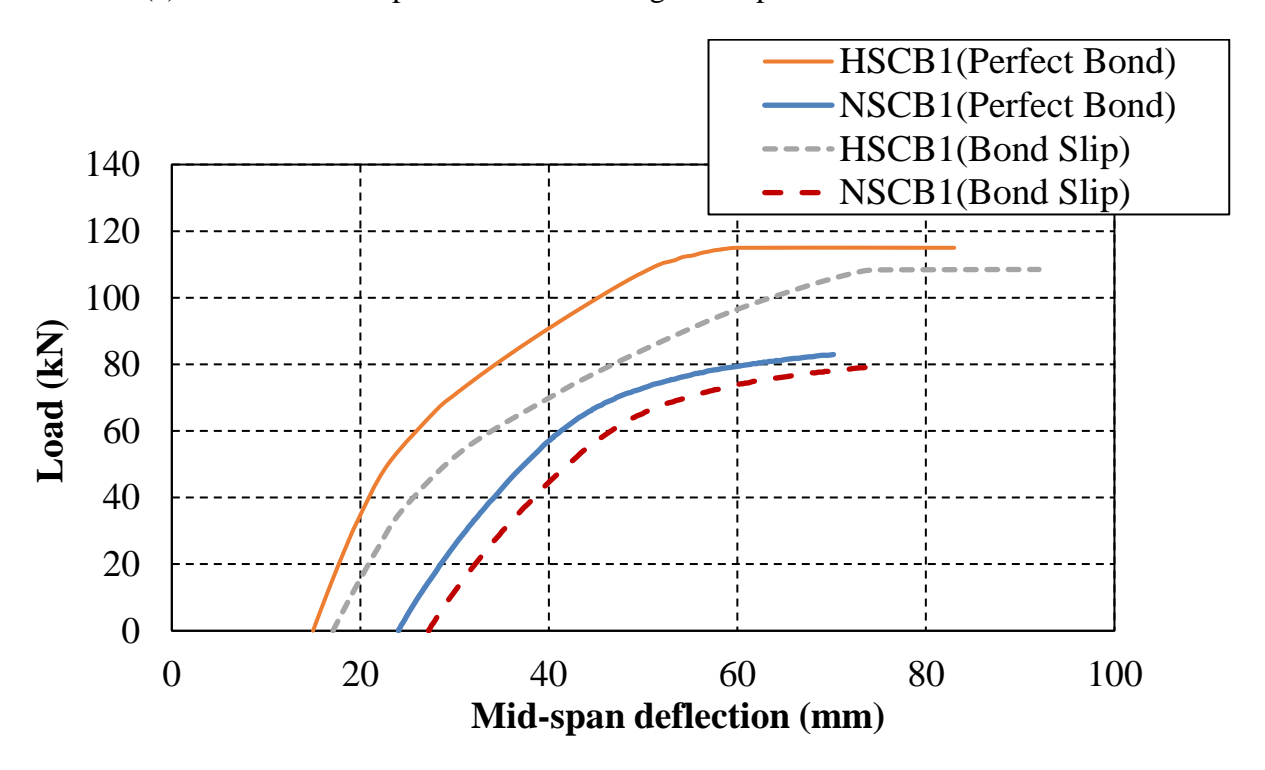


(b) Residual response for NSCB1, NSCB2, and NSCB4

Figure 4-23. Predicted and measured post-fire residual load-deflection response of fire damaged beams during Stage 3.



(a) Predicted mid-span deflection during fire exposure for HSCB1 and NSCB1



(b) Predicted residual response of beams HSCB1 and NSCB1

Figure 4-24. Effect of temperature induced bond degradation on fire behavior and residual response of RC beams following fire exposure.

5 PARAMETRIC STUDIES

5.1 General

The response of fire damaged concrete members (beams) is influenced by number of factors. It is crucial to identify and quantify the effects of these factors for understanding the residual behavior and also to evaluate residual capacity of fire damaged concrete members. Parametric studies can generate data that can be utilized to identify significant factors and also to quantify the effect of these factors on overall performance. The validated numerical, presented in Chapter 4, is applied to evaluate the effects of various factors influencing the response of fire damaged concrete beams. The results from parametric studies are be utilized to develop design guidelines on evaluating residual capacity of fire damaged concrete beams. Details analysis on procedure and results of parametric studies are discussed in the following sections.

5.2 Factors influencing fire response

A state-of-the-art review presented in Chapter 2 indicated that, RC beams retain significant level of capacity after exposure to fire. However, the extent of residual capacity in a fire exposed RC beam is dependent on fire exposure scenario, peak rebar temperature, level of loading (load ratio), restraint conditions and sectional dimensions of beam. Furthermore, since full moment capacity of a flexural member is governed by reinforcing steel, amount of concrete cover provided influences peak rebar temperatures, and hence residual capacity. Many of these factors vary significantly in different scenarios and are interdependent. Therefore, the computed residual capacity of RC members after fire exposure can vary widely based on the assumptions used in the analysis (Kodur et al. 2010c). The main factors influencing the residual response of fire damaged RC beams are:

- Fire severity
- Load level
- Axial restraint
- Cross-sectional dimensions
- Cover to reinforcement

Although previous studies reported these factors to be critical, the extent of influence of these parameters is not fully quantified. This chapter presents numerical studies in order to quantify the influence of critical factors governing residual response of fire exposed RC beams.

5.3 Parametric studies

Results from numerical studies are utilized to quantify the influence of various parameters on the response of fire exposed RC beams, and ar discussed in the following section.

5.3.1 General

Parametric study on fire damaged RC beams is performed utilizing the three-dimensional finite element based numerical model developed in Chapter 4. As part of this parametric study, four beams (designated beam BX1, BX2, BX3, and BX4) having varying span, varying cross-sectional dimensions, reinforcement details, and clear cover were analyzed. Beams BX1, BX2, and BX3 were 6 m in span, with cross-sectional sizes of 125×250 mm for beam BX1, 180 × 300 for beam BX2 and 300 × 480 mm for beam BX3, respectively. Beam BX4 was 5 m in span, with cross-sectional size of 350 × 450 mm. Beams BX1, BX2, and BX3 were assumed to be made of normal strength concrete having compressive strength of 40 MPa with reinforcing bars and stirrups having yield strength of 420 MPa and 280 MPa respectively. Beam BX4 was assumed to be made of concrete having compressive strength of 50 MPa, and reinforcing steel with yield strength 450 MPa. The flexural reinforcement in each of the three beams is provided such that it satisfies strain

conditions for tension-controlled sections as per ACI 318 (ACI 2008) guidelines. Temperature dependent material property relations for concrete and reinforcing steel at various stages are adopted based on discussion provided in Chapter 4. Beams BX1, BX2, and BX3 have identical shear reinforcement comprising of stirrups of φ 10 mm spaced at 125 mm center to center. Beam BX4 has stirrups of φ 8 mm spaced at 150 mm center to center. Typical reinforcement details for beam cross-section BX1 are illustrated in Figure 5-1a.

These beams were subject to a combination of structural and thermal loading to simulate effects of fire damage. Accordingly, all beams were subject to a similar uniformly distributed load profile with varying magnitude. Further, only 5 m of the central span for beams spanning 6 m, and 4.5 m of the central span for beams spanning 5 m, was assumed to be exposed to fire ensuring fire exposure did not extend to the support in any case. A schematic representation of the considered beam geometry, together with the assumed loading and fire exposure configuration, is shown in Figure 5-1b.

5.3.2 Range of parameters

In order to study the influence of critical factors on residual response of RC beams, four sets of analysis are carried out using the previously described numerical model. One parameter is varied within a practical range, whereas all the other properties are kept constant within each analysis set. In the first set of analysis, the residual response of RC beams is studied after exposure to four fire exposure scenarios. The time-temperature curves for these four fire exposure scenarios, which represent a wide range of compartment characteristics including fuel load and ventilation conditions, are calculated based on Eurocode 1 (EN 1991-1-2 2002) provisions. In the second set of analysis, the influence of load level present on the beam during fire exposure is studied. The load level (ratio) during fire exposure is varied from 30 to 60 percent of the ultimate capacity of the beam which to account for different level of loading that can be present during a fire exposure.

In the third set of analysis, the level of axial restraint at the beam supports is varied using four different values of axial stiffness, i.e., $10 \, \text{kN/mm}$, $25 \, \text{kN/mm}$ and $50 \, \text{kN/mm}$. No explicit rotational restraint is provided during analysis. The results from this set of analysis are used to illustrate effect of fire induced axial restraint on residual response of RC beams. For the fourth set of analysis, three beams with different cross-sectional dimensions are considered for evaluating the effect of beam size on residual response after fire exposure. The beam dimensions and reinforcement details are chosen based on the three different range of widths as in tabulated fire resistance values in ACI 216.1 (ACI216.1-97 1997). Finally, for the fifth set of analysis, influence of varying concrete cover on residual response of fire exposed concrete beams is quantified. The test parameters and the results from the tested beam have been summarized in Table 2. Analysis results for each of these parameters are discussed in detail in the subsequent sections.

5.3.3 Analysis details

The various parameters including geometry of beam, level of loading, boundary conditions, fire exposure scenario and material properties were input to the model based on the discussion in sections 4.1 and 4.2. The analysis is carried out in small time steps, with the size of each time step being automatically chosen by the computer program with a specified minimum time step of 0.2 minutes to ensure numerical convergence. In order to investigate the convergence of the finite element mesh, beam B1 tested by Dwaikat and Kodur (Dwaikat and Kodur 2009c), was modeled using different meshes. Displacement response of the beam converged within a tolerance of 1 percent when an element size of 25 mm x 25 mm x 25 mm was used. Therefore, to strike a good balance between accuracy and efficiency, this element size was adopted in all the subsequent numerical simulations for the parametric study. Also, the effect of geometric non-linearity is incorporated in the analysis using the updated Lagrangian method (Hibbitt, Karlsson & Sorensen 2012a), to account for large deflections that occur in RC beams during fire exposure. (Rafi et al.

2008; Wu and Lu 2009) Newton–Raphson method with a tolerance limit of 0.02 on the displacement norm is employed as the solution technique. The line search function is activated for rapid convergence (Crisfield 1982; Schweizerhof 1993).

5.4 Results of parametric studies

Data generated from four sets of parametric studies is utilized to trace the residual response of under different conditions. The comparative response is further utilized to quantify the effect of critical factors on residual capacity of fire exposed RC beams.

5.4.1 Effect of fire exposure

To study the effect of fire scenario on residual capacity, an RC beam, BX1, is analyzed under four different fire exposures scenarios. The flexural capacity of this beam was evaluated to be 67.3 kN-m or a total load carrying capacity of 89.7 kN from Stage 1 of analysis. A uniformly distributed load corresponding to 50 percent load ratio is applied on the beam during fire exposure.

Four parametric fire exposures are considered to cover a wide range of ventilation and fuel characteristics encountered in buildings. The respective time-temperature curves for the four parametric fire exposure scenarios (DF1, DF2, DF3 and DF4) are calculated according to Eurocode 1 (EN 1991-1-2 2002) recommendations and is as shown in Figure 5-2.

Response parameters from Stage 2 of analysis is plotted in Figure 5-3 to show comparative thermal response of RC beam under different fire scenarios. The temperature in corner tension rebar is plotted as a function of fire exposure time. The rebar does not attain its failure on reaching critical temperature (593°C) as per prescriptive requirements (ACI216.1-97 1997) in any of the considered parametric fire exposures. The rate of temperature rise, in the rebar in the case of fire scenario DF1, is lower than the rate of temperature rise in fire scenarios DF2, DF3 and DF4. These temperature trends in rebars follow temperature rise in respective fire time-temperature curves.

However, results plotted in Figure 5-3a indicate that while the peak fire temperature attained in fire scenario DF 1 (about 750°C) is significantly lower than in fire scenario DF3 (about 950°C), peak rebar temperature in fire scenario DF1 is greater by about 200°C. This can be attributed to the longer heating phase in fire scenario DF1 of about 100 minutes followed by a slower cooling rate, as compared to 20 minutes heating phase followed by a faster cooling rate in fire scenario DF3. Thus, it can be inferred that peak fire temperature alone does not give a clear indication of the maximum temperature attained in the rebar during fire exposure. Moreover, fires with lower peak temperatures may result in higher peak rebar temperatures, depending on the duration of heating phase and subsequent rate of cooling.

The progression of mid-span deflection with fire exposure time is plotted in Figure 5-3b to illustrate comparative structural response of RC beams under four fire scenarios. The deflections at early stages of fire exposure increase at a much slower rate during fire scenario DF1 than that under fire scenarios DF2, DF3 and DF4. The rate of rise in mid-span deflection correlates with the rate of rise in rebar temperature. However, due to the prolonged heating phase present in fire scenario DF1, the beam fails during fire exposure since maximum deflection limit state is exceeded. Therefore, the analysis for this case does not proceed to residual capacity evaluation (Stage 3) in the beam. In the remaining three fire scenarios (DF2, DF3 and DF4); mid-span deflections of the beam that occur during fire exposure begin to recover just as the rebar temperature starts decreasing after attaining peak value. However, part of the deflection remains as residual deflection even after cool down.

Figure 5-3c depicts load-deflection response of beam BX1 from Stage 3 of analysis (post-fire residual response), along with room temperature response prior to fire exposure. There is residual deflection in the beam, even after the beam cools down to room temperature, resulting from plastic

deformations that occurred in the loaded beam during fire exposure. The extent of these residual deformations varies with fire severity, i.e. peak fire temperatures, duration of heating phase and rate of cooling experienced during fire exposure. Residual deflections observed in fire scenario DF2 are about 50 percent more than those observed in fire scenario DF4, which is much less severe. Also, more severe fire exposure leads to lower leads to higher temperature induced degradation in mechanical properties resulting in lower residual capacity. The reduction in load bearing capacity of beam BX1 is 30, 25 and 22 percent after exposure to fire scenarios DF2, DF3 and DF4 respectively.

The maximum rebar temperature, peak deformation during fire exposure, residual deformation and residual capacity for beam BX1 exposed to four different fire exposure scenarios are summarized in Table 2. Under fire scenario DF1, beam attains the highest rebar temperatures and hence there is no residual capacity left in the beam after fire exposure. Amongst the other three fire exposures, beam BX1 experiences maximum degradation in residual capacity, about 34 percent of room temperature capacity, in fire scenario DF3, where peak rebar temperature experienced during fire exposure is the highest. The residual deformation in this case (of magnitude 72 mm) is greater than the other two cases (less than 55mm). Therefore, it can be inferred that higher rebar temperatures as well as higher residual deformations lead to a lower residual capacity in fire exposed RC beams. Moreover, the magnitude of peak rebar temperatures experienced during fire exposure and residual deformations that occur after cool down vary greatly depending on the fire exposure scenario.

5.4.2 Effect of load level

The magnitude of loading during fire exposure can have significant influence on residual capacity of fire exposed RC beams. To study the effect of level of loading on residual capacity, beam BX1 is subjected to varying load ratio of 30, 40 and 60 percent, and exposed to fire scenario DF2.

Results from the analysis are presented in Figure 5-4a-b and Table 2 to illustrate the effect of varying load ratio on residual capacity of fire exposed RC beams.

Results plotted in Figure 5-4a show that both the rate of rise in deflection, as well as maximum deflection, occurring during fire exposure increases with increasing load ratio. Also, the ratio of peak deflection during fire exposure to residual deflection, when the beam cools down to room temperature, reduces from about 2 to 1.5 indicating higher residual deflection (refer Table 2). This is primarily because a larger load ratio causes early yielding of steel reinforcement and hence higher plastic strains during fire exposure.

Figure 5-4b shows residual load-deflection response in the beam after exposure to fire under different load ratios. It can be seen that heavily loaded beams, i.e. with load ratio greater than 50 percent, have a significantly lower residual capacity. Results summarized in Table 2 show that for a load ratio of 30 percent, degradation in load bearing capacity of beam BX1 after fire exposure is about 15 percent. However, when the load ratio is increased to 60 percent, the corresponding reduction in capacity is about 26 percent. Also, while the peak rebar temperature remains unchanged under different load ratios, higher residual deformations occur at higher load ratios which result in lower residual capacity after fire exposure. These trends in results suggest that residual deformation after fire exposure is a better indicator of residual capacity than peak rebar temperature alone.

5.4.3 Effect of axial restraint

RC beams can develop significant restraint forces under fire exposure and the extent of these forces depends on support conditions. These restraint forces influence behavior of RC beams both during and after fire exposure. For studying the effect of axial restraint, residual response of beam BX2 is studied under parametric fire scenario DF4 for three different levels of axial stiffness at the end supports. Axial restraint is introduced in the beam by means of springs at the end supports

corresponding to three different axial stiffness values, i.e., $10\,kN/mm$, $25\,kN/mm$ and $50\,kN/mm$.

The results from this set of analysis are plotted in Figure 5-5a-b and summarized in Table 2.

To compare the mid-span deflection in beam BX2 during fire exposure DF4 for different support conditions is plotted in Figure 5-5a. Results indicate that the mid-span deflections are significantly reduced with increasing axial stiffness (refer Table 2). The peak deformation during fire exposure is 16 mm for an axial stiffness of 10 kN/mm which reduces to 7 mm for the case with a much higher axial stiffness of 50 kN/mm. This trend can be attributed to the arch action that gets generated in restrained RC beam due to the development of fire induced axial restraint force and this force (moment) counteracts the applied bending moment (Kodur and Dwaikat 2007). Moreover, a higher stiffness results in greater restraint forces and thereby lower deflections during

Results from residual load-deflection response of the beam for different levels of axial restraint are plotted in Figure 5-5b. Axial restraint has a relatively moderate influence on residual capacity than deformations during fire. Moreover, while peak deformations during fire exposure vary significantly for different levels of axial restraint, the residual deformations after cool down of the beam are very similar. However, a greater axial restraint results in lower post fire deformations and hence a higher residual capacity for the same fire exposure (refer Table 2).

It should be noted that the load carrying capacity of the beam with axial restraint is higher than the simply supported case due to restraint forces experienced at the supports.

5.4.4 Effect of varying size of beam

fire.

The influence of cross-sectional size of the RC beam on post-fire residual capacity is studied by exposing beams of three different cross-sections, i.e. beam BX1, BX2 and BX3, to four parametric fire scenarios (DF1, DF2, DF3 and DF 4). The response of these three beams for each of the fire scenario is summarized in Figure 5-6a-d, Figure 5-7a-c and Table 2.

Results plotted in Figure 5-6 a-d show that larger depth in the case of beam BX1 leads to relatively lower mid-span deflections during fire exposure. This is due to slower temperature rise in concrete and rebar due to the larger mass of concrete. Mid-span deflections for beams BX1 and BX2, on the other hand are relatively large due to higher temperatures attained in the cross section. Moreover, mid-span deflection in the beam recovers with decrease in rebar temperatures as the fire temperature starts to decay. The ratio between peak deformation during fire exposure and residual deformation after the beam cools down to room temperature varies between 1.6 to 1.4 for beams BX1 and BX2. However, for beam BX3, this ratio is varies from 1.3 to 1.1. This implies that deformations in beam BX3, although relatively lower in magnitude, are irrecoverable in nature. On the other hand, deformations in beam BX1 and BX2 are larger, with a greater percentage of the deformations being recovered after fire exposure. Also, while peak rebar temperature in beams of different cross section is similar since the cover to reinforcement is maintained constant, the variation in residual deformations is different and depends on cross-sectional size of the beam.

Based on results summarized in Table 2, it can be seen that reduction in capacity is lower in beams with larger cross-sectional size (such as beam BX1) or breadth to depth ratio. Results show that beam BX1 retains approximately 78 percent of its room temperature capacity after fire exposure scenario DF4, while beam BX3 having almost twice the breadth and depth of beam BX1, has a residual capacity of 84 percent after the same fire exposure scenario. Alternatively, the residual capacity of beam BX3 after fire exposure is 10 percent more than the post-fire residual capacity in beam BX1. This is due to lower overall temperatures within the cross section resulting from high specific heat and low conductivity of concrete. While rebar temperatures are similar in all three beams due to same amount of cover, reinforcing steel recovers most of its strength after cool down.

Concrete on the other hand does not depict such recovery in strength when exposed to high temperatures immediately after cool down (EN 1994-1-2 2008). Thus, lower temperatures across the cross section, due to larger size of beam, result in improved residual response of RC beams.

5.4.5 Effect of cover to reinforcement

Given that almost the full moment capacity of an RC beam is provided by the reinforcing steel, temperature induced deterioration in rebar influences level of recovery, and residual capacity of RC beams following fire exposure. Consequently, provided cover to tensile reinforcement which influences peak temperatures attained in tensile rebar, also impacts residual response of fire damaged concrete beams. In fact, damage to the RC beam during fire exposure can vary significantly with the magnitude of clear cover provided. Accordingly, beam BX4 was analyzed for two different cover thicknesses of 20 mm and 40 mm respectively.

Mid-span deflection of the beam exposed to parametric fire exposure DF5 (see Figure 5-2) for two different cover thicknesses is shown in Figure 5-8a. Mid-span deflections continue to increase well into cooling phase of fire exposure in both cases. In fact, neglecting the cooling phase of fire can lead to a significant underestimation of the maximum deflection (up to 40%). As temperatures in the member reduce significantly upon cooling, trend in mid-span deflection reverses resulting in varying degree of recovery depending on cover to reinforcement provided. As expected, lower cover thickness (20 mm) results in the tensile rebars being poorly protected from temperature ingress which then lead to higher maximum deflection at midspan and almost no recovery after cooling down. In fact, the residual deflection is almost 90% of the peak deflection experienced during fire exposure. The recovery of the deflection, however, is more pronounced in the case of greater cover depth, with residual deflection being only 70% of the peak mid-span deflection during fire exposure. Thus, cover to tensile reinforcement plays a crucial role in the magnitude of the residual displacements and the amount of recovery upon cooling.

The predicted residual load-deflection response of beam BX4 following fire exposure having two different cover thicknesses is also shown in Figure 5-8b. It can be clearly seen that lower concrete cover of 20 mm results in greater temperature induced loss of strength and stiffness in the concrete beam, compared to the case when tensile rebars are better protected from temperature ingress, having greater cover thickness of 40 mm. The residual capacity of beam BX4 following exposure to parametric fire DF5 in case of lower concrete cover (20 mm) is almost 15% lower than the case with greater concrete cover (40 mm). Thus, greater concrete cover not only improves performance of RC beams during fire exposure but has a beneficial effect on level of recovery, residual deflection, and residual capacity following fire exposure.

5.5 Summary

A nonlinear finite element analysis is applied to quantify the influence of critical factors on residual response of fire exposed RC beam. Based on the results presented in this chapter, following observations can be drawn on the residual response of fire damaged RC beams:

- Residual capacity of fire exposed RC beams is a function of type of fire exposure, load level,
 cross sectional dimensions, level of axial restraint, and assumptions regarding temperature
 induced bond degradation in RC beams.
- The reduction in residual capacity of fire exposed RC beams almost doubles when the load level increases from 30 to 60 percent of room temperature capacity of the beams. Thus, load level has significant impact on stiffness and post-fire serviceability of fire damaged concrete beams.
- Cross sectional dimensions of a fire exposed has an influence on residual capacity of fire
 exposed beams; with larger beam cross-section (higher thermal mass) leading to higher
 residual capacity.

- The extent of axial restraint has significant influence on deflection progression during both
 heating and cooling phases of fire exposure. However, the influence of axial restraint on
 resulting residual capacity of fire damaged concrete beams is fairly limited and can be ignored
 for simplicity.
- Cover to tensile reinforcement plays a crucial role in the magnitude of the residual displacements and the amount of recovery upon cooling. In fact, greater concrete cover not only improves performance of RC beams during fire exposure but has a beneficial effect on level of recovery, residual deflection, and residual capacity following fire exposure.
- RC beams exposed to most parametric fires can retain up to 70 percent of room temperature capacity, provided tensile rebar temperature does not exceed 450°C.

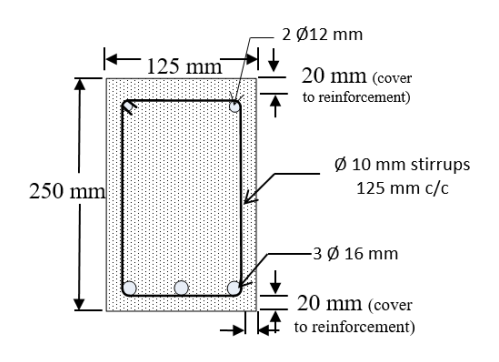
Table 5-1. Summary of test parameters and results used for parametric study

Beam designation	Beam dimensions:	Flexural reinforcement		Room temperature capacity: kN		Fire resistance
	mm	Top	Bottom	ACI 318	Model	(ACI 216):
		bars	bars			min
BX1	125X250	2 Ø 12	3 Ø 16	74.6	89.7	60
		mm	mm			
BX2	180X300	2 Ø 12	3 Ø 20	143	168.8	120
		mm	mm			
BX3	300X480	2 Ø 12	3 Ø 25	351	403.5	120
		mm	mm			
BX4	350X450	3 Ø 12	3 Ø 16	214	306	60
		mm	mm			

Table 5-2. Summary of varied parameters and results from parametric study

Parameter	Beam	Fire exposure scenario	Peak rebar temperature: °C	Load ratio: percent	Support conditions	Peak deformation: mm	Residual deformation: mm	Predicted residual load capacity: kN
Fire scenario	BX1	DF1	515	50	SS*	204	-	-
		DF2	403			125	72	64
		DF3	290			81	55	67
		DF4	174			48	35	70
Load ratio	BX1	DF2	403	30	SS	77	39	82
				40		100	52	79
				60		155	97	71
Axial restraint	BX2	DF1	498	50	SS	181	92	111
					AR**	172	84	112
		DF2	379		SS	112	65	116
					AR	109	68	117
		DF3	274		SS	76	48	118
					AR	75	50	119
		DF4	161		SS	42	25	122
					AR	41	26	123
Size of beam	BX1	DF1	515	50	SS	204	-	-
		DF2	403			125	72	64
		DF3	290			81	55	67
		DF4	174			48	35	70
	BX2	DF1	498			181	92	111
		DF2	379			112	68	116
		DF3	274			77	50	118
		DF4	161			42	26	122
	BX3	DF1	470			88	69	275
		DF2	350			64	58	305
		DF3	252			48	45	312
		DF4	142			29	25	337
Temperature induced bond degradation	BX1(Cover 20 mm)	DF5	552	55	SS	51	45	195
	BX1(Cover 40 mm)		410			42	30	231

^{*} Simply supported; ** Axially restrained



(a) Cross-section

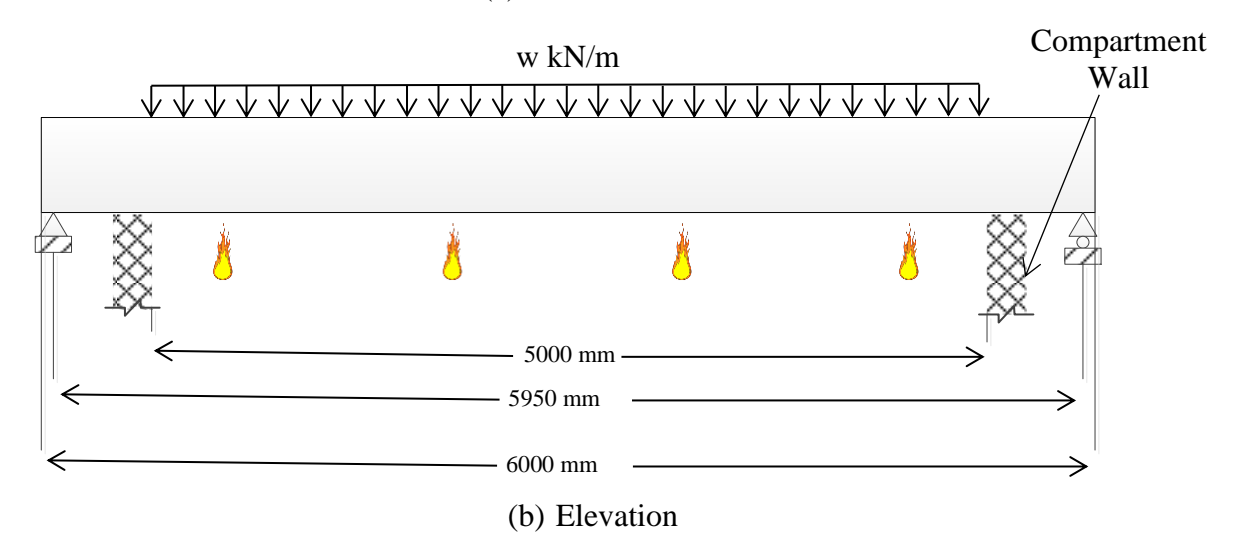


Figure 5-1. Illustration showing dimensions, loading and reinforcement details of typical beam (BX1) analyzed for parametric study

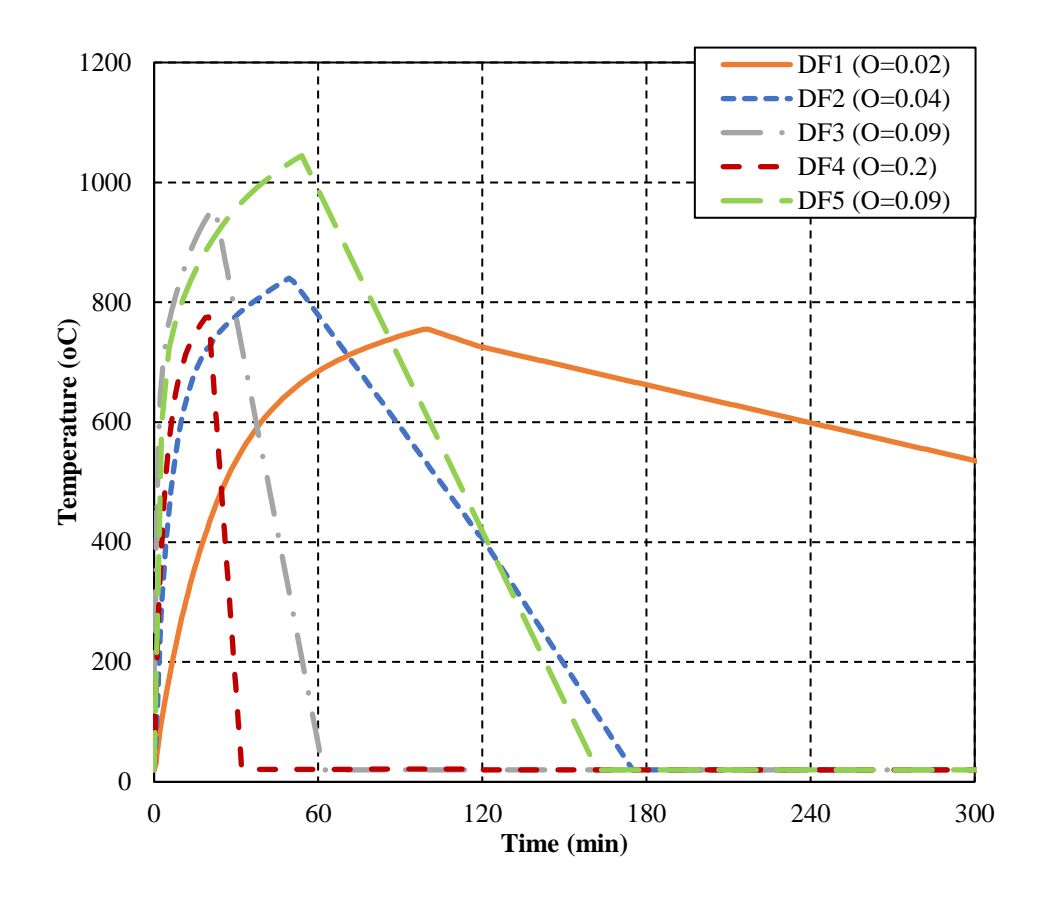
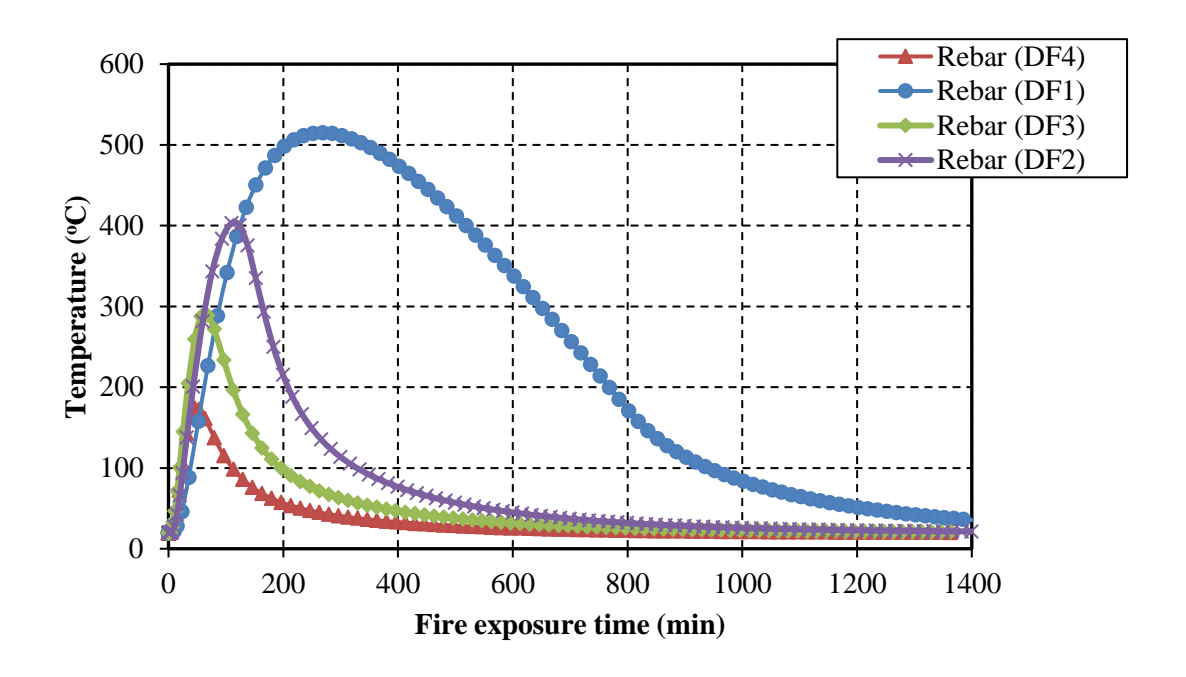
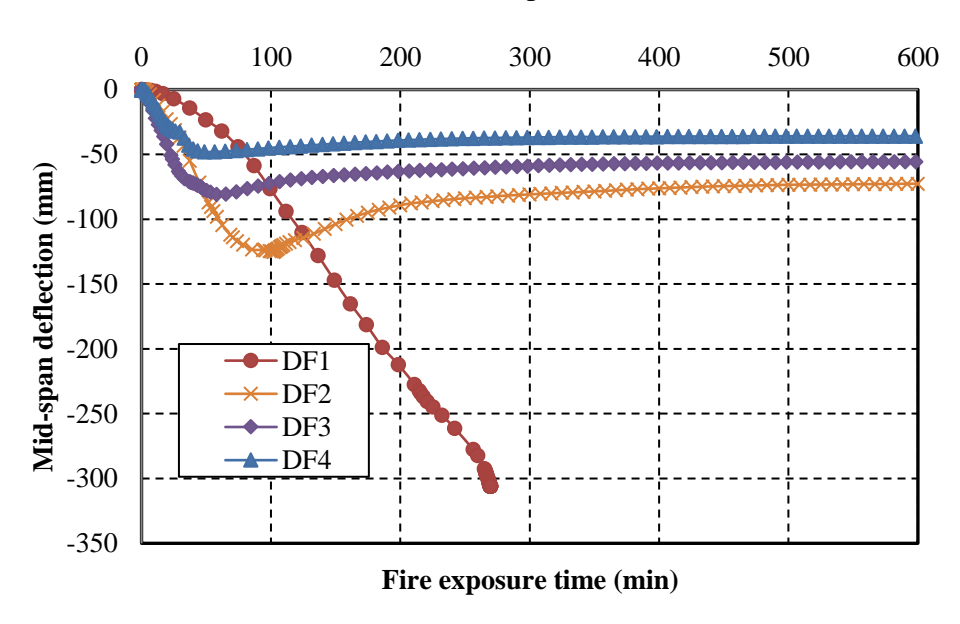


Figure 5-2. Parametric time-temperature curves for a total compartment area of 360 m², fire load density between 600 to 750 MJ/m² and four opening factors ($o = A_v \sqrt{h_{eq}}/A_t$) accounting for different area of openings (A_v), equivalent height of openings (h_{eq}), and total area (A_t).



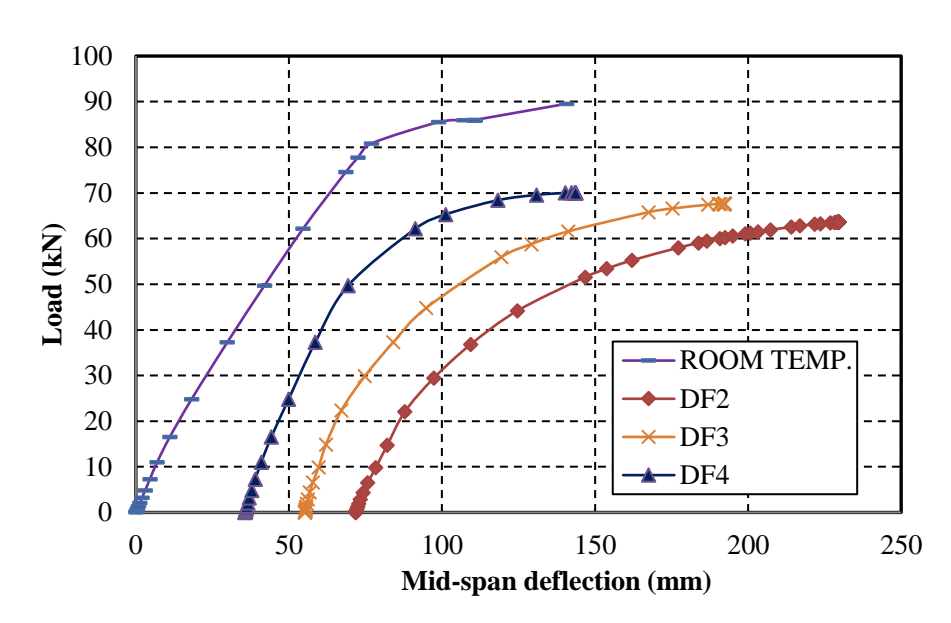
(a) Maximum corner tension rebar temperatures for beam for different scenarios



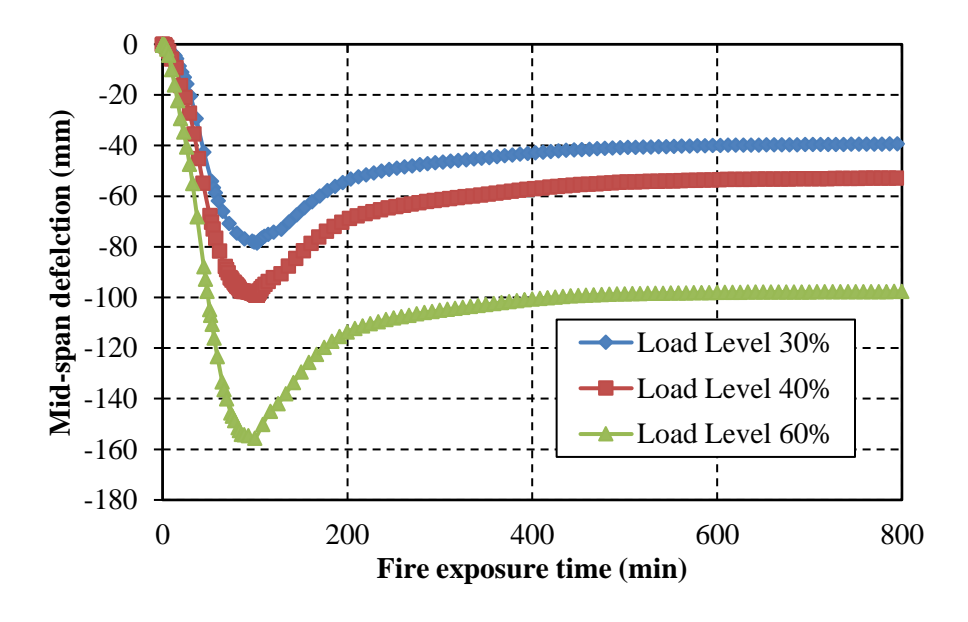
(b) Mid-span deflections for different fire scenarios for first 120 minutes

Figure 5-3. Effect of fire scenario on residual response of fire exposed RC beam BX1

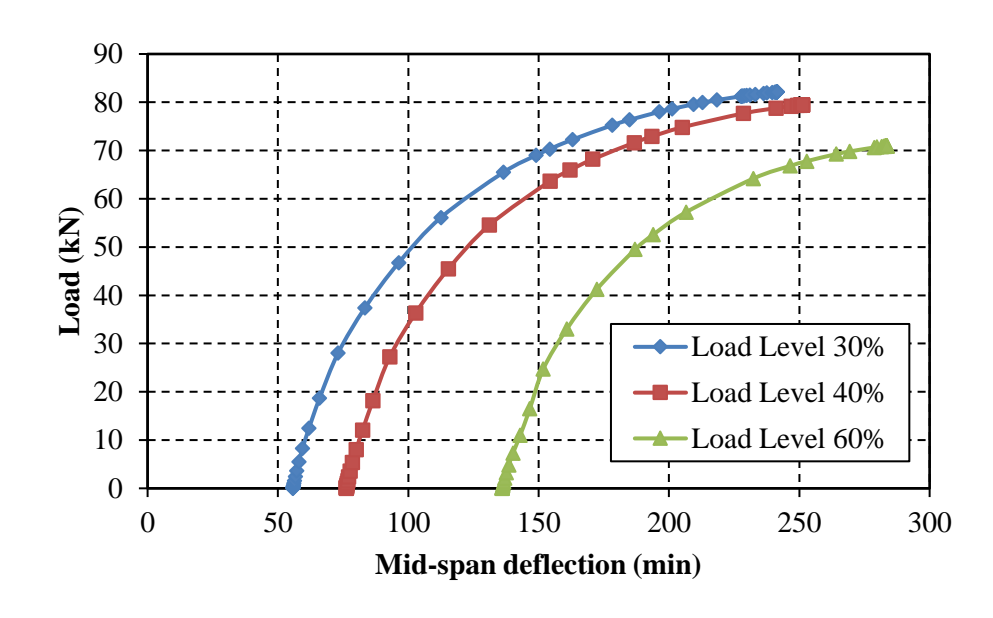
Figure 5-3 (cont'd).



(c) Residual post-fire load-deflection response for different fire scenarios

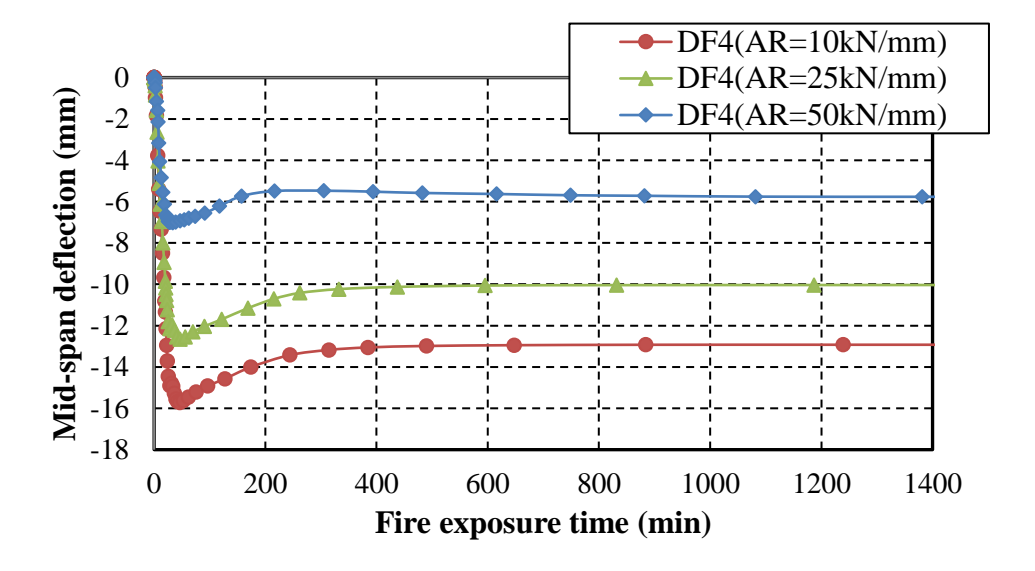


(a) Mid-span deflections during fire exposure

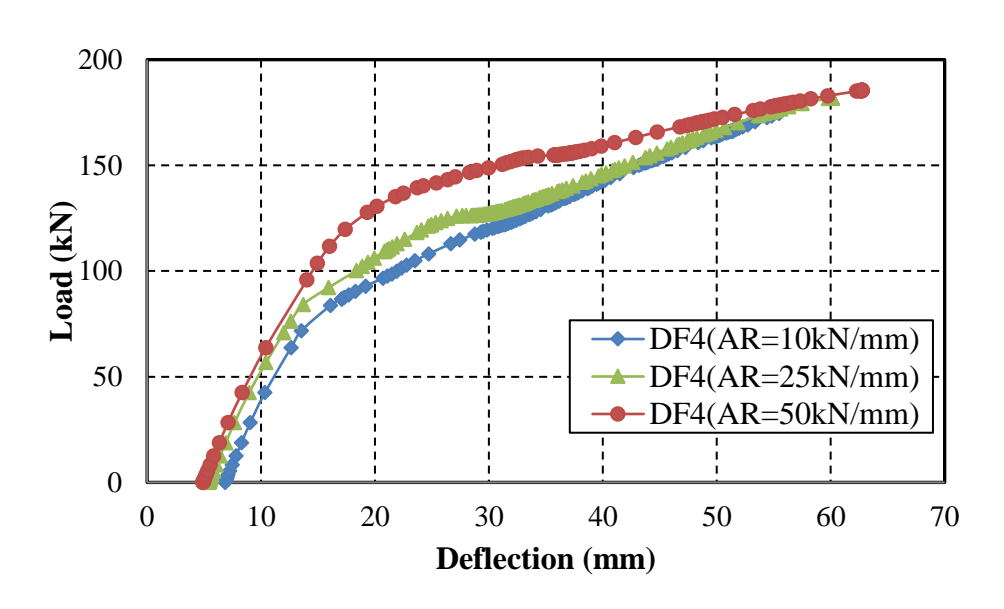


(b) Residual load-deflection response

Figure 5-4. Effect of load ratio for beam BX1 under fire exposure scenario DF2

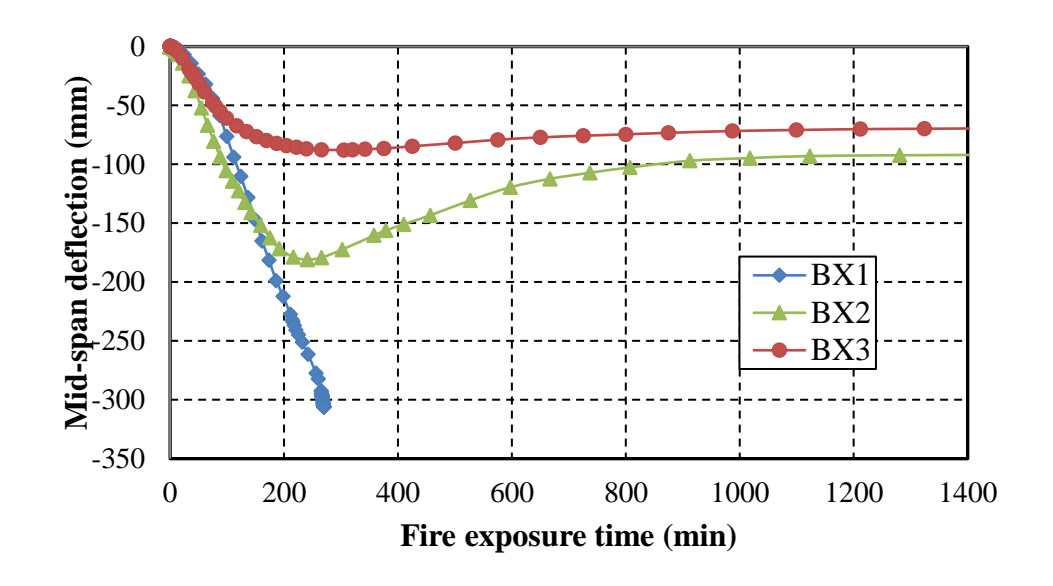


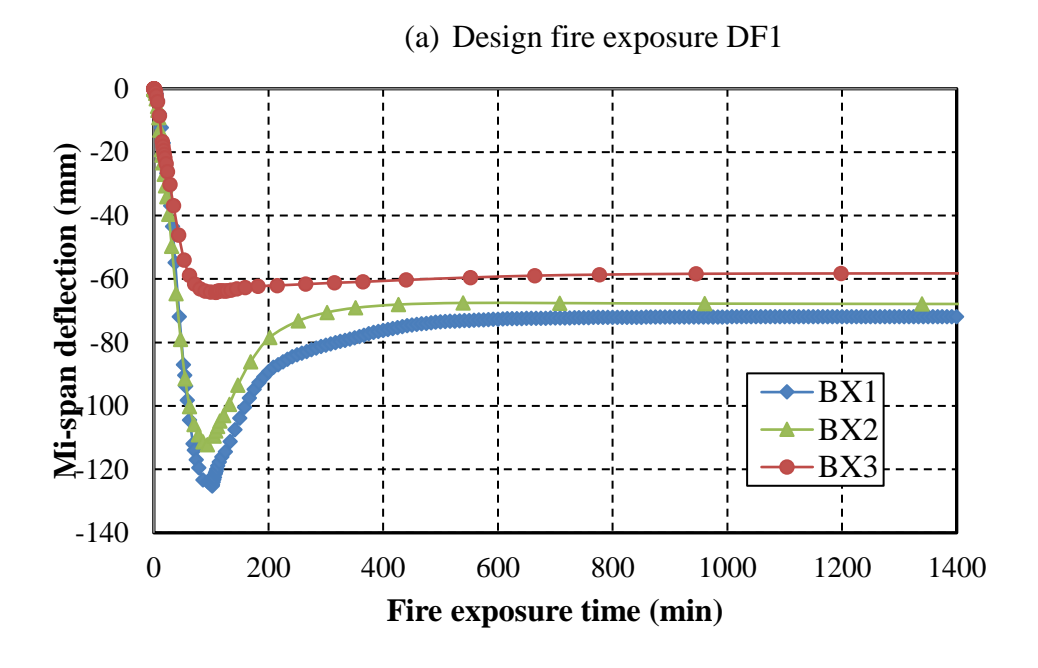
(a) Mid-span deflections for beam BX2



(b) Residual load-deflection response of beam BX2

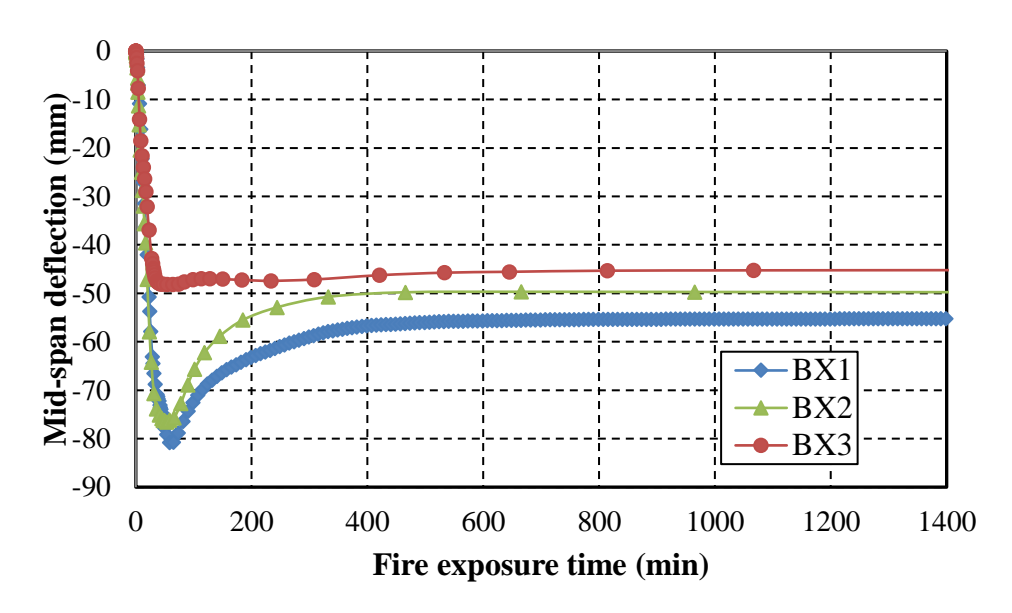
Figure 5-5. Effect of axial restraint on fire performance and residual capacity of beams BX1, BX2 and BX3 under different fire exposure scenarios



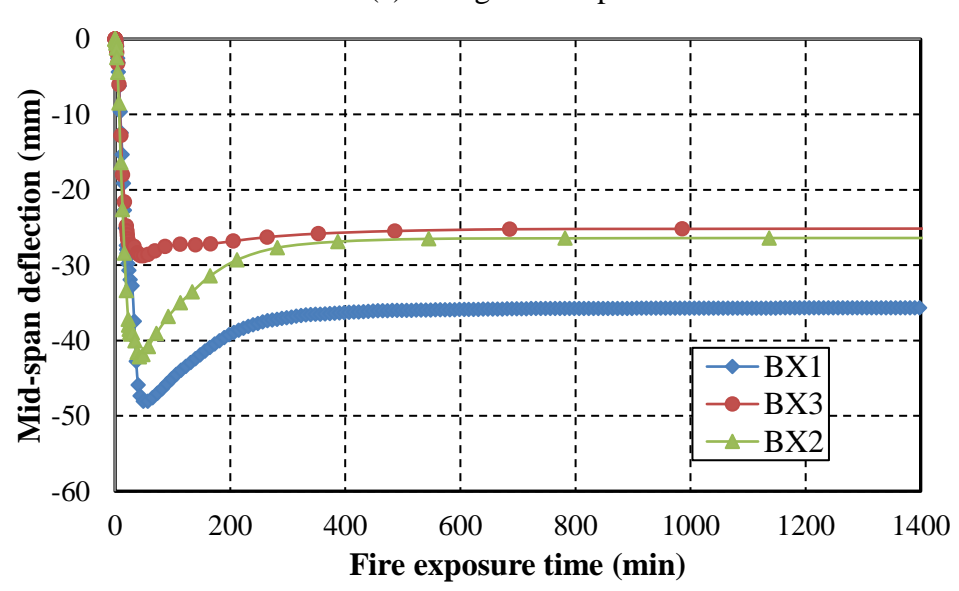


(b) Design fire exposure DF2
Figure 5-6. Effect of cross section on fire response of RC beams under different fire exposures

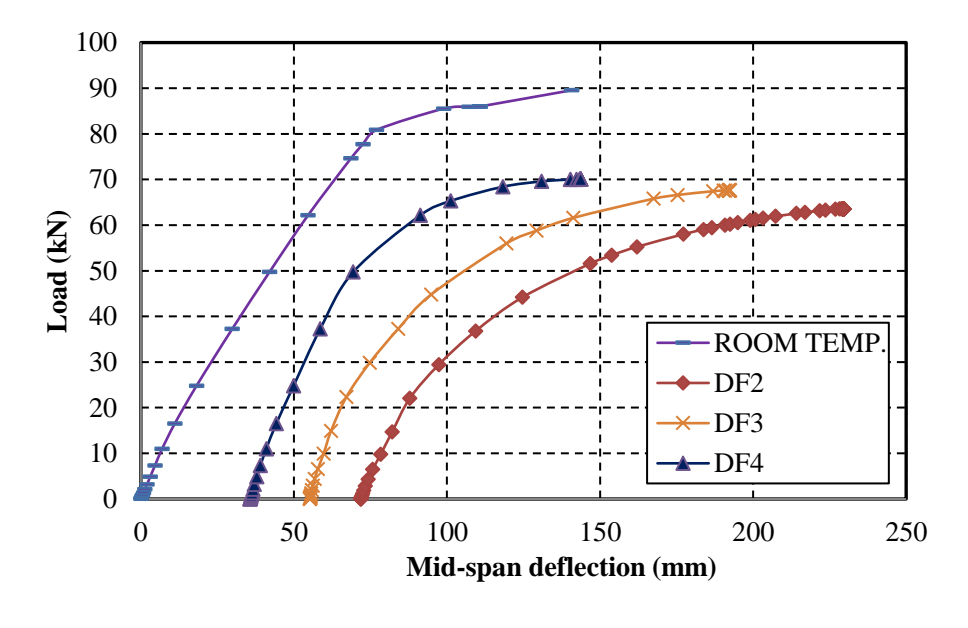
Figure 5-6 (cont'd).



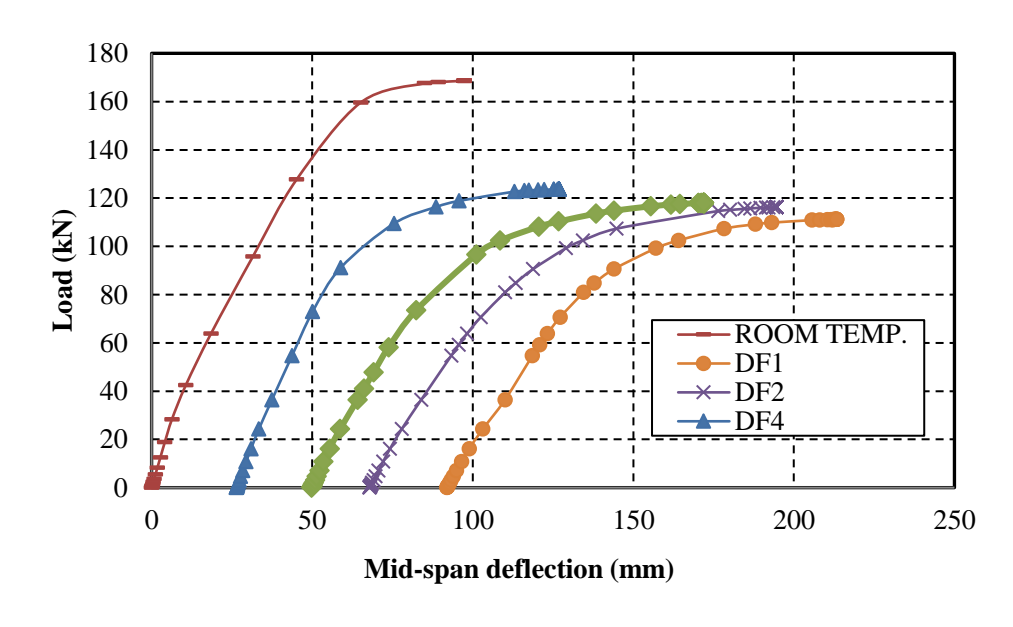
(c) Design fire exposure DF3



(d) Design fire exposure DF4



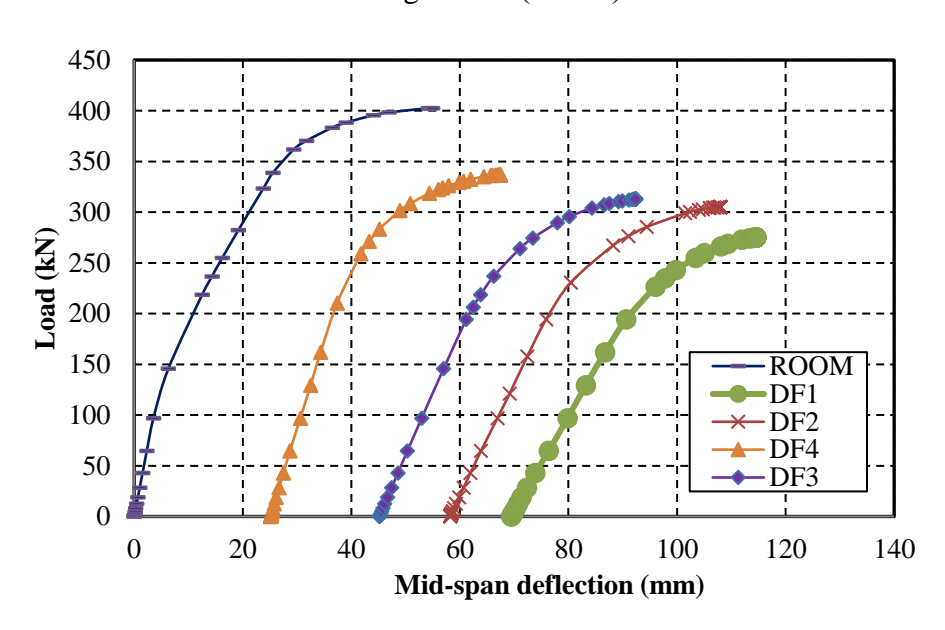
(a) Beam BX1



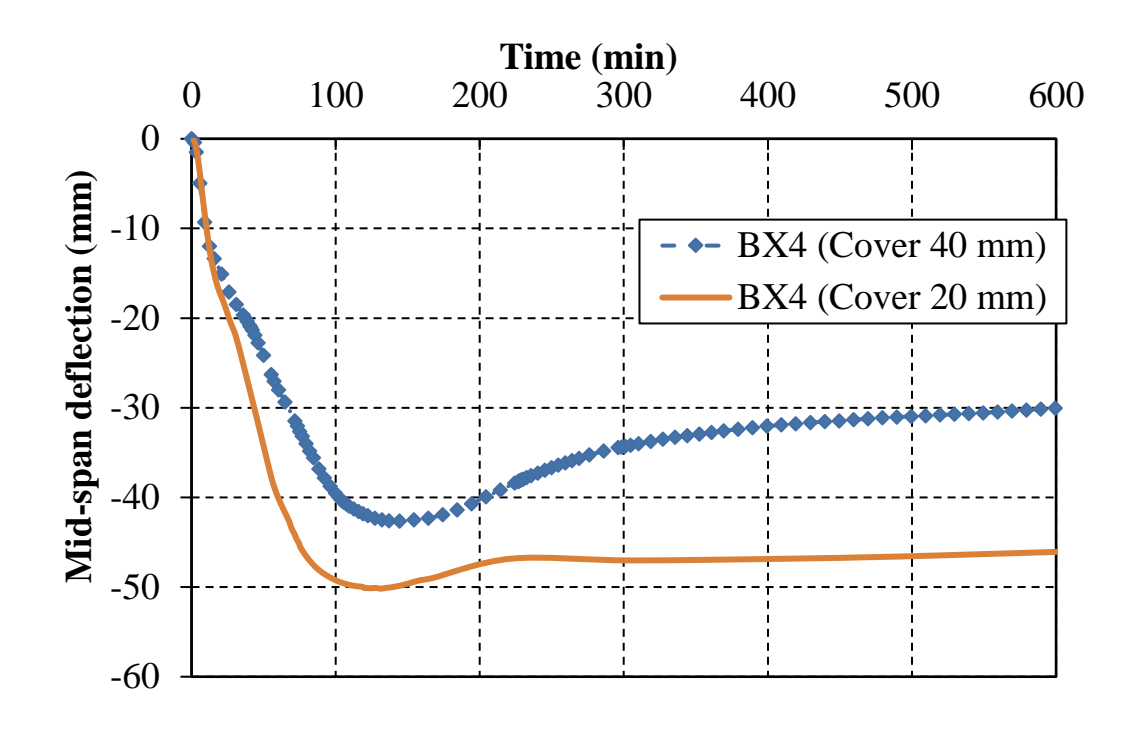
(b) Beam BX2

Figure 5-7. Effect of fire scenario on residual load-deflection response in RC beams with varying cross section

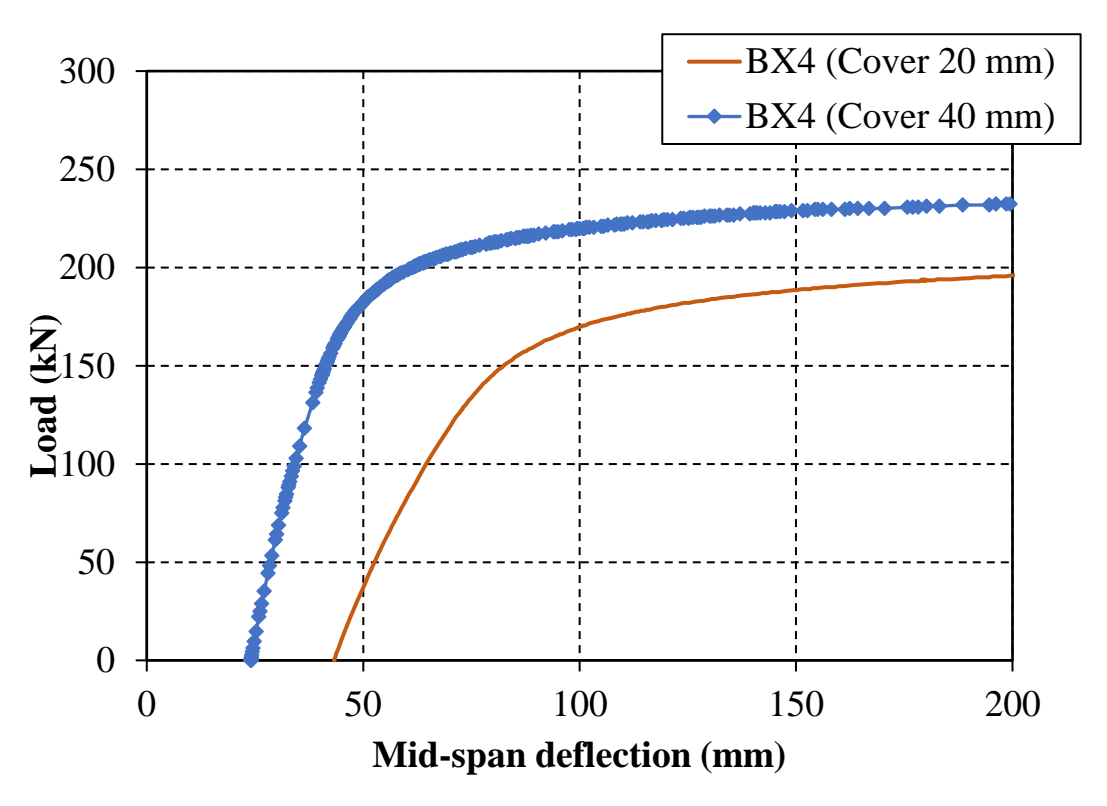
Figure 5-7 (cont'd).



(c) Beam BX3



(a) Mid-span deflection during fire exposure



(b) Post-fire residual load-deflection response

Figure 5-8. Effect of varying cover to reinforcement on structural response during fire exposure DF5 and residual response following fire exposure

6 APPROACH FOR RESIDUAL CAPACITY ASSESSMENT

6.1 General

Based on detailed results presented in Chapters 3, 4, and 5, it can be inferred that concrete structures, after most fire incidents, retain much of their residual capacity and with adequate repair and retrofitting can be brought back to service conditions. Nonetheless, extent of fire-induced damage in concrete structures can be is highly variable. In case of exposure to a severe fire, concrete members might experience significant structural damage resulting from loss of mechanical properties in concrete and rebars, possible fire induced spalling, buckling of rebars and relatively larger permanent deflections. Alternatively, exposure to moderate fire scenario may not result in noticeable deflections or loss of concrete section due to spalling, and thus loss of structural capacity of the fire exposed concrete member may not be significant. In case of minor fire exposure, concrete members may retain much of their original capacity following a fire incident. Following a moderate to severe fire exposure, it is imperative to assess if sufficient residual capacity exists in structural members prior to re-occupancy. This is further complicated by the fact that the extent of capacity required after a fire is dependent on the level of excess original design capacity available in a member. Thus, there is always uncertainty regarding level of remaining structural capacity in fire exposed concrete members. Response of a typical RC member during fire exposure and cooldown is shown schematically in Figure 6-1.

At present, there are limited guidelines for residual capacity assessment of fire-damaged concrete structures (Bai and Wang 2012; Chew 1993; Choi et al. 2013; Gosain et al. 2008; Park and Yim 2017; Short et al. 2001; Tovey 1986). There are no well-established procedures or guidance in current codes and design standards for evaluating residual capacity of concrete structures after fire

exposure. Thus, there is a need for detailed procedure and guidance for use by practitioners, engineers and firefighters for residual capacity assessment of fire-damaged concrete structures. Furthermore, a worked example illustrating the application of the proposed approach in this document to assess a concrete structure exposed to fire is discussed in Appendix A.1.

6.2 Approach for assessment

To overcome the drawbacks in current approaches, a comprehensive five-step approach for residual capacity assessment of fire-damaged concrete structures is laid out in this chapter based on extensive research conducted as part of this dissertation (Kodur and Agrawal 2019). The proposed approach utilizes a combination of visual assessment techniques and thumb rules, non-destructive testing, as well as simplified and advanced calculation methods, to assess the extent of fire-induced damage to a concrete structure. In particular, this approach provides a basis for choosing appropriate analysis methods of varying complexity, such as the numerical model developed as part of this dissertation, on a case to case basis. The approach can be applied to classify extent of fire damage, and assess residual capacity in fire damaged concrete structures. A flowchart illustrating the various steps in evaluating residual capacity of fire damaged concrete members is shown in Figure 6-2.

6.2.1 General procedure

The first step in this approach comprises of establishing fire exposure characteristics (duration of heating and cooling phase, peak temperature etc.) using fire-fighter reports (or eyewitness accounts), examination of non-structural debris, and (or) applying simplified (empirical) calculation approaches. In the second step, peak temperatures experienced at exposed surfaces of the structural member are determined. Subsequently in the third step, the extent (type) of damage

to structural members due to fire exposure is estimated using information obtained from the first two steps as well as other visual observations on the structure through physical inspection.

In cases when the extent of structural damage from fire exposure is deemed to be minor (cosmetic), there is no need for further investigation and the structure can be reinstated after undertaking needed non-structural repair, such as smoke cleaning in the compartment, painting, fixing window panes etc. However, in cases when structural damage is evident in fire exposed concrete members, further capacity assessment is needed through applying fourth and fifth steps. In the fourth step, residual mechanical properties of concrete and steel rebars are to be established, through applying empirical approaches and non-destructive or semi-destructive testing. Finally, in the fifth step, residual capacity of structural members is to be evaluated by applying simplified equations and (or) through advanced analysis. This five-step approach to evaluate residual capacity of fire-damaged structural members is illustrated in the flowchart shown in Figure 6-2.

6.2.2 Step 1: Establish fire characteristics

For assessing fire damage in a fire exposed concrete member, the duration of heating and cooling phases of fire, and the peak fire temperature need to be established. Since obtaining precise data regarding fire characteristics after a fire incident is not an easy task, a preliminary estimate of fire severity can be obtained through fire brigade records. Key information that might be useful for establishing fire severity includes any temperature measurements taken by fire-fighters (or others) using non-contact infrared thermometers, noted observations related to fire growth characteristics, length of time taken to fight the fire, length of time between the fire being noted and the arrival of the brigade, operation of any automatic fire detection or fire-fighting equipment, and degree of effort required to fight fire.

Alternatively, an indirect estimation of fire severity can be obtained by an experienced fire investigator through examining debris in the burnt out building. The nature of the burnt materials can provide information about likely temperatures developed and the duration of fire exposure at any location. As an example, upon examining such debris at the disaster zone or site, such as melting of aluminum formwork, a fire investigator can ascertain peak fire temperatures exceeded 650°C (melting point of aluminum), as indicated in Figure 6-3 (The Concrete Society 2008). A detailed list of visible temperature induced physical (noticeable) changes or degradation in common structural and non-structural materials present in buildings that can be useful for estimating fire severity (The Concrete Society 2008) are summarized in Table 6-1.

Another method for establishing fire exposure characteristics in a compartment is through applying empirical methods, such as those described in Eurocode 1 (EN 1991-1-2 2002). Knowing the type of occupancy, compartment characteristics, as well as approximate fuel load density and burning duration, a rough estimate of fire scenario (time-temperatures) that occurred can be constructed. As an illustration, different possible time-temperature curves in a building compartment having a fuel load density of 600 MJ/m² (representative of an office building), a total area of 360 m² and varying ventilation conditions are shown in Figure 6-4.

6.2.3 Step 2: Establish peak exposure (surface) temperatures experienced by structural member

Once fire characteristics (time-temperature curve) is reasonably established in the first step, peak temperatures experienced at exposed surfaces of the structural member need to be ascertained. Different structural members present within the fire compartment may experience different temperatures depending on their proximity (distance) from the heat source, emissivity of the member surface (material) etc. For instance, exposed surfaces of horizontal concrete beams (flexural members) located near the ceiling often experience higher temperatures, than vertical

concrete columns located at the corners of the compartment (building). Thus, it is critical to establish peak temperatures experienced at the exposed surfaces in order to estimate extent of temperature induced damage.

Peak temperatures experienced at the exposed surfaces of a structural member can be estimated by observing visible changes in concrete color, caused by temperature dependent microstructural changes in both cement paste and aggregate present in concrete. Such changes in color of concrete following fire provide a reasonable estimate of peak temperatures experienced by a structural member, especially on the boundary (surface) region. As an illustration, changes in color of a concrete member made of siliceous aggregate, after exposure to varying elevated temperatures in a fire are shown in Figure 6-5 (Hager 2014). Concrete made of siliceous aggregates turns red when heated between 300°C and 600°C; whitish grey between 600°C and 900°C; and buff between 900°C and 1000°C. Thus, a reasonable estimate of the peak temperatures experienced by the structural member can be made through visually observing changes in concrete color.

Besides estimating temperatures experienced at the surface level of the structural members, visual inspection of cracking patterns and spalling can provide a rough estimate of temperatures experienced within the outer layers of concrete (cover regions) as well. Thermal crazing (cracking) occurs due to differential thermal expansion at the rebar concrete interface (The Concrete Society 2008), and can be seen on the fire exposed surfaces of the structural member (see Figure 6-6a). Extensive crazing (resulting from thermal heating) following fire exposure indicates rebar temperatures to have exceeded 400°C, the temperature beyond which thermal expansion and strength loss of rebar and concrete are significantly different. Besides thermal crazing, structural members may undergo temperature induced spalling (The Concrete Society 2008) due to pore pressure developed in the member (see Figure 6-6b). In such cases, if the spalling results in

removal of cover concrete and rebar being exposed, temperatures within the spalled region (including rebar) may have exceeded 600°C.

6.2.4 Step 3: Classification of temperature induced damage during fire exposure

Temperature induced damage during fire exposure can be non-structural (cosmetic) or structural. Non-structural damage includes damage to non-load bearing members such as façade, windows, ceiling, mechanical and electrical (HVAC) installations, and any discoloration and damage of surfaces of members resulting from smoke etc. Structural damage on the other hand implies damage to mainly load bearing structural members resulting from temperature induced degradation in mechanical properties (strength and stiffness) of concrete and reinforcing steel and accompanied with loss of load bearing capacity. Based on the extent of temperature induced structural damage, structural members can then be categorized into five categories; no damage, non-structural (cosmetic) damage, moderate damage, severe damage, and complete collapse of a member. These five classes of damage (A to E) that can occur in a structural member as a result of fire exposure are tabulated in Table 6-2. Visual assessment is the first step to identify parts of the affected structure that need to be assessed in further detail.

In cases when the damage resulting from to fire is very minor such as, very limited cracking or spalling or high deflections, but blackening of walls from smoke damage that it comes under damage class A; any further detailed assessment of structural condition is generally not required. The structure can be reinstated to its original state by undertaking non-structural repair such as smoke cleaning, surface repainting etc. However, in cases when temperature induced structural damage is evident, the extent of damage needs to be classified for determining appropriate assessment and repair strategies.

Structural damage due to fire exposure is said to be moderate (damage classes B and C) when there is cracking, minor spalling or discoloration of concrete, and minimal (non-noticeable) structural

deflections (deformations) occurred. Any loss of load bearing capacity in the structural member is unlikely in these cases. Thus, residual capacity of structural members in such a scenario can be reasonably assessed by applying simplified (empirical) methods. Severe structural damage (damage classes D and E) in fire exposed concrete members is said to have occurred in case of a structural member undergoing large cracks, moderate to high concrete spalling with rebar partially or fully exposed, and large (noticeable) residual deflections or deformations. Advanced calculation methods need to be relied upon for evaluating realistic load bearing capacity of fire exposed structural members in damage classes D and E.

This damage classification (general thumb rules) can be applied for preliminary assessment of the extent of fire damage in a concrete structure through visual inspection alone. Table 6-2 summarizes a visual classification scheme that classifies structures into five different categories of temperature induced damage following fire exposure. Changes in concrete color, thermal cracking (crazing), extent of spalling, and rebar condition play an important role in determining the level of temperature induced damage as per this classification scheme. Further, this visual classification scheme is applicable to both axial (columns, walls), as well as flexural (beams, slabs) by loaded concrete members.

When the extent of fire damage in a structural member is grouped under Class A, there is no need for a detailed damage assessment as the damage is non-structural (cosmetic) in nature and the building can be re-occupied after necessary cleaning and cosmetic repair. Alternatively, if fire damage is classified as Class B, C, D or E, assessment of residual load bearing capacity of the structural member is necessary to take informed decisions regarding safe future use and needed repairs for fixing or strengthening fire-damage in members. When structural damage due to fire is minimal and can be classified under Class B, simplified approaches can be relied upon for

evaluating residual capacity of fire damaged structural members. In case of more significant temperature induced damage, i.e. when fire damage is grouped under Class C, D or E, a combination of simplified, non-destructive testing and advanced analysis methods is needed for reliable assessment of post-fire residual capacity. These methods for evaluating residual capacity constitute steps 4 and 5.

6.2.5 Step 4: Estimating residual mechanical properties of concrete and rebar

In cases when fire damage in a structural member is evident, i.e. damage classes B through E as per Table 6-2, a more detailed assessment is needed to evaluate the residual capacity of fire exposed structural member. In order to assess residual capacity, residual mechanical properties of fire exposed concrete and rebar need to be ascertained. Specifically, residual compressive strength of concrete and residual yield strength of rebar (both compressive and tensile) as functions of peak exposure temperature need to be established.

One approach to develop a relation between residual mechanical properties of rebar and concrete after reaching a certain temperature and then cooled down is to utilize published relations in literature. As an illustration, the variation of residual compressive strength of concrete after exposure to certain peak temperature (Annerel and Taerwe 2010) is shown in Figure 6-7. It can be seen that concrete continues to lose compressive strength, with time, even after cooling down to ambient conditions (room temperature) because of continuing disintegration of its microstructure resulting from heating effects (Xing et al. 2013). The compressive strength of concrete immediately after cool down (in the first week after fire exposure) is substantially higher than the compressive strength of concrete after prolonged duration following fire exposure (12 weeks). Further, the residual compressive strength of concrete is not significantly reduced when peak temperatures in concrete reached during fire exposure remain below 300°C, while for temperatures

greater than 500°C the residual strength in concrete is reduced significantly as compared to its room temperature compressive strength.

Post-fire compressive strength of concrete can also be determined directly by testing cores cut from in-situ concrete or affected rebar coupons in the fire-damaged structure. It is also essential to know the pre-fire (undamaged) compressive strength of concrete (not the design strength), to ascertain extent of temperature induced strength loss in concrete due to fire. Room temperature compressive strength should be determined by taking sufficient number of cores from an undamaged part of the fire exposed concrete structure. Similarly, cores should be extracted from concrete members directly exposed to fire to assess the extent of temperature induced damage. Also, the number and locations at which cores are extracted should be chosen to ensure that changes in structural characteristics of fire-damaged concrete can be assessed with reasonable accuracy. Critical zones (such as mid-span or support regions in flexural members) should be avoided when extracting cores such that structural capacity of the member is not weakened further. It should be noted that testing of cores provide an average value of the strength of the concrete, with little or no information on the loss of strength within the surface region of the fire exposed concrete member.

Besides temperature induced degradation in concrete, significant loss of strength may occur in reinforcing steel due to high temperatures typically experienced during fire. Temperature induced loss in strength and stiffness properties of reinforcing steel usually lead to post-fire residual deflections in concrete structural members. The residual strength in rebars primarily depends on peak temperature experienced within reinforcing steel during fire exposure. Experimental studies (Gosain et al. 2008) on residual strength of rebar indicate that steel reinforcement recovers almost 100% of its initial room-temperature yield strength upon cooling down (The Concrete Society

2008), as long as peak temperature during fire exposure do not exceed 400°C for cold formed steel, and 500°C for hot rolled steel (see Figure 6-8). If peak rebar temperatures exceed these values, reinforcing steel regains only part of its room temperature strength.

6.2.6 Step 5: Evaluating residual capacity of fire-damaged reinforced concrete elements
Residual capacity of fire damaged structural members is evaluated in the fifth step of the approach
either through simplified methods or advanced analysis. The simplified methods are quick and
easy to apply, but may not yield realistic residual capacity in certain cases due to non-consideration
of all critical factors influencing residual capacity. Advanced analysis methods can provide better
assessment of residual capacity of fire damaged structures, but involve complex set of calculations.

6.2.6.1 Simplified approach

Once the residual strength of concrete and rebar are assessed, simplified (empirical) equations can be applied to evaluate residual capacity of fire exposed concrete member. In such simplified approaches, peak cross-sectional temperatures experienced within the structural member are evaluated based on compartment fire characteristics established in the first step of the overall approach (refer Section 2.2). There are some empirical methods such as Wikstorm's (Wickström 1986) method, mainly derived for standard fire exposure, to estimate peak cross-sectional temperatures in a fire exposed concrete member. However, a major drawback of such methods is that cross-sectional temperatures are calculated based on peak fire temperature alone, and do not explicitly account for the duration of heating or cooling phase of fire exposure, which may lead to un-conservative predictions of sectional temperature. More recent method developed by Kodur et al. (Kodur et al. 2010), overcome this shortcoming by explicitly accounting for duration of heating and cooling phase of fire exposure to determine peak temperature experienced within the concrete member.

After estimating cross-sectional temperatures, the residual strength of concrete and reinforcing steel can be computed using relation between peak exposure temperature and residual strength, as discussed in step 4 (refer section 2.4). In addition, the computed residual strength of concrete and yield strength of rebar can be validated against tests on extracted cores and (or) rebar samples. This ensures accurate estimation of residual mechanical properties of concrete and reinforcing steel, and hence provides better estimate of residual capacity.

Knowing residual strengths of concrete and rebar, simplified sectional analysis procedure can be applied for evaluating residual capacity of fire exposed structural members. Such cross-sectional approaches are based on evaluating capacity of the concrete member at critical sections, such as mid-span in case of beams under flexure. Besides temperature induced degradation in material properties, any reduction in concrete cross-section (from spalling etc.) at critical regions, in both axial and flexural members need to be accounted for in evaluating residual capacity. In case of axially loaded members, the possibility of localized buckling in zones of exposed reinforcement needs to be accounted for in analysis (Kodur et al. 2013).

As an illustration, flexural capacity of a fire-damaged concrete beam (see Figure 6-9) can be calculated provided the fire characteristics (duration of heating phase, cooling phase and peak fire temperature), and cross-sectional details of the beam are known. In this method, since concrete compression zone (upper layers) in concrete is farther away from the fire exposed surface of the beam, concrete in this zone is assumed to retain its initial room temperature compressive strength. Thus, residual flexural capacity of the fire-damaged concrete beams is mostly governed by residual strength of reinforcing steel (controlled by peak rebar temperature). The peak rebar temperature can be expressed as as a function of peak fire temperature in the compartment:

$$T_{smax} = \lambda T_{fmax} \tag{6-1}$$

where, T_{smax} is the maximum rebar temperature, T_{fmax} is the maximum fire temperature and λ is a modification factor that depends on fire and cross-sectional characteristics of the beam. This modification factor λ is a function of axis distance (distance from the center of the rebar to the nearest exposed surface), the depth-to-width ratio of the concrete section and the fire duration, and can be calculated using the following equation:

$$\lambda = 1.45 \left(t_h + \frac{t_c}{2} \right)^{0.2} \left(0.4 + 0.03 \frac{H}{B} \right) - 5a \tag{6-2}$$

where, t_h is the duration of heating phase (hours), t_c is the duration of cooling phase (hours), H is the sectional depth, B is section width, and a is axis distance (m). Once the peak rebar temperature in rebar is evaluated, dimensions of the damaged concrete section are determined. Subsequently, flexural capacity of the beam can be evaluated by applying room-temperature strength design equations (e.g. ACI 318-08 (ACI 2008)). However, residual yield strength and reduced (damaged) cross-sectional dimensions are utilized instead of room-temperature yield strength and original cross-sectional dimensions of the beam when evaluating residual capacity. The flexural capacity of a fire damaged concrete beam can be expressed as:

$$M_n = A_s f_{yT} \left(d^* - \frac{A_s f_{yT}}{1.7b^* f_c'} \right)$$
 (6-3)

where M_n is the residual flexural capacity of the fire-damaged concrete beam, A_s is the area of tensile steel, f_{yT} is the residual strength of reinforcing steel, d^* is the effective depth of the damaged

concrete section, b^* is the effective width of the damaged section, and f_c' is the initial compressive strength of concrete. The residual yield strength of reinforcing steel can be estimated based on peak temperature calculated using equation 6-3, and temperature dependent yield strength relations. Furthermore, in order to determine effective cross-section breadth and depth, the 500°C isotherm within the cross-section can be calculated based on peak fire temperature. The concrete-cross section outside of the isotherm can be neglected for calculating the effective cross section of the fire damaged concrete beam. The residual flexural capacity of the fire-exposed beam is computed against bending moment from loading to check the safety limit states.

While the above sectional analysis approach is relatively straightforward, and leads to quick estimation of residual capacity, there are certain drawbacks. In particular, strain hardening effects in steel reinforcement and tension stiffening effects in concrete are usually ignored in this approach which can lead to unrealistic predictions of residual capacity. Further, critical factors such as load level present during fire, and (or) boundary conditions of the structural member cannot be accounted for in evaluating residual capacity. Finally, the sectional approach does not yield post-fire residual deflections. Thus, in scenarios when significant post-fire residual deflections occur in fire-damaged structural members, it is recommended that advanced analysis approaches be utilized for evaluating residual capacity.

6.2.6.2 Advanced analysis approach

Advanced analysis approaches are needed to evaluate residual capacity when temperature induced damage in concrete members is significant (damage classes 3, 4, and 5), and is discussed exhaustively in Chapter 4 and Chapter 5. Such an approach, based on finite element method, requires three stages of analysis for evaluating residual capacity of fire exposed concrete members;

namely, evaluating room temperature capacity of the member prior to fire exposure (Stage 1), fire resistance analysis of the member during exposure to fire (Stage 2) and finally, post-fire residual analysis of the affected member after cool down to room temperature (Stage 3). This approach can be implemented using general purpose finite element software packages such as ABAQUS (Hibbitt, Karlsson & Sorensen 2012).

As part of Stage 1 of the advanced analysis approach, room temperature capacity of the fire damaged concrete member is to be evaluated. This can be done through a detailed finite element analysis by gradually incrementing the load on the structural member till failure occurs. This room temperature capacity is the actual capacity of the member (not the design capacity) prior to fire exposure, not just the design capacity. This capacity can be utilized for comparison with the residual capacity of the member to be calculated in Stage 3 to ascertain extent of capacity degradation (fire damage) in the member.

In Stage 2 of the analysis, the response of concrete structural member is evaluated under a given fire exposure scenario, load level, and restrain conditions. The fire response analysis is carried out at various time increments till the failure of the structural member, or till the fire cools down to ambient conditions. At the end of each time increment, response parameters from thermal and structural analysis are utilized to check the state (failure) of the concrete structural member under different failure limit states. In this stage, temperature dependent thermal and mechanical properties of concrete and reinforcing steel, that are distinct during heating and cooling phases of fire exposure, are to be input into a finite element program, for evaluating realistic response.

Following the cool down of the structural member to room temperature, and if there is no failure of the structural member in Stage 2, residual capacity analysis (Stage 3) is to be carried out. The temperature induced residual stresses and strains that exist in the structural member after fire

exposure are obtained from stage 2 of the analysis in the form of residual deflections. These residual deflections result from accumulated damage in the structural member due to temperature induced material degradation and plastic strains. This state of the structural member is the initial state for Stage 3 of analysis. For this analysis, residual properties of fire damaged concrete and steel reinforcement are to be imposed on the member. The cooled-down concrete structural member is loaded incrementally till failure and the load-deflection response of the structural member is traced. The residual capacity corresponds to maximum (peak) load that the fire-damaged structural member can carry prior to attaining failure. Thus, a realistic assessment of the extent of fire damage (and residual capacity) induced in a concrete structural member can be made using this approach.

A comparison of the resulting residual capacity with room temperature capacity evaluated in Stage 1 indicates the extent of fire damage in the member. Further comparison of this residual capacity with applied loading indicate whether the structural member has sufficient capacity to withstand the loads arising during future life of the structure. The reduction in the excess capacity present prior to fire incident and after fire damage can be calculated to establish level of safety in the load carrying capacity of the member. In cases when the residual capacity is not adequate, appropriate retrofitting measures for enhancing structural capacity need to be implemented.

6.3 Limitations of approach

Although the presented approach can be applied to evaluate residual capacity of a range of structural members, there are certain inherent limitations of the approach, as listed below:

• This approach considers only structural aspects of fire damage in concrete structures.

However, besides temperature induced structural damage, the total feasibility of repair

following a fire incident in a concrete structure may also depend on direct losses such as the extent of local and global damage to the structure, damage to the facade or mechanical and electrical (M&E) installations, and indirect losses to business, for example by relocation of people, interruption of trade and the costs of cleaning smoke and combustion products, which may include cleaning to provide acceptable air quality in future. These issues have not been addressed in this study and are beyond the scope of the presented approach.

- Principles discussed in this study are primarily applicable to different type of concrete structures, including buildings, factories etc. as well as bridges. However, the proposed approach cannot be utilized to determine safety of fire damaged concrete tunnels, as an assessment of their performance will require specialized geotechnical input, which is beyond the scope of this study.
- This study presents detailed guidance on evaluating residual capacity of fire damaged concrete structures but does not discuss specific repair methods as they vary substantially on a case to case basis and are beyond the scope of this approach.

6.4 Summary

This chapter presents a general approach for assessing fire damaged concrete members. The proposed approach is developed by combining existing research and the advanced approach developed as part of this dissertation, and key findings can be summarized as following:

- A sequential five step approach is proposed for conditional assessment of fire damaged concrete structures. This approach relies upon a combination of visual inspection, expert judgement, experimental and (or) analytical (numerical) methods, to take informed decisions on repair strategies or use of the structure after fire incident.
- This approach provides a generalized framework for assessing post-fire residual capacity of fire damaged RC structures. Specifically, this approach provides the context in which the advanced methods, proposed as part of this dissertation, can be applied to evaluate residual capacity of fire damaged concrete beams.
- Depending on the extent of temperature induced structural damage after a fire incident, residual capacity of damaged concrete members can be evaluated using simplified and (or) advanced numerical methods as per the proposed approach. Subsequently, the reduction in factor of safety in load carrying capacity from pre-fire to post-fire conditions can be estimated.

Table 6-1. Assessment of temperature reached by selected materials and components in fires

Substance	Typical examples	Conditions	Approximate fire
			temperature reached
			in compartment (°C)
Paint		Deteriorates	100
		Destroyed	150
Polystyrene	Thin-wall food containers, foam, light shades,	Collapse	120
	handles, curtain hooks, radio casings	Softens	120-140
		Melts and flows	150-180
Polyethylene	Bags, films, bottles, buckets, pipes	Shrivels	120
		Softens and melts	120-140
Polymethyl-	Handles, covers, skylights, glazing	Softens	130-200
methacrylate		Bubbles	250
PVC	Cables, pipes, ducts, linings, profiles,	Degrades	100
	handles, knobs, house ware, toys,	Fumes	150
	bottles	Browns	200
	(Values depend on length of exposure to	Charring	400-500
	temperature.)	_	
Cellulose	Wood, paper, cotton	Darkens	200-300
Wood		Ignites	240
Solder lead	Plumber joints, plumbing, sanitary	Melts	250
	installations, toys	Melts, sharp edges	300-350
	•	rounded	350-400
		Drop formation	
Zinc	Sanitary installations. gutters.	Drop formations	400
	downpipes	Melts	420
Aluminum and	Fixtures, casings, brackets, small	Softens	400
alloys	mechanical parts	Melts	600
		Drop formation	650

Table 6-1 (cont'd).

Glass	Glazing, bottles	Softens, sharp	500-600
		edges	
		rounded	800
		Flowing easily,	
		viscous	
Silver	Jewellery, spoons, cutlery	Melts	900
		Drop formation	950
Brass	Locks, taps, door handles, clasps	Melt (particularly	900-1000
		edges)	
		Drop formation	950-1050
Bronze	Windows, fittings, doorbells,	Edges rounded	900
	ornamentation	Drop formation	900-1000
Copper	Wiring, cables, ornaments	Melts	1000-1100
Cast iron	Radiators, pipes	Melts	1100-1200
		Drop formation	1150-1250

Table 6-2. A visual damage classification scheme for reinforced concrete elements

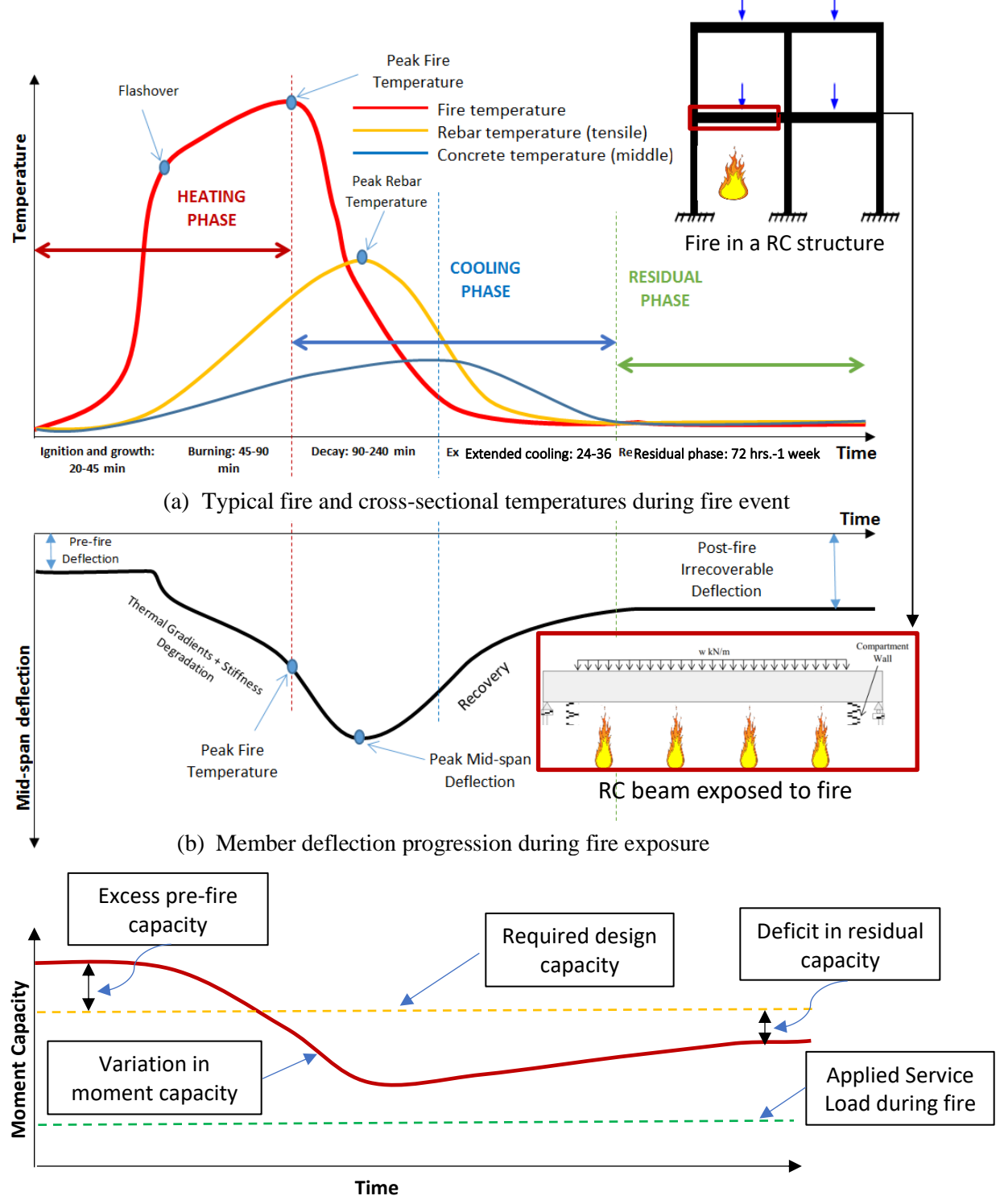
Class of	,	Surface appea	arance of	concrete	Structural co	ndition			Residual	Need (type)
Class of damage	Element	Condition of plaster/finish	Color	Crazing	Nnalling	Exposure and condition of	Cracks	Residual	capacity	of assessment

						main reinforceme- nt				
A	Any	Unaffected or	beyond ex	xtent of fir	e				No loss	No assessment needed
В	Column Wall Floor Beam	Some peeling	Normal	Slight	Minor	None exposed		monceanie	Almost no loss of capacity	Simplified approaches
	Column				IL OCALIZED TO	Up to 25% exposed, none buckled				
С	Wall Floor	-Largely peeled-off	Pink/red	Moderate	natches	Up to 10% exposed. all adhering		Barely noticeable	Very little loss of capacity	G: 1:C 1
	Beam				COTHETC	Up to 25% exposed, none buckled	Minor			Simplified and (or) advanced approaches
D	Column	Completely peeled-off	Pink/red Whitish grey	Extensive	Considerable	Up to 50% exposed, not more than one bar buckled	Moderat -e	aetarmanan	Some level of capacity is lost	

Table 6-2 (cont'd).

Wall		Consider- able to	Up to 20% exposed,		Noticeable	
		surface	generally	Wider	deformatio	
Floor		Consider-	adhering	crack	n	
		able to		width		

					soffit					
	Beam				Consider- able to corners, sides, soffit	Up to 50% exposed, not more than one bar buckled		Significant deformation		
	Column					Over 50% exposed and more than one bar buckled		Any distortion		
	Wall					Over 20%				
E	Floor	Fully removed	Whitish grey	Concrete surface removed	Almost all surface spalled	exposed, much separated from concrete		Large deformatio	Significa- nt loss of capacity	Advanced approaches
	Beam					Over 50% exposed, more than one bar buckled	Larger crack width	n-n (sag)		



(c) Moment capacity degradation with time during and after fire

Figure 6-1. Response of a typical RC beam during and after fire exposure

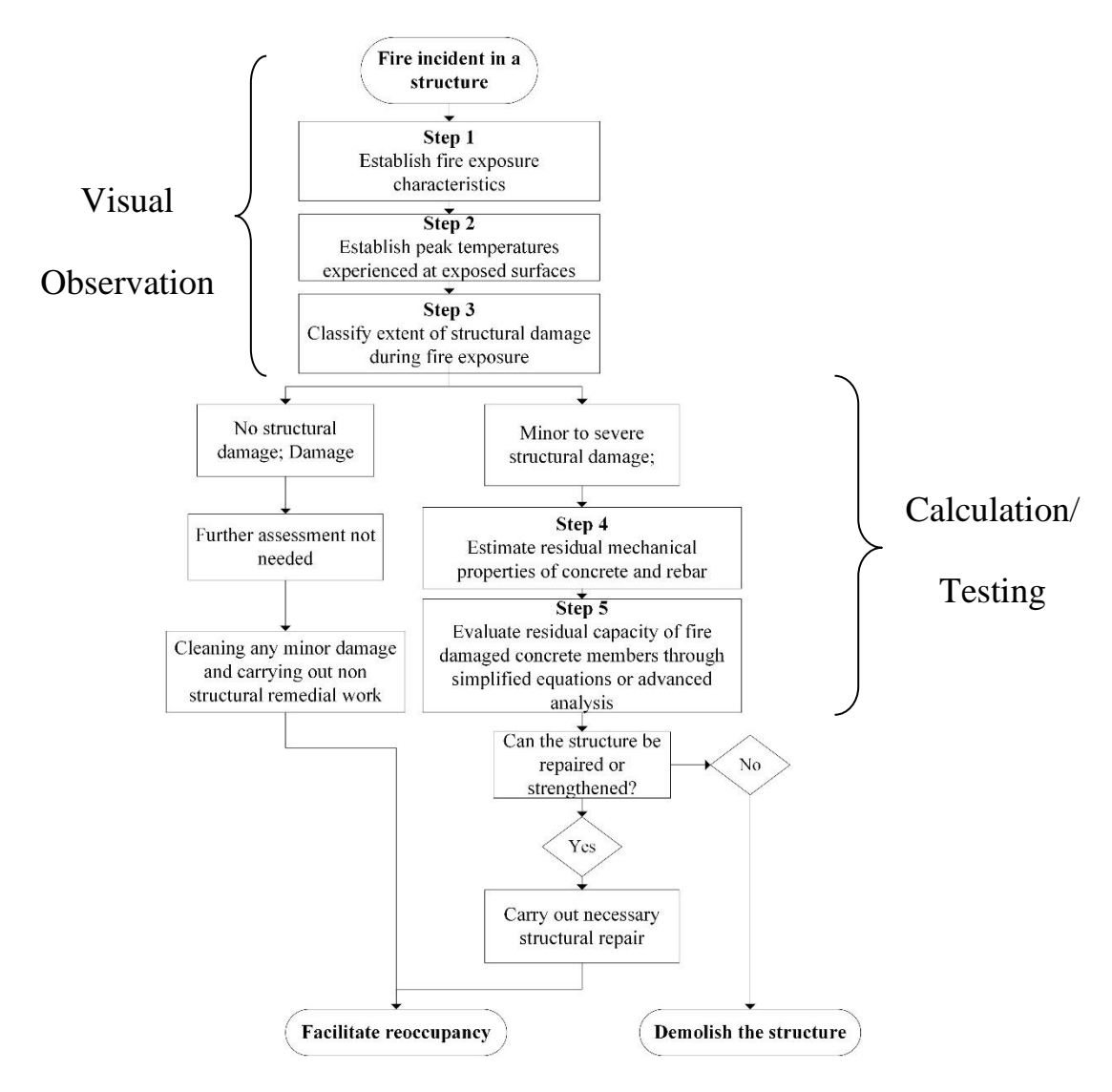


Figure 6-2. Flowchart illustrating five step approach for rapid assessment of fire-damaged concrete structures



Figure 6-3. Melting of aluminum formwork supports indicating that the fire reached temperatures in excess of 650°C

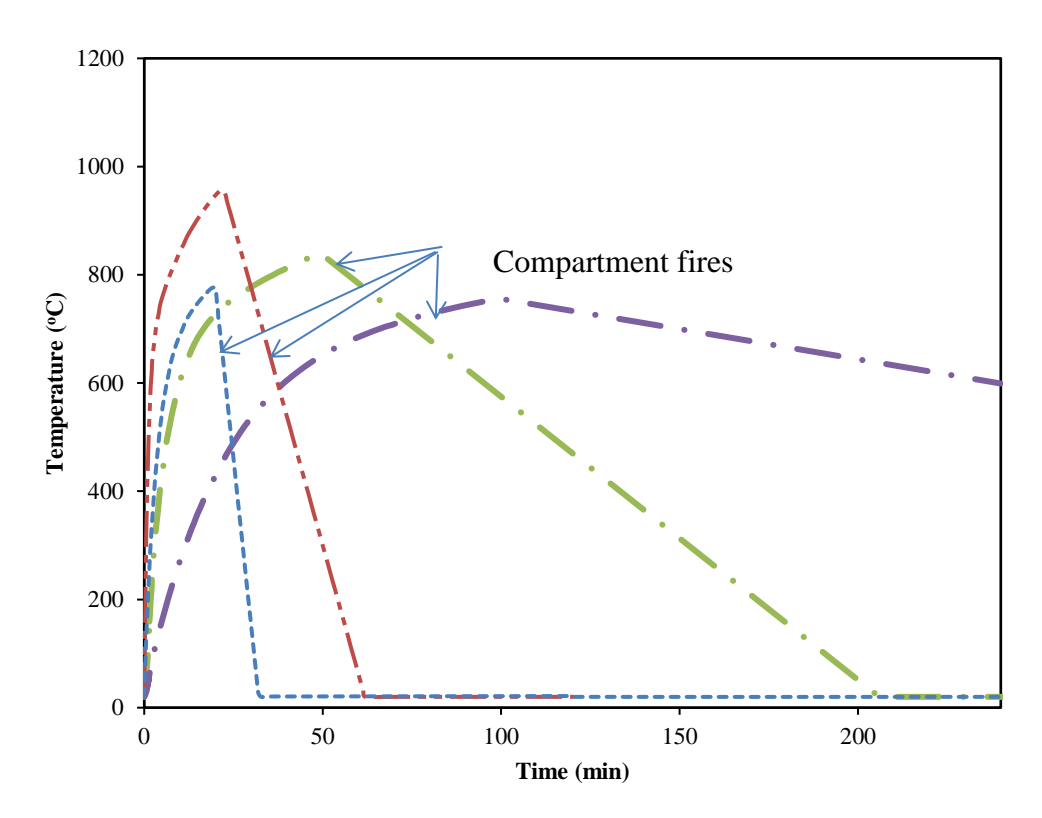
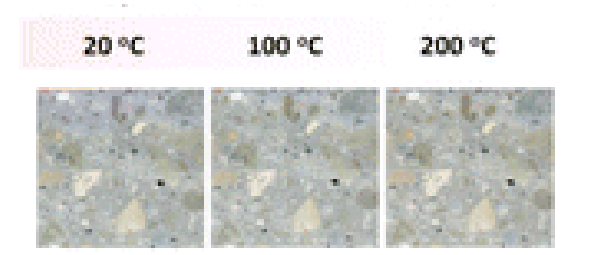


Figure 6-4. Parametric time temperature curves for different compartment conditions calculated as per Eurocode 1



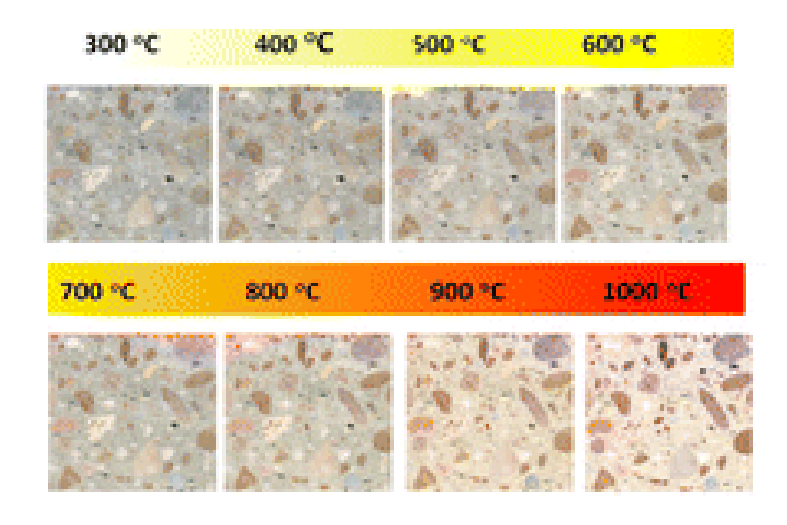


Figure 6-5. Color change of siliceous concrete, heated to temperatures ranging from 100°C to 1000°C



(a) Thermal crazing (cracking)



(b) Explosive spalling

Figure 6-6. Temperature induced damage at surface level (outer layers) of fire exposed concrete slabs

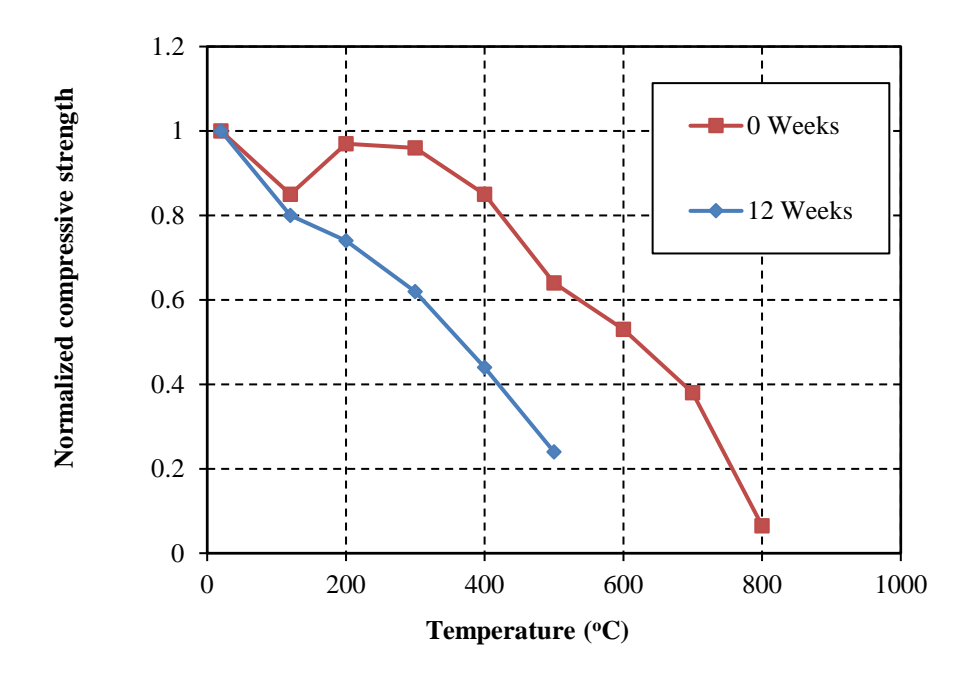


Figure 6-7. Influence of temperature and post cooling storage period on compressive strength of concrete

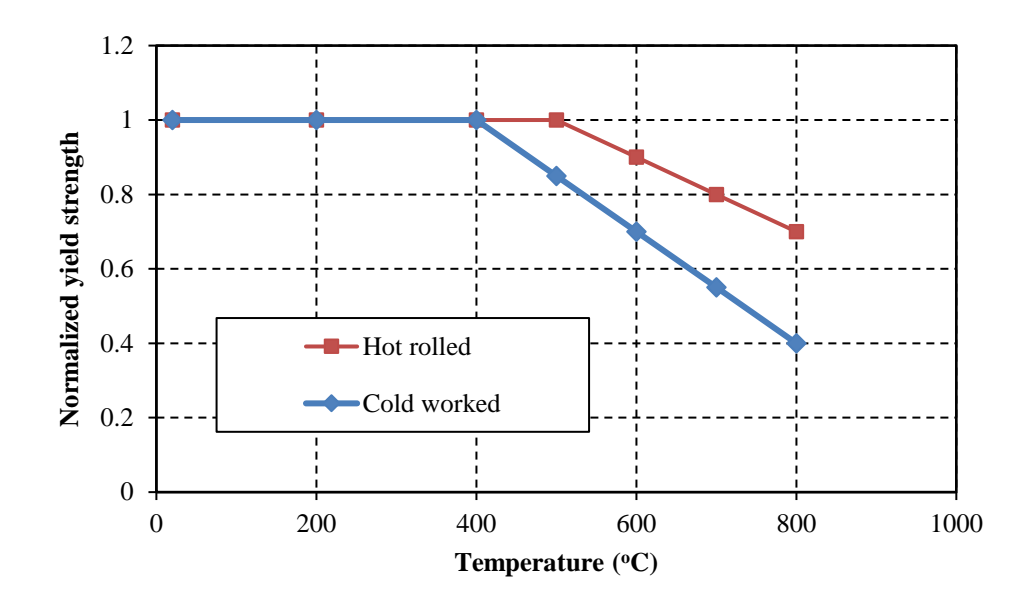


Figure 6-8. Yield strength of different types of reinforcing steel after exposure to elevated temperature

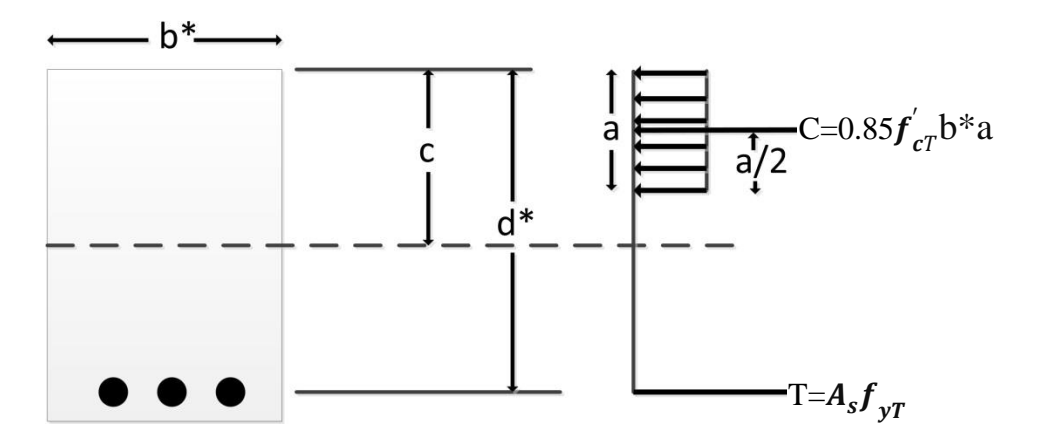


Figure 6-9. Illustration of cross-sectional capacity using simplified analysis

7 CONCLUSIONS AND RECOMMENDATIONS

7.1 General

This dissertation presented a comprehensive study on the residual response of fire damaged concrete beams. Both experimental and numerical studies were carried out to evaluate residual capacity of fire damaged concrete beams and to quantify the influence of critical factors influencing residual response of fire damaged concrete beams. As part of experimental studies, full-scale residual capacity tests were carried out on six RC beams (two HSC and four NSC) after subjecting them to realistic fire exposure scenarios with a distinct cooling phase. Data from these residual capacity tests was utilized to gauge the effect of strength of concrete, load level, fire scenario (specifically cooling phase), and residual deflections on residual capacity of fire damaged concrete beams. In addition, a series of unique bond strength tests were carried out at various temperatures to develop data on variation of temperature induced bond strength degradation for HSC and NSC, respectively. Data from these bond tests was utilized to develop empirical relations for temperature dependent bond strength of concrete in 200-600°C temperature range.

As a part of numerical studies, a general approach to evaluate residual capacity of fire exposed RC beam was developed and implemented using a three-dimensional finite element model. This numerical model, developed using ABAQUS (Hibbitt, Karlsson & Sorensen 2012) finite element software, accounts for distinct fire scenario, distinct material properties during heating, cooling and residual phases, loading and support conditions, and residual deflections in tracing residual response of fire damaged concrete beams. The validity of the model is established by comparing predicted response parameters from the numerical model against data and observations obtained

through fire exposure and residual capacity tests undertaken as part of this thesis and also with that obtained from the literature.

The validated numerical model was applied to conduct a series of parametric studies to quantify the influence of critical factors on residual response of fire damaged concrete beams. Results generated in these experimental and numerical studies, combined with other published information from existing literature were utilized to propose an approach for residual capacity assessment of fire damaged concrete beams (structures). The proposed sequential five step approach utilizes a combination of visual assessment techniques and thumb rules, non-destructive testing, as well as simplified and advanced calculation methods, to assess the extent of fire-induced damage in a concrete structure. In particular, this approach provides a basis for choosing appropriate analysis methods of varying complexity, such as the numerical model developed as part of this dissertation, on a case to case basis.

7.2 Key findings

Based on the information presented in this dissertation, the following key conclusions are drawn:

- 1. Limited test data exists on residual response of fire damaged concrete members. While these tests clearly indicate that significant residual capacity is retained in fire damaged concrete beams, there is lack of understanding on the influence of various interdependent parameters that can affect residual capacity. The influence of pre-fire service conditions, cooling phase, and residual deflections on residual capacity of fire exposed concrete members is not well established.
- 2. Three stages of analysis (testing) are required for evaluating residual capacity of fire damaged RC beams. These three stages comprise of evaluating pre-fire response

- (Stage 1), response during fire exposure including extended cool down of the member (Stage 2), and finally after complete cool down of the member (Stage 3).
- 3. The proposed numerical model, based on advanced analysis, accounts for temperature induced plastic deflections and temperature induced degradation of material properties (in both heating and cooling phases of fire) in evaluating residual capacity of fire damaged concrete beams. Incorporating temperature dependent strain hardening properties of steel reinforcement and tension stiffening properties of concrete leads to more realistic predictions of residual capacity than that based on simplified cross-sectional analysis, where such properties cannot be accounted for.
- 4. Results from experimental and numerical studies infer that type of fire exposure (especially rate of cooling), load level present during fire exposure, residual deflections, cross sectional dimensions and level of axial restraint have significant influence on residual response of fire damaged concrete beams.
 - a. Abrupt failure of RC member (beam) can occur during cooling phase of fire exposure when the cooling (phase) is at a slower rate (about 6°C per minute) representing no fire-fighting intervention, following rapid heating conditions as encountered in a severe fire. Such, rapid cooling results in greater level of strength and stiffness recovery in the RC member as it cools down to ambient conditions.
 - b. Large irrecoverable plastic deflections, significantly greater than pre-fire deflections, can occur in concrete beams due to fire exposure. The level of residual deflections is directly proportional to peak rebar temperatures experienced within the concrete beam. For similar peak rebar temperatures attained during fire

- exposure, presence of higher (by 20%) load level during fire exposure leads to significant increase (by 100%) in post-fire residual deflections.
- c. Load (stress) levels prior to and during fire exposure have limited influence on residual load carrying capacity, but adversely impact post-fire stiffness of fire damaged concrete beams. An increase in load level by about 20% can result in a 30% greater reduction in post-fire stiffness of a fire damaged concrete beams subject to similar fire exposures.
- d. Axial restraint has significant effect on fire response of concrete beams but has limited influence on residual capacity of fire damaged concrete beams.
- e. Temperature induced bond degradation has limited influence on heating phase and moderate influence on cooling phase behavior of RC beams under fire exposure. Further, the influence of considering temperature induced bond degradation on overall residual capacity of fire damaged concrete beams is minimal owing to irrecoverable tensile damage to concrete in the fire exposed regions. Thus, perfect bond may be assumed in the analysis for evaluating residual capacity of fire exposed concrete beams.
- f. Cover to tensile reinforcement plays a crucial role in the magnitude of the residual displacements and the amount of recovery upon cooling. In fact, increasing concrete cover from 20 mm to 40 mm can result in up to 15% improvement in residual capacity of RC beams following fire exposure.
- 5. A general five-step approach for residual capacity assessment of fire-damaged concrete structures was developed for use by practitioners, engineers and firefighters for residual capacity assessment of fire-damaged concrete structures. The proposed

approach utilizes a combination of visual assessment techniques and thumb rules, nondestructive testing, as well as simplified and advanced calculation methods, to assess the extent of fire-induced damage to a concrete structure. Furthermore, this approach provides a basis for choosing appropriate analysis methods of varying complexity, such as the numerical model developed as part of this dissertation, on a case to case basis.

6. Fire damaged beams may satisfy design limit state from strength consideration but may need some level of retrofitting to provide comparable level of safety (capacity) and serviceability which existed prior to the fire incident. The proposed guidance in this dissertation can be used to calculate reduction in excess capacity present prior to fire incident from fire damage in order to establish level of safety in the residual load carrying capacity of the member.

7.3 Recommendations for future research

Although this study has advanced the state-of-the-art with respect to residual response of fire damaged concrete members, additional research is required to gain further insight into some of the inherent complexities of the problem. The following are some of the key recommendations for future research in this area:

Due to the large number of parameters that can influence residual capacity, further residual
capacity assessments are needed based on the three-stage approach proposed in this thesis.

In particular, data on cooling phase behavior and post-fire residual deflections for concrete
beams with different loading, cross section, and support configurations under varying fire
scenarios is needed.

- Fire induced spalling is not incorporated in the current numerical analysis which can have significant influence on response during fire, and post-fire conditions due to loss of concrete cross-section. Further investigation is needed to evaluate the influence of temperature induced spalling on residual capacity of fire damaged concrete beams.
- Further experiments are needed to study and quantify extent of temperature induced spalling during fire exposure and its influence on residual capacity of fire damaged concrete beams. Also, numerical modeling strategies that can effectively account for early and late stage temperature induced spalling need to be developed to for more reliable predictions of residual capacity when spalling occurs.
- A better understanding of cooling phase thermal and mechanical properties needs to be
 developed through further member level tests. Such an understanding would facilitate
 accurate modeling of possible temperature induced failure during cooling phase of fire
 exposure, as well as accurate predictions of residual capacity.
- The influence of axial restraint and temperature induced bond degradation was found to be limited under some scenarios on concrete beams. Nonetheless, future studies need to focus on identifying scenarios where these parameters can significantly impact residual capacity of fire damaged concrete members.
- A large dataset of both experimental and numerical methods are needed to further refine practical guidance provided by this dissertation in assessing residual capacity of fire damaged concrete beams. While the approach for evaluating residual capacity is applied only to concrete beams, it will be beneficial to establish application of this approach in evaluating residual capacity of concrete members such as columns, slabs, walls etc.

7.4 Research impact

Residual capacity assessment of fire damaged concrete structures (beams) is required for making informed decisions with respect to re-occupancy and future safety of structure, as well as to develop needed retrofitting and strengthening measures. Nonetheless, predicting residual capacity of fire exposed beams is a complex task and can vary significantly depending on the assumptions used in analysis. At present, there is limited available empirical understanding on residual response of fire damaged concrete beams and limited approaches do not consider pre-fire conditions or extended cooling phase in evaluating residual capacity. Additionally, none of the existing approaches incorporate effect of post-fire residual deflections in evaluating residual capacity of fire damaged beams.

The experimental and numerical studies presented in this dissertation provide a comprehensive understanding of the behavior of fire damaged concrete beams. The effects of critical influencing factors, such as load intensity, fire severity (including rate of cooling), axial restraint, and temperature induced bond degradation on residual capacity are quantified. It is apparent from these studies that the realistic residual capacity can only be evaluated through a three stage approach with explicit consideration to cooling phase and residual deflections occurring due to irreversible temperature induced damage experienced in concrete and rebars during fire exposure.

Further, the numerical modelling approach presented in this study provides an effective alternative to resource and time intensive testing for evaluating residual capacity of fire damaged concrete beams. The proposed model accounts for all critical factors that affect residual behavior of fire damaged concrete beams, including distinct temperature dependent properties of concrete and reinforcing steel during heating, cooling and residual phases of analysis, strain hardening in steel reinforcement, tensile cracking in concrete, geometrical nonlinearities, realistic fire exposure with

distinct cooling phase, and built-in residual deflections. Thus, the developed model can be used to undertake detailed analysis to evaluate residual response of fire damaged concrete beams.

In addition, a sequential five-step approach is proposed for conditional assessment of fire damaged concrete structures. This approach relies upon a combination of visual inspection, expert judgement, experimental and (or) analytical (numerical) methods, to make informed decisions on re-occupancy and repair strategies for the use of the structure after fire incident. This approach provides a generalized framework for assessing post-fire residual capacity of fire damaged RC structures. Specifically, this approach provides the context in which the advanced analysis methods developed as part of this dissertation can be applied to evaluate residual capacity of fire damaged concrete beams. This approach can be applied over a wide range of structural members, so is attractive for incorporation in guidance documents for post-fire assessment of concrete structures. Overall, the research presented in this dissertation developed a comprehensive understanding on the residual response of fire damaged concrete structures after exposure to combined effects of fire and structural loading.



Appendix A: Worked example for damage assessment of an office building floor after fire

A.1 Introductory note

This appendix provides a detailed example of applying the proposed methodology laid out in this document to assess fire damage in an office building. The problem description, as well as details of each step in the assessment approach is discussed in the following sections.

A.1.1 Problem description

A severe fire has occurred in the 7th storey of a 10 storey office building, with a square ground plan of 40 m by 40 m. The construction plan of the floor exposed to fire is shown in Fig. A.1. Since every floor of the building was designed as a separate compartment, the fire brigade was successful in containing the fire to a single floor. However, the 7th floor experienced compete burnout. A preliminary assessment of the floor is needed to evaluate extent of damage to structural members. Further, an indication whether the floors immediately above the fire exposed floor can be safely re-occupied during any rehabilitation work if needed.

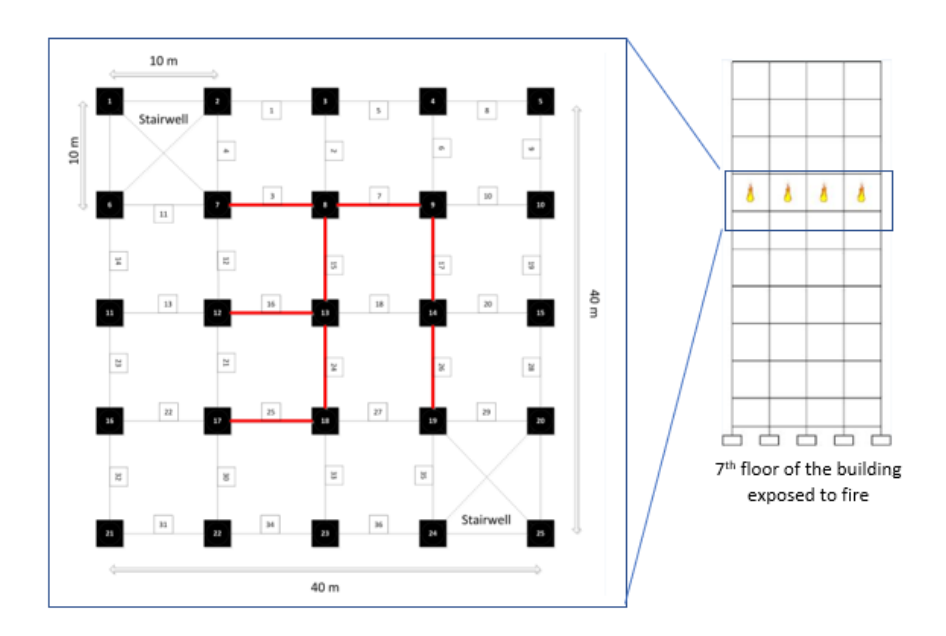


Fig. A-1. Ground plan and structural layout of the office floor and reference numbers for structural elements

The RC columns and RC beams of the concrete structure are exposed to fire. From technical design documentation on the building, dimensions of the load-bearing structural members, as well as reinforcement details are compiled. The structural members were fabricated using concrete having design strength 41 MPa and with main reinforcement having yield strength 413 MPa. The beams were designed to resist applied load of 8 kN/m (or design moment 100 kN-m), while the columns were designed to carry a design axial load of 160 kN. The RC columns are 4 m in height while the RC beams are 10 m in length. The cross-sectional dimensions and reinforcement details of the beams are shown in Fig. A.2, along with the elevation (plan) in Fig. A.1.

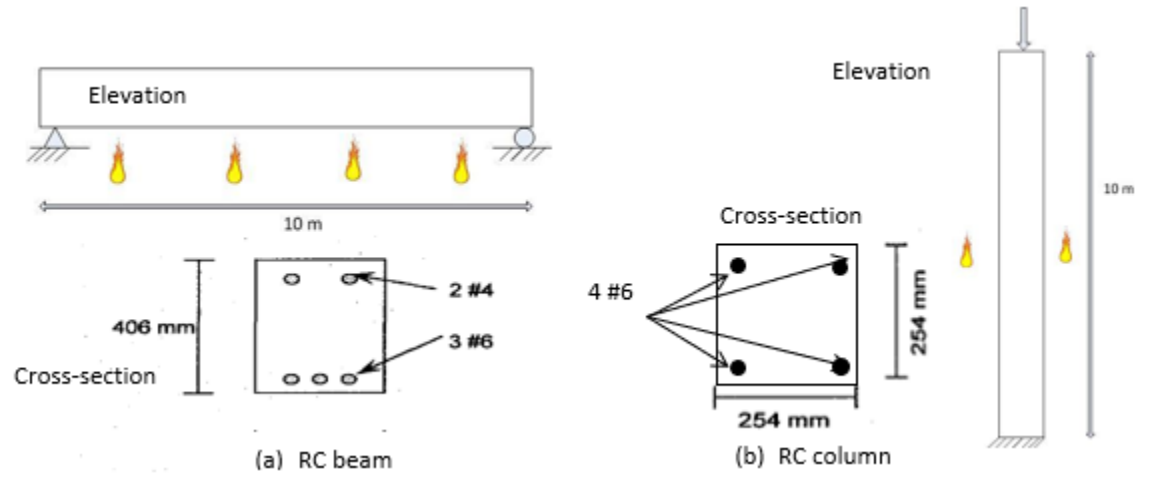


Fig. A-2. Cross-sectional dimensions and reinforcement details of beams and columns present in the fire exposed structure

Once these initial configuration details of the fire-exposed concrete structure are determined, the five step approach presented in the guidance document can be applied to assess level of safety, as well as develop targeted repair and retrofitting strategies in the fire-damaged concrete structures. Each of these steps is described in the sections below.

A.2 Step 1: Establish fire characteristics

The total duration of fire exposure (both heating and cooling phases) is initially estimated to be approximately 2 hours, based on fire-fighters' report and eyewitness interviews. Further, molten

aluminum is found upon examination of non-structural debris, indicating that peak temperatures exceeded 650°C. With such preliminary information, and based on compartment dimensions, ventilation conditions, and assumed fuel density (summarized in Table A.1), the probable time-temperature curve in the compartment is calculated as per Eurocode 1 recommendations, and is shown in Fig. A.3.

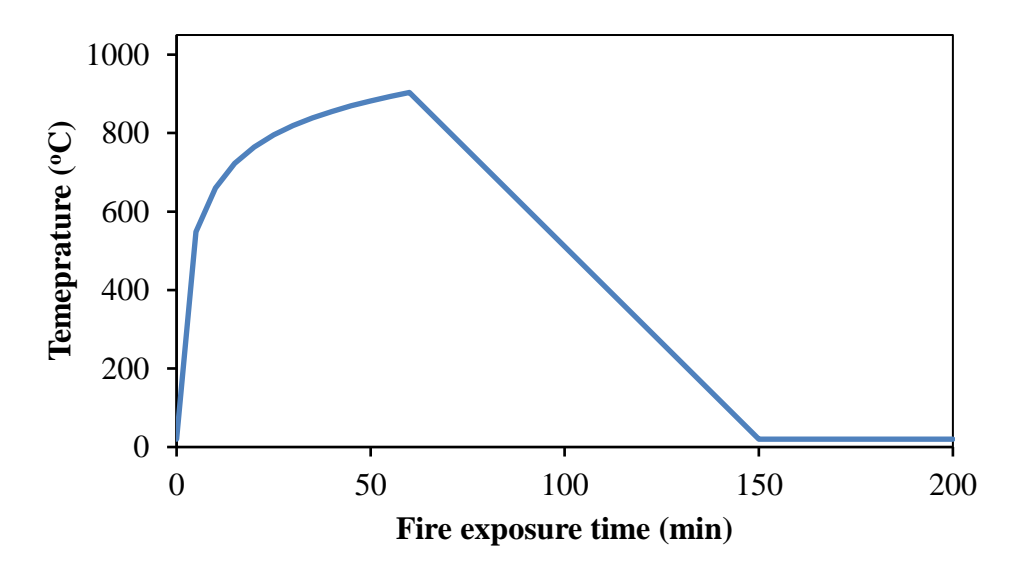


Fig. A-3. Predicted time-temperature curve of the fire compartment

The heating phase of the predicted compartment time-temperature curve lasts for 60 minutes, followed by a decay phase lasting for 90 minutes. Thus, the total duration of fire exposure is calculated to be 150 minutes which is greater than the preliminary estimate as per fire fighters' records. Furthermore, the predicted peak fire temperature is almost 900°C, corroborated by presence of molten aluminum in the debris present in the fire exposed floor. Table A.1 summarizes the key fire characteristics obtained from Step1 of assessment, and will be utilized in the subsequent steps, if needed.

Table A-1. Key fire severity characteristics

Fuel load	Peak fire	Duration of	Duration of	
density (MJ/m²)	temperature	heating phase	cooling phase	
	(°C)	(hours)	(hours)	
600	903	1	1.5	
600	903	1	1.5	

A.3 Step 2: Establish peak exposure temperatures experienced by structural member

Based on post-fire inspection by engineers, it is estimated that the RC columns (vertical members) did not experience significant rise in temperature as they were not exposed to rising convective currents (hot gases). Furthermore, walls present within fire compartment acted as an insulating layer which prevented direct exposure to high temperatures and open flame. On the other hand, RC beams (horizontal members) were directly exposed to hot gases that accumulated near the ceiling of the column. Therefore, it can be inferred that RC beams were exposed to higher temperatures than RC columns.

In addition, a visual observation of the exposed concrete surfaces in the RC beams and underneath of slabs indicates a pink coloration. Minor rounding of the corners and surface pitting (peeling) was also seen in the RC beams. This infers that the fire exposed surfaces of the beams were exposed to temperatures in excess of 700°C (as described in Section 2 of the report). On the other hand, the color of the exposed surfaces in the columns was grey, indicating the temperatures experienced at the exposed surface likely to have remained below 400°C.

In order to ascertain temperatures experienced at the rebar level, cracking patterns on the fire exposed surfaces of both RC beams and columns were recorded. No differential thermal cracks were observed in the beams which infer that the interface temperature between rebar and concrete

remained well below 600°C. Only minor surface pitting and corner (cover) spalling was seen in the fire affected members, with no reinforcement being exposed.

This information collected for each fire-exposed concrete member is utilized to classify the extent of damage in the third step of the approach.

A.4 Step 3: Classification of temperature induced damage during fire exposure

The degree of damage in RC beams and columns is ascertained based on the visual assessment scheme described in Section 2.3. The damage classification for the beams and columns is provided in Table A.2.

Table A-2. Classification of temperature induced damage based on visual observation

Structural	Class of	Member Reference Number			
Element	Damage				
	В	1-25			
Columns	С	None			
Columns	D	None			
	E	None			
	В	1,2,4-6,8-14,18-23,26-36			
Daama	С	3,7,15,16,17,24,25			
Beams	D	None			
	Е	None			

Visual classification indicates that none of the columns underwent structural damage during fire exposure. However, some beams might have undergone structural damage due to temperature induced degradation of concrete and reinforcing steel. The residual capacity of these beams needs to be ascertained.

A.5 Step 4: Estimating residual mechanical properties of concrete and rebar

No major spalling, thermal cracking or discoloration of concrete was seen as a consequence of fire exposure in the entire floor, and hence there is no need for detailed assessment to evaluate in-situ

mechanical properties of fire damaged concrete and reinforcing steel. The recommended values for strength reduction factors as proposed in section 2.4 are adopted for estimating residual strength of concrete and reinforcing steel (see Table A.3).

Table A-3. Reduction factors for residual strength of concrete and reinforcing steel after exposure to high temperature

Peak exposure Temperature in fire		e compressive rength	Reinforcing steel yield strength			
(°C)	Upper limit	Lower limit	Hot rolled	Cold formed		
20	1	1	1	1		
100	0.85	0.8	1	1		
200	0.97	0.74	1	1		
300	0.96	0.62	1	1		
400	0.85	0.44	1	1		
500	0.64	0.24	1	0.85		
600	0.53	-	0.9	0.7		

However, in-situ tests were conducted to determine compressive strength of concrete and yield strength of reinforcing steel in the unaffected regions of the structure to compare them with their design values. The in-situ compressive strength of concrete and yield strength of rebar were measured to be 55 MPa (higher than original design strength of 41 MPa), and 450 MPa respectively, significantly higher than their respective design values.

A.6 Step 5. Evaluating residual capacity of fire damaged reinforced concrete elements

Since there was no spalling or indications of loss of interfacial bond strength between reinforcing steel and concrete, a simplified approach is adopted to ascertain the residual capacity of the fire damaged RC beams. Also, no significant post fire residual deformations were observed in the beams. Further, all the beams were assumed to have undergone the same level of temperature induced degradation as they were located in the same fire compartment. The beam geometry and cross-sectional details are shown in Fig. A.4.

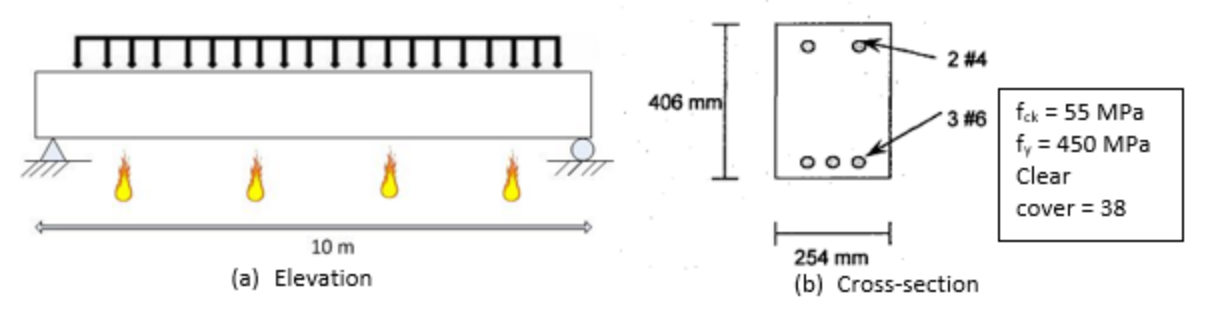


Fig. A-4. Geometry and reinforcement details of the fire damaged beams

Based on the simplified approach described in section 2.5.1 of the document, the peak rebar temperature can be ascertained depending on fire characteristics and cross-sectional details of the beam. The peak rebar temperature is calculated to be 510°C using equations 6-1 and 6-2 (section 2.5.1). Also, the effective width of the damaged cross section of the beam is measured to be 234 mm, 20 mm lower than its value prior to fire exposure. Henceforth, using residual strength of rebar and reduced (damaged) width of concrete cross section, residual flexural capacity of the beam can be calculated using modified room temperature equations (equation 3 as per section 2.5.1). It should be noted that the in-situ concrete compressive strength and yield strength of rebar, measured in step 4 are utilized in these equations. Therefore, compressive strength of concrete is 55 MPa for both room temperature and after cool down from fire exposure, while yield strength of rebar is 450 MPa at room temperature, and reduces to 427 MPa after fire exposure.

The moment capacity of the RC beam prior to fire exposure is calculated to be 129.7 kN-m which is greater than the required moment capacity of 100 kN-m. Furthermore, the residual flexural capacity of the same RC beam is calculated to be 122 kN-m using reduced values for beam width and yield strength of reinforcing steel. The calculated flexural capacity of the RC beam before and after fire exposure is summarized in Table A.4.

Table A-4. Calculated moment capacity before and after fire exposure

Peak rebar	Yield strength of rebar		Moment capacity (kN-m)		Required
temperature (°C)	(MPa)				moment
	Ambient	Residual	Ambient	Residual (%	capacity (kN-
				reduction)	m)
550	450	427	129.7	122.1 (6)	100

The residual moment capacity of the beams is about 6% lower than its room temperature capacity prior to fire exposure. Nonetheless, the predicted residual capacity of the RC beam is still greater than the required moment capacity from design consideration.

In conclusion, the fire damaged 7th floor can be re-occupied safely from a structural standpoint after necessary smoke cleaning etc. Furthermore, the floors not affected by fire and immediately above the fire exposed floor, i.e. floors 8, 9 and 10 can be re-occupied safely, similar to their prefire conditions.

Appendix B: beam design and load level calculations

B.1 Introductory note

Room temperature design and load level calculations of tested NSC and HSC beams using ACI 318 (2008), are summarized in this appendix. The reinforcement detailing, shear force diagram, and bending moment diagram of the beams is shown schematically in Figure A.1. Design calculations for deflection, and load level are summarized in two following sections (Dwaikat 2009).

B.1.1 Normal strength concrete beam

Design calculations

$$f_c' = 42 \text{ MPa}$$
 $f_v = 413 \text{ MPa}$

Neglecting compression area of steel

$$A_{st} = 855 \text{ mm}^2$$

Clear concrete cover (c) = 38 mm

$$h = 406 \text{ mm}$$
 $b = 254 \text{ mm}$

d = 352.4 mm

$$a = \beta_1 c$$

Hence, $\beta_1 = 0.75$

Therefore, c = 39.6/0.75 = 52.8 mm

Correspondingly, strain through linear interpolation

$$\epsilon_{t} = \frac{0.003}{c} (d - c) = \frac{0.03}{52.8} (352.4 - 52.8) = 0.017 > 0.005$$

Hence, $\varphi = 0.9$

Check for minimum reinforcement:

$$\rho_{min}=0.0039$$

$$\rho = \frac{A_s}{bd} = 0.00955 > \rho_{min}$$

The bending moment capacity of the beam cross-section is

$$M_n = A_s \left(d - \frac{a}{2} \right) = \frac{855 \times 413 \times (352.4 - \frac{39.6}{2})}{10^6} = 117 \text{ kN. m}$$

$$M_n = 1.4P_n$$

$$P_n = 83.9 \; kN \; \; and \; \; P_u = 75.5 \; kN$$

Shear design

Ultimate shear force at a distance d from the support face:

$$V_u = \frac{P_u}{\emptyset} = \frac{75.5}{0.5} = 100.7 \text{ kN}$$

The concrete shear strength is:

$$V_c = 0.16\sqrt{f'_c}b_wd = \frac{0.16\sqrt{42}*254*352.4}{1000} = 93 \text{ kN}$$

Let nominal shear strength be V_n , and shear reinforcement V_s , then:

$$V_n > V_c$$

$$V_s = V_n - V_c = 100.7 - 92 = 8.7 \text{ kN}$$

$$V_{s,min} = max \begin{cases} 0.344 \ b_w d \\ 0.06 \sqrt{f_c'} b_w d \end{cases} = 35 \ kN \label{eq:vsmin}$$

Thus, minimum shear reinforcement can be used

Required shear reinforcing area:

$$\frac{A_v}{s} = 0.24 \text{ mm}$$

Thus, using #2 stirrups

Area of each leg is 31.6 mm²

Hence $A_v = 2 \times 31.6 = 63.2 \text{ mm}^2$

Required spacing will be

$$s = \frac{63.2}{0.24} = 267 \text{ mm} \ge \frac{d}{2} = \frac{352.4}{2} = 176.2 \text{ mm}$$
 (ACI 318-8 11.5.4.1)

Use #2 at 150 mm c/c

Deflection check

Neglecting compressive steel, gross moment of inertia can be calculated as:

$$I_g = \frac{bh^3}{12} = 1.416 \times 10^9 \text{ mm}^4$$

Cracked moment of inertia can be calculated as:

$$E_s = 210 \text{ GPa}$$

$$E_c = 4730\sqrt{f_c'} = 30.6 \text{ GPa}$$

$$n = \frac{E_s}{E_c} = 6.9$$

$$x = \frac{\sqrt{(nA_{st})^2 + 2bdnA_{st}} - nA_{st}}{b} = 106.9 \text{ mm}$$

$$I_{cr} = \frac{bx^3}{3} + nA_{st}(d-x)^2$$

$$I_{cr} = 0.459 \times 10^9 \text{ mm}^4$$

The modulus of rupture can be calculated as:

The modulus of rupture can be calculated as:

$$M_{cr} = 0.6\sqrt{f'_c} = 4.7 \text{ MPa}$$

The cracking moment can be calculated as:

$$M_{cr} = \frac{f_r I_g}{y_t} = 26.9 \text{ kN.m}$$

Effective moment of inertia can be calculated as:

Assuming M_a to be 0.7 M_u , then:

$$M_a = 0.7 \times 117 \times 0.9 = 73.71 \text{ kN.m}$$

$$I_e = \left(\frac{M_{cr}}{M_a}\right)^3 I_g + \left[1 - \left(\frac{M_{cr}}{M_a}\right)^3\right] I_{cr} \le I_g$$

$$I_e = 0.506 \times 10^9 \, \text{mm}^4$$

$$\delta = \frac{M}{2E_C I_e} \left(\frac{L^2}{4} - \frac{a^2}{3}\right) = 6.5 \text{ mm}$$

Load level calculations

$$f_c' = 62 \text{ MPa}$$
 (On test day) $f_y = 450 \text{ MPa}$

Neglecting compression area of steel

$$A_{st} = 855 \text{ mm}^2$$

Clear concrete cover (c) = 38 mm

$$h = 406 \text{ mm}$$

$$b = 254 \text{ mm}$$

$$d = 352.4 \text{ mm}$$

$$a = \beta_1 c$$

Hence,
$$\beta_1 = 0.65$$

Therefore,
$$c = 31/0.65 = 47.7 \text{ mm}$$

Correspondingly, strain through linear interpolation

$$\epsilon_t = \frac{0.003}{c}(d-c) = \frac{0.03}{47.7}(352.4 - 47.7) = 0.0192 > 0.005$$

Hence, $\varphi = 0.9$

Check for minimum reinforcement:

$$\rho_{min} = 0.0042$$

$$\rho = \frac{A_s}{hd} = 0.00955 > \rho_{min}$$

The bending moment capacity of the beam cross-section is

$$M_n = A_s \left(d - \frac{a}{2} \right) = \frac{855 \times 450 \times (352.4 - \frac{39.6}{2})}{10^6} = 129.7 \text{ kN. m}$$

Nominal load can be calculated as:

$$M_n = 1.4P_n$$

$$P_n = 92.7 \ kN$$

Load level, defined as ratio of applied load under fire conditions to section capacity at room temperature

(Buchanan 2002) for a 60 kN load can be calculated as:

$$LL = \frac{60}{92.7} \times 100 = 53\%$$

B.1.2 High strength concrete beam

Design calculations

$$f_c' = 100 MPa$$

$$f_{v} = 450 MPa$$

Neglecting compression area of steel

$$A_{st} = 855 \text{ mm}^2$$

Clear concrete cover (c) = 38 mm

$$h = 406 \text{ mm}$$

$$b = 254 \text{ mm}$$

$$d = 352.4 \text{ mm}$$

$$a = 16.7 \text{ mm}$$

$$a = \beta_1 c$$

Hence,
$$\beta_1 = 0.65$$

Therefore,
$$c = 16.7/0.65 = 25.7 \text{ mm}$$

Correspondingly, strain through linear interpolation

$$\epsilon_t = \frac{0.003}{c}(d-c) = \frac{0.03}{25.2} (352.4 - 25.2) = 0.014 > 0.005$$

Hence, $\varphi = 0.9$

Check for minimum reinforcement:

$$\rho_{min} = 0.006$$

$$\rho = \frac{A_s}{hd} = 0.00955 > \rho_{min}$$

The bending moment capacity of the beam cross-section is

$$M_n = A_s \left(d - \frac{a}{2} \right) = \frac{855X413X(352.4 - \frac{16.4}{2})}{10^6} = 122 \text{ kN. m}$$

$$M_n = 1.4P_n$$

$$P_n = 86.8 \, kN \text{ and } P_u = 78.1 \, kN$$

Shear design

Ultimate shear force at a distance d from the support face:

$$V_u = \frac{P_u}{\emptyset} = \frac{78.1}{0.5} = 104.2 \text{ kN}$$

The concrete shear strength is:

$$V_c = 0.16\sqrt{f_c'}b_w d = \frac{0.16\sqrt{100}*254*352.4}{1000} = 165 \text{ kN}$$

Let nominal shear strength be V_n , and shear reinforcement V_s , then:

$$V_n > V_c$$
 $V_n > \frac{V_c}{2}$

$$V_{s,min} = max \begin{cases} 0.344 \ b_w d \\ 0.06 \sqrt{f_c'} b_w d \end{cases} = 54 \text{ kN}$$

Thus, minimum shear reinforcement can be used

Required shear reinforcing area:

$$\frac{A_v}{s} = 0.37 \text{ mm}$$

Thus, using #2 stirrups

Area of each leg is 31.6 mm²

Hence
$$A_v = 2 \times 31.6 = 63.2 \text{ mm}^2$$

Required spacing will be

$$s = \frac{63.2}{0.37} = 171 \text{ mm}$$

Use #2 at 150 mm c/c

Deflection check

Neglecting compressive steel, gross moment of inertia can be calculated as:

$$I_g = \frac{bh^3}{12} = 1.416 \times 10^9 \text{ mm}^4$$

Cracked moment of inertia can be calculated as:

$$E_s = 210 \text{ GPa}$$

$$E_c = 4730\sqrt{f_c'} = 47.3 \text{ GPa}$$

$$n = \frac{E_s}{E_c} = 4.4$$

$$x = \frac{\sqrt{(nA_{st})^2 + 2bdnA_{st}} - nA_{st}}{b} = 88.8 \text{ mm}$$

$$I_{cr} = \frac{bx^3}{3} + nA_{st}(d - x)^2$$

$$I_{cr} = 0.323 \times 10^9 \, \text{mm}^4$$

The modulus of rupture can be calculated as:

$$M_{cr} = 0.6\sqrt{f_c'} = 6 \text{ MPa}$$

The cracking moment can be calculated as:

$$M_{cr} = \frac{f_r l_g}{y_t} = 41.9 \text{ kN.m}$$

Effective moment of inertia can be calculated as:

Assuming M_a to be 0.7 M_u , then:

$$M_a = 0.7 \times 121.6 \times 0.9 = 76.6 \text{ kN.m}$$

$$I_e = \left(\frac{M_{cr}}{M_a}\right)^3 I_g + \left[1 - \left(\frac{M_{cr}}{M_a}\right)^3\right] I_{cr} \le I_g$$

$$I_e = 0.501 \times 10^9 \,\mathrm{mm}^4$$

$$\delta = \frac{M}{2E_c I_e} \left(\frac{L^2}{4} - \frac{a^2}{3} \right) = 4.4 \text{ mm}$$

Load level calculations

$$f_c' = 106 \text{ MPa} \text{ (On test day)} \qquad f_y = 450 \text{ MPa}$$

Neglecting compression area of steel

$$A_{st} = 855 \text{ mm}^2$$

Clear concrete cover (c) = 38 mm

$$h = 406 \text{ mm}$$
 $b = 254 \text{ mm}$

$$d = 352.4 \text{ mm}$$

$$a = 16.7 \text{ mm}$$

$$a = \beta_1 c$$

Hence,
$$\beta_1 = 0.65$$

Therefore, c = 16.7/0.65 = 25.7 mm

Correspondingly, strain through linear interpolation

$$\epsilon_t = \frac{0.003}{c}(d-c) = \frac{0.003}{25.7} (352.4 - 25.7) = 0.038 > 0.005$$

Hence, $\varphi = 0.9$

Check for minimum reinforcement:

$$\rho_{min} = 0.0057$$

$$\rho = \frac{A_s}{bd} = 0.00955 > \rho_{min}$$

The bending moment capacity of the beam cross-section is:

$$M_n = A_s \left(d - \frac{a}{2} \right) = \frac{855 \times 450 \times (352.4 - \frac{16.7}{2})}{10^6} = 132.4 \text{ kN.m}$$

Nominal load can be calculated as:

$$M_n = 1.4P_n$$

$$P_n = 94.5 \; kN$$

Load level, defined as ratio of applied load under fire conditions to section capacity at room temperature (Buchanan 2002) for a 50 kN load can be calculated as:

$$LL = \frac{50}{94.5} \times 100 = 53\%$$

Appendix C: additional images taken during different stages of testing

C.1 Introductory note

Additional images taken through the viewport at key time intervals for the tested beams are provided in this section. Also, a digital image correlation technique (DIC) was applied to track surface level strain localizations on the fire damaged beams but did not yield quantitative results possibly due to extensive surface pitting and cracking experienced during fire exposure. However, qualitative changes could be captured by the setup (refer Roya et al. (Roya et al. 2018) for more details regarding DIC setup).



Typical beam just prior to fire exposure



Typical beam (NSC) during early stages of fire exposure



Typical beam (NSC) during late stages of fire exposure

Fig. C-1. Images of Normal Strength Concrete (NSC) beam prior to and during fire exposure

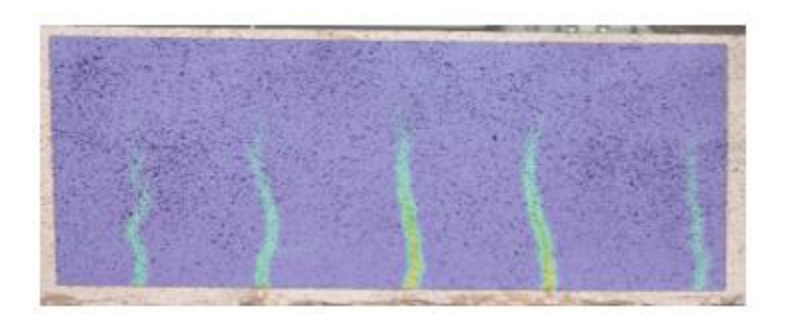


Figure C.2 Typical strain localization (redder hues indicate greater tensile strains) at critical flexural span in NSC beam B3 at service load (about 50 kN); captured using Digital Image Correlation (DIC) setup



REFERENCES

- Abrams, M., Gustaferro, A., and Lin, T. (1976). Fire endurance of continous reinforced concrete beams. 23.
- ACI. (2008). ACI 318-08: Building code requirements for reinforced concrete. ACI, Detroit, MI.
- ACI 216.1. (2008). Code requirements for determing fire resistance of concrete and masonry construction assemblies. American Concrete Institute, Farmington Hills, MI.
- Agrawal, A., Kodur, V.K.R. (2015). "Effect of temperature induced bond degradation on fire response of reinforced concrete beams." Response of Structures Under Extreme Loading Proceedings of the 5th International Workshop on Performance, Protection & Strengthening of Structures Under Extreme Loading (PROTECT2015), East Lansing, US, 28 30 June 2015, DEStech Publications, pp. 712-721.
- Agrawal, A, and Kodur, V.K.R. (2016). "Quantifying the effect of temperature induced bond degradation on fire resistance of RC beams." *Proceedings of the 9th International Conference on Structures in Fire (SIF2016)*, Princeton University, New Jersey, US, 6 8th June 2018, ISBN: 978-1-60595-320-5, pp. 62-70.
- Agrawal, A, and Kodur, V.K.R. (2018). "An experimental approach for evaluating residual capacity of fire damaged concrete members." *Proceedings of the 10th International Conference on Structures in Fire (SIF2018)*, Ulster University, Belfast, United Kingdom, 6-8th June 2018, pp. 949-958.
- Agrawal, A, and Kodur, V.K.R. (2019). "Residual response of fire-damaged high-strength concrete beams." *Fire and Materials*, 43:3, 310–322.
- Agrawal, A, and Kodur, V.K.R. (2020). "A novel experimental approach for evaluating residual capacity of fire damaged concrete." *Fire Technology*, 56, 715-735.
- Alonso, C. (2009). "Assessment of post-fire reinforced concrete structures: Determination of depth of temperature penetration and associated damage." *Concrete Repair, Rehabilitation and Retrofitting II*, 471–478.
- Annerel, E., and Taerwe, L. (2011). "Evolution of the strains of traditional and self-compacting concrete during and after fire." *Materials and Structures*, 44(8), 1369–1380.
- ANSYS. (2007). ANSYS metaphysics. ANSYS Inc., Canonsburg, PA.
- ASCE manual No. 78. (1992). *Structural fire protection*. American Society of Civil Engineers, Reston, VA.
- Aslani, F., and Samali, B. (2013). "Predicting the bond between concrete and reinforcing steel at elevated temperatures." *Structural Engineering and Mechanics*, 48(5), 643–660.

- ASTM E119-19. (2019). Test Methods for Fire Tests of Building Construction and Materials. American Society of Testing Materials, West Conshohocken, Pennsylvania, PA.
- Awoyera, P., and Akinwumi, I. (2014). "Forensic Investigation of Fire-affected Reinforced Concrete Buildings." *IOSR Journal*, 11(4), 17–23.
- Bai, L. L., and Wang, Z. Q. (2011). "Residual Bearing Capacity of Reinforced Concrete Member after Exposure to High Temperature." *Advanced Materials Research*, 368–373(2012), 577–581.
- Bazant, Z., and Kaplan, M. (1996). Concrete for high temperatures: Material properties and mathematical models. Longman Group Limited.
- Bažant, Z. P. (1970). "Constitutive equation for concrete creep and shrinkage based on thermodynamics of multiphase systems." *Matériaux et constructions*, 3(1), 3–36.
- Bažant, Z., and Thonguthai, W. (1978). "Pore pressure and drying of concrete at high temperature." *Journal of the Engineering Mechanics Division*, 104, 1059–1079.
- Beitel, J., and Iwankiw, N. (2005). "Historical Survey of Multistory Building Collapses Due to Fire." *Fire Protection Engineering*, 27, 42.
- BS 476-20. (1987). Fire tests on building materials and structures -part 20: Mehtod for determination of the fire resistance of elements of construction (general principles). BSi, UK.
- Chang, Y. F., Chen, Y. H., Sheu, M. S., and Yao, G. C. (2006). "Residual stress-strain relationship for concrete after exposure to high temperatures." *Cement and Concrete Research*, 36(10), 1999–2005.
- Cheng Fu-Ping, Kodur V. K. R., and Wang Tien-Chih. (2004). "Stress-Strain Curves for High Strength Concrete at Elevated Temperatures." *Journal of Materials in Civil Engineering*, 16(1), 84–90.
- Chew, M. Y. L. (1993). "The assessment of fire damaged concrete." *Building and Environment*, 28(1), 97–102.
- Choi, E. G., Shin, Y.-S., and Kim, H. S. (2013). "Structural damage evaluation of reinforced concrete beams exposed to high temperatures." *Journal of Fire Protection Engineering*, 23(2), 135–151.
- Crisfield, M. (1982). "Accelerated solution techniques and concrete cracking." *Computer methods in applied mechanics and ...*, 33(1–3), 585–607.
- Diederichs, U. (1981). "Bond strength at high temperatures." *Magazine of Concrete Research*, 33(115), 75–84.

- Diederichs, U., and Schneider, U. (1981). "Bond strength at high temperatures." *Magazine of Concrete Research*, 33(115), 75–84.
- Dwaikat, M. B. (2009). "Flexural response of reinforced concrete beams exposed to fire." Doctoral Dissertation, Michigan State University, East Lansing, Michigan.
- Dwaikat, M. B., and Kodur, V. K. R. (2009a). "Fire Induced Spalling in High Strength Concrete Beams." *Fire Technology*, 46(1), 251–274.
- Dwaikat, M., and Kodur, V. (2009b). "Response of restrained concrete beams under design fire exposure." *Journal of structural engineering*, 135(11), 1408–1417.
- El-Hawary, M. M., Ragab, A. M., El-Azim, A. A., and Elibiari, S. (1996). "Effect of fire on flexural behaviour of rc beams." *Construction and Building Materials*, 10(2), 147–150.
- Ellingwood, B., and Lin, T. (1991). "Flexure and shear behavior of concrete beams during fires." *Journal of Structural Engineering*, 117(2), 440–458.
- Ellingwood, B., and Shaver, J. (1979). "Fire effects on reinforced concrete members." *National Bureau of Standards*.
- Elsanadedy, H. M. (2019). "Residual Compressive Strength of High-Strength Concrete Exposed to Elevated Temperatures." *Advances in Materials Science and Engineering*, Research article, https://www.hindawi.com/journals/amse/2019/6039571/ (Oct. 30, 2019).
- EN 1991-1-2. (2002). Eurocode 1: Actions on structures Part 1-2: General actions Actions on structures exposed to fire. European Committe for Standardization.
- EN 1992-1-2. (2004). Eurocode 2: Design of concrete structures Part 1-2: General rules Structural fire design. European Committe for Standardization, Brussels, Belgium.
- EN-1994-1-2. (2008). Eurocode 4: Design of composite steel and concrete structures Part 1-2: General rules Structural fire design. European Committe for Standardization, Brussels, Belgium.
- Gao, W. Y., Dai, J.-G., Teng, J. G., and Chen, G. M. (2013). "Finite element modeling of reinforced concrete beams exposed to fire." *Engineering Structures*, 52, 488–501.
- Gawin, D., Pesavento, F., and Schrefler, B. A. (2004). "Modelling of deformations of high strength concrete at elevated temperatures." *Materials and Structures*, 37(4), 218.
- Gernay, T. (2019). "Fire resistance and burnout resistance of reinforced concrete columns." *Fire Safety Journal*, 104, 67–78.
- Gosain, N., Drexler, F., and Choudhuri, D. (2008). "Evaluation and Repair of Fire-Damaged Buildings." *Structure magazine*, (September), 18–22.

- Haddad, R. H., Al-Saleh, R. J., and Al-Akhras, N. M. (2008). "Effect of elevated temperature on bond between steel reinforcement and fiber reinforced concrete." *Fire Safety Journal*, 43(5), 334–343.
- Hager, I. (2014). "Colour Change in Heated Concrete." Fire Technology, 50(4), 945–958.
- Harada, T., Takeda, J., Yamane, S., Furumura, F., and Kesler, C. E. (ed). (1972). Strength, elasticity, and thermal properties of concrete subjected to elevated temperatures. American Concrete Insitute, Detroit.
- Harmathy, T. Z. (1967). "A Comprehensive Creep Model." *Journal of Basic Engineering*, 89(3), 496–502.
- Harmathy, T. Z. (1970). "Thermal properties of concrete at elevated temperatures." *Journal of Materials*.
- Hertz, K. (2003). "Limits of spalling of fire-exposed concrete." *Fire safety journal*, 38(2003), 103–116.
- Hibbitt, Karlsson & Sorensen, Inc. (2012). "ABAQUS standard user's manual." Pawtucket (America).
- Hsu, J.-H., and Lin, C.-S. (2008). "Effect of Fire on the Residual Mechanical Properties and Structural Performance of Reinforced Concrete Beams." *Journal of Fire Protection Engineering*, 18(4), 245–274.
- Huang, Z. (2010). "Modelling the bond between concrete and reinforcing steel in a fire." *Engineering Structures*, Elsevier Ltd, 32(11), 3660–3669.
- ISO 834-1. (1999). Fire resistance tests-elements of building construction. Part 1: general requirement. Geneva, Switzerland.
- Jendele, L., and Cervenka, J. (2006). "Finite element modelling of reinforcement with bond." *Computers & Structures*, 84(28), 1780–1791.
- J.Terro, M. (1998). "Numerical Modeling of the Behavior of Concrete Structures in Fire." *Structural Journal*, 95(2), 183–193.
- Kalaba, N, Kodur, VKR, Agrawal, A, and Bamonte, P. "Structural behaviour of R/C beams exposed to natural fires." *Proceedings of the 10th International Conference on Structures in Fire (SIF2018)*, Ulster University, Belfast, United Kingdom, 6-8th June 2018, pp. 139-146.
- Keuser, M., and Mehlhorn, G. (1987). "Finite element models for bond problems." *Journal of Structural Engineering*, 113(10), 2160–2173.
- Khaliq, W., and Kodur, V. (2011). "Thermal and mechanical properties of fiber reinforced high performance self-consolidating concrete at elevated temperatures." *Cement and Concrete Research*, 41(11), 1112–1122.

- Khan, M. I. (2002). "Factors affecting the thermal properties of concrete and applicability of its prediction models." *Building and Environment*, Retrofitting of Office Buildings: Papers from the Research Projec t Office, 37(6), 607–614.
- Khoury, G. A., Grainger, B. N., and Sullivan, P. J. (1985). "Strain of concrete during first heating to 600 C under load." *Magazine of Concrete Research*, 37(133), 195–215.
- Khoury, G. A., Majorana, C. E., Pesavento, F., and Schrefler, B. A. (2002). "Modelling of heated concrete." *Magazine of Concrete Research*, 54(2), 77–101.
- Kodur, V. K. R. (2014). "Properties of Concrete at Elevated Temperatures." *ISRN Civil Engineering*, 2014, 1–15.
- Kodur, V. K. R., Agrawal, A. and Rafi, M. M. (2014). "An approach for ascertaining residual capacity of reinforced concrete beams exposed to fire." *Advancements in Structural Engineering Proceedings of the 9th Structural Engineering Convention (SEC 2014)*, New Delhi, India, 22 24th December, 2014, Bloomsbury, ISBN: 978-9-38-489871-7, pp. 4634 -4646.
- Kodur, V. K. R., Garlock, M., and Iwankiw, N. R. (2007). *National Workshop on Structures in Fire:* State-of-the-Art, Research and Training Needs.
- Kodur, V. K. R., and Agrawal, A. (2016a). "Critical Factors Governing the Residual Response of Reinforced Concrete Beams Exposed to Fire." *Fire Technology*, 52, 967-993.
- Kodur, V. K. R. (2000). "Spalling in high strength concrete exposed to fire: concerns, causes, critical parameters and cures." *ASCE Structures Congress*, Philadelphia, 1–8.
- Kodur, V. K. R., and Agrawal, A. (2016b). "An approach for evaluating residual capacity of reinforced concrete beams exposed to fire." *Engineering Structures*, 110, 293–306.
- Kodur, V. K. R., and Agrawal, A. (2017). "Effect of temperature induced bond degradation on fire response of reinforced concrete beams." *Engineering Structures*, Elsevier Ltd, 142, 98–109.
- Kodur, V. K. R., and Alogla, S. M. (2017). "Effect of high-temperature transient creep on response of reinforced concrete columns in fire." *Materials and Structures*, 50(1), 1–17.
- Kodur, V. K. R., and Dwaikat, M. (2007). "Performance-based Fire Safety Design of Reinforced Concrete Beams." *Journal of Fire Protection Engineering*, 17(4), 293–320.
- Kodur, V. K. R., and Dwaikat, M. (2008). "A numerical model for predicting the fire resistance of reinforced concrete beams." *Cement and Concrete Composites*, 30(5), 431–443.
- Kodur, V. K. R., Dwaikat, M. B., and Fike, R. S. (2010). "An approach for evaluating the residual strength of fire-exposed RC beams." *Magazine of Concrete Research*, 62(7), 479–488.

- Kodur, V. K. R., Dwaikat Mahmud, and Fike Rustin. (2010d). "High-Temperature Properties of Steel for Fire Resistance Modeling of Structures." *Journal of Materials in Civil Engineering*, 22(5), 423–434.
- Kodur, V. K. R., and Phan, L. (2007). "Critical factors governing the fire performance of high strength concrete systems." *Fire Safety Journal*, 42(6–7), 482–488.
- Kodur V. K. R., and Sultan M. A. (2003). "Effect of Temperature on Thermal Properties of High-Strength Concrete." *Journal of Materials in Civil Engineering*, 15(2), 101–107.
- Kodur V. K. R., Agrawal A. (2019). "Approach for assessment of fire damaged concrete structures." *Proceedings of the 6th International Conference on Applications of Structural Fire Engineering (ASFE'19)*, Nanyang Technological University (NTU) Singapore, Singapore, 13-14th June 2019. pp 1-9.
- Kodur, V. K. R., and Agrawal, A. (2020). "A numerical approach for evaluating residual capacity of fire damaged concrete members." Revista ALCONPAT, 10(2), 230 242.
- Krešimir, N., Ožbolt, J., and Boko, I. (2016). "The influence of continuing reinforcement on the load capacity of a RC beam previously exposed to high temperatures." *Građevinar*, 68(12), 967–978.
- Kumar, A., and Kumar, V. (2003a). "Behaviour of RCC Beams after Exposure to Elevated Temperatures." *Institution of Engineers India Civil Engineering Division*, 84, 165–170.
- Kwak, H., and Kim, S. (2001). "Bond–slip behavior under monotonic uniaxial loads." *Engineering structures*, 23(2001), 298–309.
- Lakhani, H., Kamath, P., Bhargava, P., Sharma, U., and Reddy, G. (2013). "Thermal Analysis of Reinforced Concrete Structural Elements." *Journal of Structural Fire Engineering*, 4(4), 227–244.
- Lakhani, H., Singh, T., Sharma, A., Reddy, G. R., and Singh, R. K. (2014). "Prediction of post fire load deflection response of RC flexural members using simplistic numerical approach." *Structural Engineering and Mechanics*, 50(6), 755–772.
- Lee, J., and Fenves, G. L. (1998). "Plastic-Damage Model for Cyclic Loading of Concrete Structures." *Journal of Engineering Mechanics*, 124(8), 892–900.
- Li, L., and Purkiss, J. (2005). "Stress–strain constitutive equations of concrete material at elevated temperatures." *Fire Safety Journal*, 40(7), 669–686.
- Li, Y. H., and Franssen, J. (2011). "Test results and model for the residual compressive strength of concrete after a fire." *Journal of Structural Fire Engineering*, 2(1), 29–44.
- Lu, L., Yuan, Y., Caspeele, R., and Taerwe, L. (2015a). "Influencing factors for fire performance of simply supported RC beams with implicit and explicit transient creep strain material models." *Fire Safety Journal*, 73, 29–36.

- Lubliner, J., Oliver, J., Oller, S., and Onate, E. (1989). "A plastic-damage model for concrete." *International Journal of solids and ...*, 25(3), 299–326.
- Mindess, S., Young, J. F., and Darwin, D. (2003). *Concrete*. Prentice-Hall Inc., Englewood Cliffs, New Jersey.
- Molkens, T., Van Coile, R., and Gernay, T. (2017). "Assessment of damage and residual load bearing capacity of a concrete slab after fire: Applied reliability-based methodology." *Engineering Structures*, 150, 969–985.
- Morley, P. D. (1983). "Response of the bond in reinforced concrete exposed to high temperature." *Magazine of Concrete Research*, 35(123), 67–74.
- Nassif, A. (2006). "Postfire full stress-strain response of fire-damaged concrete." *Fire and Materials*, 30(5), 323–332.
- Neves, I. C., Rodrigues, J. P. C., and Loureiro, A. de P. (1996a). "Mechanical Properties of Reinforcing and Prestressing Steels after Heating." *Journal of Materials in Civil Engineering*, 8(4), 189–194.
- Nilsson, L. (2002). "Long-term moisture transport in high performance concrete." *Materials and Structures*, 35(December), 641–649.
- Ožbolt, J., Bošnjak, J., Periškić, G., and Sharma, A. (2014). "3D numerical analysis of reinforced concrete beams exposed to elevated temperature." *Engineering Structures*, 58, 166–174.
- Panedpojaman, P., and Intarit, P.-I. (2016). "Maximum temperature prediction for concrete sections during cooling phase." *KKU Engineering Journal*, 43, S2.
- Panedpojaman, P., and Pothisiri, T. (2014). "Bond characteristics of reinforced normal-strength concrete beams at elevated temperatures." *ACI Structural Journal*, 111(6), 1351–1362.
- Park, G.-K., and Yim, H. J. (2017). "Evaluation of Fire-Damaged Concrete: An Experimental Analysis based on Destructive and Nondestructive Methods." *International Journal of Concrete Structures and Materials*, 11(3), 447–457.
- Poon, C.-S., Azhar, S., Anson, M., and Wong, Y.-L. (2001b). "Strength and durability recovery of fire-damaged concrete after post-fire-curing." *Cement and Concrete Research*, 31(9), 1307–1318.
- Pothisiri, T., and Panedpojaman, P. (2012). "Modeling of bonding between steel rebar and concrete at elevated temperatures." *Construction and Building Materials*, Elsevier Ltd, 27(1), 130–140.
- Rafi, M., Nadjai, A., and Ali, F. (2008). "Finite element modeling of carbon fiber-reinforced polymer reinforced concrete beams under elevated temperatures." *ACI Structural Journal*, 105(6), 701–710.

- Razafinjato, R., and Beaucour, A. (2016). "High temperature behaviour of a wide petrographic range of siliceous and calcareous aggregates for concretes." *Construction and Building Materials*, 123, 261–273.
- Reichel, V. (1978). "How fire affects steel-to-concrete bond." *Batiment International, Building Reasearch and Practice*, 6(3), 176–187.
- Schäfer, H. (1975). "A contribution to the solution of contact problems with the aid of bond elements." *Computer methods in applied mechanics and engineering*, 6, 335–354.
- Schneider, U. (1988). "Concrete at high temperatures—a general review." *Fire safety journal*, 13, 55–68.
- Schweizerhof, K. (1993). "Consistent concept for line search algorithms in combination with arclength constraints." *Communications in Numerical Methods in Engineering*, 9(9), 773–784.
- Shamseldein, A., Elshafie, H., Rashad, A., and Kohail, M. (2018). "Assessment and restoration of bond strength of heat-damaged reinforced concrete elements." *Construction and Building Materials*, 169, 425–435.
- Shi, X., Tan, T., Tan, K., and Guo, Z. (2004). "Influence of Concrete Cover on Fire Resistance of Reinforced Concrete Flexural Members." *ASCE Journal of Structural Engineering*, 130(8), 1225–1232.
- Shin, K.-Y., Kim, S.-B., Kim, J.-H., Chung, M., and Jung, P.-S. (2002). "Thermo-physical properties and transient heat transfer of concrete at elevated temperatures." *Nuclear Engineering and Design*, 212(1), 233–241.
- Tao, Z., Wang, X., and Uy, B. (2013). "Stress-Strain Curves of Structural and Reinforcing Steels after Exposure to Elevated Temperatures." *Journal of Materials in Civil Engineering*, 25(September), 1306–1316.
- Tastani, S. P., and Pantazopoulou, S. J. (2010). "Direct Tension Pullout Bond Test: Experimental Results." *ASCE Journal of Structural Engineering*, 136(6), 731–743.
- Thongchom, C., Lenwari, A., and Aboutaha, R. S. (2019). "Effect of Sustained Service Loading on Post-Fire Flexural Response of Reinforced Concrete T-Beams." *ACI Structural Journal*, 116(3).
- Torić, N., Boko, I., and Peroš, B. (2013). "Reduction of Postfire Properties of High-Strength Concrete." *Advances in Materials Science and Engineering*, 2013, 1–9.
- Tovey, A. K. (1986). "Assessment and Repair of Fire-Damaged Concrete Structures-an Update." *Special Publication*, 92, 47–62.

- The Concrete Society. (2008) Assessment, Design and Repair of Fire-damaged Concrete Structures. Cement and Concrete Industry Publications Forum. CCIP-040, Camberley, UK.
- Ulaga, T., Vogel, T., and Meier, U. (2003). "The bilinear stress-slip bond model: Theoretcial background and significance." *FRPRCS-6 Conference*, Singapore, 1–10.
- Van Coile, R. (2015). "Reliability-based decision making for concrete elements exposed to fire." Doctoral Dissertation, Ghent University, Ghent, Belgium.
- Wickström, U. (1986). A very simple method for estimating temperature in fire exposed concrete structures. Swedish National Testing Institute, 186–194.
- Wu, B., and Lu, J. Z. (2009). "A numerical study of the behaviour of restrained RC beams at elevated temperatures." *Fire Safety Journal*, 44(4), 522–531.
- Wu, H., Lie, T., and Hu, J. (1993). Fire resistance of beam-slab specimens-experimental studies. Canada.
- Xing, Z., Hébert, R., Beaucour, A.-L., Ledésert, B., and Noumowé, A. (2013). "Influence of chemical and mineralogical composition of concrete aggregates on their behaviour at elevated temperature." *Materials and Structures*, 47(11), 1921–1940.
- Xu, Y. Y., Wu, B., Jiang, M., and Huang, X. (2012). "Experimental Study on Residual Flexural Behavior of Reinforced Concrete Beams after Exposure to Fire." *Advanced Materials Research*, 457–458, 183–187.
- Youssef, M. A., and Moftah, M. (2007). "General stress–strain relationship for concrete at elevated temperatures." *Engineering Structures*, 29(10), 2618–2634.